Optical Limiting and Nonlinear Optical Properties of Photo Responsive Materials: Tetratolylporphyrins, Pure and iron doped $Bi_{12}SiO_{20}$ crystals and Codoped Ag-Cu Metal Nanoclusters

A Thesis submitted for the degree 6f

DOCTOR OF PHILOSOPHY

by

P. Prem Kiran

School of Physics

University of Hyderabad

Hyderabad-500 046

India

February 2004

DECLARATION

I hereby declare that the matter embodied in this thesis entitled "Optical Limiting and Nonlinear Optical Properties of Photo Responsive Materials: Tetratolylporphyrins, Pure and iron doped $Bi_{12}SiO_{20}$ crystals and Codoped Ag-Cu Metal Nanoclusters" is the result of investigations carried out by me in the School of Physics, University of Hyderabad, India, under direct supervision of Prof. D. Narayana Rao.

Place: Hyderabad

Date: 24·02·04

P. Prem Kiran

CERTIFICATE

This is to certify that, the work described in this thesis has been carried out by **Mr. P. Prem Kiran** under my direct supervision and this has not been submitted for any degree or diploma at this or any other University.

Place: Hyderabad
Date: 24·02·04

D. Narayana

U. s. s. Sastry

Dean

School of Physics

DEAN
School of Physics
University of Hyderabad
Hyderabad-500 046, INDIA

*To My Parents
&Teachers*

Contents

Chapter 3   Axial ligated Phosphorus (V) Tetratolylporphyrins

Chapter 4   Axial-bonding type hybrid porphyrin arrays with basal
Tin (IV) Tetratolylporphyrin scaffold

Chapter 5 $Bi_{12}SiO_{20}$ and $Bi_{12}SO_{20}$:Fe crystals

Chapter 6   Ag-Cu nanoclusters codoped in SiO_2 Sol-Gel films

Chapter 7   Summary and future perspective   191

List of Publications   **195**

Acknowledgements

It is indeed a great pleasure to thank all those who have, directly or indirectly, helped in successful completion of this thesis.

At the outset I wish to thank my thesis supervisor Prof. D. Narayana Rao who was by my side always, patiently and constantly inspiring, encouraging, guiding me throughout the course and sharing the elegant way of doing science. And I think that now, I finally understand that "why" is as important as "how" one does an experiment. My association with him for over five years was a rewarding experience, which I never wish to forget.

I would like to thank the Dean, School of Physics, for making available all the facilities required for the experiments. I also thank all the non-teaching staff for their co-operation.

I would like to thank Prof's S.P. Tewari, C.S. Sunandana, and S. Dutta Gupta, and Dr. P. Anantha Lakshmi, for their constant support and inspiring association. Special thanks to Dr. Suneel Singh for his help in solving rate equations and his support throughout. I would like to thank all my teachers who always supported and encouraged me to reach this level.

I would like to thank my friends Naga Srinivas, Sastry GRGK, Vikas, **Shekar,** Shiva, Sastri CV and Vijayanand for their constant encouragement and support through the ups and downs during this period.

I would like to thank Prof. Bhaskar G. Maiya and Mr. D. Raghunath Reddy, School of Chemistry for providing me with large amounts of samples of Tetratolylporphyrins when required and for their co-operation extended throughout my course. I would also like to thank Prof. T.P. Radhakrishnan, School of Chemistry for his valuable association through out the course. I would like to thank Dr. Goutam De, CGCRI, Kolkata for the sol-gel films, Prof. H.L. Bhat, Department of Physics, IISc., Bangalore and his group members Deepthi, Brahadeeswaran, Vijay and Vanish for help with cutting and polishing of BSO crystals and for the nice time at SERC school. I would like to thank Prof's D. Mathur and G. Ravindra Kumar for extending the picosecond and femtosecond laser facility at TIFR, and for their valuable discussions. I thank Dr.'s M.

Chapter 1

Motivation and Introduction

Fundamental concepts and various mechanisms responsible for optical limiting in various classes of materials are described. The materials chosen for the present study and the motivation for choosing these materials are explained. Chapter wise division of the thesis is given.

1.1   Optical Limiting

Lasers have caused revolutionary changes in many fields of science and technology. Since 1960, six orders of magnitude, from 10^{-9} to 10^{-15} seconds, have been added to time-resolved observation of fast phenomena. New subfields of science, including femtochemistry and femtobiology, have been created. In addition, the domain of power flux densities has been extended from 10^{12} to 10^{19} Wcm^{-2} by the use of short focused pulses. This has given experimental access to new phenomena, including ultrafast phase transitions in electronic structure, above-threshold ionization of atoms, and high-order harmonic generation and acceleration of relativistic electrons by light pulses. Some representative examples of transient Raman scattering and of impulsive and displacive excitations in molecules and crystals illustrate the usefulness of picosecond and femtosecond pulse techniques **[1].** Even though lasers revolutionized major fields of science, the dramatic advances in semiconductor and solid-state lasers that are far more portable, compact and efficient are finding application in the realm of laser weaponry [2]. High-power diode-pumped solid-state lasers promise the military the same advantages they offer industry. With such an advent of high power laser sources over wide range of wavelengths and pulse durations, the necessity for protection of sensors and eyes has enormously increased over the last few years. In this context, optical limiters have received significant attention. An ideal limiter exhibits a linear transmission below a threshold and clamps the output to a constant above it, thus providing safety to sensors or eye. The minimum criteria identified for a material to act as an

effective optical limiter are (1) Low limiting threshold and large dynamic range (2) High optical damage threshold and stability (3) Sensitive broadband response to long and short pulses (4) Fast response time (5) High linear transmittance through out the sensor band width, optical clarity, and robustness [3]. Wide varietiy of organic and inorganic materials are being studied to achieve efficient optical limiting [4]. Various approaches have been developed towards better optical limiting based on, e.g., electro-optical **[5],** magneto-optical [6], and all-optical [7] mechanisms. The all-optical limiters rely on materials that exhibit one or more of the nonlinear optical mechanisms: Two-photon absorption (TPA), Excited State Absorption (ESA), Free carrier absorption, Thermal defocusing and scattering, photorefraction, nonlinear refraction, induced scattering [8]. Coupling two or more of these mechanisms has also achieved enhancement in optical limiting, like self-defocusing in conjunction with TPA [9], TPA of one molecule with ESA in another molecule [10]. Different experimental geometries like cascaded limiters [11] are also studied to achieve large figure of merit and dynamic range.

1.2   Processes leading to optical limiting

The **first** experimental demonstration of optical power limiter reported by Leite *et al.* [12] is based on the laser induced thermal lens effect using 488 nm cw Ar$^+$ laser beam as incident light and nitrobenzene as the linearly absorbing medium with an aperture in front of the detector. Though the change of power through the aperture was only 3% of the total input power change at high input levels, the original idea and setup is still the basis of most popular optical limiting designs using organic dye solutions **[13],** semiconductors [14] and other materials [15] as linearly absorbing media. Optical limiting can be achieved by means of various nonlinear optical mechanisms, including self-focusing, self-defocusing, induced scattering, induced-refraction, induced aberration, excited state absorption, two-photon absorption, photorefraction and free-carrier absorption in nonlinear optical media [16]. Although there is a great variety of optical limiting

devices most of them can be divided into two categories. One is the energy-spreading type of devices and the other is the energy-absorbing type of devices.

1.3   Energy-spreading type optical limiters

For energy-spreading type of devices, the key requirement is to place an aperture or pinhole in front of a detector. The limiting of the detected laser beam is based on the fact that, after passing through a nonlinear medium, the spatial energy distribution of the transmitted laser beam has changed. When the input laser intensity (or fluence) increases, there will be more portions of the incident laser energy spreading to a wider solid-angle range; as a result the portion passing through the aperture will decrease accordingly.
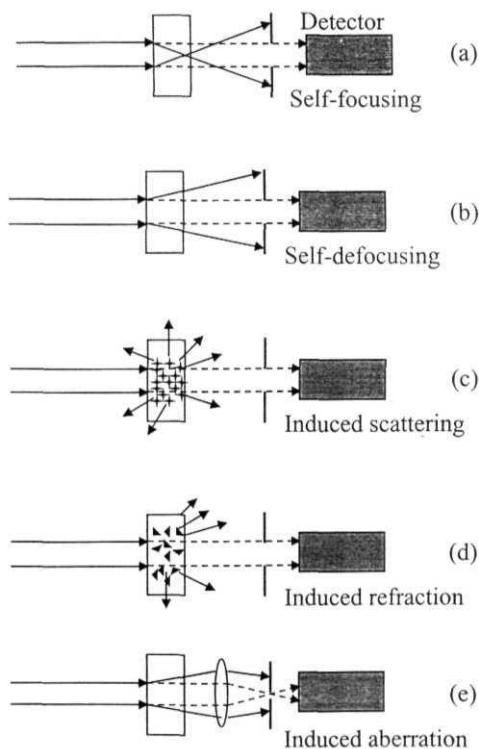
Figure 1.1: Schematic illustrations of energy-spreading type of optical limiters

In these cases the observed limiting behaviour depends not only on the input laser intensity (or fluence) and the nonlinear medium, but also on the pinhole size and the geometric configuration of the optical system for a given device. For most of this type of devices, thermally induced refractive index change plays a major role. Typical designs for the energy-spreading type of optical limiting devices are schematically shown in Fig 1.1. In all these cases the opening size of the aperture is chosen such that for a very low input fluence (or intensity) level, the transmitted laser beam after passing through the medium can just totally pass through the aperture without blocking.

In Figs 1.1 (a) and (b) the design based on self-focusing and self-defocusing are shown. In both the cases at high input levels the detected energy portion can be significantly reduced due to the energy spreading in the aperture plane. Fig 1.1 (c) shows the optical limiter based on laser-induced and intensity dependent scattering. In this case, the limiting medium is a system of linearly absorbing particles randomly distributed in a transparent host material. For a weak input light beam, the temperature and refractive index changed due to the particles' absorption in the system are negligible, whereas for strong laser beam, the absorption-induced temperature change of the particles is no longer negligible and each particle forms an individual heating center. As a result of this local heating effect, the medium becomes highly inhomogenous and the considerable portions of the energy will spread out into a wider spatial range and the portion of the light passed through the aperture will be limited [17]. The device shown in fig 1.1 (d) uses a similar idea, where the medium is a mixed system composed of two microscopic components that have the same static refractive index but are in a different phase states, e.g. one in liquid and other is solid. If one component is transparent and the other is linearly absorptive to the incident laser beam, as a result of selective opto-heating process, the whole system becomes inhomogenous in the boundary between the two components [16]. Another mechanism shown in fig 1.1 (e) is based on induced aberration. It is well known that the induced refractive index change is a function of the local intensity distribution of the laser beam inside the medium. An irregular spatial distribution of local light intensity may lead to a random refractive index change at higher

intensity levels, which may cause severe aberration influences on the wavefront of the transmitted laser beam. By keeping a small pinhole in the focal plane of a focusing lens, the portion of the laser energy passed through the pinhole will decrease as the induced aberration becomes greater [18]. Although, all optical limiting devices of energy spreading type are based on the laser induced refractive index change and featured by using an aperture, in some experimental devices no aperture is used, the limited sensitive area of the detector still plays the role of aperture.

Comparing with all other nonlinear optical effects related to refractive index changes, the opto-thermal effect induced refractive index change is considered to be important, even it has a slow temporal response. The specific origins that cause thermally induced refractive index changes can be given as following: (1) The presence of small amount of impurities or external particles giving rise to a nonzero residual linear absorption in transparent and non-resonantly absorptive medium. At higher input laser intensity (or fluence) the small residual linear absorption might be strong enough to create a remarkable thermally induced refractive index change. (2) For a resonant and linearly absorbing media such as dye solution or semiconductor crystal, thermally induced refractive index change will be significant even for a weaker cw laser beam or low fluence pulsed laser beam. (3) An aperture involved in front of a detector, while working with a nonlinear absorbing material working with RSA or TPA mechanism, the contribution from the thermal effect may be more responsible for the observed optical limiting behavior than the contribution from pure nonlinear absorption.

1.4   Energy-absorbing type optical limiters

Nonlinear absorption is another type of mechanism that is employed for optical limiting. In this case no aperture or pinhole is necessary, and the optical limiting relies on the fact that the transmission of nonlinear absorbing media decreases when the input laser intensity (or fluence) increases. The major nonlinear absorption mechanism employed for optical limiting is RSA [19]. The

optical limiting devices based on this mechanism can be called the energy-absorbing type of optical limiters and figure 1.2 (a) shows the common design for optical limiting devices for this type of limiters. In this case the processes leading to optical limiting can be one of the following: two-photon absorption (TPA), excited state absorption (ESA), and free-carrier absorption (FCA). ESA is the process leading to nonlinear absorption in organic molecules and a similar process in semiconductors, metals and metal nanoparticles is called FCA. In this thesis, mechanisms that use RSA are discussed in detail.
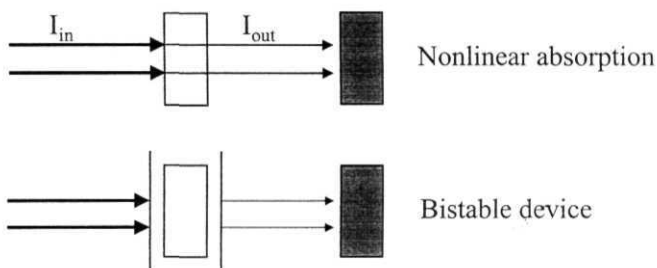
Figure 1.2: (a) Schematic of optical limiting device based on nonlinear absorption and (b) optical bistability.

Materials showing RSA become more strongly absorbing as the input optical intensity (or fluence) is increased. This nonlinear optical response can be exhibited when chromophores have a weak ground-state absorption over some spectral range and strong excited-state absorption in the same wavelength range. Although a variety of materials and mechanisms have been and are being explored for use in optical limiting, interest in reverse saturable absorber chromophores is increasing for many reasons, few of which are listed here. First, for chromophores having large ratio of excited-state to ground-state absorption cross sections ($\sigma_{ex}/\sigma_g \gg 1$) there is a potential for achieving large nonlinear attenuation and maintaining high linear transmittance. Second, since optical energy is absorbed and converted to heat as opposed to being spread, as in nonlinear refractive or scattering media, the limiting may be more reliable and may be applied in fast (highly convergent) optical systems. Third, chromophores

with prompt singlet excited-state absorption and long-lived triplet-state absorption may be effectively used to optical limiting of a wider range of pulse widths (sub-picosecond to microsecond duration). Finally, the ability to modify systematically the photophysical properties of chromophores through rational changes in molecular structure enables molecular engineering approaches to the development of chromophores with enhanced limiting responses [20].

1.5   Reverse Saturable absorption

Reverse saturable absorption was first observed by Giuliano and Hess,[21] who were studying various organic dye molecules (e.g. Indanthrone and Sudanschwarz B) for potential applications for the Q-switching of a laser cavity. They noticed that under intense laser pulses, these organic dyes did not show bleaching (saturable absorption) as expected, but became darker at high intensities.

Chromophores exhibit reverse saturable absorption when an excited state, which is populated by optical excitation, has an absorption cross-section, σ_{ex}, which is larger than the ground-state absorption cross-section, σ_g, over a certain spectral range. If an optical pulse passes through a medium containing such molecules, the transmittance decreases as the pulse intensity or **fluence** increases. Fig 1.3 shows simplified version of the nonlinear absorptive response for reverse saturable absorbers. At low incident pulse energies, the transmittance is governed by the ground-state absorption and can be written as $I_0 - e$ and after excitation the initial ground-state population is transferred to the excited state, the transmission drops and approaches a value governed by the excited state cross-section $T_{sat} - e'$, The rate constant for optical pumping of population from the ground state to an excited state depends on the irradiance I, the photon frequency v, and the photon flux ϕ and is given by $\kappa_{gex} = \sigma_g I / h v = \sigma_g \phi$. Thus to produce a large excited-state population σ_g must be sufficiently large during the pulse. In order to get a strong optical limiting

response it is necessary to have a large value ,of σ_{ex}/σ_g and to rapidly and efficiently transfer the ground-state population to the excited state. Large ground state absorption can often lead to saturation of absorption, which is an unwanted mechanism for optical limiting devices, though it is useful for saturable absorbers that are used for passive mode-locking of lasers. The saturation of absorption can be reduced and can be effectively manipulated in certain cases to enhance RSA by the following phenomenon. (1) By exciting the population to further higher excited states (2) by relaxing the population back to the ground state very rapidly i.e., timescales much shorter than the excitation pulse width, (3) by transferring the population sufficiently fast to the levels from where further excitation is possible. Thus the population dynamics of the molecule plays a crucial role in deciding the capability of the material as optical limiter.
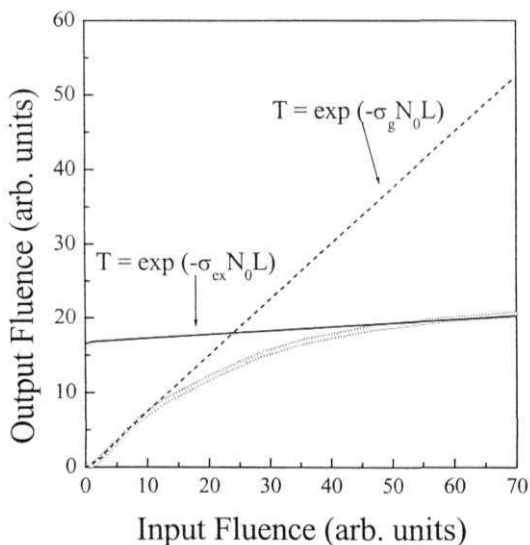
Figure 1.3: Illustration of the nonlinear absorptive response of a reverse saturable absorber.

The population dynamics of reverse saturable absorbers under laser pulse excitation can be described by simple rate equations neglecting the coherence effects as in many systems investigated for nonlinear absorption / optical limiting applications since dephasing is usually ultrafast (on a sub picosecond time scale) under the conditions where large-molecules are usually applied [22]. General energy level scheme to explain the population dynamics in relevance to nonlinear absorption and optical limiting in RSA chromophores is given in Fig 1.4. Detailed description of the rate equations and methodology for evaluating the excited state cross sections is given in the Chapter 2 of the thesis.
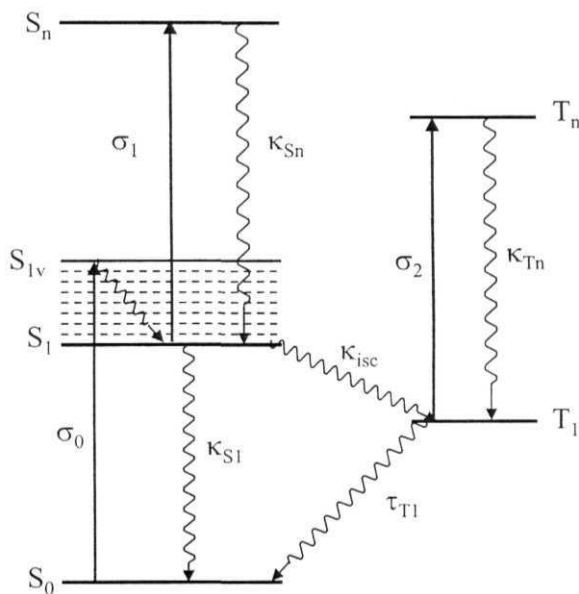
Figure 1.4: Schematic energy level diagram for a chromophore with a singlet ground state.

The populations of the various states of a chromophore can attain values that become independent of time during the pulse when the time constant for return of population to the ground state is shorter than the pulse duration, which is the case of "fast-absorbers" which is the steady-state condition for the populations [22]. To illustrate the steady-state behaviour, consider a system

comprised of So, S_1 and S_n states where, in addition to having ultrafast relaxation from S_n to S_1, the relaxation time from S_1 to S_0 is shorter than the pulse duration. At sufficiently high intensity the response time of the "fast" reverse saturable absorber is essentially instantaneous. As a result of this fast response, there is minimal change in shape of the pulse after passing through the reverse saturable absorber. Molecules having two-photon absorption can be considered in this category. Using TPA as optical limiting mechanism exhibits the advantage of (1) negligible linear absorption loss for weak signal, (2) extremely fast temporal response, and (3) retaining beam quality for the transmitted signal. TPA-based devices are suitable not only for optical limiting but also for other application purposes such as optical power stabilization, optical pulse reshaping and optical spatial-field reshaping [23]. When the return of population to the ground state is slow compared to the pulse width, reverse saturable absorber is considered to be "slow". Molecules that allow formation of triplet states via intersystem crossing, which slows down the relaxation to ground state, like porphyrins, phthalocyanines, fullerenes having dominant excited state absorption from the triplet states come under this category.

The important parameters (figures of merit) characterizing the response of RSA chromophores are the saturation fluence, which control the excited-state population, and the ratio of the effective excited-state to ground state absorption cross-section, (σ_1/σ_0). When there is a triplet-triplet absorption contribution, the intersystem-crossing rate is also important, and for strong pumping, the triplet population is controlled by the product $\kappa_{isc} \times (\sigma_2 \ /an)$. The optical bandwidths associated with the linear transmittance and the excited-state absorption of reverse saturable absorbers is also important in evaluating materials for optical limiting [24].

1.6   Free carrier absorption

Free-carrier absorption is a phenomenon that is analogous to excited state absorption in organic molecules. It has similar qualitative characteristics to ESA. In semiconductors/band gap materials like photorefractives, the absorption of a

photon with energy greater than the band gap will promote an electron to the conduction band, where it is a free carrier and can contribute to current flow when a field is applied. The excited electron will rapidly thermalize and relax to the bottom of the conduction band. From there it will recombine with an excited hole in the valence band after a characteristic recombination time. However, at sufficiently high intensities, it can with high probability absorb another photon while it is in the conduction band. This process is called free carrier absorption. Once free carriers are generated in semiconductors, they may experience phonon-assisted absorption to higher lying (lower-lying) states in the conduction (valence) band. In the weak absorption regime, the attenuation can be described by

$$\frac{\partial I}{\partial Z} = -\alpha_0 I - \sigma_c N_c(I)I \qquad\qquad \textbf{(1.1)}$$

where $N_c(I)$ is the intensity dependent carrier density, and σ_c is the free carrier cross-section given by

$$\sigma_c = \frac{e^2}{\varepsilon_0 n_0 cm^* \omega^2 \tau} \qquad\qquad \textbf{(1.2)}$$

where m^* is the effective carrier mass, ω is the optical frequency and r is the free-carrier decay time (mean collision time). It has the $1/\omega^2$ dependence of a high-frequency conductivity and thus is most important for infrared radiation in semiconductors. The free-carrier density is governed by rate equation given by

$$\frac{\partial N_c}{\partial t} = \frac{\alpha_0 I}{\hbar\omega} - \frac{N_c}{\tau_c} \qquad\qquad \textbf{(1.3)}$$

where τ_c is the free-carrier relaxation time due to electron-hole recombination and carrier diffusion. In general, eqns. (1) and (3) have to be solved numerically to determine the transmittance of the material. When the incident pulse is short compared to the carrier relaxation time, second term in Eqn (3) can be neglected and Eqns (1) and (3) can be integrated over time to obtain the fluence attenuation given by

$$\frac{\partial F}{\partial Z} = -\alpha_0 \left(1 + \frac{F}{2F_s}\right) F \qquad (1.4)$$

where $F = \hbar\omega / \sigma_{_,}$ is the saturation fluence.

1.7   Two-Photon assisted excited state absorption

When TPA is particularly strong in a material, it can lead to significant population of a two-photon allowed state. Often there are allowed radiative transitions from this state to higher-lying states of the system, i.e., ESA can ensue from the two-photon pumped state. This occurs both in polyatomic molecules and in semiconductors, especially when excited with ultrashort pulses. The attenuation and excited state population can be given by

$$\frac{\partial I}{\partial Z} = -\alpha I - \beta I^2 - \sigma N I \qquad (1.5)$$

and

$$\frac{\partial N}{\partial t} = \frac{\beta I^2}{2\hbar\omega} - \frac{N}{\tau_1} \qquad (1.6)$$

where α is the linear absorption coefficient for impurity absorbers, and τ_1 represents the lifetime of two-photon excited states. These equations are solved numerically to determine the nonlinear transmittance of the system. The detailed procedure to solve the equations is explained in chapter 2 of this thesis.

1.8   Materials for Optical limiting

Varieties of materials are studied for optical limiting purposes based on different processes. Improved nonlinear materials with more sensitivity and less linear loss are being developed to incorporate them into optical systems and their ability to protect real sensors. More attention focuses around pulsed lasers in the visible and near infrared bands, in view of the importance and vulnerability the eye [25]. In the UV-near IR transmission band, suspensions lead to optical limiting using scattering mechanism [26]. Dyes lead to OL in selected portion of the visible band because of nonlinear absorption and refraction. The most

extensively studied materials are the macrocyclics including phthalocyanines and naphthalocyanines [27], porphyrins [28] and fullerenes [29] and their derivatives in which long-lived triplet excited state can be produced copiously. Liquid crystals are another class of materials studied in the visible to mid IR region via refraction and TPA [30]. Various other materials like, photorefractive materials [31], photonic band gap materials [32], nanomaterials and nanotubes **[33],** nonlinear absorbers doped **in** xerogels and sol-gel films [34], glasses [35], filters [36], organic/inorganic clusters [37], layered systems [38] and bacteriorhodopsin [39] are studied for their optical limiting properties.

Out of various materials discussed in the literature, some show low limiting thresholds with CW beams and ns/ps pulses and low damage thresholds as well. Some of the materials show very high damage thresholds but high limiting thresholds. Some materials have a broadband spectral response with high $I_{1/2}$ and some have narrowband response with lower $I_{1/2}$. Our aim has been to study both organic and inorganic materials to bring some of these in tandem to achieve eye-safe limiting thresholds as well as high damage thresholds for ns and ps pulses with **in** the visible region of the spectrum. In pursuit of this we studied porphyrins, photorefractive materials and nanoclusters, which have low limiting thresholds and high damage thresholds and can be very easily modified to enhance limiting behaviour.

1.9   Outline of the thesis

This thesis is an attempt to identify new materials for all-optical limiting mechanisms based on RSA and aims at a detailed investigation of the basic nonlinear optical processes leading to optical limiting properties and to move towards the eye-safe limiters. Chapter 2 of the thesis explains the experimental geometries and the general properties of the materials studied.

Porphyrins, a class of tetrapyrrolic chromophores, are among the most effective optical limiters in the visible region known to date [28]. Of the various processes leading to optical limiting, ESA plays a very important role for optical limiting in porphyrins. The contribution of structural modifications to optical

limiting in Phosphorus (V) tetratolylporphyrin based materials with axial chlorine and azoarene subunits are addressed in Chapter 3 of this thesis.

Optical limiting properties of 'axial-bonding' type hybrid porphyrin arrays - dimer, trimer and hexamers based on a Tin (IV) scaffold are studied to understand the effect of different metal atoms substituted at different positions in the porphyrin oligomer structure on optical limiting and optical nonlinearity. Chapter 4 of the thesis gives the details of the optical limiting and nonlinear optical properties.

Photorefractive materials are one of the promising candidates for optical limiting. Photorefractive crystals are studied for their optical limiting properties using the photorefractive nonlinearities, photo-induced lensing and light controlled electro-optic effect [31]. Photorefractive crystals possess large number of donor sites and trap levels, which can be manipulated by appropriate doping, the absorption from which plays an important role at higher intensities. The experimental results on optical limiting in BSO and BSO:Fe under high power nanosecond laser excitation at different wavelengths have shown that these materials can be used for broadband optical limiting applications in the visible region. Chapter 5 of the thesis describes the nonlinear absorption properties of these materials in detail.

Recently nanomaterials are emerging as a new class of optical limiting materials. Some metal and semiconductor nanoparticles have been found to exhibit excellent optical limiting responses toward nanosecond pulses [7,33]. Chapter 6 of the thesis presents the optical limiting properties of co-doped Ag-Cu nanoclusters with Cu/Ag molar ratio of 1,2 and 3 respectively deposited on silica glass by the sol-gel process. These films are characterized at different excitation wavelengths in order to find out the contribution of surface plasmon resonance towards OL.

The final chapter (7) of the thesis summarizes the work carried out on the materials described above. Various processes and structural modifications leading to optical limiting, enhanced RSA and optical nonlinearity are summarized. Future attempts towards the widely acceptable optical limiter to arrive at the demanding low damage threshold for eye are proposed.

1.10   References

1. N. Blombergen, *Rev. of Modern Physics,* 71, S283 (1999).

2. J. Hecht, *Optics & Photonics news,* 42, Jan 2003.

3. R. Sutherland, R. Pachter, P. Hood, D. Hagan, K. Lewis, J.W. Perry, eds., *Materials for Optical limiting II,* Vol.479 of Mater. Res. Soc. Proc. (MRS, Pittsburrgh); *Nonlinear Optics* 27 (2001) Full issue *Proceedings of The Second International Symposium on Optical power limiting,* (ISOPL 2000), Venice Italy, 2-5 July, (2000); E.W. Van Stryland, M.J. Soileau, S. Ross, and D.J. Hagan, *Nonlinear Optics* 21, 29 (1999).

4. R.C. Hollins, *Current Opinion in Solid State & Mat. Sc.* 4, 189 (1999).

5. J. Guo, T.Y. Chang, I. McMichael, J. Ma, and J.H. Hong, *Opt. Lett.* 24, 981 (1999).

6. R. Frey and C. Flytzanis, *Opt. Lett.* 25, 838 (2000).

7. E.V. Becker, E.A. Romanova, L.A. Melnikov, T.M. Benson, and P.Sewell, *Appl. Phys.B* **73,** 531 (2001); D. Pelinovsky, J.Sears, L. Brzozowski, and E.H. Sargent, *J.Opt. Soc. Am.B* 19, 43(2002); D. Pelinovsky, and E.H. Sargent, *J.Opt. Soc. Am.B* **19,** 1873 (2002); Y.-P. Sun and J.E. Riggs, *Int. Rev. Phys. Chem.* 18, 43 (1999); Y-P. Sun, J.E. Riggs, K.B. **Henbest,** and R.B. Martin, *J. Nonlinear Opt. Physics & Materials.* **9,481** (2000).

8. L.W. **Tutt** and T.F. Boggess, *Prog. Quant. Elcetron.* **17,** 299 (1993).

9. E.W. Van Stryland, H. Vanherzeele, M.A. Woodall, M.J. Soileau, A.L. Smirl, S. Guha, and T.F. Boggess, *Opt. Engg.* 24, 613 (1985).

10. M.P. Joshi, J. Swiatkiewicz, F. Xu, P.N. Prasad, B.A. Reinhardt, and R. Kannan, *Opt. Lett.* 23, 1742(1998).

11. F.E. Hernandez, S. Yang, E.W. Van Stryland, and D.J. Hagan, *Opt. Lett.* 25, 1180 (2000); A.C.Walker, A.K.Kar, W.Ji, U.Keller, and S.D.Smith, *Appl Phys. Lett.* 48, 683(1986); D.J.Hagan, T.Xia, A.A.Said, T.H.Wei and E.W. Van Stryland, *Int. J. of Nonlinear Opt. Phys.* 2, 483(1993).

12. R.C.C. Leite, S.P.S. Porto, and T.C. Damen, *Appl. Phys. Lett.* **10,** 100 (1967).

13. B.L. Justus, A.J. **Campillo,** and A.L. Huston, *Opt. Lett.* 19, 673 (1994); T.J. Bunning, L.V. Natarajan, M.G. Schmitt, B.P. Epling and R.L. Crane, *Appl. Opt.* 30, 4341 (1991); B.L. Justus, A.L. Huston and A.J. Campillo, *Appl. Phys. Lett.* 63, 1483 (1993); R. Chari, S.R. Mishra, H.S. Rawat, and S.M. Oak, *Appl. Phys.B* 62, 293

(1996); R.C. Hoffman, K.A. Stetyick, R.S. Potember, and D.C. McLean, *J. Opt. Soc. Am.B* 6, 772 (1989); O.V. Przhonska, J.H. Lim, D.J. Hagan, E.W. Van Stryland, M.V. Bonder, and Y.L. Slominsky, *J. Opt. Soc. Am.B* **15,** 802 (1998); S. Hughes, G. Spruce, B.S. Wherrett, K.R. Welford, and A.D. Lloyd, *Opt. Commun.* **100,** 113 (1993); S. Hughes, and B. Wherrett, *Phys. Rev. A* 54, 3546 (1995); D.N. Rao, E. Blanco, S.V. Rao, F.J. Aranda, D.V.G.L.N. Rao, S. Tripathy, and J.A. Akkara, *J. Sci. Ind. Res.* 57, 664(1998).

14. D.J. Hagan, E.W. Van Stryland, Y.Y. Wu, T.H. Wei, M. Sheik-Bahae, A.A. Said, K. Mansour, J. Young, and M.J. Soileau, *Proc. of SPIE*, **1105,** 103 (1989); E.W. Van Stryland, H. Vanherzeele, M.A. Woodall, M.J. Soileau, A.L. Smirl, S. Guha, and T.F. Boggess, *Opt. Engg.* 24, 613 (1985); E.W. Van Stryland, Y.Y. Wu, D.J. Hagan, M.J. Soileau, and K. Mansour, *J. Opt. Soc. Am.B* 5, 1980 (1988); D.J. Hagan, E.W. Van Stryland, M.J. Soileau, Y.Y. Wu, and S. Guha, ***Opt. Lett.*** 13, 315 (1988).

15. R. Vijaya, Y.V.G.S. Murti, T.A. Vijayaraj, and G. Sundararajan, *Curr. Sci.* 72, 507 (1997); J. Staromlynska, T.J. McKay, J.A. Bolger, and J.R. Davy, *J. Opt. Soc. Am. B* **15,** 1731(1998); G.R. Allan, D.R. Labergerie, S.J. Rychnovsky, T.F. Boggess, A.F. Smirl, and L.W. Tutt, *J. Phys. Chem.* 96, 6313 (1992); L. Brzozowski, and E.H. Sargent, *IEEE J. Quantum. Electron.* **36,** 1237 (2000); G. Fang, Y. Song, Y. Wang, X. Zhang, C. Li, L-C. Song, and P-C. Liu, *Opt. Commun.* **183**, 523 (2000); J. Zhou, E.Y.B. Pun, and X.H. Zhang, *J.Opt. Soc.Am.B* **18**, 1456 (2001); Y. Morel, J. Zaccaro, A. Ibanez, and P.L. Baldeck, ***Opt.*** *Commun.* **201**, 457 (2002); Z. Sun, M. Tong, H.Zeng, L. Ding, Z. Wang, J. Dai, G. Bian, and Z. Xu, ***J.Opt.*** *Soc. Am.B* 18, 1464(2001).

16. T.F. Boggess, S.C. Moss, I.W. Boyd and A.L. Smirl, ***Opt. Lett.*** 9, 291 (1984); T.F. Boggess, A.L. Smirl, S.C. Moss, I.W. Boyd and E.W. Van Stryland, *IEEE J. Quantum Electron.* **QE-21,** 488 (1985); W. Ji, A.K. Kukaswadia, Z.C. Feng and S.I I. Tang, */. Appl. Phys.* **75**, 3340 (1994).

17. M.J. Soileau, W.E. Williams, E.W. Van Stryland, ***IEEE J.*** *Quant. Electron.* **QE-19,** 731 (1983); J-G. Tian, C. Zhang, G. Zhang, and J. Li, *App. Opt.* 32, 6628 (1993); I.C. Khoo, R.R. Michael and G.M. Finn, ***Appl.*** *Phys. Lett.* 52, 2108 (1988).

18. G.S. He, S.H. Liu, *Physics of Nonlinear Optics,* World Scientific Publishing Co. Pte. Ltd., Singapore, Chapter 13, 1999; R.L. Sutherland, *Handbook of Nonlinear Optics,* Marcel Dekker Inc., New York, USA, Chapter 9, 1996.

19. Y.B. Band, *J. Chem. Phys.* 83,5453 (1985); D.J. Harter, M.L. Shand, and Y.B. Band, *J. Appl. Phys.* 56, 865 (1984); K.P.J. Reddy, *Curr. Sci.* 61, 520 (1991); S. Kim, D. McLaughlin, and M. Potasek, *Phys. Rev. A* 61, 025801 (2000); R. Lepkowicz, A. Koyakov, D.J. Hagan, and E.W. Van Strylabd, *J.Opt. Soc. Am.B* 19, 94(2002).

20. J.W. Perry, in *"Nonlinear optical properties of Organic molecules and polymers"*, eds: H.S. Nalwa and S. Miyata, CRC press, USA (1997).

21. C.R. Giuliano and L.D. Hess, *IEEE J. Quant. Electron.* QE-3, 358 (1967).

22. M. Hercher, *Appl. Opt.* 6, 947, (1967); M. Hercher, W. Chu and D.L. Stockman, *IEEE J Quant. Electron.* QE-4, 954 (1968).

23. G.S. He, L. Yuan, J.D. Bhawalkar, P.N. Prasad, *Appl. Opt.* 36, 3387 (1997); J. Schwatz, C.S. Naiman, and R.K. Chang, *Appl. Phys. Lett.* 11, 242 (1998); G.S. He, R. Gvishi, P.N. Prasad, and B.A. Reinhardt, *Opt. Commun.* 117, 133 (1995); G.S. He, L. Yuan, N. Cheng, J.D. Bhawalkar, P.N. Prasad, L.L. Brott, S.J. Clarson, and B.A. Reinhardt, *J.Opt. Soc. Am. B* 14, 1079 (1997).

24. P.A. Miles, *Proc. SPIE.* 2143, 251 (1994); J.A. Hermann, P.B. Chappie, J. Staromlynska, and P.J. Wilson, *Proc. SPIE,* 2229, 178 (1994).

25. G.L. Wood, A.G. Mott, and E.J. Sharp, *Proc. SPIE,* 1692, 2 (1992); R.C. Hollins, *Nonlinear Optics,* 27, 1(2001).

26. K. Mansour, E.W. Vanstryland, M.J. Soileau, *Proc. SPIE* 1105, 91(1989); K.J. McEwan, P.A. Madden, *J. Chem.Phys.* 97, 8748 (1992); F. Fougeanet, D. Riehl, *Nonlinear optics,* 21, 435 (1999); K.J. McEwan, P.K. Milsom, D.B. James, *Proc. SPIE* 3472, 42 (1998); O. Durand, V. Grolier-Mazza, and R.Frey, *Opt. Lett.* 23,1471 (1998); R. Goedert, R. Becker, A. Clements, T. Whittaker, *J.Opt.Soc.Am.B* 15 1442 (1998); P.R. Schuster, C.A. Viands, R.S. Potember, M.G. Smitt, *J. Nonlinear Opt. Phys. Mater.6,* 141 (1997); K. Mansour, M.J.Soileau, E.W.Van Stryland, *J. Opt. Soc. Am.B* 9, 1 100 (1992); R.R. Micheal, and C.M.Lawson, *Opt. Lett.* 17, 1055 (1992); F.E. Hernandez, W.Shensky III, I.Cohanoschi, D.J. Hagan, and E.W. Van Strylabd, *Appl. Opt.*41, 1103 (2002).

27. J.W. Perry, K. Mansour, and P. Miles, *Mat. Res. Soc. Syrnp. Proc.*374, 257 (1995); T.C. Wen, and I.D. Lian, *Synthetic Metals,* 83, 111 (1996); D. Dini, M.Barthel, and M. Hanack, *Eur. J. Org. Chem.3759* (2001); J.S. Shirk, R.G.S. Pong, F.J. Bartoli, and A.W. Snow, *Appl. Phys. Lett.* 63, 1880 (1993); J.W. Perry, L.R. Khundlar, D.R. Coulter, D. Alvarez, Jr., S.R. Marder, T.H. Wei, M.J. Sence, E.W. Van Stryland, and D.J. Hagan, *"Organic molecules for Nonlinear Optics and Phtotonics",*

eds.J.Messier, Kluwer Academic Publishers, Netherlands, 369 (1991); D.R. Coulter, V.M. Miskowski, and J.W. Perry, *Proc. SPIE* **1105**,42 (1989).

28. W. Su, T.M. Cooper, and D. McLean, *Proc.ofSPIE* 3472,136 (1998); K.J. McEwan, J.M. Robertson, and H.L. Anderson, *MRS symposium Proc series,* **479,** 29 (1997); F.M. Qureshi, S.J. Martin, A.K. Kar, and H.L. Anderson, *Chem. Phys.*231, 87 (1998); F.Z. Henari, W.J. Blau, L.R. Milgrom, G. Yahioglu, D. Phillips, and J.A. Lacey, *Chem. Phys. Lett.* **267,** 229 (1997); N. Tang, and T.M. Cooper, *MRS symposium Proc series,* **479,** 47 (1997); P.P. Kiran, N.K.M.N. Srinivas, D.R. Reddy, B.G. Maiya, A.S. Sandhu, A. Dharmadhikari, G.R. Kumar and D.N. Rao, *Opt. Commun.* **202,** 347 (2002); P.P. Kiran, D.R. Reddy, B.G. Maiya, A. Dharmadhikari, G.R. Kumar and D.N. Rao, *Applied Optics, LPEO* 41, 7631 (2002).

29. B.Z.Tang, H.Peng, S.M.Leung, N.-T.Yu, H.Hiroka, and M.W.Fok, **Mat. Res. Soc. Symp. Proc. 479,** 69 (1997); L. Smilowitz, D. McBranch, V. Klimov, M. Grigorova, J.M. Robinson, B.J. Weyer, A. Koskelo, B.R. Mattes, H. Wang, and F. Wudl, *Synthetic Metals* **84,** 931 (1997); B. Ma, J.E. Riggs, and Y.-P. Sun, *J. Phys. Chem. B* **102,** 5999 (1998); B. Taheri, H. Liu, B. Jassemnejad, D. Appling, R.C. Powell, and J.J. Song, *Appl. Phys. Lett.* 68, 1317 (1996); Y-P. Sun, J.E.Riggs, and B.Liu, *Chem. Mater.* 9, 1268(1997); D. Vincent, and J. Cruickshank, *Appl. Opt.* 36, 7794, (1997); I.V. Bezel, S.V. Chekalin, Y.A. Matveets, A.G. Stepanov, A.P. Yartsev and V.S. Letokhov, *Chem. Phys. Lett.* **218,** 475 (1994). L.W. Tutt and A. Kost, *Nature* **356,** 225 (1992); A. Kost, L.W. Tutt, M.B. Kelvin, T.K. Dougherty and W.E. Elias, *Opt. Lett.* 18,334(1993).

30. I.C. Khoo, M.V. Wood, M. Lee, and B.D. Guenther, *Opt. Lett.* 21, 1625 (1996); I.C. Khoo, M.V. Wood, B.D. Guenther, M.-Y. Shih, and P.H. Shen, *J. Opt. Soc. Am. B* 15, 1533 (1998); H. Ono, and N. Kawatsuki, *Opt. Commun.* **139,** 60 (1997); M.J. Soileau, E.W. Van staryland, S. Guha, E.J. Sharp, G.L. Wood, and J.L.W. Pohlmann, *Mol. Cryst.Liq. Cryst.* **143,** 139 (1987).

31. M. C. Golomb, and A. Yariv, *J. Appl. Phys.* 57, 4906 (1985); S. Thai, J. Malowicki, and Q.W. song, C. Zhang, X. Dang, Q. Sheng, and J. Tian, *Optical Memory And Neural Networks,* 3, 399 (1994); D. N. Rao and P.P. Kiran, *Nonlinear Optics* 27, 347 (2001).

32. M. Scalora, J.P. Dowling, CM. Bowden, and M.J. Blemer, **Phys.** *Rev. Lett.* 73, 1368 (1994); K.S. Bindra, R. Chari, V. Shukla, A. Singh, and S.M. Oak, **J.Opt.** *A: Pure. Appl. Opt.* 1, 1 (1999).

33. Y-P. Sun, J.E. Riggs, H.W. Rollins, and R. Guduru, *J. Phys. Chem.* **103**, 77 (1999); 7071 (2000); X. Sun, Y. Xiong, P. Chen, J. Lin, W. Ji, J.H. Lim, S.S. Yang, D.J. Hagan, E.W. Van Stryland, *Appl. Opt.* 39, 1998 (2000); S.R. Mishra, H.S. Rawat, S.C. Mehendale, K.C. Rustagi, A.K. Sood, R. Bandyopadhyay, A. Govindaraj, C.N.R. Rao, *Chem. Phys. Lett.* **317**, 510 (2000); X. Sun, R.Q. Yu, G.Q. Xu, T.S.A. Hor, and W. Ji, *Appl. Phys. Lett.* **73**, 3632 (1998); P. Chen, X. Wu, X. Sun, J. Lin, W. Ji, and K.L. Tan, *Phys. Rev. Lett.* **82**, 2548 (1999); L. Vivien, E. Anglaret, D. Riehl, F. Hache, F. Bacou, M. Andrieux, F. Lafonta, C. Journet, C. Goze, M. Brunet, and P. Bernier, *Opt. Commun.* **17** A, 271 (2000); J. E. Riggs, D.B. Walker, D.L. Carroll, and Y-P. Sun, *J. Phys. Chem. B* **104**, 7071 (2000).

34. M. Brunei, F.L. Luyer, M. Canva, A. Brun, F. Chaput, L. Malier, and J.C. Boilot, *Appl. Phys. B* 58, 443 (1994); D. McBranch, B.R. Mattes, A. Koskelo, J.M. Robinson, and S.P. Love, *Proc. SPIE* **2284**, 15 (1994); F. Bentivegna, M. Canve, P. Georges, A. Brun, F.Chaput, L. Malier, and J.C. Boilot, *Appl. Phys. Lett.* 62, 1721 (1993); R. Singnorini, M. Zerbetto, M. Meneghetti, R. Bozio, M. Maggini, C.De faveri, M. Prato, and G. Scorrano, *Chem. Commun.* 1891 (1996); K.Mansour, P. Fuqua, S.R. Marder, B. Dunn, and J.W. Perry, *Proc. SPIE* **2143**, 239 (1994); E. Blanco, D.N. Rao, F.J.Aranda, D.V.G.L.N. Rao, S. Tripathy, J.A. Akkara, R. Litran, and M.R. del-Solar, *J. Appl. Phys.* **83**, 1 (1998); J. Schell, D. Brinkmann, D. Ohlmann, B. Honerlage, R. Levy, M. Joucia, J.L. Rehspringer, J. Scrughetti, and C. Bovier, *J. Chem. Phys.* **108**, 8599 (1998).

35. K.S. **Bindra**, S.M. Oak, and K.C. Rustagi, *Opt. Commun.* **124**, 452 (1996); D.M.C. **Branch, L. Smilowitz**, V. Klimov, A. Koskelo, J.M. Robinson, B.R. Mattes, J.C. **Hummelen, F.** Wudl, J.C. Withers, and N.F. Borrelli, *Proc. SPIE* 2530, 196, (1995).

36. G.L. Fischer, R.W. Boyd, T.R. Moore, and J.E. Sipe, *Opt. Lett.* **21**, 1643 (1996).

37. C. Zhang, Y. Song, B.M. Fung, Z. Xue, and X. Xin, *Chem.Commun.* 843 (2001); L.W. **Tutt** and S.W. McCahon, *Opt. Lett.* 15, 700 (1990); L.W. Tutt, S.W. McCahon and M.B.Klien, *Proc. SPIE,* **1307,** 315 (1990); S. Shi, W. Ji, and S.H. Tang, J.P. Lang and X.Q. Xin,./. *Am. Chem. Soc.* **116,** 3615 (1994); W. Ji, S. Shi, H.J. Du, P. Ge, and S.H. Tang, X.Q. Xin, *J.Phys.Chem.* 99, 17297 (1995); W. Ji, J. Du, S.H. Tang, and S. Shi, *J. Opt. Soc. Am. B* **12,** 876 (1995); M.K.M. Low, H. Hou, H. Zheng, W. Wong, G. Jin, X. Xin, and W. Ji, *Chem. Commun.* 505 (1998); W. Ji, W. Xie, S.H. Tang, S. Shi, *Materials Chemistry and Physics* **43,** 45 (1996); W. Ji, P. Ge, W. Xie, S.H. Tang, S. Shi, *J. Luminescence* **66&67,** 115 (1996); T. Xia, A. Dogariu,

K. Mansour, D.J. Hagan, A.A. Said, E.W. Van Stryland, and S.Shi, *J. Opt. Soc. Am. B* 15, 1497 (1998); S. Banerjee, G.R. Kumar, P. Mathur, and P. Sekar, *Chem. Commun.* 299 (1997); P. Mathur, S. Ghose, M.M. Hossian, C.V.V. Satyanarayana, S. Banerjee, G.R. Kumar, P.B. Hitchcock, and J.F. Nixon, *Organometallics* 16, 3815 (1997).

38. L.M. Kahn, *Phys. Rev. B* 53, 1429 (1996); J.A. Hermann, *J. Opt. Soc. Am. B* 1, 729 (1984); C.J. Herbert, W.S. Cpinski, and M.S. Malcuit, *Opt. Lett.* 17, 1037 (1992).

39. D.N. Rao, C.S. Yelleswarapu, S.R. Kothapalli, and D.V.G.L.N. Rao, *Optics Express* 11, 2848 (2003); Q.W. Song, C. Zhang, R. Gross, and R. Birge, *Opt. Lett.* 18, 775 (1993); G. E. Dovgalenko, M. Klotz, G. J. Salamo, and G.L. Wood, *Appl. Phys. Lett.* 68, 287 (1996).

Chapter 2

Experimental techniques and fundamental details of the materials studied

This chapter presents the details of the experimental techniques employed for different studies carried out, A brief introduction to Degenerate Four Wave Mixing (DFWM), Z-scan technique, and OL setup and their applicability to nonlinear absorption and dynamics are given. A brief introduction to the fundamental properties of the materials studied in this thesis is presented.

2.1   Introduction

The magnitude and response of third-order nonlinear susceptibility are important parameters in characterizing and determining the applicability of any material as a nonlinear optical device. There are several techniques [1-8] for measuring these parameters that include

1. Degenerate Four Wave Mixing (DFWM): For measurement of both magnitude and response time of the third-order nonlinearity.
2. Third Harmonic Generation: For measurement of magnitude of third-order nonlinearity only.
3. Z-scan: For measurement of sign, magnitude of third-order nonlinearity.
4. Electro-Absorption technique: Dispersion studies of third-order nonlinearity.
5. Time-resolved Optical Kerr Effect and Transient Absorption techniques: For the study of photo-physical processes determining the nonlinearity.
6. Time Correlated Single Photon Counting (TCSPS) technique to measure the radiative (fluorescence) lifetimes

Among which DFWM and Z-scan are widely used techniques.

2.2   Degenerate Four Wave Mixing (DFWM)

A Four Wave Mixing experiment can be considered as an interaction of three optical fields in a medium leading to the generation of fourth field, via third

order polarization. The presence of a third-order optical nonlinear susceptibility $\chi^{(3)}$ leads to the creation of various components of material polarization, giving rise to new optical fields. If the phase-matching condition is fulfilled (i.e. the phase relation between the waves emitted by different parts of the nonlinear medium leads to constructive build up of the resulting wave), new beams of light are created. If the fields are of identical frequencies, the process is called Degenerate Four Wave Mixing and the output beam will have the same frequency. The time resolution of the FWM measurements depends on two parameters. The first is related to the time duration of the laser pulses and the second is related to the coherence time of the laser pulses.

DFWM provides information about the magnitude and response of the third-order nonlinearity. In this process, three coherent beams incident on a nonlinear medium generate a fourth beam due to the third order nonlinearity. The strength of this fourth beam is dependent on a coupling constant that is proportional to effective $\chi^{(3)}$ and hence measurements on observed signal will yield information about the $\chi^{(3)}$ tensor components of the medium [9]. DFWM can be employed in backward (or generally called the Phase Conjugate), forward or boxcar configurations, with the choice on the experimental conditions and the requirements. Using different polarizations of the three beams it is possible to measure all the independent $\chi^{\scriptscriptstyle\backslash}$ tensor components of a material. Some of the several advantages of this technique are

1. The Phase Conjugate (PC) signal is distinguishable from others by simple spatial separation and the signal has a characteristic dependence on the input intensities, which can be used for verification of the experiment.
2. The sample could be in any form (isotropic) and all the independent tensor components of $\chi^{(3)}$ can be measured in a single experiment.
3. Beams other than true Gaussian modes can be employed.
4. The time dependence of the probe beam gives information about the response times of the nonlinearity.

2.2.1   Phase Conjugate Geometry

The backward wave geometry is also called the Phase conjugate geometry. In this geometry two counter-propagating waves called forward and backward pump beams interact with a third wave called the probe beam in a nonlinear medium. The probe beam is incident at a small angle with respect to the pumps. As a result of the interaction a fourth wave called the phase conjugate or signal beam is generated. A simplified schematic of the experimental set-up used with 6ns pulses is shown in Fig. 2.1.
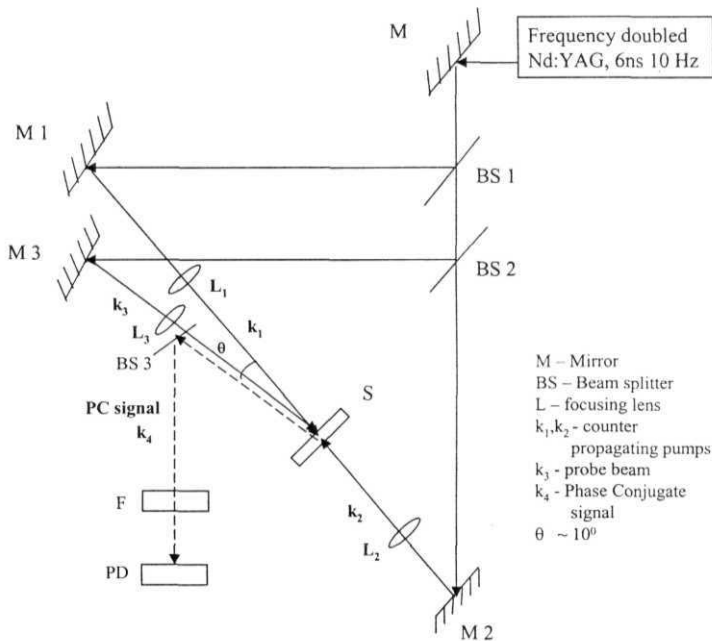
Figure 2.1: Simplified experimental setup of Degenerate Four Wave Mixing using 6ns pulses.

The beam is initially collimated using two convex lenses and an aperture is used to cut the scattered background and achieve good spatial filtering of the beam. Two beam splitters (30-70, 50-50) are used to obtain three beams of

almost equal intensity. All the three beams have a diameter of ~ 2.5 - 3 mm, which could be, varied further using an iris. In the phase conjugate configuration, beam 1 is fixed whereas beams 2 and 3 pass through variable delays. Beam 1 ($\mathbf{k_1}$) is designated as forward pump, beam 2 ($\mathbf{k_2}$) is backward pump and beam 3 ($\mathbf{k_3}$) is the probe. Beam 2 passes through a variable delay (a micrometer screw). Beam 3 passes through another delay line mounted on a micrometer screw to adjust the delays between the pumps and the probe. The angle between the forward pump and the probe is ~ 10°. All the beams are focused into the sample taken in 1-mm thick quartz cell using lenses of focal length of ~ 20 cm. The beam waist at focus measured using knife-edge technique, at low power densities of the laser beam, is ~ 70±5 μ. The polarization state of each individual beam is controlled using a Half Wave Plate (HWP). Proper care is taken to ensure that the counter-propagating and the probe beams are overlapped in the sample, both spatially and temporally. Using a pinhole at the sample position and maximizing the transmission through pinhole facilitates spatial alignment. Temporal overlap is accomplished by varying the path length of each of the beams to maximize the PC signal in a standard sample like CS_2. The phase conjugate signal (in $-\mathbf{k_3}$ direction) is isolated using a beam splitter and is passed through an aperture (to reduce the scattered background) and focused on to a fast photodiode (PD, FND 100, rise time ~ 1 ns). Various neutral density filters (NDF) are used for attenuating the probe and the signal beams. The signal collected using the fast photodiode is observed on an oscilloscope (Tektronix TDS 210, 60 MHz) to ensure the PD does not get saturated.

The whole process of four wave mixing can be looked in another way and treating it as creation of the transient gratings by interference of pairs of waves and Bragg diffraction of the other wave from the grating formed in the material by it's nonlinear response to spatially modulated light intensity. At the crossing of two beams, the spatial modulation of their electric fields varies due to constructive and destructive interference. The molecules in the interaction region experience varying electric field intensities according to their position and this leads to the formation of a transient grating of polarized molecules in space. The

formation of the grating does not require that the two crossing beams coincide in time as long as the coherence is maintained in the sample. Based on the relative timing of the three fields one can envision different gratings formed as shown in Fig. 2.2 [1]. The grating formed by $\mathbf{k_1}$ and $\mathbf{k_2}$ waves gets diffracted by $\mathbf{k_3}$ beam to yield the output at $\mathbf{k_3} \pm (\mathbf{k_1} - \mathbf{k_2})$. The one formed by $\mathbf{k_2}$ and $\mathbf{k_3}$ gets diffracted by $\mathbf{k_1}$ to yield the output at $\mathbf{k_1} \pm (\mathbf{k_2} - \mathbf{k_3})$. They are illustrated in the Fig. 2.2 for the special case of $\mathbf{k_1} = - \mathbf{k_2}$. The output waves are expected in the directions $- \mathbf{k_3}$ and $\mathbf{k_3} \pm 2\mathbf{k_1}$. The generation of output in $- \mathbf{k_3}$ direction is phase-matched, and is known as phase conjugate signal, while in the other directions is not. Thus usually only the output at $\mathbf{k_4} = - \mathbf{k_3}$ needs to be considered for measuring the nonlinearities.
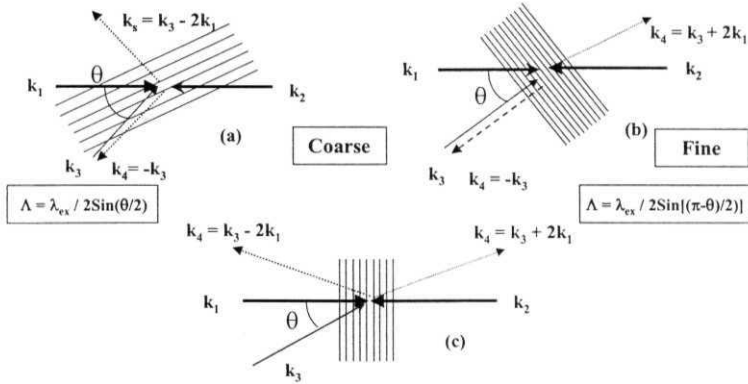
Figure 2.2: Different gratings formed with interference of any two beams.

In the phase conjugate configuration, the backward pump is delayed with respect to other to observe the decay of the grating. For small values of 9 the grating 'written' by the forward pump and probe pulses will have a large spatial period $A = \lambda/(2n_0 \, Sin(0/2))$. When the pulses coincide in time two other gratings are also formed, a small period grating generated by the interaction of the backward pump and the probe pulses and a two-photon temporal coherence grating. However the spacing of the small-period grating (given now by A =

$\lambda/(2n_0 \, Sin((\pi\text{-}\theta)/2)))$ is considerably smaller than the large-period one. In our case the spacing of the large-period grating is found to be ~ 2-3 μ (depending on the angle 9 and the refractive index of the solvent) and for the small-period grating it is calculated to be 0.2–0.3 μ. If diffusive processes are present the small-period grating washes out rapidly. The contribution of the two-photon grating is usually negligible, and can be observed under special conditions of strong enhancement due to two-photon resonance.

The expression for the induced nonlinear polarization corresponding to the generated field is given by

$$P_i \, (\omega) = \chi_{ijkl}^{\cdots} \, (-\omega; \; \omega, \; \omega, -\omega E_j(\omega)E_k(\omega)E_l^*{}_{(to)} \qquad (2.1)$$

The wave equation with the nonlinear polarization above can be solved using slowly varying envelope approximation, which considers that the features of the pulse (the envelope and instantaneous phase) vary little during an optical period, and assuming that there is no pump beam depletion. The efficiency of the DFWM/OPC is described by the reflectivity $R = I_{opc}/I_p$. The solution of the wave equation is given by

$$I_{opc} = \frac{\omega^2}{4c^2 n^2} \left| \chi^{(3)} \right|^2 l^2 \, I_f I_b I_p \qquad \textbf{(2.2)}$$

I_f and I_b are the intensities of the strong forward and backward pumps and I_p is that of the weak probe. This result is valid under the assumption that there is no linear or nonlinear absorption, no pump depletion, and low reflectivity. If three input beams are derived from the same fundamental beam, then it is clear that the phase conjugate signal shows a cubic dependence on the fundamental intensity. However at very high input intensities achieved using ultrashort pulses and with materials having strong nonlinear absorption the phase conjugate signal shows higher order dependencies on the fundamental intensity like fifth and higher.

The applications of Four-Wave Mixing (FWM) can be divided into three categories. First, the creation of a dynamic grating via a material excitation and the subsequent probing of the grating using another beam allow us to study the material excitation processes. Such a spectroscopic technique is versatile and extremely powerful, and has found many applications in various disciplines [9,10]. Second, under specific conditions with the creation of a static grating, the output of FWM is a phase-conjugate (PC) signal. This is the real time holography and can be used in real-time image construction in different applications like optical image and data processing. Third, the possible generation of new frequency components in FWM permits the extension of coherent light sources to new frequency regions in the IR, UV, and XUV where there are not many available.

2.2.2   Measurement of <γ> using DFWM:

The value of the cubic hyperpolarizability <γ> is calculated using the equations [11]:

$$\chi_s^{(3)} = \left(\frac{n_0}{n_{ref}}\right)^2 \left(\frac{I_{ref}}{I}\right) \left(\frac{A}{A_{ref}}\right)^{\frac{1}{2}} \left(\frac{\alpha l\, \exp(\alpha l/2)}{1 - \exp(-\alpha l)}\right) \chi_{ref}^{(3)} \qquad \textbf{(2.3)}$$

and

$$<\gamma> = \frac{\chi^{(3)}}{L^4 N} \; ; \; L = \frac{n^2 + 2}{3} \qquad \textbf{(2.4)}$$

where n is the refractive index, 1 is the length of the sample, A is **the** coefficient of the cubic term of a least square fit to the plot of PC signal versus input intensity, a is the absorption coefficient (cm^{-1}). L is the local field correction factor. We have taken the value of $\chi^{(3)}$ for the reference sample CS_2 as 1.7×10^{-12} esu for ns pulses and 4.0×10^{-13} esu for ps pulses [12]. N is the number density of the solute molecules in solution. Both concentration and intensity dependent studies are done to measure the second hyperpolarizability <γ>. For a solution of

non-interacting particles, the effective $\chi^{(3)}$ assuming a pair wise additive model [12] is given by

$$\chi^{(3)}_{solution} = L^4 \left[N_{solvent} \; \gamma_{solvent} + N_{solute} \; \gamma_{solute} \right] \qquad \textbf{(2.5)}$$

where N_{solute}, $N_{solvent}$ are the number densities of molecules of the solute and the solvent respectively. For dilute solutions with:

$$N_{solute} = \frac{A \times C}{M} \text{, we may write}$$

$$\chi^{(3)}_{solution} = \chi^{(3)}_{solvent} + \frac{L^4 \gamma_{solute} A}{M} \times C \qquad (2.6)$$

with 'A' being the Avagadro's number, 'M' being the molecular weight and 'C the concentration of the solute in g/ml. For lower concentrations $|\chi^{(3)}|$ of the solution follows a linear relationship with respect to the concentration of the solute. $\chi^{(3)}$ may have both real and imaginary components originating from the solute as well as solvent. The real part is responsible for the nonlinear refraction whereas the imaginary part is responsible for nonlinear absorption. SA, TPA or ESA. The real part can be positive or negative.

2.2.3   Degenerate Four-Wave Mixing with 25 ps pulses (DFWM-PS)

The experimental set-up for the $\chi^{(3)}$ measurements and time-delayed four wave mixing using the ps pulses is shown in Fig. 2.3. The input beam is from a hybrid mode-locked Nd: YAG laser emitting 532 nm and the pulses are of 25 ps duration at 10 Hz. The maximum pulse energy is ~ 30 mJ. The input beam is passed through an aperture to get a spatially filtered beam of ~ 7 mm diameter. Using a beam splitter a part of it is split and used for the backward pump (beam 3, which goes through a microprocessor controlled, high precision delay line) and is focused using a 1m lens. The rest of the beam is again split using another beam splitter. The second beam, which is the probe, (beam 2) goes through a delay line (micrometer screw) and comes at an angle to the forward pump. Beam 1 (forward pump) reaches the sample at a fixed delay and is focused onto the

sample using a 2m focal length lens. All the beams have neutral density filters in their paths to change the intensities accordingly. The angle between the forward pump (beaml) and the probe (beam 2) is ~ 5.1°. A half wave plate (HWP) is introduced in the probe beam to change its state of polarization. A part of the forward pump is picked up by a photodiode (NRC 818J-09B) to monitor the pulse-to-pulse fluctuations. All the samples, in the form of solution, are placed in a 1 -mm quartz cuvette.
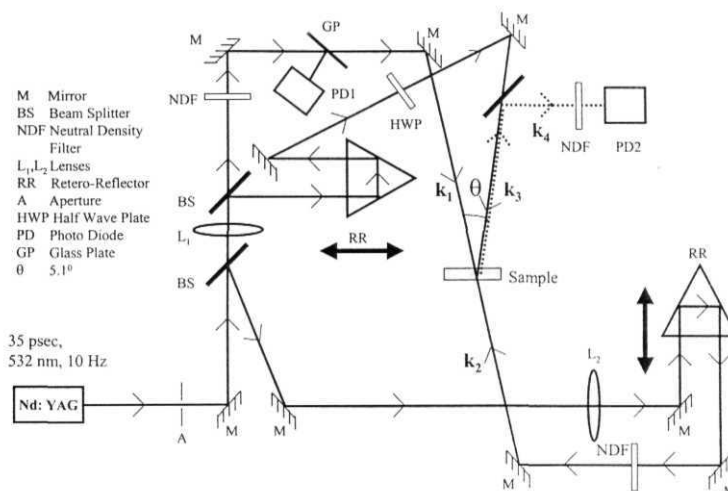
Figure 2.3: DFWM-PC setup with 25 ps pulses.

Schematic of the time-resolved DFWM setup is shown in Fig 2.4. Beams 1 and 2 are focused using a 2m lens and beam 3 is focused using a lm lens. Beam 2 is the probe for the measurements. PC signal is recorded by delaying the beam 2 with other beams at zero delay. The peak intensities incident on the sample are limited to about 200-600 MW cm^{-2}. The delay line is in the probe beam is microprocessor controlled and has a resolution of 1.3 um corresponding to 8.7 fs (with a retro-reflector). The DFWM signal picked up by a fast photodiode is fed to a digital storage oscilloscope where it is averaged over successive pulses before recording. Appropriate neutral density filters are used to

attenuate the probe beam and the PC signal to avoid saturation of the photodetector. The ratio of the intensities of the beams 1, 2 and 3 are 1:0.2:1 respectively.
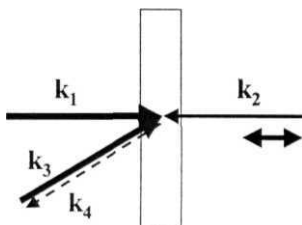
Figure 2.4: Schematic of the time-resolved DFWM-PS setup.
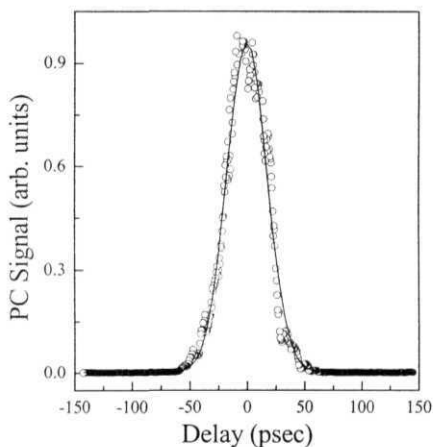
Figure 2.5: Phase conjugate signal with CS_2. The line shows the fit to Gaussian of width 34.9 ps corresponding to pulse width of ~25 ps.

Autocorrelation trace for CS2 is shown in Fig 2.5. Open circles are the experimental data and the solid line is the fit assuming the Gaussian profile of the pulse. Since the two orientational relaxation times of CS2 are 200fs and 2 ps [13], which are smaller than the half-width of the pump pulse i.e. 25 ps, the CS_2 signal serves as an auto-correlation trace of the pump pulse.

2.3 Optical limiting setup

Optical limiting properties are studied by keeping the sample at the focus in f/5 geometry. This geometry is used as a standard, because human eye is equivalent to f/5 optical geometry [14]. The input energy is varied using calibrated neutral density filters, while the output is collected using a calibrated fast photodiode (FND 100). Typical OL setup is shown in Fig 2.6.
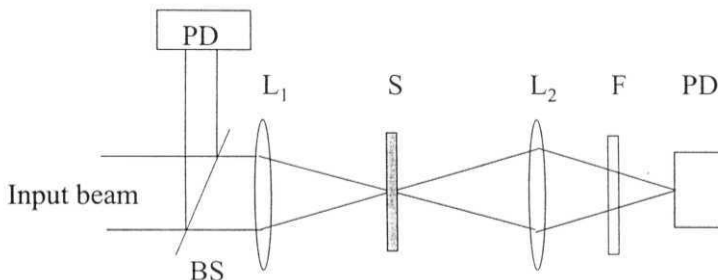
Figure 2.6: Optical Limiting test bed f/5 geometry: L_1, L_2 - Lenses, S - Sample, BS - Beam Splitter, F - Neutral density filter, PD - Photodiode.

The input energy where the transmitted output becomes half of the linear **transmittance** is called the limiting threshold ($I_{1/2}$) of the material and an important factor for choosing a material as optical limiter. Each experimental point shown in the OL curves is an average of 128 laser pulses to get a better signal to noise ratio. The experiments are repeated to ascertain the reproducibility and to determine the error. An experimental error of 5-10% is observed due to the modification while preparing the solutions for the required linear transmission of 70 -75 %.

2.4 Z-scan

The Z-scan technique is **a** single beam technique, which allows the determination of the real and imaginary parts of the susceptibility [8]. Fig 2.7 shows a typical Z-scan experimental setup. This technique is a simple, sensitive,

single beam method that uses the principle of spatial beam distortion to measure both the sign and the magnitude of refractive nonlinearities of optical materials. The experiment uses a Gaussian beam from a laser in tight focus geometry to measure the transmittance of a nonlinear medium through a finite aperture in the far field as a function of the sample position Z, from the focal plane. In addition to this, the sample transmittance without an aperture is also measured to extract complementary information about the absorptive nonlinearities of the sample. The transmittance characteristics of the sample with a finite aperture depend on the nonlinear refractive index, as elucidated below.
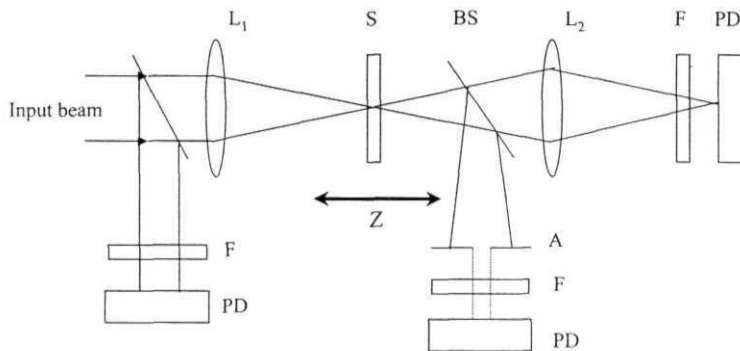
Figure 2.7: Z-Scan setup: L_1, L_2 - Lenses, BS - Beam Splitter, S - Sample, F - Neutral density filter, PD - Photodiode

This technique has several *advantages,* some of which are:

- Simplicity: No complicated alignment except for keeping the beam centered on aperture.
- Simultaneous measurement of both sign and magnitude of nonlinearity.
- Data analysis is quick and simple except for some particular conditions.
- Possible to isolate the refractive and absorptive parts of nonlinearity unlike in DFWM.
- High sensitivity, capable of resolving a phase distortion of A/300 provided the sample is of high optical quality.

Some of the *disadvantages* include:

- Stringent requirement of high quality Gaussian TEM$_{00}$ beam for absolute measurements.
- For non-Gaussian beams the analysis is completely different. Relative measurements against a standard samples allows relaxation on requirements of beam shape
- Beam walk-off due to sample imperfections, tilt or distortions.
- Not suitable for measurement of off-diagonal elements of the susceptibility tensor except when a second non-degenerate frequency beam is employed.

The Z-scan technique has been used extensively to study different materials like semiconductors, nanocrystals, semiconductor-doped glasses, liquid crystals, organic materials, biomaterials etc. To enhance it's sensitivity and applicability new extensions have been added. A much more sensitive technique, EZ-scan (eclipsed Z-scan), has been developed which utilizes the fact that the wings of a circular Gaussian beam are much more sensitive to the far-field beam distortion. A reflection Z-scan technique was introduced to study the optical **nonlinearities** of surfaces. Z-scan with top-hat beams, elliptical Gaussian beams has also been performed. The dual wavelength (two-color) extension of the standard Z-scan technique has been used to measure the non-degenerate nonlinearities. This has been further used to time-resolve the dynamics of the nonlinear process by introducing a delay between the pump and probe beams. A comprehensive review of different techniques of Z-scan could be found in the references listed in [15].

2.4.1   Closed-aperture Z-scan for sign and refractive nonlinearity

Consider, for instance, a material with a negative nonlinear refraction and of thickness smaller than the diffraction length ($\pi\omega_0^2/\lambda$) of the focused beam being positioned at various positions along the Z-axis (fig. 2.7). This situation can be regarded as treating the sample as a thin lens of variable focal length due to the

change in the refractive index at each position ($n = n_0 + n_2I$). When the sample is **far from the** focus and closer to the lens, **the** irradiance is low and the transmittance characteristics are linear. Hence the transmittance through the aperture is fairly constant in this region. As the sample is moved closer to the focus, the irradiance increases inducing a negative lensing effect. A negative lens before the focus tends to collimate the beam. This causes the beam narrowing leading to an increase in the measured transmittance at the aperture. A negative lens after the focus tends to diverge the beam resulting in the decrease of transmittance. As the sample is moved far away from the focus, the transmittance becomes linear in Z as the irradiance becomes low again. Thus the curve for Z versus transmittance has a peak followed by a valley for a negative refractive nonlinearity. The curve for a positive refractive nonlinearity **will** give rise to the opposite effect, i.e. a valley followed by a peak.

2.4.2 Open-aperture Z-scan for absorptive nonlinearity

In the above discussion a purely refractive nonlinearity was considered assuming that absorptive nonlinearities are absent. The presence of multi-photon (two or more) absorption suppresses the peak and enhances the valley, while saturation of absorption produces the opposite effect. The sensitivity of the experiment to refractive nonlinearities is entirely due to the aperture. The removal of the aperture will make the Z-scan sensitive to absorptive nonlinearities alone. Thus by doing the Z-scan with and without aperture both the refractive and absorptive nonlinearities of the sample can be studied. Z-scan studies of all the samples are performed using broadband source ns / ps pulses. Spatially filtered input beam is focused using a lens of focal length ~ 80 **mm.** For Z-scan with ps pulses a longer focal length lens is used since the peak intensities are large compared to ns pulses. The sample is scanned across the focus using a stepper motor controlled by PC. A part of the input beam split using a glass plate is monitored using a PD to know the fluctuations in the input laser beam and is used to trigger the boxcar averager used for data collection. The transmitted light is then collected using another large area lens of f ~ 100 mm and another fast

photodiode. The output beam is again split using a beam splitter and one part is used to get for closed aperture information and the other for open aperture. For the closed aperture Z-scans an aperture of known size is placed after the sample and the light passing through the aperture is collected using a similar photo-diode. Different neutral density filters are used for attenuation to ensure that the photodiode does not get saturated. The photodiode output is fed to a lock-in amplifier (SRS 830 or Princeton Applied Research) or a boxcar averager/gated integrator and is finally recorded. In the boxcar averager the gate width is fixed at 25 ns and the signal coming from the PD's is synchronized to fall within the gate, which reduces the noise level. The number of averages from in boxcar is varied accordingly to obtain a good signal to noise ratio. The averaged signal is then sent to an interfaced ADC card and then to a computer.

Experimentally one first obtains a closed aperture Z-scan for a reference sample of CS_2 in order to establish empirically the radius of the focal spot and thereby the intensity at the focal plane. Furthermore, the value of the real part of $\chi^{(3)}$ for the unknown sample can be readily obtained by simply comparing the observed ΔT_{p-v} (the difference between transmittance of peak and valley in closed aperture Z-scan) for CS_2 with that of the sample obtained under identical conditions.

$$\chi^{(3)}_{sample} = \chi^{(3)}_{ref} \frac{\left(\Delta T_{p-v} . n_0\right)_{sample}}{\left(\Delta T_{p-v} . n_0\right)_{ref}} \tag{2.7}$$

The normalized transmittance for the open aperture Z-scan is expressed by

$$T(z, s=1) = \sum_{m=0}^{\infty} \frac{\left[-q_0(z)\right]^m}{(m+1)^{3/2}} \quad \text{for } |q_0(0)| < 1, \tag{2.8}$$

$$\text{where } q_0(z) = \beta I_0 L_{eff} / \left(1 + z^2/z_0^2\right) \tag{2.9}$$

By numerical simulations to the open aperture Z-scan data one can obtain TPA coefficient β and other contributions like excited state absorption. The values of n_2 and $\chi^{(3)}$ are related in MKS units by

$$Re\ \chi^{(3)} =\ 2\ n_0^2\ \varepsilon_0\ c\ \gamma \qquad\qquad (2.10)$$

$$Im\ \chi^{(3)} =\ (\lambda/2\pi)n_0^2\ \varepsilon_0\ \ c\ \beta \qquad\qquad (2.11)$$

In general nonlinear absorption arises not only due to two-photon absorption but also from processes like ESA, TPA, Multi-photon absorption and TPA generated ESA in organic molecules, free carrier absorption in semi conductors, surface plasmon absorption and inter/intraband transitions in case of nanoparticles. In such a case a generalized rate equations that are appropriate to the material under study have to be solved in order to estimate the nonlinear absorption.

2.5   Time Correlated Single Photon counting (TCSPC) Techinique:

Fluorescence lifetime of the fluorphores is measured using various methods among all, time correlated single photon counting (TCSPC) is rated as the best. TCSPC is a digital technique, which counts the photons that are time correlated with the excitation pulse. The heart of the method is a time-to-amplitude converter. The schematic of the experimental setup is given in Fig 2.8.

The mode locked Tsunami picosecond laser second **harmonic** (405 nm, FWHM ~1.2 ps) operated at 4 MHz is the excitation source. For decay measurements fluorescence lifetime spectrometer (Model 5000U, IBH, UK) is used. The excitation beam is focused in the sample and fluorescence is collected at right angles to the excitation beam and is detected by a MCP-PMT (Hamamatsu R3809U) after passing through a monochromator. Signal from PMT is fed into the discriminator and output from discriminator served as a stop signal for TAC (Time to Amplitude Converter). The start signal was derived from the high-speed silicon detector (Thor Labs Inc., DET210). The photodiode signal was converted to TTL by pulse converter (IBH, Model TB-01) and the output was used as start pulse for TAC. The TAC output was fed to the MCA card (Oxford Corp., UK). Repetitive laser pulsing and emitted photon collection produced a histogram of time versus counts representing the fluorescence decay.

The data analysis was carried out by the software provided by IBH (DAS-6), which was based on reconvolution technique using iterative nonlinear least square methods [16].
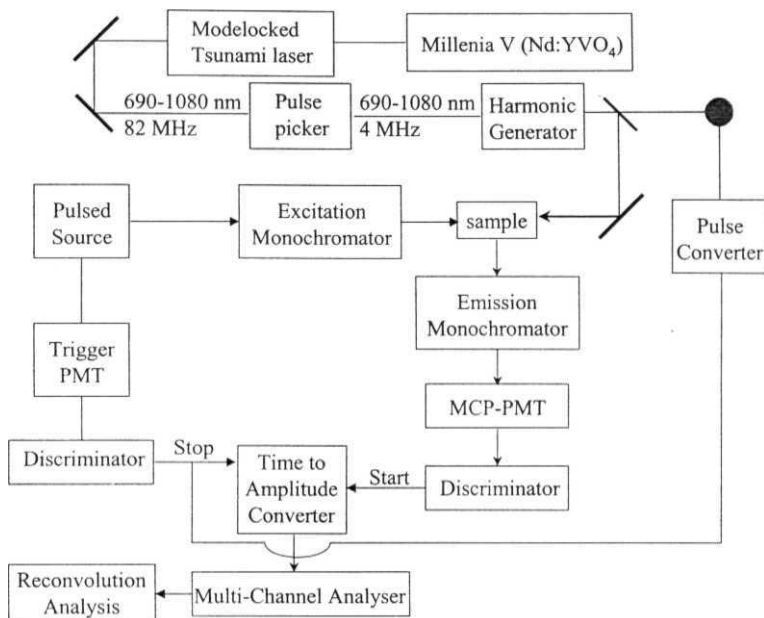
Figure 2.8: Schematic of the picosecond laser and TCSPC setup.

2.6   Nonlinear scattering measurement for nanoclusters

Frequency doubled Nd:YAG laser (532 nm) with 6 ns, 10 Hz repetition rate is used for this experiment. Nonlinear scattering experiments are carried out using f/30 geometry and scattering curves are collected at different angles (θ) from the axis using a fast photodiode, which is connected to data acquisition system consisting of boxcar averager and computer. The experimental setup is shown in Fig 2.9.
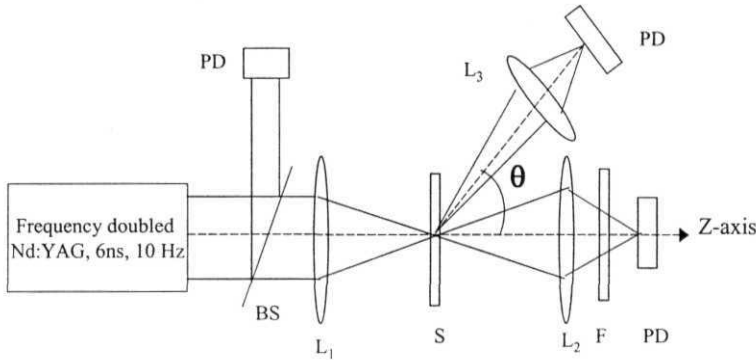
Figure 2.9: Nonlinear scattering setup L_1, L2, L_3 - Lenses, S - Sample, BS - Beam Splitter, F - Neutral density filter, PD - Photodiode. 6- angle at which scattered light was collected.

2.7   Laser Systems

The experiments with nanosecond pulses are performed using second harmonic at 532 nm from Nd:YAG laser Continuum 660 B-10, 10 Hz, 6 ns FWHM, 100 mJ/pulse and Spectra-Physics INDI-40, 10 Hz, 500 mJ/pulse. These sources are used to in turn pump Raman shifter and RhB dye laser, which were explained in the sections 2.7.1 and 2.7.2 respectively. Experiments with 25 ps pulses were done using a hybrid mode-locked Nd: YAG laser emitting 532 nm at 10 Hz repetition rate with maximum pulse energy of ~ 30 mJ.

2.7.1   Raman Shifter

Second harmonic of the Nd:YAG laser is used as the pump source for the Raman shifter. Fig 2.10 shows the schematic of the Raman shifter used. The Raman cell is made of stainless steel and is 30 cm long. Input laser beam is focused into the Raman cell with a plano-convex lens of 30 cm focal length and is collimated back using another 30 cm plano-convex lens. The Stokes and anti-Stokes lines are separated by means of a Pellin-Broca prism mounted on a

rotating stage. The cell is filled with H_2 gas after evacuating it with a rotary pump. Since the vibration mode of H_2 is 4155 cm^{-1}, the first stokes line for 532 nm at 683 nm (14642 cm^{-1}) and the first anti-Stokes line at 435.7 nm(22952 cm^{-1}) are used for the optical limiting studies [17].
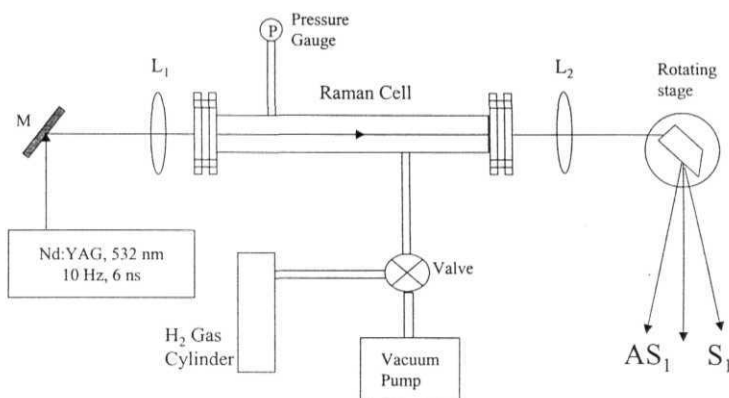
Figure 2.10: Raman shifted lines from a H_2 gas cell. S| and AS, are first Stokes and Anti-Stokes lines respectively.

2.7.2   RhB Dye Laser

Fig. 2.11 shows the schematic of the dye laser [18] set-up used for optical limiting studies. It has an oscillator and a single stage amplifier. Rhodamine B (RhB) in methanol (107 mg/lit) is used as the gain medium and a pump is used to circulate the liquid (at the rate of 1 litre/minute) to minimize the laser scattering and reduce the possibility of decomposition during the experiment. 8% of the frequency doubled Nd: YAG laser power split by a plane glass plate, is first expanded by a plano-concave lens of focal length ~ 50 mm and then focused by a cylindrical lens of f ~ 50 mm into the dye cell of approximately 3 mm (diameter) x 15 mm (length) dimensions. The oscillator cavity consists of a 100% R mirror and ~ 8% R glass plate which produces output of maximum bandwidth. The total length of the oscillator cavity is ~ 17 cm. With both the high reflectivity mirror and the output coupler window being parallel, the resonator cavity is barely stable

and hence the alignment has to be made very carefully to avoid any spurious feedback and intensity fluctuations. Necessary care is taken to avoid mechanisms leading to the formation of cavity modes, which leads to undesirable structure in the laser spectrum. The output pulses from the oscillator are amplified using the remaining 92% of the power. Concentration of solution used for amplification is 37.4 mg/lit. Maximum average power that could be achieved after amplification is approximately 20 mW. The output has a FWHM of ~ 7 - 8 nm.
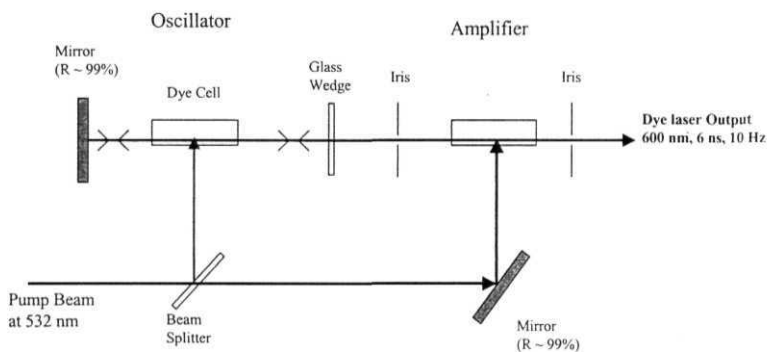
Figure 2.11: Home built RhB dye laser.

2.8 Photophysics of porphyrins

In molecules, the absorption of electromagnetic radiation results in the excitation of an electron from a lower to a higher molecular quantum state. The electronically excited molecule is energetically unstable with respect to ground state. If the molecule does not rearrange or fragment it will find some way of losing its excitation energy to the ground state. In fact, there are number of different possible de-excitation pathways and the ones that are most favourable depend on the type of molecule and the nature of electronic states involved [19]. The de-excitation pathways are often characterized by very rapid rates. One of the most interesting properties of electronically excited molecules is their

tendency to re-emit radiation on returning to the ground state. The absorption of ultraviolet or visible light by an organic molecule causes the excitation of an electron from an initially occupied, low energy orbital to a high energy, unoccupied orbital. The energy of the absorbed photon is used to energize an electron and cause it to jump to a higher energy orbital. Two excited electronic states derive from the electronic orbital configuration produced by light absorption in a molecule. In one state, the electron spins are paired (anti-parallel) and in the other state the electron spins are unpaired (parallel). The state with paired spins has no resultant spin magnetic moment. A state with paired spins remains a single state in the presence of a (laboratory) magnetic field, and is termed as singlet state. A state with unpaired spins interacts with a (laboratory) magnetic field and splits into three quantized states, and is termed as triplet state. An energy diagram is a display of the relative energies of the ground state, the excited singlet states, and triplet states of a molecule for a given, fixed nuclear geometry.

An energy level diagram characteristic of a typical porphyrin molecule is shown in Fig. 1.4. The electronic ground state of the molecule is a singlet state, designated as So, which spans a range of energies determined by the quantized vibrational and rotational excitation of the molecule. The typical energy between the vibrational levels is of the order of 100 cm^{-1}. The rotational levels provide a near continuum of states between the vibrational levels. The higher singlet states are denoted as S_1 and S_n. Each electronic state has similar broad continuum of levels and the optical transitions between these continua leads to broad absorption and emission spectra. Transition between singlet states are spin-allowed, giving rise to strong absorption bands. When a laser pulse is incident, the molecules are excited from the lowest levels of the ground state S_1 (S_{10}) to the highest vibrational states of S_1 (S_{1v}). The decay from S_{1v} to S_{10} is non-radiative and occurs within few ps. From S_{10} the molecules can relax back to the ground state radiatively or non-radiatively to the ground state or crossover to the triplet state (Intersystem Crossing). The radiative decay, which is spontaneous, from S_{10} to So is known as Fluorescence and is governed by the lifetime of the S_1 state. For organic molecules the lifetime is typically of the order of few ns. The energy

difference between absorption and emission processes is taken by the non-radiative decay in the S_1 and S_0 states and the relaxation of the molecules from S_{10} to the lowest triplet state T_1 is governed by the intersystem crossing rate. The intersystem-crossing rate constant is typically 10^{11} to 10^7 s^{-1} due to spin restriction factor. Another important process of de-activation of the S_1 state is the Internal Conversion, which is the non-radiative decay of S_{10} to So. The decay from T_1 to So can be radiative or non-radiative and is termed as Phosphorescence if it is the former type. Typical phosphorescence life times are in the range of ms to μs. The lifetime of the triplet state T_1 is generally large since the triplet-singlet transition is dipole forbidden. In the first excited singlet and triplet states, under special experimental conditions (higher intensities), the molecule may be promoted to the higher states S_n and T_n respectively. These higher states relax back to the S_1 and T_1 on a very fast time scale (few hundred fs) and in the process generate a vibrationally excited state (Kasha's rule). Higher triplets can also be populated by intersystem crossing from higher singlet states if the rate constants are competitive for internal conversion and intersystem crossing in the upper states. Thus, although direct absorption from ground singlet to triplet state is forbidden by selection rules, it can be populated indirectly. We will be using vibrational relaxation time also to represent the dephasing time for the S_n and S| states. This is so because of band of vibrational levels, closely spaced, in the S_n states leading to very fast dephasing time T_2. Since the vibrational levels in S| state are far more separated, the dephasing (τ_{vib}) is expected generally slow compared to that of in the S_n states. Electronic spectra of metalloporphyrins are not only sensitive to the porphyrin structure and the nature of the central atom of the metal, but also depend on what axial ligand is added to the metal. The absorption spectra of all the samples have been presented in Chapter 3 & 4. The S_1 state for all the samples fall in the spectral region of 500 - 650 nm corresponding to 20,000 cm^{-1} - 15,400 cm^{-1} and S_2 state fall in 390 - 450 nm region corresponding to 25,640 cm^{-1} - 22,222 cm^{-1}. The excitation at 532 nm corresponding to 18,797 cm^{-1} is off resonance with linear absorption peaks in some porphyrins and will match the lower levels of the S_1 in some cases.

2.9   Photorefractive materials

Using a general definition, a photo-refractive effect is every effect that produces a change of the refractive index of a material under illumination. In this sense, every refractive index change of a material that is due to large light intensities can be called photorefractive. In this category we find the optical Ken-effect, light induced absorption and changes of linear optical properties through thermal effects, or light induced change of the polarisability of a material. In electro-optic materials, large refractive index changes can be obtained through internal electric fields that are due to light-induced charge redistribution. Although these kinds of photorefractive effects can be found only in materials that are both photoconductive and electro-optic, it has the advantage of large changes in refractive index already at comparatively low light intensities.

The photorefractive effect was observed for the first time in 1966 at Bell Laboratories [20] as an undesired local refractive index change in $LiNbO_3$ and $LiTaO_3$ caused by intense blue or green laser beams focused into the crystals. This index inhomogeneity leads to distortions of the wavefront of transmitted beams, and to decollimation/fanning and scattering of light. Since it hindered the use of these materials in this spectral region it was first referred to as a "laser damage effect". Later it was found that the crystals can be returned to their initial homogenous state by briefly heating them to above 200°C, and that the origin of the effect is quite different from the irreversible catastrophic damage which occurs at much higher intensities. Although the refractive index change observed was not permanent, it influenced the phase matching condition for second harmonic generation in an unpredictable way. However, the potential of the photorefractive effect was soon realized [21]. Many experimental and theoretical studies were undertaken in the next ten years [22-24], which led to a better understanding of the mechanisms of the photorefractive effect and to the proposal of a number of new applications [25]. The theoretical studies culminated in the work of Kukhtarev and co-workers that presented a complete band-transport model in 1976 and 1979 [26]. For a more detailed review of the photorefractive effect and its history, see Refs [27]. Here, we briefly present the basic building

blocks of the band transport model, focusing on their general significance. Photorefractive materials are defined as electro-optical materials in which photo-induced space-charge fields via the electro-optic effect change refractive indices. With the development of highly photosensitive electro-optic and photoconductive crystals such as $Bi_{12}SiO_{20}$, $Bi_{12}GeO_{20}$, reduced $KNbO_3$ various applications in real time devices, and the possibility of correcting distorted laser wavefronts by four-wave interaction have been achieved [28].

Impurities, vacancies or defects in the crystal act as charge donors and acceptors; these extra charges are rearranged when light strikes the crystal. Present models propose that the charges, either electrons or holes or both, are excited by light to the closest energy band, where the charges drift, diffuse and eventually become trapped in the crystal. Another possible mechanism is light-assisted tunneling or hopping, directly between trapping sites. Whatever the transport mechanism, if the charges arc illuminated continuously, they eventually arrange themselves into an equilibrium pattern. When the light is turned off, the charges stay put (if the crystal is a good insulator in the dark), so that they "remember" the light pattern. Even though the charges may be present in very small concentrations, typically one part per million, their electric fields can distort the crystal lattice significantly. If the crystal lacks the inversion symmetry, then the electric field surrounding each charge can cause a large, first-order change in the crystal's index of refraction. An interesting difference between photorefractive materials and almost everything else is that if the crystal is good insulator in the dark, its optical nonlinearity is independent of the intensity of the optical beams, thereby permitting spectacular nonlinear effects even with weak laser beams. The optical intensity determines the speed but not the magnitude of the nonlinearity. How fast a photorefractive crystal responds to light and builds up its charge pattern depends on the rate at which photons hit the crystal. To create the static electric fields observed in these crystals requires the rearrangement of about 10^{16} charges per cubic centimeter. Even if each charge required only one photon to move from its initial to final location in the crystal, it would take a few milliseconds to supply sufficient photons, assuming an incident light beam with an intensity 1 Wcm^{-2}. Using high intensity pulsed lasers, which

increases the photon arrival rate, increases the speed of photorefractive effect from few seconds to few picoseconds [29].
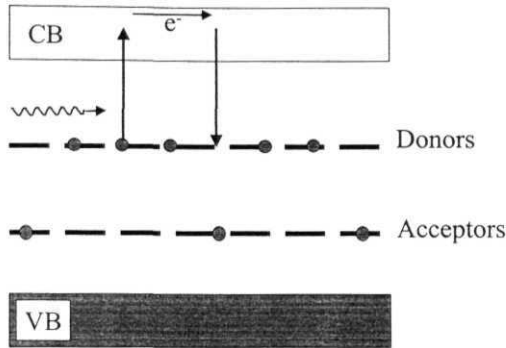
Figure 2.12: Qualitative representation of the intra band-gap energy levels introduced by an impurity atom.

The first step in the photorefractive interaction between light beams is photoexcitation of charge carriers in the material. In an insulator electrons completely occupy the valence band, which is separated from the empty conduction band by a forbidden energy gap. For many transparent dielectrics like $BaTiO_3$, $KNbO_3$ or $Bi_{12}SiO_{20}$, this gap is roughly 3 eV wide and direct photoexcitation of electron-hole pairs is possible for ultraviolet light (wavelengths smaller than approximately 400 nm). Visible light can excite charge earners if impurities introduce energy levels in the band gap that can act, depending on the valency of the dopants, as electron acceptors or donors. In the first case an electron can be photoexcited from the valence band to the impurity level (photoexcitation of holes), while in the second case an impurity electron can be excited to the conduction band (photoexcitation of electrons). Fig 2.12 gives view of simple band explaining basic PR effect.

2.10 **Nanomaterials**

Between the well-established and conventional domain of the atomic & molecular physics and that of the physics of condensed matter, there is an intermediate region dealing with the properties of small aggregates, clusters or small particles, which are neither quite microscopic nor quite macroscopic. The study of the systems in this intermediate region is rather important from a technological point of view for the understanding of problems related to aerosols, catalysis, chemisorption, powder metallurgy etc. From a more fundamental point of view, the study of this state of matter, intermediate between that of a molecule and a solid, generally known as nanomaterial, seems to be crucial and very interesting because it touches on some of the basic points of physical principles, usually concealed if one deals with infinitely large systems [30]. Availability of various kinds of fabrication and characterization techniques revolutionized the field of nanoscience and technology. Varieties of materials like metal and semiconductors have been studied as nanoparticles/ nanocrystallites dispersed in dielectrics, to name a few. Since a small particle is necessarily surrounded by a dielectric, the interface of between the particle and dielectric leads, through the surface-plasmon resonance, to the dielectric anomaly that is the origin of the beautiful colours of metal colloids [31]. It was also observed that the width of the absorption band of such a colloid, which is roughly proportional to the imaginary part of the susceptibility, increases when the size of the particle decreases [32]. This effect was accounted for classically in terms of limited free path [33] or quantum mechanically in terms of the quantum size effect [34]. Despite their disparity, all the materials that are formed by uniformly dispersed metal and semiconductor crystallites in a liquid or solid transparent dielectric share two important features that have essential impact on their properties in the optical frequency range. First, in the metal or semiconductor nanocrystals or microcrystals, the otherwise, delocalized valence electrons in the bulk can find themselves confined in regions much smaller than their delocalization length, which is infinite in the ideal metal and of the order of several tens to a hundred Angstroms in a perfect semiconductor; this drastically modifies their quantum

motion as probed by optical beams but also their interaction with other degrees of freedom. Second, because the size of the crystallites is much smaller than the wavelength and their dielectric constant is very different from that of the surrounding transparent dielectric, the electric field that acts on and polarizes the charges of these crystallites can be drastically different from the macroscopic Maxwell field. These two-effects, the first quantum-mechanical and the second classical are known as quantum and dielectric confinements, are particularly striking in the optical frequency range [35]. In chapter 6 of the thesis, we discuss the effect of laser excitation on metal nanoparticlcs.

2.11   Rate equations

The contribution of different nonlinear optical processes leading to RSA and thus OL are found by writing rate equations describing various processes and by solving them numerically. Eqs 10-16 describes the processes leading to nonlinear absorption in porphyrin molecule with singlet states So, S| & S_n and the triplet states T_1 and T_n. σ_0 is the ground state absorption cross-section, σ_1 and σ_2 are the excited state absorption cross-sections from S_1 and T_1 states respectively, β is the two-photon cross-section, N_0, N_1, N_2, $N3$ and N_4 arc the populations in So, S_1, S_n, T|, and T_n states respectively.

$$\frac{dN_0}{dt} = -\frac{\sigma_0 I N_0}{\hbar\omega} - \frac{\beta I^2}{2\hbar\omega} + \frac{N_1}{\tau_1} + \frac{N_3}{\tau_3} \qquad (2.12)$$

$$\frac{dN_1}{dt} = -\frac{\sigma_1 I N_1}{\hbar\omega} + \frac{\sigma_0 I N_0}{\hbar\omega} - \frac{N_1}{\tau_1} - \frac{N_1}{\tau_{ISC}} + \frac{N_2}{\tau_2} \qquad (2.13)$$

$$\frac{dN_2}{dt} = \frac{\sigma_1 I N_1}{\hbar\omega} + \frac{\beta I^2}{2\hbar\omega} - \frac{N_2}{\tau_2} \qquad (2.14)$$

$$\frac{dN_3}{dt} = -\frac{\sigma_2 I N_3}{\hbar\omega} - \frac{N_3}{\tau_3} + \frac{N_1}{\tau_{ISC}} + \frac{N_4}{\tau_4} \qquad (2.15)$$

$$\frac{dN_4}{dt} = \frac{\sigma_2 I N_3}{\hbar\omega} - \frac{N_4}{\tau_4} \qquad (2.16)$$

and the intensity transmitted through the sample is given by

$$\frac{dI}{dz} = -\sigma_0 I N_0 - \sigma_1 I N_1 - \sigma_2 I N_3 - \beta I^2 \tag{2.17}$$

with

$$I = I_{00} \times (\frac{\omega_0^2}{\omega^2(z)}) \times \exp(-\frac{t^2}{\tau_p^2}) \times \exp(-\frac{2 \times r^2}{\omega^2(z)}) \tag{2.18}$$

and

$$\omega(z) = \omega_0 \left\{ 1 + \left(\frac{z}{z_0}\right)^2 \right\}^{\frac{1}{2}} \quad ; \quad z_0 = \frac{\pi \times \omega_0^2}{\lambda}$$

$\tau_1, \tau_2, \tau_3,$ and τ_4 are the lifetimes of the excited states $S_{10}, S_n, T_1,$ and T_n respectively. z_0 is the Rayleigh range, ω_0 is the beam waist at focus, τ_p is the input pulse width used, and τ_{ISC} is the intersystem crossing rate. I is intensity as a function of r, t, and z, I_{00} is peak intensity at the focus of the Gaussian beam. The differential equations are first de-coupled and then integrated over time, length, and along the radial direction, are solved numerically using Runge-Kutta fourth order method. Assuming the input beam to be a Gaussian, the limits of integration for r, t, and z are varied from 0 to ∞, -∞ to ∞, and 0 to L (length of the sample) respectively. Typical number of slices used for r, t, and z are 60, 30, and 5 respectively. $\sigma_1, \sigma_2,$ (3 and τ_{ISC} are then estimated through least square fit of the experimental data [36]. The rate equations are different for porphyrins and photorefractive materials as the energy level structure varies. Rate equations are written accordingly to describe the processes leading to OL. Same rate equations are also used to fit the OL curves.

2.12   References

1. Y.R. Shen, *The Principles of Nonlinear Optics,* New York: Wiley, USA, 1984; Y.R. Shen, *IEEE J. Quant. Electron.* QE-22, 1196 (1986).

2. N. Bloembergen, *Nonlinear Optics,* Benjamin, New York, 1977.

3.   M.D. Levenson, *Introduction to Nonlinear Laser Spectroscopy,* New York: Academic, 1982.

4.   R.A. Fischer, *Optical Phase Conjugation*, New York: Academic, USA, 1983.

5.   H.J. Eichler, P. Gunter, and D.W. Pohl, *Laser-Induced Dynamic Gratings,* Springer-Verlag, Berlin, Heidelberg, Germany, 1986.

6.   B. Ya. Zeldovich, N.F. Philipetsky, V.V. Shkunov, *Principles of Phase Conjugation*, Springer series in optical sciences, Vol. 42, Springer, Berlin, Germany, 1985.

7.   D.M. Pepper, Ed. *Opt. Engg.* **21,** 2, 1982.

8.   M. Sheik-Bahae, A.A. Said, T.H. Wei, D.J. Hagan, and E.W. Van Stryland, *IEEE J. Quant. Electron.* **QE-26,** 760 (1990).

9.   A.D. Walser, G. Coskun, and R. Dorsinville, *Electrical and Optical Polymer Systems,* ed.'s D.L. Wise, G.E. Wnek, D.J. Trantolo, T.M. Cooper, and J.D. Gresser, Marcel Dekker Inc., New York, 423-452; M. Zhao, Y. Cui, M. Samoc, P.N. Prasad, M.R. Unroe, and B.A. Reinhardt, *J. Chem. Phys.* 95, 3991 (1991); S.K. Ghoshal, P. Chopra, B.P. Singh, J. Swiatkiewicz, and P.N. Prasad, *J. Chem. Phys.* 90, 5078 (1989); B.P. Singh, M. Samoc, U.S. Nalwa, and P.N. Prasad, *J. Chem. Phys.* 92, 2756 (1990); Y. Pang, M. Samoc, and P.N. Prasad,./. *Chem. Phys.* 94, 5282 (1991); B.P. Singh, P.N. Prasad, and F.E. Karasz, *Polymer* 29, 1940 (1988); M. Samoc, and P.N. Prasad, *J. Chem. Phys.* 91, 6643 (1989); Y. Cui, M. Zhao, G.S. He and P.N. Prasad, *J. Phys. Chem.* 95, 6842 (1991); M.K. Casstevens, M. Samoc, J. Pfleger, and P.N. Prasad,./. *Chem. Phys.* 92, 2019 (1990).

10. R.R. Rojo, Ph.D. Thesis, Heriott-Watt University, April 1994, UK; F.J. Aranda, Ph.D. Thesis, University of Massachusetts, Lowell, USA, 1995;

11. R.L. Sutherland, *Handbook of Nonlinear optics,* Marcel-Dekker Inc., New York, USA (1996).

12. M.-T. Zhao, B.P. Singh, and P.N. Prasad, ./. *Chem. Phys.* 89, 5535 (1988); C. Meloney, H. Byrne, W.M. Dennis, W. J. Blau, and J.M. Kelly, *Chem. Phys.* **121,** 21 (1988); D.V.G.L.N. Rao, F.J. Aranda, J.F. Roach and D.E. Remy, *Appl. Phy. Lett.* 58, 1241 (1991); S. Guha, K. Kang, P. Porter, J.F. Roach, D.E. Remy, F.J. Aranda, and D.V.G.L.N. Rao, *Opt. Lett.* **17,** 264 (1992); T. Sakaguchi, Y. Shimizu, M. Miya, T. Fukumi, K. Ohta, and A. Nagata, *Chem. Lett.* 281, (1992); J. Qin, T. Wada, and H. Sasabe, *Mol. Cryst. Liq. Cryst.* **217,** 47 (1992); S.V. Rao, N.K.M.N. Srinivas, D.N. Rao, L. Giribabu, B.G. Maiya, R. Philip, G.R. Kumar, *Opt. Commun.* **182,** 255 (2000).

13. T. Kobayashi, A. Terasaki, T. Hattori, K. Kurokawa, *Appl. Phys. B 41,* 107 (1988).

14. D.B. James and K.J. McEwan, *Nonlinear Optics* 21, 377 (1999); T.J. Mc Kay, J. Staromlynska, J.R. Davy and J. Bogler, *J. Opt. Soc. Am. B* 18, 358 (2001).

15. P.B. Chappie, J.M. Staromlynska, J.A. Hermann, and T.J. McKay, J. *Nonlinear Opt. Phys. and Mat.* 3, 251 (1997); T. Xin, D.J. Hagan, M. Sheik-Bahae, and E.W. Van Stryland, *Opt. Lett.* 19, 317 (1994); D.V. Petrov, *J. Opt. Soc. Am. B* 13, 1491 (1996); J.-G. Tian, W.-P. Zang, and G. Zhang, *Opt. Commun.* **107,** 415 (1994); S.M. Mian, B. Taheri, and J.P. Wicksted, *J. Opt. Soc. Am. B* 13, 856 (1996); M. Sheik-Bahae, A.A. Said, D.J. Hagan, M.J. Soileau, and E.W. Van Stryland, *Opt. Engg.* 30, 1228 (1991); S.V. Kershaw, *J. Mod. Opt.* 42, 1361 (1995).

16. National facility at National Center for Ultrafast processes, Chennai.

17. D.N. Rao, V.N. Kumar and B. Geeta, Proceedings of National Laser symposium 1994, India; R.W. Minck, R.W. Terhune and W.G. Rado, *Appl. Phys. Lett.* 3, 181 (1963); A.Z. Grasyuk, *Sov. J. quant. Electron.* 4, 269 (1974); J. Cahen, M.Clerc and P. Rigny, *Opt. Commun.* 21, 387 (1977); V. Wilke and W. Schmidt, *Appl. Phys.* 18, 177 (1979); A. Yariv, Quantum Electronics, John, Wiley & sons, New York (1989).

18. V.N. Kumar, Ph.D. Thesis, University of Hyderabad, January 1997; S. V .Rao, Ph.D. Thesis, University of Hyderabad, January 2001; M. Maeda, Laser Dyes, Academic Press, New York, 1984; U. Brackmann, Lambda Chrome Laser Dyes, Lambda Physik, Gottingen, 1986; G. Yamaguchi, F. Endo, S. Murakawa, S. Okamura, and C. Yamanaka, *Japn. J. Appl. Phys.* 7, 179, 1968; F.P. Schafer, in *Dye Lasers,* F.P. Schafer Ed., Springer Verlag, 1977; F.P. Schafer, *Liquid Lasers* in Laser handbook, Edited by F.T. Areechi and E.O. Schulz-Dubois (North-Holland, 1972), Vol. 1.

19. N.J. Turro, "Modem Molecular Photo-Chemistry", The Benjamin/Cummings Publishing Co. Inc., 1978; K.K. Rohatgi-Mukherjee, "Fundamentals of Photo-Chemistry", Wiley Eastern Ltd., New Delhi, 1992; M. Gouterman, in The Porphyrins, vol. III, Academic press, (1978); K. Kalyanasundaram, Photochemistry of polypyridine and porphyrin complexes, Academic Press, (1992).

20. A. Ashkin, G.D. Boyd, J.M. Dziedzic, R.G. Smith, A.A. Ballman, J.J. Levinstein, K. Nassau, *Appl. Phys. Lett.* 9, 72 (1966).

21. F.S. Chen, J.T. LaMacchia, D.B. Fraser, *Appl. Phys. Lett.* 13, 223 (1968).

22. J.J. Amodei, *RCA Review* 32, 185 (1971).

23. A.M. Glass, D. Von der Linde, T.J. Negran, *Appl. Phys. Lett.* 25, 233 (1974).

24. D.M. Kim, R.R. Shah, T.A. Rabson, F.K. Tittcl, *Appl. Phys. Lett.* 28, 338 (1976); R.W. Hellwarth, *J. Opt. Soc. Am.* 67, 1-3 (1977).

25. J. Khoury, V. Ryan, C. Woods, and M.C. Golomb, *Opt. Commun.* 85, 5 (1991); **M. Belic, M.** Petrovic, and F. Kaiser, *Opt. Commun.* **123,** 657 (1996).

26. N. V. Kukhtarev, *Sov. Tech. Phys. Lett.* 2, 438 (1976); N. V. Kukhtarev, V. B. Markov, S. G. Odulov, M. S. Soskin, and V. L. Vinetskii, *Ferroelectrics* **22,** 949 (1979).

27. P. Gunter, ***Phys. Rep.*** **93,** 199 (1982); T.J. Hall, R. Jaura, L.M. Connors, P.D. **Foote,** *Prog. Quant. Electron.* **10,** 77 (1985); D.M. Pepper, J. Feinberg, N.V. Kukhtarev, *Scientific American* **263,** 34 (1990); P. Gunter and J.P. Huignard, eds., *"Photorefractive Materials and their Applications, "* Vols. I and II, Springer-Verlag, Berlin Heidelberg (1988).

28. J.P. Huignard and F. Micheron, *Appl. Phys. Lett.* 29, 591 (1976); P. Gunter and A, Krumins, *Appl. Phys.23,* 199 (1980); D.M. Pepper and A. Yariv, *Opt. Lett.* 5, 59 (1980); J.P. Huignard, J.P. Herriau, P. Auborg and E. Spitz. ***Opt. Lett.*** 4, 21 (1979).

29. G.C. Valley, A.L. Smirl, M.B. Klein, K. Bohnert, and T.F. Boggess, *Opt. Lett.* **11** 647 (1986); N.J. Berg, B.J. Udelson and J.N. Lee, *Appl. Phys. Lett.* **31** 555 (1977); C.T. Chen, D.M. Kim and D. Von der Linde, ***Appl.*** *Opt.* **20** 2\73 (1981).

30. J.A.A.J. Perenboom, P. Wyder, P. Meier, *Phys. Rep.* 78, 173 (1981).

31. G. Mie, ***Ann.*** *of Phys. (Leipzig)* 25, 377 (1908), J.C. Maxwell-Garnet, *Philos. Trans. R. Soc. London,* **203,** 385 (1904); **205,** 237 (1906)

32. R.H. Doremus, *J. Chem. Phys.,* 40,2389 (1964); 42, 414 (1965).

33. W.J. Doyle, *Phys. Rev.* **111**, 1067(1958).

34. A. Kawabata and R. Kubo, *J. Phys. Soc. Jpn.* 21, 1765 (1966); L. Genzel, T.P. Martin, and U. Krcibig, Z ***Phys.*** *B* **21,** 339 (1975).

35. C. Flytzanis, F. Hache, M.C. Klein, D. Ricard, and P. Roussignol, vol. XXIX, 321 in: E. Wolf Ed., Progress in Optics, North Holland, Amsterdam, (1991).

36. S.V. Rao, D.N. Rao, J.A. Akkara, B.S. De Cristofano, and D.V.G.L.N. Rao, ***Chem. Phys. Lett.*** **297,491** (1998).

Chapter 3

Axial ligated
Phosphorus (V) Tetratolylporphyrins

This chapter explains optical limiting characteristics of Phosphorus (V) Tetratolylporphyrins (P (V) TTP's) with axial chlorine atoms, leading to heavy atom effect and with axial azoarene subunits which introduces charge transfer states. Heavy atom effect exerted by the two axial chlorides is found to lower the limiting threshold by 30 times in the ns regime and by three times in ps regime. The introduction of axial azoarene groups into the phosphorus porphyrin structure is found to reduce the limiting threshold by a factor of two in the ns regime. In the ps regime these molecules show saturation of ESA at higher intensities. The experimental results on the measurement of third order optical nonlinearity in the ns and ps domain, in these porphyrin molecules (TTP), using degenerate four wave mixing (DFWM) and Z-Scan techniques are also discussed. Time-resolved studies indicate an ultra-fast temporal evolution of the nonlinearity in these molecules.

3.1   Porphyrin media for NLO applications

Porphyrins are macrocyclic aromatic molecules having four pyyrole rings occupying the position at four corners of a square and connected by unsaturated methane bridges to complete the macrocycle.   Metalloporphyrins are highly colored molecules with strong absorption in the visible region due to the cyclic conjugated tetrapyrrole chromophore. Various porphyrin systems are considered as being derived from the simplest parent ligand called porphine. Porphyrins and related macrocycles provide an extremely versatile synthetic base for a variety of materials applications.   The exploration of metalloporphyrin assemblies as building blocks for tailored materials has found rapid growth during the past decade [1]. The interest in metalloporphyrins is many-fold. In particular they have strong electronic transitions ($\epsilon_{max} \approx 10 - 10' \, M'' \, cm^{-1}$) in the visible and near infrared (NIR), whose energies can be shifted, both by chemically modifying the ring and by changing the coordinated metal. Because these transitions are unusually sharp (FWHM $\approx 500 - 1500 \, cm^{-1}$) [2], the nonlinear susceptibilities may be enhanced near resonance, without incurring significant linear absorption losses. These are chemically and thermally robust surviving to over 400°C in

some cases [2] and are stable under intense optical irradiation. Strong nonlinearity and fast response times, are the desired criteria for making porphyrins useful for photonic devices [3]. Because of the two-dimensional delocalization of the π-electrons throughout the macrocycle ring, porphyrins are interesting chromophores for second and third order NLO properties. Porphyrins have been studied extensively for their second order NLO properties using various techniques like HRS, EFISHG etc [4]. Third-order NLO properties are also studied in variety of porphyrin molecules, like tetraphenylporphyrins (TPP) [5], tetrabenzoporphyrins (TBP) [6], tetrakispentadecylphenylporphyrins [7], octaethylporphyrins (OEP) [8], Octaphenyltetraazaporphyrin (OPTAP)[9], baskethandle porphyrins [10], conjugate polymers [11], tetratolylporphyrins (TTP) [12] to name a few. These molecules are among the most effective third-order NLO materials possessing high second hyperpolarizabilities. Porphyrins were also studied as composites with C_{60} in thin films using various techniques like DFWM, Z-scan and THG [13]. Porphyrins, owing to strong ESA from both singlet and triplet states, are among the most effective optical limiters in the visible region known to date [14]. Since the mechanism of limiting in such materials depends on the absorption of excited molecules, it is important to characterize the excited state dynamics and evaluate parameters like excited state absorption cross-sections, lifetimes etc. so as to optimize their properties for the realization of a functional device [15]. Study of the optical nonlinearity and elucidation of the dynamics associated with excited states of such molecules is therefore important from a fundamental as well as technological point of view. One way of altering the excited state properties is by changing the structural geometry and hence electronic structure of these macrocycles.

Structural modifications to the porphyrin ring can be expected to result in molecules with diverse photophysical and photochemical properties that will in turn affect their optical nonlinearity. This would possibly lead to a desirable change in a variety of excited state processes including enhanced internal conversion and intersystem crossing (ISC), ion-association, excitation energy transfer (EET), photoinduced electron transfer (PET) etc. One of the key structural modifications in this regard, is the introduction of heavy atoms in the

porphyrin ring, which in turn, due to faster ISC rate reduces **the** fluorescence yield, increase triplet formation and hence further enhancing absorption from T_1 $\rightarrow T_n$. Photoinduced electron transfer (PET) is another phenomenon that comes into play due to the presence of additional donor/acceptor units in the molecule. Such effects can be conveniently harnessed to enhance the third order nonlinearity, limiting performance and hence to develop promising materials for optical limiting. This chapter explains the effect of structural modifications like internal heavy atom effect and the introduction of charge-transfer states on the limiting behavior of phosphorus (V) tetratolylporphyrins.

3.2   Heavy atom effect in 5,10,15,20-(tetratolyl) porphyrinato phosphorus(V) dichloride

3.2.1   Heavy atom effect and its relevance to Nonlinear Optics

The transition between two given energy states in organic molecules are governed by selection rules. The rule governing the transitions between the states of like multiplicities is most stringently obeyed. A transition is allowed only when the selection rules are obeyed; otherwise it is called a forbidden transition. In an ideal situation, transitions between singlet and triplet state are strictly forbidden. But under the influence of intramolecular and intermolecular perturbations, these transitions do occur, which mixes the pure singlet and triplet states. These perturbations arc functions of the magnetic field near the nucleus and are therefore a function of atomic mass coming into play due to the presence of heavier atom in a molecule (intramolecular) or in the surrounding (intermolecular or external) are governed by the heavy atom effect [16].

The hamiltonian operator, which causes mixing of the states of unlike multiplicities, is expressed as

$$H_{so} = K\xi \,(L \bullet S)$$ (3.1)

where ξ is a function which depends on the field of the nucleus, $(L \bullet S = a\ cos\theta)$ is **the** scalar product of orbital and spin angular momentum vectors respectively and K is the constant for the molecule. The wave function obtained on such spin-

orbit coupling interactions which cause mixing of the pure triplet ψ_T and pure singlet ψ_S^0 is expressed as

$$\psi_{SO} = \psi_T^0 + \lambda \psi_S^0 \qquad \textbf{(3.2)}$$

where *X* indicates the degree of mixing and is given by

$$\lambda = \frac{\int \psi_S^o \, H_{SO} \, \psi_T^o \, d\tau}{|E_{ST}|} \approx \frac{V_{SO}}{|E_{ST}|} \qquad \textbf{(3.3)}$$

EST is the energy gap between the singlet and triplet states and V_{SO} is the interaction energy that flips the electronic spin. Thus, smaller is the energy gap E_{ST} the larger is the mixing coefficient *X. Vso* will be large also if the molecule is paramagnetic. Therefore, under spin-orbital coupling interaction the transition moment *M* is given as

$$|M| \propto \frac{\xi \int \psi_S^o \, L.S \, \psi_T^o \, d\tau}{|E_{ST}|} \qquad \textbf{(3.4)}$$

and is seen to be directly related to ξ and inversely to the energy separation between the singlet and triplet states. ξ is a function of the potential field near a nucleus and has a high value for an orbital, which can penetrate close to the nucleus.

Heavy atom effects in the transitions between singlet and triplet states are usually interpreted in terms of the coupling of the relativistic magnetic field of the motion of a nuclear charge around an electron considered to be fixed, and the magnetic field of the electron-spin motion (spin-orbit coupling). Those effects are proportional to the (square of the) spin-orbit coupling factor, ξ, of an atom with a high atomic number, Z, that outweighs all the other atoms ($\xi \approx Z^4$) [16]. Heavy atom effect in organic molecules is one of the very important phenomenon to modify the spin-orbit interactions [17], which in turn modify the singlet and triplet state properties like lifetimes of the states, fluorescence and phosphorescence emission. In order to maximize the quantum yield for triplet formation one usually resorts to an internal heavyatom effect [16]. This systematic study of heavy-atom effects is rationalized through the use of a model for radiationless transitions in large molecules [17]. Additionally, just like other

radiationless transitions in the weak-coupling limit [18], intersystem crossing rates present an inverse relationship with the difference in energy, E_{ST}, of the singlet and triplet states and are proportional to the relative number of vibrational modes, η, involved in the transition [19]. Thus, even if the nature of the excited states is not affected by the heavy atom substitution and symmetry characteristics do not reduce heavy atom/porphyrin orbital overlap, intersystem crossing rates are a function of ξ^2, E_{ST} and η.

When the halogen atom is an integral component of the molecule (i.e. present as a substituent) the effect is termed internal heavy atom effect. Heavy atom effects due to halogens are also observed when they are present externally in the neighborhood (as counter ions in solvent for example), known as external heavy atom effect. Both these effects show a dramatic enhancement of S→T transition, which is said to borrow intensity from S→S transition. A quite extensive research has been undertaken on the study of both internal and external heavy atom effects in halogenated porphyrins and metalloporphyrins [20-24]. The role of halogen atoms in promoting spin-orbit coupling is fairly well established. Studies of the photophysics of condensed aromatic and heterocyclic molecules have shown that the enhancement of spin-orbit coupling through the heavy atom is indirectly observed in the shortening of the triplet state lifetime and in an increase in the phosphorescence yield upon increasing the atomic weight of the halogen [23]. In this section, we explain the nonlinear absorption and optical limiting properties of 5,10,15,20-(tetratolyl) porphyrinato phosphorus (V) dichloride ($[(TTP)P^V Cl_2]^+$), with introduction of heavy Cl^- in place of (OH)" in 5,10,15,20-(tetratolyl) porphyrinato phosphorous (V) dihydroxide $[(TTP)P^V(OH)_2]^+$. With the substitution of Cl" in place of OH", significant variations in the singlet state are observed. The fluorescence yield (ϕ_{fl}), the singlet (τ_{S1}) and triplet lifetime (τ_{T1}) for these molecules in dichloromethane given in Table 3.2.1, show the effect of halogenation. Singlet state properties measured in different environments also showed a similar behavior where ϕ_{fl} has reduced considerably and τ_{S1} is faster.

3.2.2   Molecular structure and linear optical properties

Samples of $[(TTP)P^V Cl_2]^+$ and $[(TTP)P^V(OH)_2]^+$ are synthesized and purified according to the reported procedures in the literature [25]. Each sample is subjected to a column chromatographic purification process prior to the measurements. In all experiments, sample solutions in chloroform are taken in a quartz cell of 1-mm path length. The molecular structure and absorption spectra of these molecules are shown in Fig. 3.2.1 and 3.2.2 respectively. This molecule shows linear absorption features of typical metalloporphyrins, namely the high energy B (Soret) band and the low energy Q band(s).

$$X = OH \qquad [(TTP)P^V(OH)_2]^+$$
$$= Cl \qquad [(TTP)P^V Cl_2]^+$$
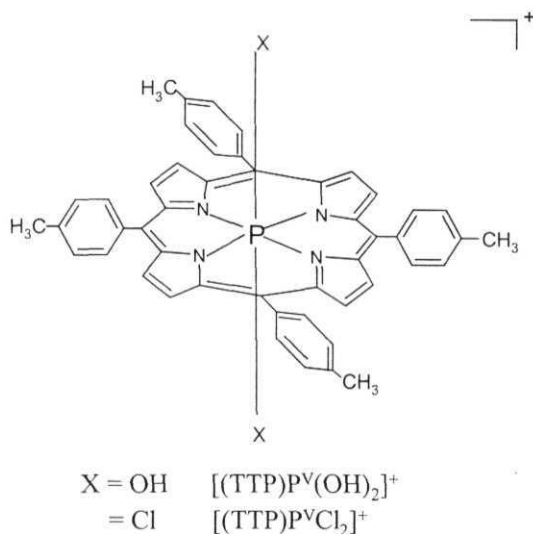
Figure 3.2.1: Molecular structure of 5,10,15,20-(tetratolyl) porphyrinato phosphorus (V) dichloride

	τ_{S1}	$\varnothing_{fl}$	τ_{T1}
$[(TTP)P^V(OH)_2]^+$	1 ns (27), 3.45 (72)	0.056	68 µs
$[(TTP)P^V Cl_2]^+$	0.7 ns (87), 3.5 (12)	0.036	17 µs

Table 3.2.1: Fluorescence yield, singlet and triplet state lifetimes.

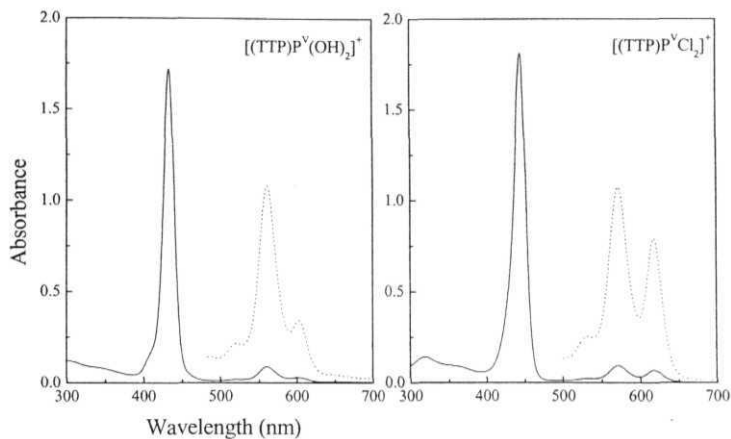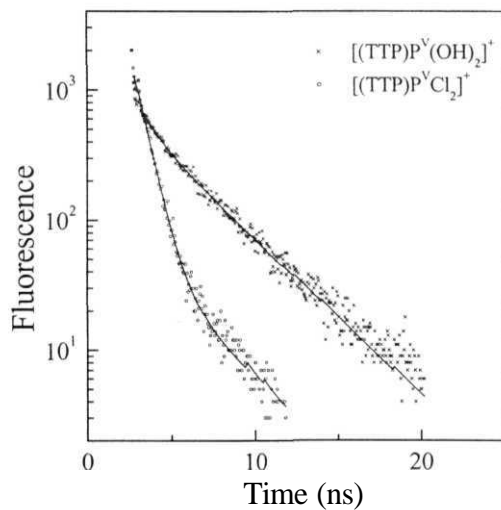Figure 3.2.2: Absorption spectra of $[(TTP)P^V(OH)_2]^+$ and $[(TTP)P^VCl_2]^+$

Figure 3.2.3: Fluorescence decays of $[(TTP)P^V(OH)_2]^+$ and $[(TTP)P^VCl_2]^+$

Fluorescence lifetimes and the percentage contribution of each lifetime are given in Table 3.2.1. The decay curves are shown in Fig. 3.2.3 and both these molecules show a bi-exponential decay representing both slow and fast decay. In

the reference porphyrin $[(TTP)P^V(OH)_2]^+$ the slower decay has more contribution (72%) and with chlorine introduction the faster component has more contribution (87%), which is a well-expected effect of heavy atom effect.

3.2.3   Third order nonlinear optical properties

Frequency doubled Nd: YAG lasers with 25 ps and 6 ns pulse widths, 10 Hz repetition rate are used for the experiments. We have employed standard backward DFWM-PC geometry for the measurement of $\chi^{(3)}$. Optical limiting and open aperture Z-scan studies are carried out by focusing the input beam on to the sample with linear transmission of approximately 75% at 532 nm using lenses of 500 mm and of 125 mm focal length to 60 urn and 30 μrn spot size at focus in case of 25 ps and 6 ns pulses respectively, and the transmitted light is collected with a fast photodiode. The peak fluences used in the Z-scan experiments with 25ps and 6 ns pulses are approximately 0.25-1.3 Jcm^{-2} and 0.5-1.5 Jcm^{-2} respectively. The optical limiting and Z-scan studies are performed at the same concentration of $\sim 10^{-4}$ M ensuring identical experimental conditions for both ps and ns regimes. The sample remains stable even after exposure to laser pulses for a long period of time, which is confirmed from indistinguishable absorption spectra recorded before and after the measurements.

Intensity dependence curves of the phase conjugate (PC) signal for $[(TTP)P^VCl_2]^+$ and the reference $[(TTP)P^V(OH)_2]^+$ shown in Fig 3.2.4 clearly indicates the large enhancement in the PC signal. At higher intensities we have not observed any higher order nonlinearities for this molecule. The log-log plot of PC signal to the input intensity gives a slope of 3.2 $\pm$ 0.2, indicates that the nonlinearity is predominantly third order. Effective microscopic second hyperpolarizability $<\gamma>$ measured with 25 ps pulses and 6 ns pulses for $[(TTP)P^V(Cl)_2]^+$ is (8.49 $\pm$0.46) x 10^{-30} esu and (174.48 + 7.2) x 10^{-27} esu respectively. These values are found to be greater than the corresponding values of $[(TTP)P^V(OH)_2]^+$ by one order in ps regime and by three orders in ns regime respectively [12].
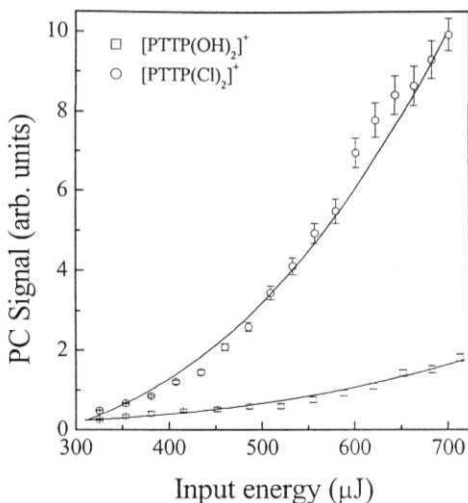
Figure 3.2.4: Intensity dependence of the PC Signal with 35 pulses. Solid lines show the cubic fit to the data.

The ratio of the signals for the conjugate beam in nanosecond DFWM experiment for parallel and perpendicular probe polarizations dropped down by just about 1/3, indicating that the nonlinearity is predominantly electronic in origin. Large enhancement in $\langle\gamma\rangle$ at nanosecond timescale is attributed to the contribution of excited triplet state. Greater polarization emanating from electronegative chlorine in the phosphorus porphyrin structure was shown to lead to a rise in the measured $\langle\gamma\rangle$ values. Similar enhancement of $\langle\gamma\rangle$ with axial electronegative ligand substitution by one order has been reported earlier in TPP systems [26].

3.2.4   Optical limiting and nonlinear absorption

Significant reduction in the limiting threshold level for $[(TTP)P^{V}Cl_2]^{+}$ compared to $[(TTP)P^{V}(OH)_2]^{+}$, with 6 ns pulses can be seen in Fig. 3.2.5. The limiting threshold ($I_{1/2}$) has reduced by 30 times, from 3 Jcm^{-2} to 0.1 Jcm^{-2} in ns time regime, and by three times from 0.264 Jcm^{-2} to 0.0884 Jcm^{-2} in ps regime.

ESA is the most important mechanism leading to optical limiting in porphyrins [27]. Heavy atom effect in brominated porphyrins [28], a class of group III and group IV metalloid porphyrins [29], and halogenation and alkylation [30] is known to enhance RSA. Third order nonlinearities [31] of thiophene homologues due to heavy atom effect are also reported. Enhancement of optical limiting in heavy atom containing phthalocyanines due to spin-orbit coupling and nonlinear absorption is found to increase with Z [32]. Heavy atom effect has been reported in metalloporphyrins like TPP and ZnTPP with planar shape, H_2OBP with saddle [33] and ZnOBP with ruffled saddle conformation [34]. Ring nonplanarity increases the matrix element $\langle S_1 | H | T \rangle$, allowing for mixing of $\pi\sigma^*$ and arc* triplet states with $S_1(\pi\pi^*)$ and "free rotor effect", simultaneously shortening the intersystem crossing and triplet lifetimes [35,36].
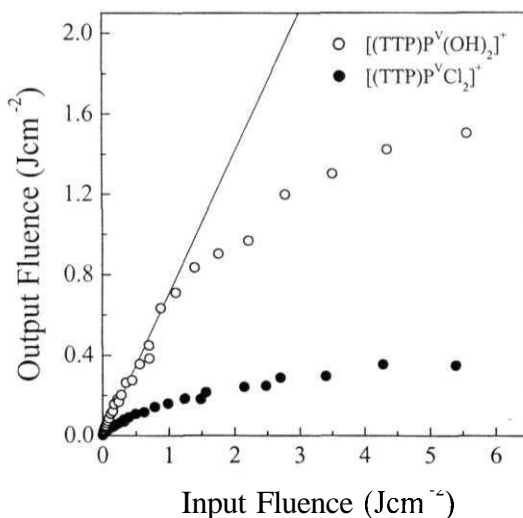
Figure 3.2.5: OL curves of $[(TTP)P^V(OH)_2]^+$ (o) and $[(TTP)P^VCl_2]^+$ (•) with 6ns pulses. Line represents 75% linear transmission.

Metals forming complexes with porphyrins are classified into three types: closed shell metals, open shell paramagnetic metals, and open shell diamagnetic metals [37]. In OBP's with open shell paramagnetic ions the nonlinear absorption efficiency scaled as ZnOBP > CdOBP > H_2OBP > PbOBP > CuOBP

= CoOBP a trend reflecting the spin state of the metals. Both Cu^{2+} and Co^{2+} are open shell paramagnetic ions with unfilled d orbitals. Whereas, in the closed shell metal OBP series a reverse trend $Zn^{2+} > Cd^{2+} > Pb^{2+}$ appeared [28]. Contributions to spin-orbit coupling coming from the central metal ion, the peripheral bromines, and the distortion of the porphyrin ring are found to be the factors that increase the intersystem crossing rate and decrease the triplet lifetime [36].
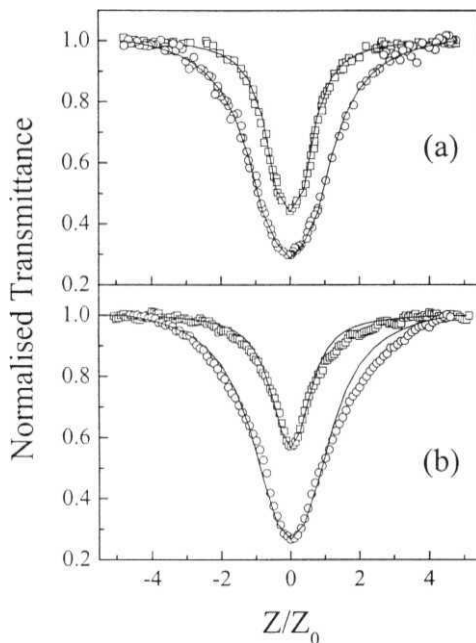
Figure 3.2.6: Open aperture Z-scan curves of $[(TTP)P^V(OH)_2]^+$ (□) and $[(TTP)P^VCl_2]^+$ (o) showing RSA at low fluences (a) with 25ps pulses with peak fluences of 0.35 Jcm^{-2} at focus and (b) with 6ns pulse widths. Solid lines show theoretical fit generated using a five level model.

Among the various factors that can be invoked to explain improvement of the optical limiting performance of $[(TTP)P^VCl_2]^+$ in the ns time regime, faster intersystem crossing rate due to the axial chloride substitution due to heavy atom effect is the most important as it plays a significant role by enhancing the population of the triplet state. The long lifetime of the T_1 state compared to the

ns pulse duration, leads to larger effective ESA from $T_1 \rightarrow T_n$, leading to reduction in optical limiting threshold and enhancement in $\langle\gamma\rangle$. Though anomalous heavy atom effect on optical limiting performance is reported in lanthanide diphthalocyanines [38] and in some of the porphyrins [28], we have not observed any anomaly in our case, as the chloride substitution is in the axial site.

Figure 3.2.7: Open aperture Z-scan curves of $[(TTP)P^V(OH)_2]^+$ showing SA followed by RSA with 25ps pulse widths. Peak Intensity I_{00} is also shown.

In order to estimate the limits to which these molecules would be showing the limiting behavior due to RSA is seen by recording the Z scan curves at different fluences for the ps and ns regimes. With 25 ps pulses, both the molecules have shown RSA till the fluences of 0.40 Jcm^{-2} (Fig. 3.2.6 (a)). But above this fluence level, both the molecules show a gradual transition to SA near focus due to the saturation of ESA from S_1 to S_n with increasing input fluence.

The Z-scan data with ns pulses (Fig. 3.2.6 (b)) shows only RSA even at high fluences. We observed stronger RSA with the introduction of Cl" both in ps and ns regimes.

We have also observed saturation of absorption in RSA at fluences larger than 0.5 Jcm$^-$ with picosecond pulses. Saturation in absorption at high fluences based on higher excited state absorption is reported in cadmium texaphyrin solution [39], 1,1',3,3,3',3'-hexamethylindotricarbocyanine iodide (HITC1) [40] and in chloroaluminium phthalocyanine dye [41]. Fig. 3.2.7 and 3.2.8 show the open-aperture Z-scan curves at different fluences above 0.40 Jcm^{-2} with picosecond pulses showing SA followed by RSA for $[(TTP)P^V(OH)_2]^+$ and $[(TTP)P^VCl_2]^+$ respectively. The symmetrical traces indicate that no other processes such as scattering, photo degradation or damage occur. The fluence at which the saturation of excited states has started (S_{th}) is given in Table 3.2.2. Saturation of the excited states is more in $[(TTP)P^VCl_2]^+$ compared to that in $[(TTP)P^V(OH)_2]^+$.
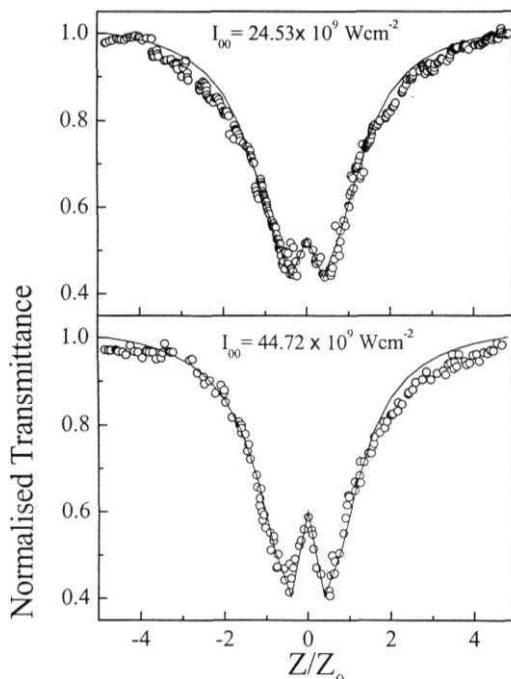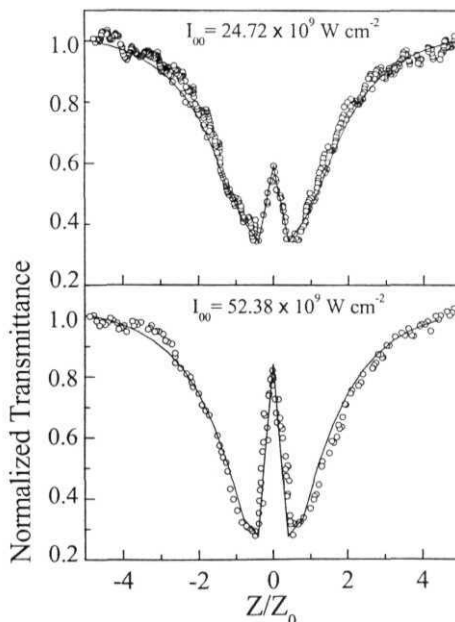

Figure 3.2.8: Open aperture Z-scan curves of $[(TTP)P^VCl_2]^+$ showing SA followed by RSA with 25ps pulse widths. Peak Intensity I_{00} is also shown.

The enhancement in the nonlinear absorption with nanosecond pulses and the saturation effects with picosecond pulses at higher fluences are investigated by a generalized five-level model and the rate equations describing different mechanisms, like ground state absorption from $S_0 \to S_1$, ESA from $S_1 \to S_n$, $T_1 \longrightarrow T_n$ and different relaxation times in the molecule. The rate equations are solved numerically using Runge-Kutta fourth order method as explained earlier in section 2.11 of chapter 2. In the ps regime, the singlet levels So, S_1 and S_n play a major role. Hence the five level model effectively becomes a three level model, neglecting the ISC from $S_1 \to T|$, as the pulse duration is much shorter than τ_{ISC}. While modeling the ns data, we observe that $S_1 \longrightarrow S_n$ absorption shows insignificant contribution, which is due to large population in the T_1 state due to stronger intersystem crossing from $S_1 \longrightarrow T\backslash$.

From the theoretical fit to open aperture Z-scan curves with 25ps pulses, the ESA from $S_1 \to S_n$ (σ_1) and the lifetime of the higher singlet state τ_{Sn} are estimated. The ESA cross-section (σ_2) from $T_1 \to T_n$ and ISC rate (τ_{isc}) are estimated from the theoretical fit of the ns data. Excited singlet state S_1 will have different decay channels: (1) radiative decay measured using picosecond time resolved fluorescence measurements typically few nanoseconds, (2) the population relaxation measured using DFWM-PS typically few tens to hundreds of picoseconds and (3) the vibrational relaxations with in the singlet states which is typically in few picoseconds. The contribution from all these processes is taken as the effective singlet lifetime used in the rate equations. The estimated values from the theoretical fits, the widely used figures of merit, the ratios σ_1/σ_0, σ_2/σ_0, where σ_0 is the ground-state cross section along with the parameters used for the estimation of these parameters are shown in Table 3.2.2. τ's are the lifetimes of the levels and Φ_{fl} is the fluorescence yield. The higher figure of merit σ_1/σ_0 for $[(TTP)P^V Cl_2]^+$ than $[(TTP)P^V(OH)_2]^+$ confirms that enhancement in the nonlinear absorption at lower fluences with picosecond pulses is more due to ESA from $S_1 \to S_n$. In case of $[(TTP)P^V Cl_2]^+$, though the onset of saturation started at slightly higher fluences than $[(TTP)P^V(OH)_2]^+$, saturation of the excited states is more predominant even with slight increase in the input fluence.

This is due to the longer lifetime of the high lying excited states S_n [42] leading to saturation in the absorption from the first excited singlet state S| at higher fluences.

	$[(TTP)P^V(OH)_2]^+$	$[(TTP)P^VCl_2]^+$
[a] τ_{Sn}	450 fs	600 fs
[a] σ_1/σ_0	2.67	3.56
[b] σ_2/σ_0	2.086	12.15
[b] τ_{isc}	1 ns	100 ps
[b] S_{th}	0.560 Jcm^{-2}	0.618 Jcm^{-2}

Table 3.2.2: Calculated figures of merit for optical limiting. [a] estimated from ps data and [b] ns data.

Faster ISC rate observed in $[(TTP)P^VCl_2]^'$ is in agreement with a similar observation made earlier for halogenated porphyrins [22,23], the difference being that in our case the substitution is in the axial site. The heavy atom effect arising from the spin-orbit coupling decreases the fluorescence quantum yield (On), hence increasing ISC. Even though the triplet lifetime is reduced, the ESA from triplet states is not reduced, as its lifetime (τ_{Tl}) is much larger than the exciting ns pulse duration.

3.2.5   Population relaxation - DFWM-ps results

Methods for the study of vibrational relaxation dynamics of excited state, fluorescence [43] from high lying states in a variety of porphyrins like TBP [44], OEP [45], TPP [46] and many other molecules include transient absorption spectroscopy, pump-probe studies and Raman spectroscopy [47]. Different relaxation pathways as well as the effects of solvent, temperature and metal-ions have been extensively studied using picosecond [48] and femtosecond [49] laser pulses.

Fig 3.2.9 (a) and (b) show the DFWM-ps signal for $[(TTP)P^V(OH)_2]^+$ and $[(TTP)P^VCl_2]^+$ respectively. Since the two orientational relaxation times of CS_2 are 200 fs and 2 ps [50], which are much smaller than the half-width of the pump

pulse, the CS_2 signal serves as an auto-correlation trace of the pump pulse. Open circles (o) are the experimental data for the samples and the solid line in Fig 3.2.9 is correlation curve with the reference sample CS2. Inset in Fig 3.1.9 shows the decay component and the fit for the decay. For both the molecules there is an obvious slower component in the decay. The decays are fitted to single exponential, from which the value of population relaxation time (TO is estimated. T, values are 46.95 ± 1.6 ps and 48.5 ± 2.7 ps for $[(TTP)P^V Cl_2]^+$ and $[(TTP)P^V(OH)_2]^+$ respectively. Temporal evolution of the signal has been checked at longer time delays (> 600 ps) also, and no thermal contribution was observed, as reported in certain other porphyrins (e.g. basket handle porphyrins) [51]. The values of T_1 are slightly faster than that of the other TTP's with different central metal atoms reported earlier [15]. No change is observed with the halogen substitution in these time scales.
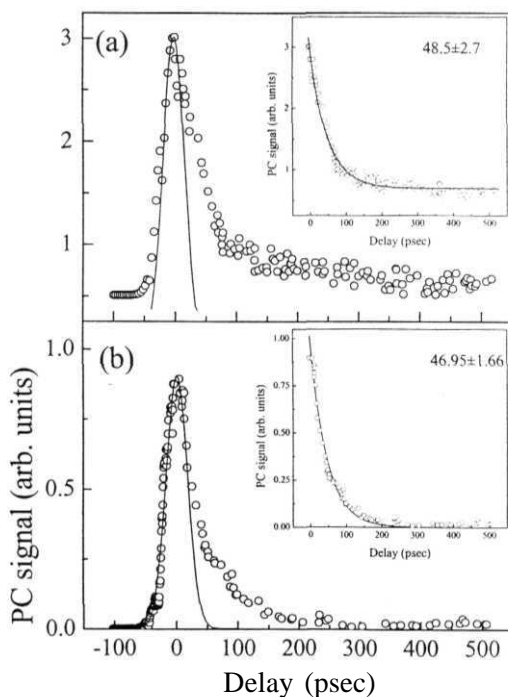
Figure 3.2.9: DFWM-ps relaxation of (a) $[(TTP)P^V(OH)_2]^+$ and (b) $[(TTP)P^V Cl_2]^+$. Inset shows the fit to the decay part of the signal.

3.2.6   <u>Conslusions</u>

➢ Greater polarization emanating from electronegative chlorine in the phosphorus porphyrin structure lead to a rise in the measured <y> values.

> Enhancement in <y> values by one order in ps regime and by three orders in ns regime respectively.

➢ Large enhancement in <y> at nanosecond timescale due to the excited triplet state.

> Reduction in the limiting threshold ($I_{1/2}$) by 30 times and 3 times with nanosecond and picosecond pulses respectively due to variation in the S_1 state because of heavy atom effect.

> Greater reduction in $I_{1/2}$ with the nanosecond pulses is due to faster ISC and enhanced ESA from triplet states.

3.3   Effect of charge transfer states on optical limiting: azoarene appended phosphorus (V) tetratolylporphyrins

3.3.1   <u>Photoinduced Electron Transfer (PET) and Excitation Energy Transfer (EET), Relevance of Charge-transfer states to Nonlinear Optics</u>

The basis of the photochemically active compounds (chromophores) is that following absorption of a photon of light they enter a long-lived electronically excited state. Of course all chemical compounds are in principle capable of electronic transitions in which an electron is promoted to a higher-energy state usually a HOMO→LUMO transition but in the vast majority of cases the excited state collapses very quickly back to the ground state, with evolution of heat as the electronic energy is converted to increased vibrational motion of the molecule. However, if the electronic excited state of the molecule survives for long enough, there is a possibility that it can interact with another molecule before it is deactivated, and the reactions of molecules in their electronically excited state are completely different from those which they under go in their ground state [52]. If no such interaction occurs then the excited state will be deactivated thermally, or sometimes by emission of photon (luminescence). Luminescent complexes are particularly useful as they tend to have long-lived excited states, and the loss of luminescence (quenching) is an obvious sign that the excited state complex is reacting with another group rather than undergo radiative decay.

The two main mechanisms by which an electronically excited molecule can pass its energy on to another molecule (a quencher) are electron transfer and energy transfer. These are illustrated schematically in Fig 3.3.1. It will be seen that promotion of an electron from a filled orbital to higher-energy empty orbital means that in the excited state the molecule is simultaneously a stronger oxidizing agent and a stronger reducing agent than it was in the ground state. The promoted electron is in a high-energy orbital and can transfer out to an electron poor quencher; i.e. it acts as a reducing agent. Alternatively, the low-energy hole left by the promoted electron can accept an electron from an

electron-rich quencher; i.e. the excited-state chromophore acts as an oxidizing agent. The type of electron transfer that occurs depends on the nature of the species that is interacting with the chromophore. In electron transfer, the excited state can be an electron donor or acceptor. In electron transfer, the energetics are dictated by the redox potentials of the donor and acceptor, as well as the energy of the excited state.
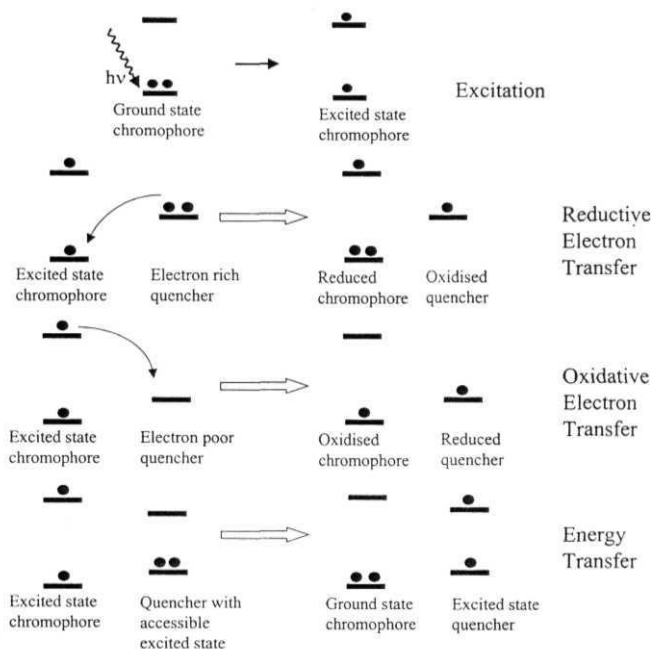
Figure 3.3.1: Electron transfer and energy transfer quenching of a chromophore excited state.

Energy transfer, in contrast, involves no net electron transfer; instead the excited state energy of the chromophore is transferred to the quencher, which itself enters an electronically excited state. This is more likely to occur if the quencher has a low-energy excited state available and is not amenable to oxidation or reduction. In energy transfer, the excited state is exclusively an energy donor. Energy transfer can operate by a dipole-dipole (coulombic) mechanism involving the mutual interaction of electrons. Since the mutual

contact between the reactants is not required, the dipole-dipole mechanism can be operative over large distances, sometimes greater than 50 A. Energy transfer by electron exchange, however, requires a closer approach of the reactants to allow for the mutual exchange of electrons. In this respect, energy transfer by electron exchange is similar to electron transfer. Efficient energy transfer requires that the excited-state energy of donor exceed that of acceptor. The media showing PET and EET are generally called as donor-acceptor (D-A) systems.

The phenomenon of photoinduced electron transfer (PET) is a result of one of the remarkable achievements of photochemistry. Certain molecules become powerful electron donors or acceptors on photoexcitation. This phenomenon of PET has attracted the interest from many fields. Interest in PET has uncovered novel pathways for synthesis of organic molecules [53], development of solar energy storage and conversion systems utilizing transition metal complexes [54], photosynthesis and electron-transport in biological systems [55], design of molecular computing devices, imaging, chemical sensors and photonic devices [56]. In PET, an electron migrates between a photo-excited and ground-state species. According to this concept, PET can be classified as a quenching pathway. In fact, like quenching by energy transfer, PET also involve a dynamic interaction between a photo-excited state and neighboring ground-state species.

Porphyrins and its arrays are one of the well-known media for PET and EET processes [57]. Donor-acceptor systems containing azulenic molecules are reported to show optical limiting properties [58]. Straightforward to synthesize and stable, porphyrins have an extended aromatic π-electron system that supports reversible electron transfer at accessible redox potentials. The HOMO-LUMO gap is in the visible region, making photoexcitation convenient in these molecules. A wide range of metal ions can be inserted into the porphyrin macrocycle, forming robust complexes that still have axial coordination sites available for simplistic ligand chemistry. In view of these properties, photoexcitation of the porphyrin *nn** electronic transitions can be harnessed to useful catalytic reactions via transient reduction or the oxidation of the central metal. Transition metals can introduce *d* orbitals at energies within HOMO-

LUMO gap, resulting in **the availability** of ligand→metal charge transfer (CT), metal → ligand CT, and/or *dd* excited states at energies below the lowest $\pi\pi^*$ state, and therefore accessible to photoexcitation via the strongly allowed *nn** transitions.   The CT states have metal ions that are transiently reduced or oxidized, while the porphyrin is transiently oxidized or reduced. Redox reactions of coordinated ligands can therefore be envisaged for CT states of metalloporphyrins. Because the recombination between the redox partners in intimate contact is facile, these states are usually short lived.

In this section, studies on a family of new class of phosphorus (V) tetratolylporphyrins with axial azobenzene chromophores are reported.   In these **porphyrins,** donor/acceptor levels and a charge transfer (CT) state is introduced due to the introduction of azoarene (AZT = 4-hydroxy, 4'-methyl azobenzene, AZB = 4-hydroxy azobenzene, AZN = 4-hydroxy, 4'-nitro azobenzene) subunits in place of H **in** axial (OH)" in 5,10,15,20-(tetratolyl) porphyrinato phosphorous (V) dihydroxide $[(TTP)P^V(OH)_2]^+$ without any charge-transfer states.   An intramolecular PET from the axial azoarene donors to the singlet-excited state of the basal phosphorus (V) porphyrin is responsible for quenching of fluorescence in these complexes [61]. We observed stronger RSA in the ns regime with the introduction of axial a/.oarene units. We also observed saturation of absorption of the S_1 states at higher fluence in the ps regime whereas, no such saturation of absorption behavior is observed with nanosecond pulses. The observed nonlinear absoiption and the phenomenon leading to such behavior is explained using a self-consistent rate equation model.

3.3.2   Molecular structure and linear optical properties

The samples are synthesized and purified according to the procedures reported in the literature [59]. The molecular structures and absorption spectra of the axial azoarene appended phosphorus (V) porphyrins are shown in Fig. 3.2.2 and Fig 3.2.3 respectively.   These molecules show linear absorption features typical of metalloporphyrins, with the high-energy B (Soret) band and the low energy Q bands. Each new molecule shows an additional moderately intense

absorption band in the UV region (~350nm) due to the axial azoarene chromophores. This band is absent in the spectrum of $[(TTP)P^V(OH)_2]^+$. The negative free energy change AG calculated using cyclic voltammetry [60] is an indication to the photoinduced electron transfer and the presence of the CT states. Each sample is subjected to a column chromatographic purification process prior to the measurements. In all experiments, sample solutions in chloroform are taken in 1-mm quartz cuvettes. The compounds remain stable even after long exposure to laser pulses for a long period of time, which was confirmed from the identical absorption spectra recorded before and after the exposure.

$R = H$ $[(TTP)P^V(-O-AZB)_2]^+$
$R = NO_2$ $[(TTP)P^V(-O-AZN)_2]^+$
$R = CH_3$ $[(TTP)P^V(-O-AZT)_2]^+$
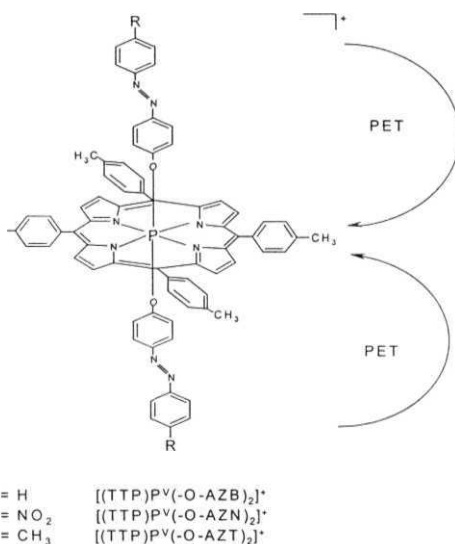
Figure 3.3.2: Molecular structure of Phosphorus (V) azoarene porphyrins

Fluorescence decay curves are shown in Fig 3.3.4 and all these three molecules show slow as well as faster components. The lifetimes are tabulated in Table 3.3.1. The fluorescence yield has gone down with the introduction of azoarene subunits. The fluorescence lifetimes varied quite considerably compared to the reference porphyrin $[(TTP)P^V(OH)_2]^+$. For $[(TTP)P^V(AZB)_2]^+$ the faster component is more dominant and for the other two molecules, the

slower components are dominant. A clear slowing down of the decay is observed
as expected.

Porphyrin	λ_{max} (nm)	ϕ	ΔG (eV)	τ_{S1} ns, (%)
$[(TTP)\,P^V(AZN)_2]^+$	630,679	0.069	-0.17	0.53 (30), 2 (33), 4.39 (36)
$[(TTP)\,P^V(AZB)_2]^+$	630,682	0.015	-0.16	0.26 (88), 2.33 (11)
$[(TTP)\,P^V(AZT)_2]^+$	631,680	0.003	-0.13	0.87 (31), 3.35 (68)

Error limits: λ_{em}, ± 2 nm ; ϕ, $\pm 10\%$

Table 3.3.1: Fluorescence yields (ϕ) and the singlet state lifetimes
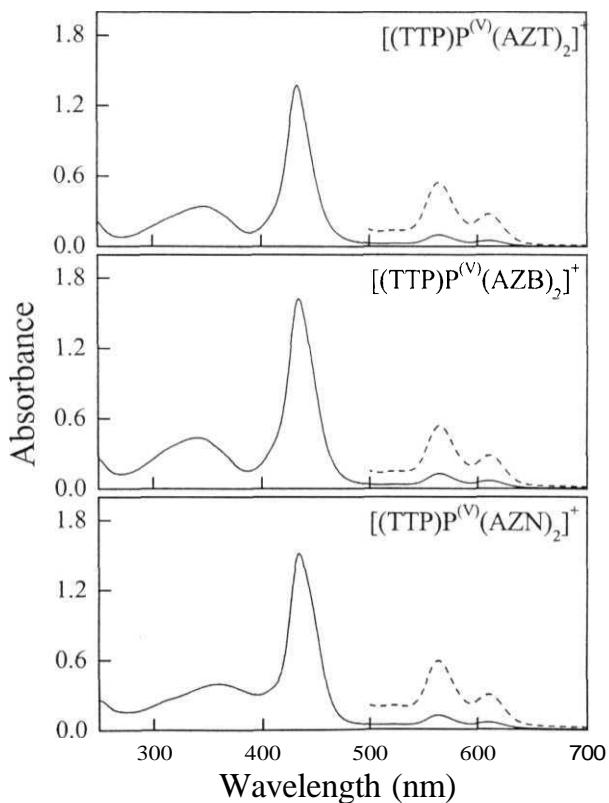
Figure 3.3.3: Absorption Spectra of Phosphorus (V) azoarene porphyrins
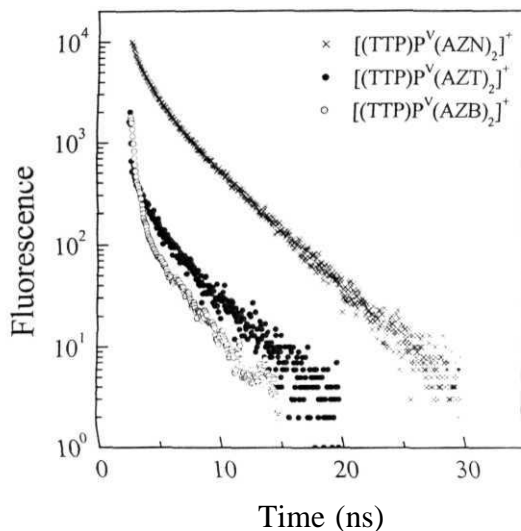
Figure 3.3.4: Fluorescence decays of axial-azoarene appended P^V TTP's.

Frequency doubled Nd: YAG lasers with 25 ps and 6 ns pulse widths, 10 Hz repetition rate are used for the experiments. We have employed standard backward degenerate four wave mixing (DFWM) geometry for the measurement of third order optical nonlinearity $\chi^{(3)}$. Optical limiting studies are performed using f/5 test bed and open aperture Z-scan studies are carried out, by focusing the input beam onto the sample with linear transmission of approximately 75% using lenses of 500 mm and of 125 mm focal length in case of ps and ns pulses respectively. The transmitted light is collected with a fast photodiode. The peak fluences used in the Z-scan experiments with 25 ps and 6 ns pulses are approximately 0.25-1.2 Jcm^{-2} and 3-4 Jcm^{-2} respectively. The studies are performed at the same concentration of ~10^{-4} M ensuring identical experimental conditions for both ps and ns regimes.

3.3.3   Third order nonlinear optical properties

The intensity dependence of phase conjugate signal with 25 ps pulses is shown in Fig. 3.3.5. Concentration dependence of the PC signal is shown in Fig. 3.3.6. The enhancement in the DFWM signal is quite obvious with the introduction of axial azoarene subunits. Solid line gives the fit to the cubic dependence of this signal with input intensity. The ratio of the signals for the conjugate beam in nanosecond DFWM experiment for parallel and perpendicular probe polarizations dropped down by just about 3 times, indicating that the nonlinearity is predominantly electronic in origin. The values of the effective microscopic second hyperpolarizability $<\gamma>$ with 25 ps pulses and 6 ns for the samples arc given in Table 3.3.2.
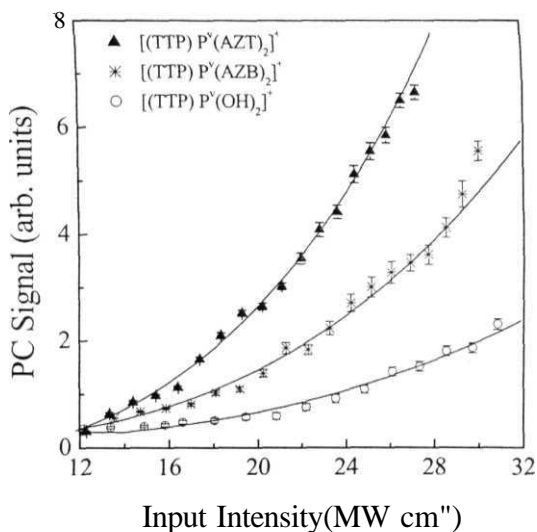
Figure 3.3.5: Intensity dependence of the PC Signal for Azoarene porphyrins with 25ps pulses. Solid lines show the cubic fit of the input intensity to the PC signal.

The second hyperpolarizability of these molecules is higher than that of the reference molecule $[(TTP)P^V(OH)_2]^+$ without CT states [12], by one order of magnitude in ps regime and by two orders of magnitude in the ns regime. This

clearly indicates that introduction of the azoarene groups into the phosphorus porphyrin structure leads to a rise in the measured <y> values. Similar enhancement in the hyperpolarizabilties is reported in CT complexes of C_{60} with aromatic amines [61]. Enhancement in <γ> due to the multidirectional intramolecular charge transfer transitions from the periphery to the center (PC-CT) [62] and due to nitro group in bis(N-phenyldithiocarbimato) Ni(II) complexes [63] is well reported.
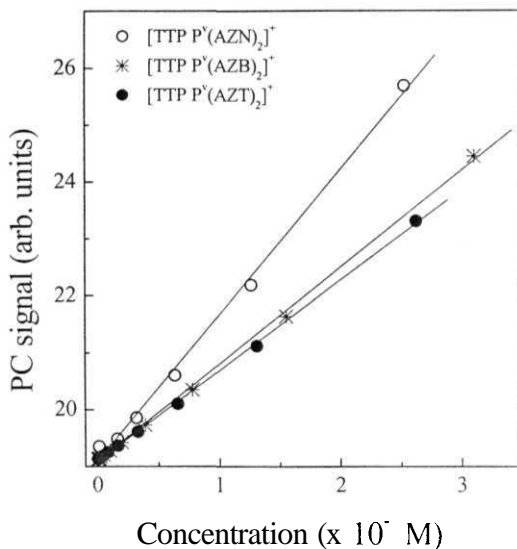
Figure 3.3.6: Concentration dependence of the PC signal of Azoarene porphyrins with 6 ns pulses. Solid lines show the cubic fit of the input intensity to the PC signal.

Porphyrin	<γ> ($*10^{-30}$esu)	<γ> ($*10^{-28}$esu)	$I_{1/2}$ (J/cm^2)
	25 ps	6 ns	6 ns
$[(TTP)P^V(OH)_2]^+$	0.286	3.2550	3.00
$[(TTP)P^V(AZT)_2]^+$	3.13±0.2	123.42±12	2.02
$[(TTP)P^V(AZB)_2]^+$	1.60±0.2	149.56±16	1.52
$[(TTP)P^V(AZN)_2]^+$	4.01±0.3	252.94±20	1.30

Table 3.3.2: Second hyperpolarizabilities of phosphorus (V) azoarene porphyrins with 25 ps pulses and 6 ns pulses. $I_{1/2}$ is the limiting threshold.

3.3.4   Optical limiting and nonlinear absorption

The optical limiting curves for these molecules with 6ns pulses are shown in Fig. 3.3.7 for a linear transmission of 75%. The limiting threshold is reduced in azoarene-appended porphyrins by a factor of two as can be seen from the threshold values $I_{1/2}$ given in Table 3.3.2. Figure 3.3.8 shows the optical limiting curves for one of the representative azoarene molecules $[(TTP)P^V(AZT)_2]^+$ at 80%, 60% and 40% linear transmittance. The clamping levels can be seen to reduce linearly with increasing ground state absorption. Photoinduced electron transfer from the excited state of conjugated polymers onto C_{60} [64] and in porphyrin-viologen dyads [65] is reported to enhance nonlinearity and optical limiting performance. In these molecules the population from the first singlet state S_1 can relax to triplet T_1 or to ground state So via non-fluorescent CT state in addition to $S_1 \rightarrow S_0$ and $S_1 \rightarrow T_1$ transitions.
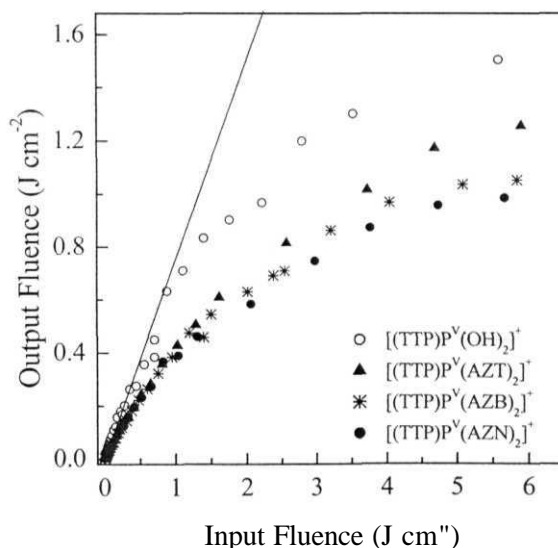
Figure 3.3.7: Optical limiting curves of azoarene porphyrins at 75% linear transmittance with 6ns pulses.
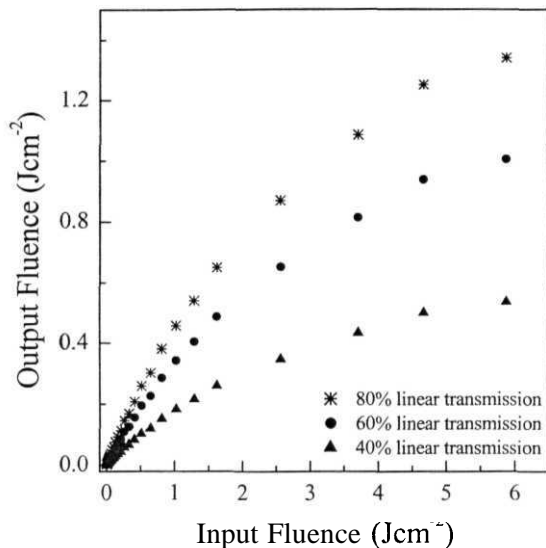
Figure 3.3.8: Optical limiting curves of $[(TTP)P^V(AZT)_2]^+$ at linear transmittances of 80%, 60% and 40%.

Fig. 3.3.9 shows the open aperture Z-scan curves with 25ps pulses. The open aperture Z-scan curves with 6 ns pulses for these molecules are shown in Fig. 3.3.10 with a normalized transmittance at focus (To) of 0.431, 0.476 and 0.521 for $[(TTP)P^V(AZN)_2]^+$, $[(TTP)P^V(AZB)_2]^+$ and $[(TTP)P^V(AZT)_2]^+$ respectively. Peak fluences used for the experiment are also shown in Fig. 3.2.10. In the ns regime open aperture Z-scan curves shows only RSA even at high fluences indicating the dominance of ESA from $T_1 \rightarrow T_n$ through ISC from $CT \rightarrow T_1$.

In our attempts to explain the results of the 6 ns and 25 ps experiments, a six-level model explaining various mechanisms occurring in these molecules has been used (Fig. 3.3.11). A self-consistent theoretical analysis, based on the rate equations describing the different mechanisms in the molecule and the output transmittance is developed. The rate equations are solved numerically using Runge-Kutta fourth order method as explained in section 2.11. Solid lines in the figures with Z-scan curves show the theoretical fits.
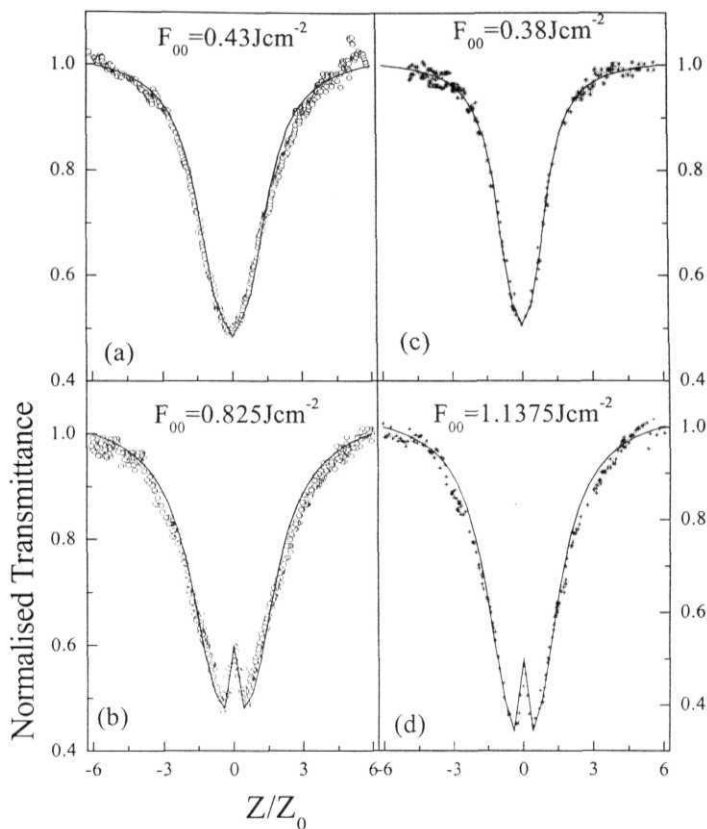
Figure 3.3.9: Open aperture Z-scan curves of (a,b) $[(TTP)P^V(AZN)_2]'$ and (c,d) $[(TTP)P^V(AZB)_2]'$ with 25ps pulses at different peak fluences(F_{00}). Solid lines show the theoretical fit using energy level diagram.

Laser light excites molecules from the ground state S_0 into one of the manifold of vibrational-rotational states in the first excited singlet state $S_0 \rightarrow S_1$ (do), which relaxes very rapidly ($\sim$ ps) to the lowest level of this electronic state. This level relaxes either by nonradiative decay into the CT state and from there to first triplet state (ISC), or by both radiative and nonradiative decay within the singlet system. ESA can occur from the singlet state S_1 up to a higher singlet state S_n (a,) and from the triplet state up to a higher triplet state $T_n(\sigma_2)$. For ps

pulse excitation, triplet level contribution to the nonlinear absorption can be neglected due to the slower intersystem crossing rate and absorption due to the CT states is included in σ_1 cross section. Whereas with ns pulse excitation the triplet levels play an important role. In the ps regime only three singlet levels (So, S_1 and S_n) along with the charge transfer level (CT) play a major role and hence the six-level model effectively becomes a four level model. In the ns regime, So, S_1, T_1, T_n and charge transfer (CT) states including ISC from CT $\rightarrow T_1$ will play a dominant role.
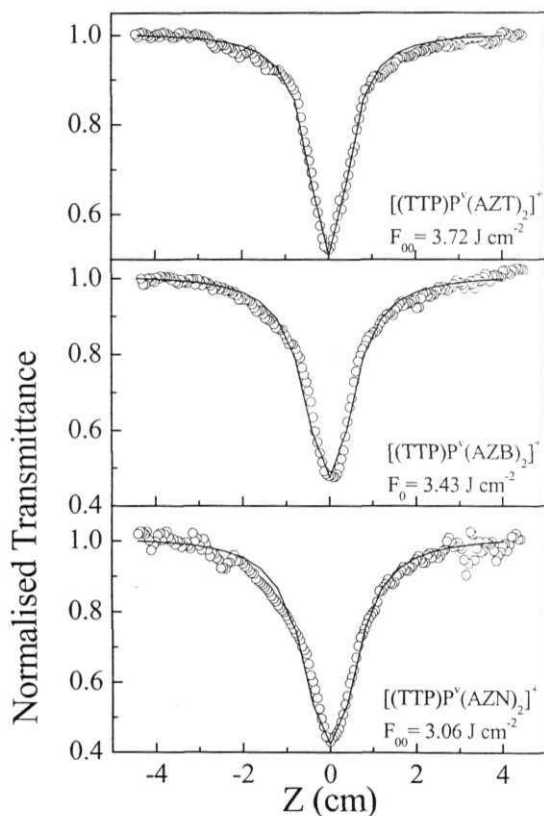
Figure 3.3.10: Open aperture Z-scan curves of azoarene appended P^VTTP's with 6 ns pulses. Solid lines show the theoretical fit using energy level diagram. Peak fluence(F_{00}) is also shown.

The parameters leading to enhanced limiting performance and nonlinear absorption with ns pulses and ps pulses, along with the parameters used for the estimation are given in Tables 3.3.3 and 3.3.4. Lifetimes of higher excited singlet state and the ISC obtained from theoretical modeling are also given. The fluence at which the saturation of excited states has started, saturation threshold (S_{th}), which is one of the important parameters in deciding the capability of a material as optical limiter, is also given in Table 3.3.3. S_{th}, (0.628 - 0.802 Jcm^{-2}) for the these molecules is found to be higher than that for $[(TTP)P^V(OH)_2]^+$ (0.56 Jcm^{-2}). The figures of merit (σ_1/σ_0 and *ty/oo)* for our molecules are compared with reference porphyrin $[(TTP)P^V(OH)_2]^+$ (Table 3.3.4). The enhancement in σ_1/σ_0 and σ_2/σ_0 due to the presence of additional CT state can be clearly seen compared to the reference porphyrin. The values of σ_1/σ_0 and σ_2/σ_0 for these porphyrins was found to be higher than some of the earlier reported molecules and comparable to some of the porphyrins, dyes [40-42,67,44] and fullerenes and fullerene derivatives [68].
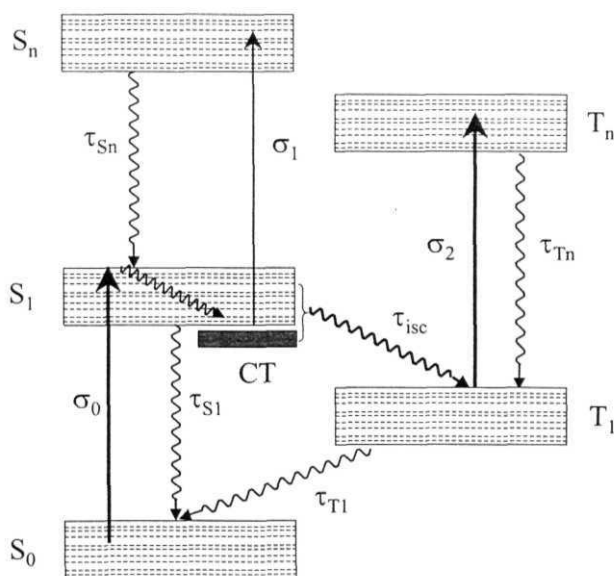
Figure 3.3.11: Energy level diagram of phosphorus (v) azoarene porphyrins

The presence of CT state, and internal conversion from CT state to singlet So and intersystem crossing from CT to triplet T_1 plays a significant role in enhanced RSA in ns regime. In the ps regime, as population from S_1 can relax faster to So, via CT states, the saturation of ESA in $S_1 \rightarrow S_n$ transition, which leads to SA in RSA at higher intensities is also reduced considerably increasing S_{th}.

Porphyrin	$^a\tau_{Sn}$ (fs)	$^b\tau_{isc}$ (ps)	$^aS_{th}$(Jcm^{-2})
$[(TTP)P^V(AZB)_2]^+$	440	750	0.802
$[(TTP)P^V(AZT)_2]^+$	415	620	0.628
$[(TTP)P^V(AZN)_2]^+$	375	500	0.712

Table 3.3.3: Lifetimes of higher excited state, ISC times and saturation threshold of the phosphorus (V) azoarene porphyrins. Estimated from Z-scan curves with ^{a}25 ps pulses and from ^{b}6 ns pulses. S_{th} is the saturation threshold.

Porphyrin	σ_1/σ_0	
$[(TTP)P^V(OH)_2]^+$	2.67	2.086
$[(TTP)P^V(AZB)_2]^+$	2.93	4.76
$[(TTP)P^V(AZT)_2]^+$	2.88	8.44
$[(TTP)P^V(AZN)_2]^+$	3.07	9.28

Table 3.3.4: Figures of merit for optical limiting for the phosphorus (V) azoarene porphyrins, estimated from Z-scan curves with 25 ps pulses and from 6 ns pulses. Values for $[(TTP)P^V(OH)_2]^+$ are also given for comparison.

3.3.5   Population relaxation - DFWM-ps results

Porphyrins have been at the center of the intramolecular electron transfer using covalently attached electron donor acceptor molecules because of the convenience of photoexcitation in initiating the electron transfer [69]. Donor-acceptor groups have been attached to the periphery of the porphyrin ring, and porphyrin-based molecular triads, tetrads and pentads have been created and reported to support quite long charge-separated states [70]. By covalently attaching one or more donors or acceptors, it might be possible to further transfer

the electron or hole localized on the porphyrin in a CT state before it recombines with the hole or electron on the metal ion resulting in the extended lifetime of the charge-separated state.

Regular metal porphyrins display a strong transition around 420 nm denoted by soret band. Upon absorption, the S_2 state of the porphyrin is populated. The energy difference between the S_1 and S_2 state is almost 1 eV. This large energy difference contributes to make the lifetime of the S_2 state relatively long, according to the energy gap law. Electron transfer reactions from different excited states in porphyrins and the effect of changing the energy of the link connecting the donor and acceptor are well studied. When an electron acceptor was attached to the porphyrin, electron transfer was reported to compete with S_2 to S_1 relaxation. Porphyrins have been used in number of synthetic model systems for photosynthetic reactions and electron transfer has been demonstrated to occur on a subpicosecond time scale [71,72]. These studies have all considered electron transfer reactions from the S_1 state. Despite the large number of porphyrin donor-acceptor studied, reports on reactions from the S_2 state are relatively less [73]. Energy transfer from the S_2 state of a Zn-porphyrin linked to $Ru(bpy)_3{}^{2+}$ was reported [74] with a lifetime of few ps for the S_2 state, electron transfer reactions could occur prior to internal conversion to S_1, if the donor and acceptor are strongly coupled.

The presence of donor-acceptor subunits is reported to vary the relaxations considerably and population relaxation has varied considerably with the axial azoarene subunit (Fig.3.3.12). The porphyrin with AZN subunit has a longer relaxation of 126.19 ± 4.91 ps compared to the porphyrins with AZT and AZB subunits having faster relaxations of 45.08 ± 1.42 ps and 52.1 ± 1.1 ps respectively. Donor-acceptor porphyrins having a CT state are well studied using various techniques like ps transient absorption spectroscopy and pump-probe spectroscopy. Electron transfer demonstrated by pump-probe spectroscopy in water-soluble $ZnTPPS^4$ to methyl viologen (MV^{2+}) is very fast (< 200 fs) in the complex where as in the absence of MV^{2+}, the lifetime is 1.3 ps [73]. In Co(ll)porphyrins [75], the ground state recovery time was estimated to be less

than 50ps. Similar studies in Co" and Co^{III} octaethylporphyrins (in toluene) [76] revealed two distinct time scales with different spectral signatures.
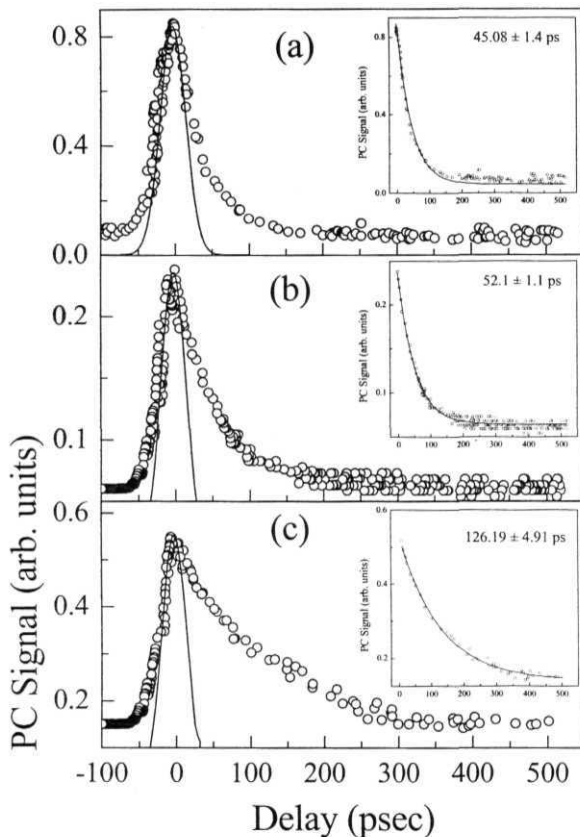
Figure 3.3.12: DFWM-ps curves for (a)$[(TTP)P^{(V)}(AZT)_2]^+$, (b)$[(TTP)P^{(V)}(AZB)_2]^+$ and (c) $[(TTP)P^{(V)}(AZN)_2]^+$. Inset shows the fit to the decay part.

In Co" porphyrin the mixing of the state, which is due to the unpaired electron with the normal singlet and tiplet states produces doublets and quartets. The ground state becomes a doublet; the lowest excited states become the singdoublet $[^2Q(\pi,\pi^*)]$, the tripdoublet $[^2T(\pi,\pi^*)]$, and tripquartet $[^4T(\pi,\pi^*)]$. The two lifetimes of the former were estimated to be <10 and 10-20 ps, which

were attributed to the **deactivation** of the $^2T(\pi,\pi^*)$ and the CT state. The lifetimes for Co^{III} sample was found to be ~ 5ns. Femtosecond dynamics in solvents of varying polarity and structure [77] for Co(II)TTP revealed the relaxation time-scales to be 0.2,2,20-200 ps in different solvents. The longest component is found to be different for each of the solvent: benzene (16 ps), dichloroethane (23 ps), pyridine (40 ps) and piperidine (190 ps) due to the presence of a CT state. In excited Cu(II) protoporphyrins the ground state recovery time increases rapidly from highly polar solvents like pyridine (~ 45 ps) to nonpolar solvents like benzene (~ 400 ps) due to the presence of CT state involved with the axial coordination of more polar solvents [77]. For Cu(II) porphyrin, after ps excitation a Frank-Condon state of $^2S_1$ is populated which decays into the $^2T_1$ within 8 ps. This state relaxes with time constant of ~450 ps to the $^2T_1$ state and $^4T_1$ equilibrium state from which phosphorescence is emitted [79]. In Cu(II)TPP and OEP ring-to-metal CT state is found to have lifetime as long as 30-40 ns [80] In case of water soluble Cu porphyrin, the relaxation dynamics of the excited states to be completed within 100 ps and the different timescales observed were 100 fs, 1.2, 4 and 25 ps due to the split triplet states and a new quenched state [81]. In case of Cu it is well understood that the unpaired electrons split the singlet S_1 and triplet T_1 thereby creating new pathways of relaxations including the presence of a CT state or metal state.

3.3.6   Conclusions

➢ Enhancement in <y> due the appended axial azoarene subunits to porphyrin ring

➢ One order higher in ps regime, greater than that of some Tetrabenzoporphyrins.

➢ Higher nonlinearity in ns regime by two orders is predominantly electronic in origin.

➢ Enhancement in optical limiting performance is due to enhanced excited state absorption from $T_1 \rightarrow T_n$ because of faster intersystem crossing from CT state to T_1 due to charge transfer states.

> Limiting Threshold has lowered by a factor of 2.

➢ Faster relaxations from the excited states become slightly longer with higher electronegative AZN subunit.

> Saturation of ESA has reduced considerably compared to porphyrin with axial (OH) and chlorine substituents

> Can be easily doped into polymers to increase the stability.

3.4   References

1. J.-H. Chou, M.E. Kosal, H.S. Nalwa, N.A. Rakow and K.S. Suslick, in *The Porphyrin Handbook,* Vol.6, Ch. 41, eds: K. Kadish, K. Smith, R. Guilard, Academic Press, New York, 2000; N.R. Armstrong, *J. Porphyrins Phthalocyanines,* 4, 414 (2000); K.S. Suslick, *Comprehensive supramolecular chemistry; Bioinorganic systems;* Elsevier: Oxford, Vol.5 1996; R.F. Abrahams, B.F. Hoskins, N.M. Michall, and R. Robson, *Nature* **369,** 727 (1994).

2. M. Gouterman, In *The Porphyrins,* Vol 3, pp1-165, ed.: D. Dolphin, Academic, New York (1978).

3. P.O. Schouten, J.M. Warman, M.P. de Haas, M.A. Fox, and H.-L. Pan, *Nature* **353,** 736 (1991); C.Y. Liu, H.-L. Pan, H. Tang, M.A. Fox, and A.J. Bard, *J. Phys. Chem.* 99, 7632 (1995); B.A. Gregg, M.A. Fox, and A.J. Bard, *J. Phys. Chem.* 94, 1586 (1990); C.-H. Liu, H.-L. Pan, M.A. Fox, and A.J. Bard, *Science,* 261, 897 (1993); *Chem. Mater.* 9, 1422 (1997); G.R. Fleming, J.-L. Martin, and J. Breton, *Nature* **333,** 190 (1988); M.P. Debreczeny, W.A. Svec, and M.R. Wasielewski, *Science* **274,** 584 (1996).

4. K.S. Suslick, C.T. Chen, G.R. Meredith, and L.T. Cheng, *J. Am. Chem. Soc.* **114,** 6928 (1992); H. Chou, C.T. Chen, K.F. Stork, P.W. Bohn, and K.S. Suslick, *J. Phys. Chem.* 98, 383 (1994); A. Sen, P.C. Ray, P.K. Das, and V. Krishnan, *J. Phys. Chem.* **100,** 19611 (1996); A. Sen, and V. Krishnan, *J. Chem. Soc, Faraday Transactions.* 93, 4281 (1997); S. Priyadarshy, M.J. Therien, and D.N. Beratan, *J. Am. Chem. Soc.* **118,** 1504 (1996); S.M. LeCoers, H.W. Guan, S.G. Dimango, CH. Wang, and M.J. Therien, *J. Am. Chem. Soc.* **118,** 1497 (1996); L. Karki, F.W. Vance, J.T. Hupp, S.M. LeCoers, and M.J. Therien, *J. Am. Chem. Soc.* **120,** 2606 (1998); M. Yueng, A.C.H. Ng, M.G.B. Drew, E. Vorpagel, E.M. Breitung, R. McMahon, and D.K.P. Ng, *J. Org.Chem.* 63, 7143 (1998); I.D.L. Albert, T.J. Marks, and M.A.

Ratner, *Chem. Mater.* 10, 753 (1998); D. Li, B. Swanson, J.M. Robinson, and M.A. Hoffbauer, *J.Am. Chem. Soc.* **115,** 6975 (1993).

5. C. Mclony, H. Byrne, W.H. Dennis, W.J. Blau, and J.M. Kelly, *Chem. Phys.* **121,21** (1992).

6. D.V.G.L.N. Rao, F.J. Aranda, J.F. Roach, and D.E. Remy, *Appl. Phys. Lett.* **58,** 1241 (1991); S, Guha, K. Rang, P. Porter, J.F. Roach, D.E. Remy, F.J. Aranda, and D.V.G. L.N. Rao, *Opt.Lett.* 17, 264 (1992); D.V.G.L.N. Rao, F.J. Aranda, D.E. Remy, and J.F. Roach, *Int. J. of Nonlinear Opt. Phys.* 3, 511 (1994).

7. T. Sagakuchi, Y. Shimizu, M. Miya, T. Fukumi, K. Ohta, and A. Nagata, *Chem. Lett.* 281 (1992).

8. M. Hosada, T. Wada, A.F. Garito, and H. Sasabe, *Jpn. J. Appl. Phys.* 31, L249 (1992); J. *Phys. Chem.* 96, 10534 (1992).

9. R.A. Norwood, and J.R. Sounik, *Appl Phys. Lett.* 60, 295 (1992).

10. G.R. Kumar, M. Ravikanth, S. Banerjee, and A. Sevian, *Opt. Commun.* **144,** 245 (1997).

11. H.L. Anderson, S.J. Martin, and D.D.C. Bradley, *Angew. Chem.* **Int.** *Ed. Engl.* 33, 655 (1994); Z. Bao, and L. Yu, *Proc. ACS meeting. Polym. Mater. Sci. (PMSE)* 71, 781 (1994); A. Sinha, B. Bihari, K. Mandal, and L. Chen, *Macromolecules*, **28,** 5681 (1995).

12. S.V. Rao, N.K.M.N. Srinivas, D.N. Rao, L. Giribabu, B.G. Maiya, R. Philip, G.R. Kumar, *Opt. Commun.* **182,** 255 (2000); P.P. Kiran, D.R. Reddy, B.G. Maiya, and D.N. Rao, *Opt. Materials.* 21,565 (2002).

13. Z.H. Kafafi, S.R. Flom, H.W. Sarkas, R.G.S. Pong, CD. Merritt, and F.J. Bartoli, *Proc. SPIE* **2284,** 134 (1994); S.R. Flom, R.G.S. Pong, F.J. Bartoli, and Z.H. Kafafi, *Nonlinear Optics* 10, 183 (1995); F. Kajzar, Y.O. Shudo, C. Merritt, and Z.H. Kafafi, *Synthetic Metals,* 94, 91 (1998).

14. W.J. Blau, H. Byrne, W.M. Dennis and J.M. Kelly, *Opt. Commun.* 56, 25 (1985); A. Sevian, M. Ravikanth and G. R. Kumar, *Chem. Phys. Lett.* 263, 241 (1996); N.K.M.N. Srinivas, S.V. Rao, D.V.G.L.N. Rao, B.K. Kimball, M. Nakashima, B.E. Decristofano and D.N. Rao, *J. Porphyrins Phthalocyanines*, 5, 549 (2001); P.P. Kiran, D.R. Reddy, B.G. Maiya, A. Dharmadhikari, G.R. Kumar and D.N. Rao, *Appl. Opt.* **41,** 7631 (2002); N. Tang, W. Su, T. Cooper, W. Adams, D. Brandelik, M. Brant, D. McLean, and R. Sutherland, *Proc. of SPIE.* **2853,** 149 (1996).

15. D.N. Rao, S.V. Rao, F.J. Aranda, D.V.G.L.N. Rao, M. Nakashima, and J.A. Akkara, *J. Opt. Soc. Am. B* **14,** 2710 (1997); S. V. Rao, N.K.M.N. Srinivas, D.N. Rao, L. Giribabu, B.G. Maiya, R. Philip, and G.R. Kumar, *Opt. Commun.* **192,** 123 (2000).

16. S.P. McGlynn, T. Azumi, M. Kinoshita, "*Molecular Spectroscopy of the Triplet State",* Prentice-Hall, Englewood Cliffs, NJ, 1969.

17. S.J. Formosinho, *J. Chem. Soc. Faraday Trans.* -II, 70, 605 (1974).

18. R. Englmar, and J. Jortner, *Mol. Phys.* 18, 145 (1970).

19. O.S. Mortensen, W. Siebrand, A.W. Tarr, *Chem. Phys.* **125,** 231 (1988).

20. S.I. Yang, J. Seth, J.-P. Strachan, S. Gentemann, D. Kim, D. Holten, J.S. Lindsey, D.F. Bocian, *J. Porphyrins Phthalocyanines* **3,** 117 (1999); M. Pineiro, A.L. Carvalho, M.M. Pereira, A.M.D.A.R. Gonsalves, L.G. Arnaut, S.J. Formosinho, *Chem. Eur. J.* 4, 2299 (1998); J.R. Darwent, P. Douglas, A. Harriman, G. Porter, M.-C. Richoux, *Coord. Chem. Rev.* **44,** 83 (1982).

21. R. Bonnet, A. Harriman, A.N. Kozyrev, *J. Chem. Soc. Faraday Trans.* 88 763 (1992).

22. K.M. Smith, *"Pophyrins and Metalloporphyrins",* Elsevier: Amsterdam, (1975).

23. K. Kalyanasundaram, "*Photochemistry of Polypyridine and Porphyrin Complexes",* Academic Press, New York, (1992); M.C. Tamargo and D.O. Cowan, *J. Am. Chem. Soc,* **104,** 1107 (1982); K. Okada, M. Yamaji and H. Shizuka, *Chem. Phys. Lett.* **254,** 79 (1996); K. Ruud, B. Schimmelpfennig, and H. Agren, *Chem. Phys. Lett.***310,** 215 (1999); K.B. Eisenthal and M.A. El-Sayed, *J. Am. Chem. Soc.* 794 (1964).

24. M. Gouterman, F.D. Schwarz, P.D. Smith and D. Dolphin, *J. Chem. Phys.* 59, 676 (1973); D. Dolphin, T.G. Taylor and L.Y. Xie, *Acc. Chem. Res.* 30 251 (1997); D.J. Quimby and F.R. Long, *J. Am. Chem. Soc.* 97, 5111(1975); R.A. Freitag and D.G. Whitten, *J. Phys. Chem.* 87, 3918 (1983); R. Bonnett, I.H. Campion-Smith, A.N. Kozyrev, and A.F. Mironov, *J. Chem. Res.* 138, (1990); F. D'Souza, A. Villard, E. Van Caemelbecke, M. Franzen, T. Boschi, P. Tagliatesta, and K.M. Kadish, *Jnorg. Chem.* 32, 4042 (1993). T. Takeuchi, H.B. Gray, and W.A. Goddard, *J. Am. Chem. Soc.* **116,** 9730 (1994); J.A. Hodge, M.G. Hill, and H.B. Gray, *Inorg. Chem.* 34, 809 (1995); K.M. Baskigia, M.D. Barber, J. Fajer, C.J. Medforth, M.W. Renner, and K.M. Smith, J. *Am. Chem. Soc.* **112,** 8851 (1990); P. Ochsenbein, K. Ayougou, D. Mandon, J. Fischer, R. Weiss, R.N. Austin, K. Jayaraj, A. Gold, J. Terner, J. Fajer, *Angew. Chem. Int. Ed. Engl.* **33,** 348 (1994).

25. T. Barbour, W.J. Belcher, P.J. Brothers, C.E.F. Rickard, and D.C. Ware, *Inorg. Chem.* 31,746(1992).

26. K. Kandasamy, S.J. Shetty, P.N. Puntambekar, T.S. Srivastava, T. Kundu and B.P. Singh, *J. Porphyrins Phthalocyanines,* 3, 81 (1999); K. Kandasamy, S.J. Shetty, P.N. Puntambekar, T.S. Srivastava, T. Kundu and B.P. Singh, *Chem. Commun.* **1159** (1997).

27. S. Guha, K. Kang, P. Porter, J.F. Roach, D.E. Remy, F.J. Aranda, and D.V.G.L.N. Rao, *Opt. Lett.* **17,** 264 (1992); B.R. Kimball, M. Nakashima, B.S. DeCristofano, N.K.M.N. Srinivas, P.P. Kiran, D.N. Rao, A. Panchangam and D.V.G.L.N. Rao, *Proc. of SPIE,***4106,** 264 (2000).

28. W. Su, T.M. Cooper, M.C. Brant, *Chem. Mater.* 10, 1212 (1998).

29. W. Su, T.M. Cooper, K. Nguyen, M.C. Brant, D. Brandelik, D.G. McLean, *Proc. SPIE.* **3472,** 136 (1998).

30. A. Krivokapic, H.L. Anderson, G. Bourhill, R. Ives, S. Clark, and K.J. McEwan, *Adv. Mater.* 13 652(2001).

31. K. Kamada, T. Sugio, M. Ueda, K. Tawa, Y. Shimizu, K. Ohta, *Chem. Phys. Lett.* **302,** 615 (1999).

32. K. Mansour, D. Alvarez, K.J. Perry, I. Choong, S.R. Marder and J.W. Perry, *SPIE Org. Biol. Optoelectron.* **1853,** 132 (1993); J.W. Perry, K. Masour, S.R. Marder, K.J. Perry, D. Alvarez Jr., and I. Choong, *Opt. Lett.* 19, 625 (1994); C. Liu, X. Wang, Q. Gong, Y. Liu, W. Qiu and D. Zhu, *Chem. Phys. Lett.* 347, 378 (2001).

33. P. Bhyrappa, M. Nethaji, and V. Krishnan, *Chem. Lett.* 869 (1993).

34. D. Mandon, P. Ochsenbein, J. Fischer, R. Weiss, K. Jayaraj, R.N. Austin, A. Gold, P.S. White, O. Brigaud, P. Battioni, and D. Mansuy, *Inorg. Chem.* **31,** 2044 (1992); E.R. Birnbaum, J.A. Hodge, M.W. Grinstaff, W.P. Schaefer, L. Henling, J.A. Labinger, J.E. Bercaw, and H.B. Gray, *Inorg. Chem.* 34, 3625 (1995).

35. S. Gentemann, C.J. Medforth, T.P. Forsyth, D.J. Nurco, K.M. Smith, J. Fajer, and D. Holten, */. Am. Chem. Soc.* **116,** 7363 (1994);

36. N.J. Turro, pp 153-198, "*Modern Molecular Photochemistry*", University Science Books, Sausalito, (1994).

37. M. Gouterman, *7. Mol. Spectroscopy* 6, 138 (1961).

38. X. Wang, C. Liu, Q. Gong, Y. Huang and C. Huang, *Opt. Commun.* **197,** 83 (2001).

39. J. Si, M. Yang, Y. Wang, L. Zhang, C. Li, D. Wang, S. Dong, and W. Sun, *Appl. Phys. Lett,* **64,** 3083 (1994).

40. S.N.R. Swatton, K.R. Welford, S.J. Till and J.R. Sambles, *Appl. Phys. Lett.* 66, 1868 (1995).

41. T-H. Wei, T-H. Huang, H-D. Lin and S-H Lin, *Appl. Phys. Lett.* **67,** 2266 (1995).

42. S. Huges, G. Spruce, B.S. Wherrett, K.R. Welford, and A.D. Lloyd, *Opt. Commun.* **100,** 113 (1993); X. Deng, X. Zhang, Y. Wang, Y. Song, S. Liu, and C. Li, *Opt. Commun.* **168, 207 (1999).**

43. A. Harriman, *J. Chem. Soc. Faraday Transactions* 1, 76, 1978 (1980); ibid *J. Chem. Soc. Faraday Transactions* 1, 77, 369 (1981); *J. Chem. Soc. Faraday Transactions 2,* 77, 1281 (1981); J. Rodriguez, C. Kirmaier and D. Holten, *J. Am. Chem. Soc.* **111,** 6500(1989).

44. G.G. Gurzadyan, T.-H. Tran-Thi, and T. Gustavsson, *J. Chem. Phys.* **108,** 385 (1998); H. Stiel, A. Volkmer, 1. Ruckmann, A. Zeug, B. Ehrenberg and B. Roder, *Opt. Commun.* **115,** 135 (1998); P. Chen, I.V. Tomov, A.S. Dvornikov, M. Makashima, J.F. Roach, D.M. Alabran and P.M. Rentzepis, *J. Phys. Chem.* **100,** 17507(1996).

45. N. Serpone, T.L. Netzel, and M. Gouterman, *J. Am. Chem. Soc.* **104,** 246 (1982).

46. M.M. Devane, *Opt. Commun.* **52,** 136 (1984).

47. J. Rodriguez, C. Kirmaier and D. Holten, *J. Chem. Phys.* 94, 6020 (1994); C. Galli, K. Wynne, S.M. LeCours, M.J. Therien and R.M. Hochstrasser, *Chem. Phys. Lett.* 206, 493 (1993); R. Kumble, S. Palese, V.S.-Y. Lin, M.J. Therien and R.M. Hochstrasser, *J. Am. Chem. Soc.* **120,** 11489 (1998); R. Khairutdinov, and N. Serpone, *J. Phys. Chem.B* **103,** 763 (1999); J.R. Andrews, and R.H. Hochstrasser, *Chem. Phys. Lett.* 76, 21 (1980); D. Kim, D. Holten, M. Gouterman and J.W. **Buchler,** *J. Am. Chem. Soc.* **106,** 4015 (1984); S. Akimoto, T. Yamazaki, I. Yamazaki and A. Osuka, *Chem. Phys. Lett.* **309,** 177 (1999); I. Yamazaki, S. Akimoto and T. Yamazaki, *ActaPhysica Polonica A* 95, 105 (1999).

48. J. Aaviskoo, A. Freiberg, S. Savikhin, G.F. Stelmakh, and M.P. Tsvirko, *Chem. Phys. Lett.* **111,** 275 (1984); S. Gentemann, C.J. Medforth, T. Ema, N.Y. Nelson, K.M. Smith, J. Fajer and D. Holten, *Chem. Phys. Lett.* **245,** 441 (1995); D. Kim, C. Kirmaier and D. Holten, *Chem. Phys.* 75, 305 (1983); O. Bilsel, J. Rodriguez, D. Holten, *J. Phys. Chem.* 94, 3508 (1990).

49. G.E.O'Keefe, G.J. Denton, E.J. Harvey, R.T. Phillips, R.H. Friend, and H.L. Anderson, *J. Chem. Phys.* **104,** 805 (1996).

50. T. Kobayashi, A. Terasaki, T. Hattori and K. Kurokawa, *Appl. Phys.B* 47, 107 (1988).

51. G.R. Kumar, M. Ravikanth, S. Banerjee and A. Sevian, *Opt. Commun.* **144,** 245 (1997).

52. A. Juris, V. Balzani, F. Barigelletti, S. Campagna, P. Belser, and A. von Zelewsky, *Coord. Chem. Rev.* **84,** 85 (1988); T.J. Meyer, *Acc. Chem. Res.* **22,** 163 (1989); M.D. Ward, *Chem. Soc. Rev.* **26,** 365 (1997).

53. G.J. Kavarnos, and N.J. Turro, *Chem. Rev.* **86,** 401 (1986); G. Pandey in Topics in Current Chemistry **168,** *Photoinduced Electron Transfer V,* ed: J. Mattay, Springer-Verlag(1993).

54. I. Willner, E. Kaganer, E. Joselevich, H. Durr, E. David, M.J. Gunter, and M.R. Johnston, *Coord. Chem. Rev.* **171,** 261 (1985); L. Flamigni, F. Barigelletti, N. Armaroli, J.-P. Collin, I.M. Dixon, J.-P. Sauvage, and J.A.G. Williams, *Coord. Chem. Rev.* **190-192,** 1299 (1999); J.S. Connolly Ed., *Photochemical conversion and storage of solar energy,* Academic, New York (1981).

55. K.I. Zamarev, and R.F. Khairutdinov, in *Photoinduced Electron Transfer IV,* Topics in Current Chemistry, 163, Springer-Verlag (1992); P. Piotrowiak, *Chem. Soc. Rev.* **28,** 143 (1999); A. Gust, T.A. Moore, in *Supramolecular photochemistry,* ed V. Balzani, (1987).

56. G.J. Kavarnos, in *Photoinduced Electron Transfer I,* Topics in Current Chemistry, **156,** Springer-Verlag (1992); J.J. Hopfield, J.N. Onuchic, and D.N. Bcratan, *Science* **241,** 817 (1988); R. Purrello, S. Gurrieri, and R. Lauceri, *Cood. Chem. Rev.* **190-192,** 683 (1999); P. Belser, S. Bernhard, C. Blum, A. Beyeler, L. DeCola, and V. Balzani, *Coord. Chem.* tfev.190-192, 155 (1999); A. Credi, V. Balzani, S.J. Langford, and J.F. Stoddart, *J. Amer. Chem. Soc.* **119,** 2679 (1999); D.F. Eaton, *Photoinduced Electron Transfer I,* Topics in Current Chemistry, **156,** Springer-Verlag (1992); R.A. Bissel, A.P. deSilva, H.Q.N. Gunaratne, P.L.M. Lynch, C.E.M. Maguire, C.P. McCoy, and K.R.A.S. Sandanayake, *Photoinduced Electron Transfer V,* Topics in Current Chemistry, **168,** Springer-Verlag (1993).

57. H.E. Toma, and K. Araki, *Coord. Chem. Rev.* **196,** 307 (2000); J.L. Sessler, A.E. Vivian, D. Seidel, A.X. Burrell, M. Hoehner, T.D. Mody, A. Gebauer, S.J. Weghorn, and V. Lynch, *Coord. Chem. Rev.* **216,** 411 (2001).

58. D.A. Oulianov, I.V. Tomov, A.S. Dvornikov, and P.M. Rentzepis, *Nonlinear optics* 27, 139(2001).

59. D.R. Reddy and B.G. Maiya, *J. Chem. Soc. Chem. Commun.* Issue 1, 117 (2001).

60. G.A. Mabbot, *J. Chemical Education,* **60,** 697 (1983); J.J. Van Benschoten, J.Y. Lewis, W.R. Helneman, D.A. Roston, and P.T. Kissinger *J. Chemical Education,* **60,** 772 (1983); C.A. Marrese and C.J. Carrano, *J. Chem. Soc. Chem. Commun.* 1279 (1982).

61. M. Ichida, T. Sohda and A. Nakamura, *J. Phys. Chem. B* **104**, 7082-7084 (2000).

62. D.R. Greve, S.B. Schougaard, T. Geisler, J.C. Petersen, and T. Bjornholm, *Adv. Mater.* 9, 1113 (1997).

63. S.B. Schougaard, D.R. Greve, T. Geisler, J.C. Peterson, and T. Bjornholm, *Synthetic Metals* 86, 2179 (1997).

64. M. Cha, N.S. Sariciftci, A.J. Heegar, J.C. Hummelen and F. Wudl, *Appl. Phys. Lett.* 67, 3850 (1995).

65. B. Dupuis, C. Michaut, I. Jouanin, J. Delaire, P. Robin, P. Feneyrou and V. Dentan, *Chem. Phys. Lett.* 300, 169 (1999).

66. P.P. Kiran, N.K.M.N. Srinivas, D.R. Reddy, B.G. Maiya, A.S. Sandhu, A. Dharmadhikari, G.R. Kumar and D.N. Rao, *Opt. Commun.* 202, 347 (2002).

67. A. Sevian, M. Ravikanth, and G.R. Kumar, *Chem. Phys. Lett.* 263, 241 (1996).

68. F.Z. Henari, W.J. Blau, L.R. Milgram, G. Yahioglu, D. Phillips, and J.A. Lacey, *Chem. Phys. Lett.* 267, 229 (1997); F.Z. Henari, J. Callaghan, H. Stiel, W. Blau and D.J. Cardin, *Chem. Phys. Lett.* 199, 144 (1992).

69. D. Gust, T.A. Moore, A.L. Moore, L.R. Makings, G.R. Seely, X. Ma, T.T. Trier, and F. Gao, *J. Am. Chem. Soc.* 110, 7567 (1988); Y. Sakata, H. Tsue, Y. Goto, S. Misumi, T. Asahi, S. Nishikawa, T. Okada, and N. Mataga, *Chem. Lett.* 1307 (1991).

70. M.R. Wasielewski, G.L. Gaines III, M.P. O'Neil, W.A. Svec, and M.P. Niemczyk, *J. Am. Chem. Soc.* 112, 4559 (1990); M.P. O'Neil, M.P. Niemczyk, W.A. Svec, D. Gosztola, G.L. Gaines III, M.R. Wasielewski, *Science* 257, 63 (1992).

71. F.J. Vergelt, R.B.M. Koehorst, T.J. Schaafsma, J.-C. Lambry, J.-L. Martin, D.G. Johnson, M.R. Wasielewski, *Chem. Phys. Lett.* 182, 107 (1991); A. Harriman, M. Hissler, O. Trompette, R. Ziessel, *J. Am. Chem. Soc.* 121, 2516 (1999); A. Vlcek Jr., Chemtracts - *Inorg. Chem.* **12**, 863 (1999).

72. M.R. Wasielewski, *Chem. Rev.* 92, 435 (1992); D. Gust and T. Moore, *Acc. Chem. Res.* 26, 198 (1993); H. Kurreck, and H. Huber, *Angew. Chem. Int. Ed. Engl.* 34, 849 (1995); A. Harriman, and J.-P. Sauvage, *Chem. Soc. Rev.* 41 (1996); N.J. Head, J. Thomas, M.J. Shephard, M.N. Paddon-Row, T.D.M. Bell, N.M. Carbal, and K.P. Ghiggino, *J. Photochem. Photobiol.A: Chem* 133, 105 (2000); S.L. Springs, D. Gosztola, M.R. Wasielewski, V. Kral, A. Andrievsky, and J. Sessler, *J. Am. Chem. Soc.* **121**, 2281 (1999); G.P. Wiederecht, M.P. Niemczyk, W.A. Svec, and M.R. Wasielewski, *J. Am. Chem. Soc.* **118**, 81 (1996); A. Osuka, G. Noya, S. Taniguchi, T. Okada, Y. Nishimura, I. Yamazaki, and N. Mataga, *Chem. Eur. J.* 6, 33 (2000); H. Tsue, H. Imahori, T. Kaneda, Y. Tanaka, T. Okada, K. Tamaki, and Y. Sakata, *J.*

Am. Chem. Soc. **122,** 2279 (2000); D. Kilin, U. Kleinekathofer, and M. Schreiber, *J. Phys. Chem. A* **104,** 5413 (2000); L. Flamigni, N. Armaroli, F. Barigilletti, V. Balzani, J.-P. Collin, J.-O. Dalbavie, V. Heitz, and J.-P. Sauvage, *J. Phys. Chem. B* **101,** 5936 (1997); M.A.J. Rodgers, and S.L. Loguniv, *J. Phys. Chem.* 96, 8697 (1992); W. Frey, R. Klann, F. Laerner, T. Elasser, E. Baumann, M. Futscher, and H.A. Staab, *Chem. Phys. Lett.* **190,** 567 (1992); H. Heitele, F. Pollinger, T. Haberle, M.E. Michel-Beyerle, and H.A. Staab, *J. Phys. Chem.* 98, 7402 (1994); K. Wynne, S. LeCours, C. Galli, M.J. Therien, and R.M. Hochstrasser, *J. Am. Chem. Soc.* **117,** 3749 (1995); Y. Shibata, H. Chosrowan, N. Mataga, and A. Osuka, *J. Lumin.* **87-89,** 757 (2000); E.I. Zenkevich, A.M. Shulga, S.M. Bachilo, U. Rempel, J. von Richthoflen, and Ch. Von Borczyskowski, *J. Lumin.* **76&77,** 354 (1998); K. Hirakawa, H. Segawa, *J. Photochemistry & Photobiology A: Chemistry.* **123,** 67 (1999).

73. M. **Andersson,** J. Davidsson, L. Hammarstrom, J.K. Tommola, and T. Peltola, *J. Phys. Chem. B* **103,** 3258 (1999); H. Chosrowjan, S. Tanigichi, T. Okada, S. Takagi, T. Arai, and K. Tokumaru, *Chem. Phys. Lett.* **242,** 644 (1995).

74. D. LeGourrierec, M. Andersson, J. Davidson, E. Mukhtar, L. Sun and L. Hammarstrom, *J. Phys. Chem. A* **103,** 557 (1999).

75. G.R. Loppnow, D. Melamed, A.L. Leheny, A.D. Hamilton, and T.G. Spiro, *J. Phys. Chem.* 97,8969(1993).

76. C.D. Tait, D. Holten, and M. Gouterman, *Chem. Phys. Lett.* **100,** 268 (1984).

77. H.Z. Yu, J.S. Baskin, B. **Steiger,** C.Z. Wan, F.C. Anson, and A.H. Zewail, *Chem. Phys. Lett.* 293, 1 (1998)

78. E. Hilinski, K.D. Straub, and P.M. Rentzepis, *Chem. Phys. Lett.* **111,**333, (1984).

79. T. Kobayashi, D. Huppert, K.D. Straub, and P.M. Rentzepis, *J. Chem. Phys.* 70, 1720 (1979).

80. X. Yan and D. Holten, J. *Phys. Chem.* 92, 5982 (1988).

81. S.C Jeoung, S. Takeuchi, T. Tahara, D. Kim, *Chem. Phys. Lett.* **309,** 369 (1999).

Chapter 4

Axial-Bonding Type Hybrid Porphyrin Arrays with basal Tin (IV) Tetratolylporphyrin Scaffold

Optical limiting properties of 'axial-bonding' type hybrid porphyrin arrays - trimers and hexamers based on a Tin (IV) scaffold are studied. The effect of different central metal atoms substituted in the adjacent porphyrin ring in the oligomer structure is discussed in the nanosecond and picosecond regime. In the nanosecond regime the optical limiting performance has increased considerably with increasing number of porphyrins in the array and ESA from singlet and triplet states found to play a major role. However, in the ps regime the higher order nonlinear processes takeover at higher intensities leading to interesting switching behaviour of nonlinear absorption. The second hyperpolarizability $<y>$ is three orders of magnitude higher compared to the monomer $Sn^{(IV)}TTP$.

4.1 Conjugated molecules / arrays for NLO applications

Organic materials with delocalized electrons have got a great deal of importance because of their large nonlinear optical susceptibilities, architectural flexibility, and ease of fabrication. The relation between the molecular structures and the third-order nonlinear optical susceptibilities ($\chi^{(3)}$) has been the main interest in these molecules [1,2]. Generally the delocalization of an electron in the molecular frame will enhance the optical nonlinearity and it has been one of the most successful strategies for designing the molecules. The optical and electronic properties of many oligomeric conjugated systems have been thoroughly investigated [3] for better understanding of both the basic physics in small, well-defined molecular systems as well as to determine structure/property relations applicable to the corresponding polymers. Conjugated organic materials have been widely investigated in search of suitable chromophores for all-optical applications like switching, and limiting [4]. Simple conjugated polymers such as poly(p-phenylene) and poly(p-phenylenevinylene) exhibit useful properties, like semiconductivity and electroluminescence [5]. Metalloporphyrin and metallophthalocyanines form an important class of electronic materials because of the large rc-electron system with two-dimensional conjugated molecular

structure [6]. At the same time, another class of organic systems, conjugated polymers, shows promise as suitable materials due to an expected large nonlinearity that is caused by one-dimensionally delocalized electrons [7]. Interest in advanced electronic and photonic materials recently has led to the exploration of conjugated polymers of more complex units, such as porphyrins [8]. The high polarizability and optical oscillator strength of the porphyrin macrocycles gives these materials remarkable nonlinear optical (NLO) behaviour, making them potentially useful for ultra-fast switching technologies. High values of the nonlinear refractive index, n_2 (which is proportional to the real part of the third order susceptibility, $\chi^{(3)}$) are essential for electro-optical and all-optical switching [9], whereas high nonlinear absorption coefficients, β (proportional to the imaginary part of $\chi^{(3)}$) are important for optical limiting [10]. High values of $\chi^{(3)}$ are associated with large, polarizable π-systems, long conjugation lengths and small HOMO-LUMO gaps [11], makes porphyrins good building blocks for such materials. The possibilities of substitution around the porphyrin periphery and of varying the metal at the center of the porphyrin provide extra ways of optimizing the performance of these materials [12]. Although number of studies have focused on the third-order nonlinear properties of porphyrin based materials [13], the majority of these involve macrocycle chromophores that arc electronically uncoupled or weakly coupled to one another. Several alkync-linked [14] and edge-fused [15] conjugated dimers and trimers have been investigated [16]. In this chapter we discuss the optical limiting and nonlinear optical properties of 'axial-bonding' type hybrid trimer and hexamer arrays based on $Sn^{IV}TTP$ scaffold; in which photoinduced electron transfer (PET) and excitation energy transfer (EET) play a significant role in modifying the singlet state properties.

4.2   Molecular Structure and linear optical properties

The molecular structures of monomer and dimer are shown in Fig. 4.1. The nomenclature of monomer and dimer molecule is *meso*-5,10,15,20-(tetratolyl) porphyrinato tin(IV) dihydroxide; [(TTP)Sn^{IV}(OH)$_2$] and [μ-[5,10,15-

Tri(*p*-tolyl)-20-[4-[2-[4-[10,15,20-tri(*p*-tolyl)-5-porphyrinyl] phenoxy] ethoxy] phenyl]porphyrinato]] di(tin) (IV)Tetrahydroxide; [(TriTP)-Sn^{IV}(OH)$_2$]-O(CH$_2$)$_2$O-TriTP)Sn (OH)$_2$] respectively. Dimer molecule has two monomers linked at meso position with ethoxy spacer. Monomer and dimer are synthesized following the procedure reported in the literature [17,18]. For the sake of simplicity we mention them as SnTTP and Sn-Sn(TTP)$_2$ in this chapter. Sn^{IV} porphyrin based, "axial-bonding" type hybrid trimers and hexamers are constructed by employing 'building-block' approach. The approach involves simple inorganic reactions such as axial bond formation of main group element containing porphyrins and insertion of metal/metalloid ions into the porphyrin cavity. The architecture of the trimer arrays [19] is such that Sn^{IV} complex of *meso*-5,10,15,20-(tetratolyl)porphyrin forms the basal scaffolding unit, the free-base, Ni porphyrins occupy the two axial sites via an aryloxy bridge. The nomenclature of the porphyrin trimer arrays discussed here is as follows: (free-base porphyrin)$_2$ (tin(IV)porphyrin) = [(TTP)-Sn^{IV}(H$_2$TriTP(O))$_2$] and (nickel (II) porphyrin)$_2$ (tin(IV)porphyrin) *s* [(TTP)-Sn^{IV}(NiTriTP(O))$_2$]. For simplicity these trimers are referred as Sn-(H$_2$)$_2$(TTP)$_3$ and Sn-Ni$_2$(TTP)$_3$ respectively.

Sn(IV)TTP

Sn(IV)TTP dimer
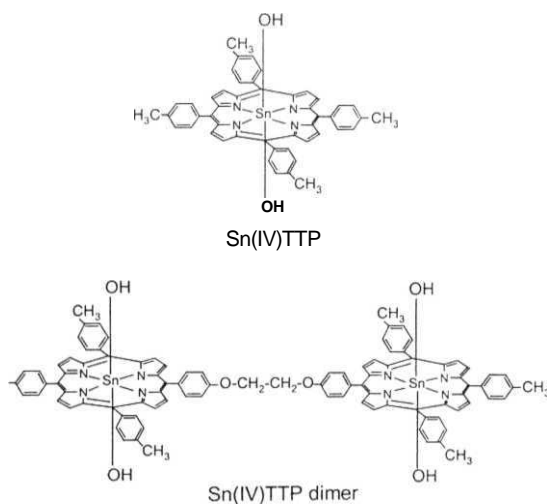
Fig. 4.1: Molecular structure of Sn^{IV} monomer and dirtier

The scheme of construction of **hexamer** arrays employs a synthetic protocol involving sequential "organic" and "inorganic" reactions conducted, respectively, at the peripheral *meso-* phenyl ring and the central Sn^{IV} ion of the porphyrin scaffold. The architecture of **hexamers** [18] are based on a covalently linked Sn^{IV} porphyrin **dimer**, with each of the two Sn^{IV} porphyrins centers trans-axially ligated to two free-base, zinc(II) porphyrins. The nomenclature of the hexamers is given as follows: $[(TTP)-Sn^{IV}(H_2TriTP(O))_2]-O(CH_2)_2O-[(TTP)-Sn^{IV}(H_2TriTP(O))_2]$ and $[(TTP)-Sn^{IV}(ZnTriTP(O))_2]-O(CH_2)_2O-[(TTP)-Sn^{IV}(ZnTriTP(O))_2]$. These arrays are referred as $Sn_2-(H_2)_4(TTP)_6$ and $Sn_2-Zn_4(TTP)_6$ arrays. The molecular structure of the trimers and hexamers are shown in Fig. 4.2 and 4.3 respectively. UV-VIS absorption spectrum of all these molecules is shown in Fig. 4.4.
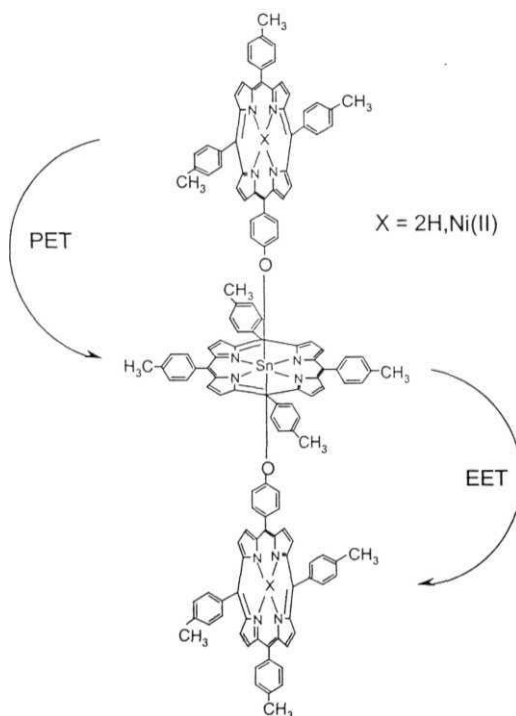
Fig 4.2: Molecular structure of "axial-bonding"-type tin (IV) trimers. Arrows indicate the PET and EET.

A comparison of the UV-VIS spectrum of a given **trimer** and hexamer with the spectra of the corresponding monomeric porphyrins suggested that the λ_{max} values of these array are in the same range as those of the reference compounds. In addition, the molar absorptivities at the peak maxima (e) values of the bands due to trimers and hexamers are nearly equal to the sum of those due to their constituent monomers. Minor variations in the spectral features of the trimers with respect to the corresponding monomers are ascribed to the 'substituent effects' i.e., differences in the axial ligands of Sn^{IV} porphyrins and the meso substituents of the free-base porphyrins/ metalloporphyrins.
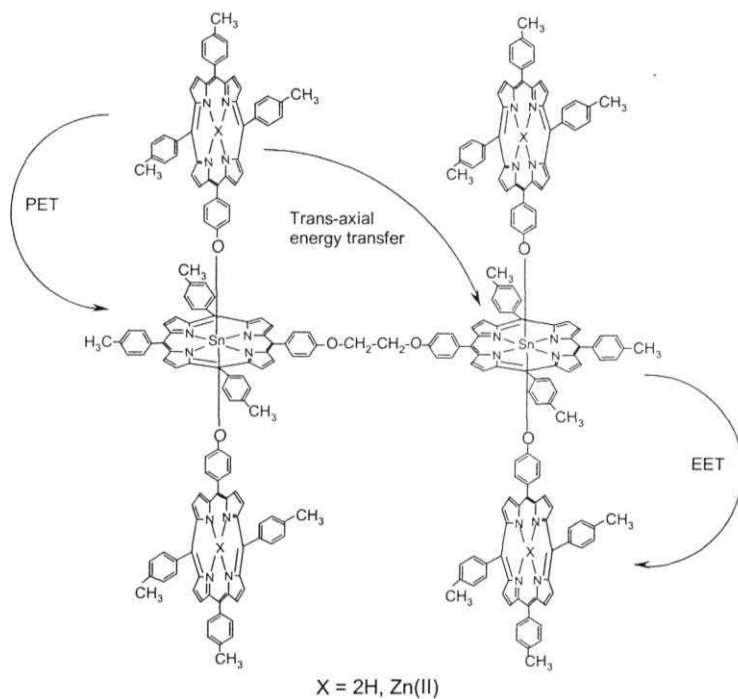
Fig 4.3: Molecular structure of Sn_2-$(H_2)_4$ hexamers

These indicate that there is minimal perturbation of the electronic structures of the individual macrocyclic π-systems in these arrays. Specifically

there exists no indication of the presence of exciton coupling between the porphyrin rings i.e., basal-basal, basal-axial, or axial-axial interaction in these arrays. Their redox potential data are also close to those of the corresponding constituent monomeric species. On the other hand, the singlet state activities of these oligomers are quite different from those of the precursor reference compounds as probed by steady-state fluorescence.
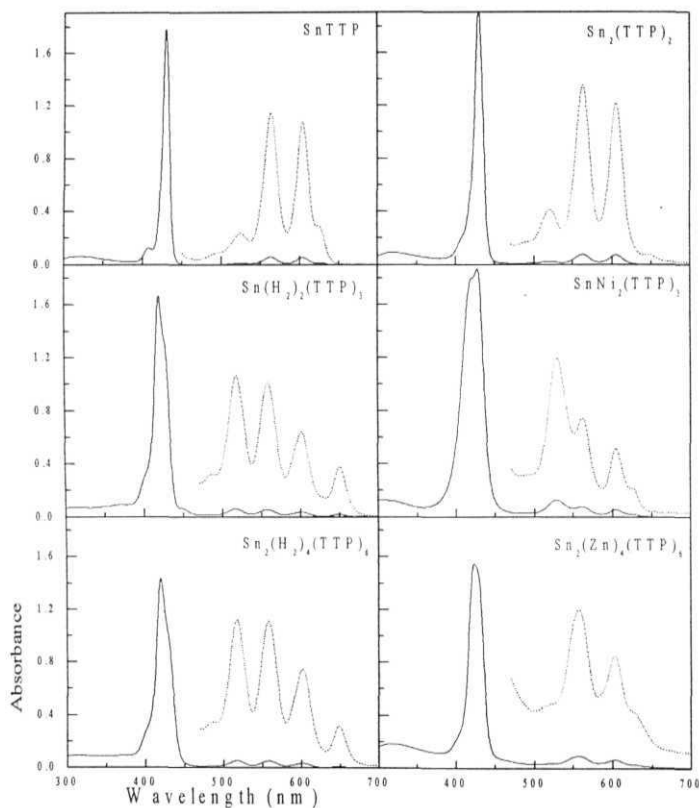
Fig 4.4: UV-Vis spectra of Sn(IV) oligomers.

In the case of trimers, fluorescence due to both the basal and axial porphyrins is considerably quenched in comparison with that due to the monomeric chromophores. Whereas, the spectral shapes and the wavelengths of

maximum emission for the individual chromophores of these arrays remains close to those due to the corresponding monomeric entities. Thus, the singlet state energy values (E_{0-0} values of H_2, Zn^{II} and Sn^{IV} porphyrins are 1.94, 2.07 and 2.04 eV respectively) of the individual components of these arrays are assumed to be essentially similar to those of their constituent monomers.

In the case of hexamers, strong quenching of fluorescence is observed. The percent quenching is close to 100, with the band that is characteristic of Sn^{IV} porphyrin emission being totally absent in the spectra. This is in contrast with the partial quenching observed in case of trimers. In trimer molecules, PET occurs from the axial porphyrin to the basal Sn^{IV} porphyrin and EET occurs from basal Sn^{IV} porphyrin to axial acceptors. In the case of hexamers, in addition to the EET from the basal Sn^{IV} porphyrin to its own two axial free-base acceptors, additional energy transfer from a given Sn^{IV} porphyrin to the free bases ligated at the neighbouring Sn^{IV} centers i.e., "*trans*-axial" energy transfer is likely to occur leading to more efficient quenching. A very high efficiency of energy transfer from the basal Sn^{IV} porphyrin to the axial acceptors is observed in these axial-bonding type donor-acceptor hexamer assemblies [18].

4.2.1 Fluorescence lifetimes

Fluorescence lifetimes and the respective quantum yields are given in Table 4.1. All these molecules have bi-exponential decays for τ_{S1} representing slow and fast decay. For SnTTP the lifetime is between 0.562 to 1 ns. In the case of trimers, τ_{S1} has increased to 0.74 - 5.93 ns in $Sn-(H_2)_2$ $(TTP)_3$ trimer and with metal substitution in case of $Sn-Ni_2$ $(TTP)_3$ τ_{S1} is ~ 0.62 - 2.13 ns. As the array is becoming larger, the contribution of slowly decaying (long lived) component has increased. In case of $Sn_2-(H_2)_4$ $(TTP)_6$ S_1 lifetime is 0.454-7.25 ns whereas for Sn_2-Zn_4 $(TTP)_6$ it is 0.663-1.73 ns. The lifetimes of the first excited singlet state have varied considerably with the metal substitution in hexamers. Substitution of Zn as central metal atom in porphyrin ring is reported to vary the singlet state properties and triplet state formation quite significantly [18,19]. As the excitation pulse is 6ns, the longer S_1 lifetime of $Sn_2-(H_2)_4$ $(TTP)_6$

will help in enhanced ESA and ISC, which lead to better optical limiting performance. Fluorescence decay curves for monomer, trimer and hexamer are shown in Fig. 4.5(a) and 4.5(b) respectively.

Porphyrin	τ_{S1} ns, (% fluorescence yield)
Sn(TTP)	0.562 (71), 1 (28)
Sn-Sn (TTP)$_2$	0.57 (95), 4.94 (5)
Sn-(H$_2$)$_2$ (TTP)$_3$	0.744 (71), 5.93 (28)
Sn-Ni$_2$ (TTP)$_3$	0.62 (70), 2.13 (29)
Sn$_2$-(H$_2$)$_4$ (TTP)$_6$	0.454 (28), 1.95 (23), 7.25 (47)
Sn$_2$-Zn$_4$ (TTP)$_6$	0.667 (30), 1.73 (69)

Table 4.1: Fluorescence lifetimes and % yields of Sn(IV) TTP oligomers
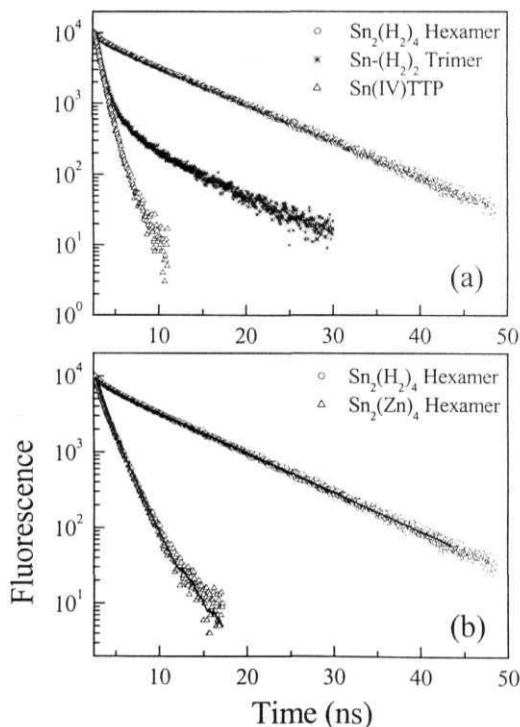
Fig 4.5: Fluorescence decay curves **for (a) Sn(IV)** TTP monomer, Sn-(H$_2$)$_2$ trimer and Sn-(H$_2$)$_4$ hexamer and (b) Sn$_2$-(H$_2$)$_4$ hexamer and Sn$_2$-Zn$_4$ hexamer.

Excitation energy transfer (EET) and photoinduced electron transfer (PET) are found to be responsible for the observed variation in the singlet state properties. The number of acceptors (free-base porphyrins) in the neighborhood of a given donor (Sn(IV) porphyrin) increases as one moves from the lower homologue to the higher donor-acceptor assemblies. Thus in the case of hexamer arrays additional energy transfer, called trans-axial energy transfer, from a given Sn^{IV} porphyrin to the free bases ligated at the neighboring Sn^{IV} centers is likely to occur in addition to the EET from the basal Sn^{IV} porphyrin to its two axial free-base acceptors which is the case with trimers. PET from ground-state free-base porphyrin to the singlet-state Sn^{IV} porphyrin leads to a charge transfer state of $Sn^{IV}P^{\cdot}$—H_2P^+ and involves free-energy changes leading to formation of charge transfer states (Fig. 4.6). These charge transfer states lead to localization of singlet states and the spread in the singlet states is quite large and the fluorescence emission wavelength is red shifted quite considerably.
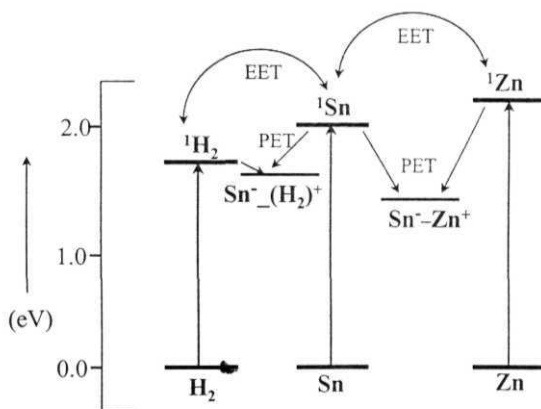
Fig 4.6: A generalized energy level diagram illustrating the singlet state dynamics and charge transfer states pertaining to the photoactive arrays of trimer and hexamer. The effect of PET, EET and the CT states formed in these oligomers are found to vary the singlet state properties and in these effects were considered while estimating the figures of merit.

4.3   Measurement of <γ> and higher order nonlinearities

DFWM-PC geometry is used to measure the second hyperpolarizability <γ> of these oligomers using 25 ps pulses. In the case of Sn(IV) oligomers <γ> has increased from monomer to dimer, trimer and hexamer arrays. However <γ> saturates for trimer arrays and decreases as one moves on to hexamer arrays. The <γ> value is three orders of magnitude higher for hexamers compared to that of monomer [20]. For dimer molecule, in which two SnTTP monomers were edge linked via ethoxy spacer, the <γ> value is four orders of magnitude higher. The log-log plot of input energy and phase conjugate signal for dimer and Sn_2-Zn_4 $(TTP)_6$ hexamer are shown in Fig. 4.7(a) and 4.7(b) respectively.

These molecules show log-log slope of ~ 3 at lower intensities (<10 GW cm^{-2}) and above that the slope approaches ~ 5, suggesting contributions from the higher excited states and the presence of higher order nonlinearities to the observed nonlinearity. For dimer molecule higher order slope appeared at a relatively lower intensities (~ 9 $GWcm^{-2}$) compared to that for trimer and hexamer (~ 15 $GWcm^{-2}$) molecules. The values of <γ> measured from cubic fit of the phase conjugate signal at lower intensities where the slope is ~ 3 are given in Table 4.2.

The chain length dependence of $\chi^{(3)}$ for several molecular arrays and polymers has been investigated earlier and it is known that the magnitude depends on the number of monomer unit N [1, 21]. Usually it is a function of power of the chain length [1],

$$\gamma \propto N^{a(N)} \tag{4.1}$$

For conjugate compounds with a small monomer unit such as polythiophene, $a(N)$ is almost constant in an intermediate region (3-7 units) and finally $a(N)$ becomes less than unity which indicates the saturation effect. For instance, in the case of thiophene oligomers, reported by Hein *et al.* absolute value of $\chi^{(3)}$ was enhanced with increasing the thiophene unit; however, γ per monomer unit was saturated at about 4 units. It is also reported that the saturation of the oligothiophenes occurs at about 7-8 units [1]. It is interesting to

note that for the oligomers and arrays of larger monomer unit such as porphyrin, the enhancement is more drastic and it saturates at a much shorter length [22]. Effects of alternation and saturation of y have been reported earlier for cyanines [23].
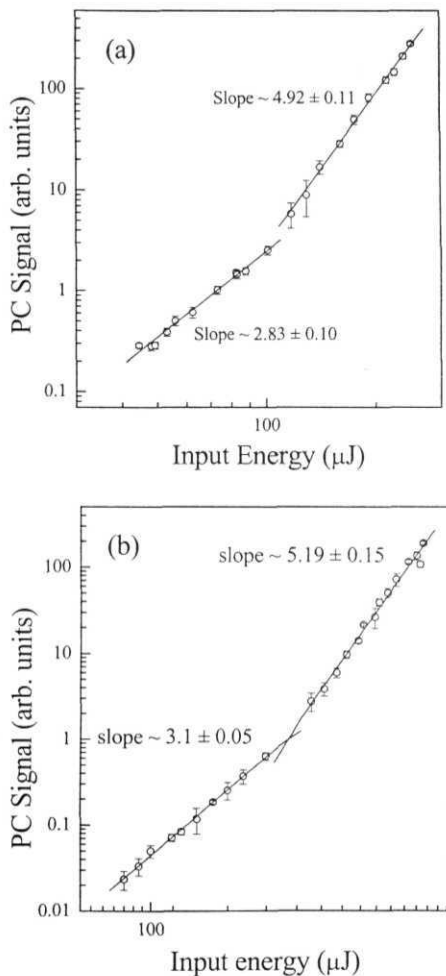
Fig 4.7: Log-log plot of phase conjugate signal and the input energy for (a) Sn-Sn dimer and (b) Sn_2-Zn_4 hexamer with 25 ps pulses.

Porphyrin	$\langle\gamma\rangle$ ($\times 10$ esu)
Sn(TTP)	0.368×10^{-3}
Sn-Sn (TTP)$_2$	2.99 ± 0.4
Sn-(H$_2$)$_2$(TTP)$_3$	0.9328 ± 0.06
Sn- Ni$_2$(TTP)$_3$	0.6142 ± 0.04
Sn$_2$-(H$_2$)$_4$(TTP)$_6$	0.333 ± 0.02
Sn$_2$-Zn$_4$(TTP)$_6$	0.385 ± 0.03

Table 4.2: Second hyperpolarizability $\langle\gamma\rangle$ of Sn(IV)TTP oligomers

Large third-order electronic polaraizabilities in porphyrin oligomers [22,24] and polymers [25] are reported earlier. The deviations from the cubic behaviour of the phase conjugate signal where the log-log slope approaching ~ 5 are observed earlier in tetramer, pentamer and polymers of porphyrin [25]. In isolated molecules in solution, strongly coupled pairs of excitations created by a TPA or ESA processes would create a two-photon grating that would produce a scattering proportional to the fifth power of the laser intensity, and an effective $\chi^{(5)}$ process. The nonlinearity would be expected to be rapid on the time-scale of the pulse duration because S$_n$ excited states of organic molecules commonly decay rapidly to S$_1$. Ultrafast measurements [26] of the dynamics of S$_n$ —> S$_1$ in analogous *meso*-linkedethynyl bridged porphyrin oligomers show the relaxation occurs in a sub 100 fs timescalc. Similar results of the fifth-order nonlinearity are reported in stilbazolium derivative [27] due to TPA and TPA generated ESA.

Four-wave description of the DFWM interaction specifies only the number of beams involved and does not constrain the interaction to a third-order nonlinearity. The most general form of the third-order polarization density for the backward DFWM geometry can be expressed as

$$\vec{P}^{(3)} = \chi^{(3)}_{fp} \ (\vec{\varepsilon}_f \cdot \vec{\varepsilon}_p^{\bullet})\vec{\varepsilon}_b \ + \chi^{(3)}_{bf}(fit \ \cdot \vec{\varepsilon}_p^{\bullet})\vec{\varepsilon}_f \ +2C\chi^{(3)}_{fp}(\vec{\varepsilon}_f \ \vec{\varepsilon}_b)\vec{\varepsilon}_p^{\bullet} \quad (4.2)$$

The first two terms are identified as spatial grating terms and the third term corresponds to the scattering of the probe wave from a spatially uniform

two-photon coherence. The susceptibility C is usually negligible unless there is a strong resonant enhancement from a two-photon transition. Depending on the polarization state of the input waves and the conjugated signal different terms contribute to the nonlinear polarization. In our experimental setup all the four waves are linearly polarized and all the three terms contributing to $P^{(3)}$ will be present [28]. The order of the susceptibilities and the specific terms that contribute significantly to the DFWM signal, depend on the nonlinear interaction. For instance, when the nonlinear mechanism is due to two-photon transitions, terms involving both third order and fifth order nonlinear susceptibilities will generally be significant and the dominance of one over the other will depend on details such as the two-photon transition probability, the dephasing rate of the two-photon coherence. Even for the case of a single-photon transition, terms of higher than third order may contribute, but such conditions are usually negligible unless significant population changes are involved.

The polarization density terms leading to DFWM can be written as

$$P^{NL}(co) - P^{(3)} + P^{(5)} + (higher\text{-}order\ \ terms) \qquad (4.3)$$

In contrast to the single-photon resonant terms in P^{NL}, in two-photon resonant media a much more significant contribution to the net polarization density P^{NL} may occur from $P^{(5)}$ and higher order terms, even when the population changes are negligible. For DFWM interaction some of the terms that are phase matched to radiate in the conjugate-wave direction are shown in table 4.3 below.

In the presence of an intermediate state one can expect term $\chi_c^{(5)}$ to dominate, owing to the formation of a relatively long lived intermediate state population. If this intermediate state is already well saturated at the light intensities of interest, this term essentially reduces to a third order term. If the population relaxation times for the states are generally longer than the dephasing times of the coherences $\chi_a^{(5)}$, $\chi_b^{(5)}$ be significantly longer than $\chi_d^{(5)}$ and $\chi_c^{(5)}$, and the corresponding polarization terms may be expected to result in DFWM signals comparable to the third-order 2ω coherence term. Each term in $P^{(5)}$ has

functional dependence on the amplitudes of the input waves. For instance $\chi_b^{(5)}$ has a cubic dependence on the intensity of the backward beam. With appropriate polarization selection, and by intensity and angular dependence experiments, it is possible to study the individual contributions of these terms to the DFWM signal.

Typical term in $P^{(5)}(\omega)$	Physical sequence in the nonlinear polarization density
$\chi_a^{(5)}\left[\left(\bar{\varepsilon}_f \cdot \bar{\varepsilon}_f\right)\bar{\varepsilon}_f^* \cdot \bar{\varepsilon}_p^*\right]\bar{\varepsilon}_b$	2ω coherence $\rightarrow$ spatial grating
$\chi_b^{(5)}\left[\left(\bar{\varepsilon}_f \cdot \bar{\varepsilon}_b\right)\bar{\varepsilon}_b^* \cdot \bar{\varepsilon}_p^*\right]\bar{\varepsilon}_b$	2ω coherence $\rightarrow$ spatial grating
$\chi_c^{(5)}\left[\left(\bar{\varepsilon}_f \cdot \bar{\varepsilon}_f^*\right)\bar{\varepsilon}_f \cdot \bar{\varepsilon}_p^*\right]\bar{\varepsilon}_b$	Population of intermediate state $\rightarrow$ spatial grating
$\chi_d^{(5)}\left[\left(\bar{\varepsilon}_f \cdot \bar{\varepsilon}_b\right)\bar{\varepsilon}_f^* \cdot \bar{\varepsilon}_f^*\right]\bar{\varepsilon}_p^*$	2ω coherence only no spatial grating
$\chi_e^{(5)}\left[\left(\bar{\varepsilon}_f \cdot \bar{\varepsilon}_f^*\right)\bar{\varepsilon}_f \cdot \bar{\varepsilon}_b\right]\bar{\varepsilon}_p^*$	2ω coherence only no spatial grating

Table 4.3: Nature of P terms in two-photon resonantly enhanced materials

The population distribution of porphyrins with 25 ps pulse excitation can be explained by the following rate equations

$$\frac{dN_0}{dt} = -\frac{\sigma_0 I N_0}{\hbar\omega} - \frac{\beta I^2}{2\hbar\omega} + \frac{N_1}{\tau_1} \tag{4.4}$$

$$\frac{dN_1}{dt} = \frac{\sigma_0 I N_0}{\hbar\omega} - \frac{\sigma_1 I N_1}{\hbar\omega} - \frac{N_1}{\tau_1} + \frac{N_2}{\tau_2} \tag{4.5}$$

$$\frac{dN_2}{dt} = \frac{\sigma_1 I N_1}{\hbar\omega} + \frac{\beta I^2}{2\hbar\omega} - \frac{N_2}{\tau_2} \tag{4.6}$$

As the relaxations from the excited singlet state S_2 are very fast compared to the excitation pulse width the population N_2 can be assumed to be not changing at very high intensities

i.e., $dN_2/dt = 0. \Rightarrow \quad \dfrac{N_2}{\tau_2} = \dfrac{\sigma_1 I N_1}{\hbar\omega} + \dfrac{\beta I^2}{2\hbar\omega}$ **(4.7)**

Substituting this in to eqn (4.6), gives

$$\frac{dN_1}{dt} = \frac{\sigma_0 I\, N_0}{\hbar\omega} - \frac{N_1}{\tau_1} + \frac{\beta I^2}{2\hbar\omega} \tag{4.8}$$

The effective population describing the nonlinear property

$$\frac{dN_1}{dt} - \frac{dN_0}{dt} = 2\frac{\sigma_0 I\, N_0}{\hbar\omega} - 2\frac{N_1}{\tau_1} + 2\frac{\beta I^2}{2\hbar\omega}$$

$$2\frac{N_1}{\tau_1} = \frac{1}{\tau_1}\left[(N_1 - N_0) + (N_1 + N_0)\right] = \frac{1}{\tau_1}\left[N_{eff} + N_{eff}^0\right] \tag{4.9}$$

Where $N_{eff} = N_1 - N_0$ is the effective population contributing to the nonlinear polarization and $N_{eff}^0 = N_1 + N_0$ is the population at zero field, which is a constant N_0.

The effective population density leading to the nonlinear polarization properties can be given by

$$\frac{dN_{eff}}{dt} = 2\frac{\sigma_0 I\, N_0}{\hbar\omega} - \frac{1}{\tau_1}\left[N_{eff} + N_{eff}^0\right] + 2\frac{\beta I^2}{2\hbar\omega} \tag{4.10}$$

The resulting nonlinear polarization source term P^{NL} is proportional to EN_{eff}. At higher intensities the two-photon term have dominant contribution to the nonlinear polarization is

$$N_{eff}(t) \propto \int_{-\infty}^{\infty} I_{eff}^2\, dt' \tag{4.11}$$

At higher intensities assuming TPA to be the dominant process and in the DFWM geometry $I^2 - (E_f + E_b + E_p)^4$. Concentrating only on the terms which contain $E_f E_p*$ and neglect the terms in $|E_p|^2 E_p*$ since $|E_p| \ll |E_f|, |E_b|$. Then the component *of I^2* producing a grating leading to the DFWM signal is I_{eff}^2 x $(|E_f|^2 + 2|E_b|^2)[2E_f E_p* + c.c.]$. Note that while I_{eff}^2 is real, it has been broken down into the sum of two complex conjugate terms. The first gives rise to the

conjugate signal, the second to a term, which radiates with a wave vector of $\mathbf{k_p}$ - 2kf and is not phase matched.

Assuming the phase distortions on E_p to be small, $E_p{}^* = E_{p0} \, exp\{+ik_p \, (z \, cos\theta + x \, sin\theta)\}$ and $E_f = Ep \, \{-ik_f z\}$, so that N_{eff} can be written as

$$N_{eff} \propto 2\cos[K_g x] \int_{-\infty}^{\infty} \left| E_f(t') \right|^3 \left| E_p(t') \right| dt' \tag{4.12}$$

where $K_g = k_f - k_p$ is the grating wave vector. In the limit of small G, $K_g \sim 2\pi\theta/\lambda$, where λ is the free-space wavelength. Since $E_{opc} \propto P^{Nl}$, the total irradiance dependence of the DFWM signal is

$$I_{opc} \propto I_b I_p I_f^3 \tag{4.13}$$

The observed fifth-order nonlinearity can be considered to be arising from a sequential $\chi^{(3)} : \chi^{(1)}$ nonlinearity. Such sequential nonlinearities leading to fifth and seventh order contributions to phase conjugation are reported in semiconductors [29]. In case of Sn-Sn dimer the log-log slope of the phase conjugate signal to the input energy varied as 2.83 ± 0.10 and 4.92 ± 0.11 at lower and higher intensities respectively. Where as for trimer and hexamers the slopes are higher than 3 and 5 at lower and higher intensities respectively. At higher intensities slopes higher than 5 observed in trimers and hexamers may be due to the additional localization coming due to the presence of PET and EET, which localize the singlet states, in turn changing the population densities contributing to nonlinear polarization. Whereas in dimer molecule the possibility of PET and EET is absent and only conjugation is present. In general for a medium that is m-photon resonant (m>l) the lowest-order term that may contribute significantly to a DFWM signal is of order 2m - 1, whereas the lowest-order term with a spatial modulation is of order 2m +1 [29].

4.4   Optical limiting and nonlinear absorption

Optical limiting and nonlinear absorption studies are performed for these samples both in ns and ps regime. The nonlinear absorption behaviour observed in these hybrid arrays is totally different at ns and ps timescales. In the nanosecond regime all these molecules show good RSA even at higher intensities. However, in the picosecond regime the behaviour switches from RSA to SA and then again to RSA as the intensity increases.

4.4.1   With 6 ns pulses

Optical limiting studies are done using 6 ns pulses with 10 Hz repetition rate from frequency doubled Nd: YAG laser. We have employed f/5 geometry. The linear transmission is approximately 70-75% for 1-mm path length of the sample. The input iluence is varied in the range of $30 \mu Jcm^{-2}$ to $70Jcm^{-2}$. OL curves for monomer SnTTP, trimer $Sn_2-(H_2)_2$ $(TTP)_3$ and hexamer $Sn_2-(H_2)_4$ $(TTP)_6$ at ~75% linear transmission at 532 nm shown in Fig. 4.8 clearly indicates the enhanced limiting behavior as one moves to higher homologues.
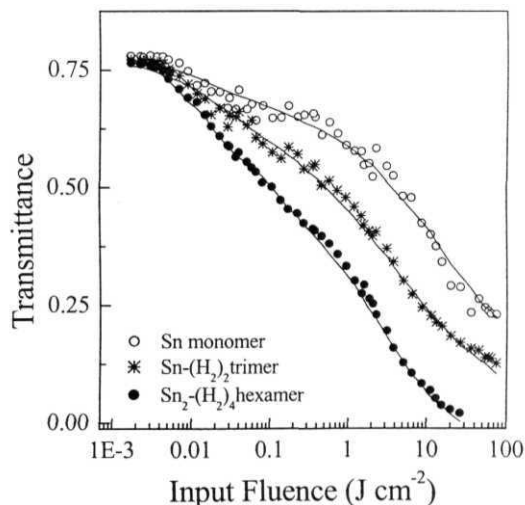
Fig 4.8: Optical limiting curves of Sn(IV) TTP monomer, trimer and hexamer at 75% linear transmission with 6 ns pulses. Lines show the fits to the limiting curves.

Figure 4.9 (a) and (b) show the variation in the limiting curves for SnTTP and Sn-Sn(TTP)$_2$ at different linear transmissions of 85% and 70%. These oligomers start showing considerable limiting performances from the concentrations corresponding to 75% linear transmission at 532 nm and the limiting performance increases with increasing concentration (decreasing linear transmission at 532 nm).
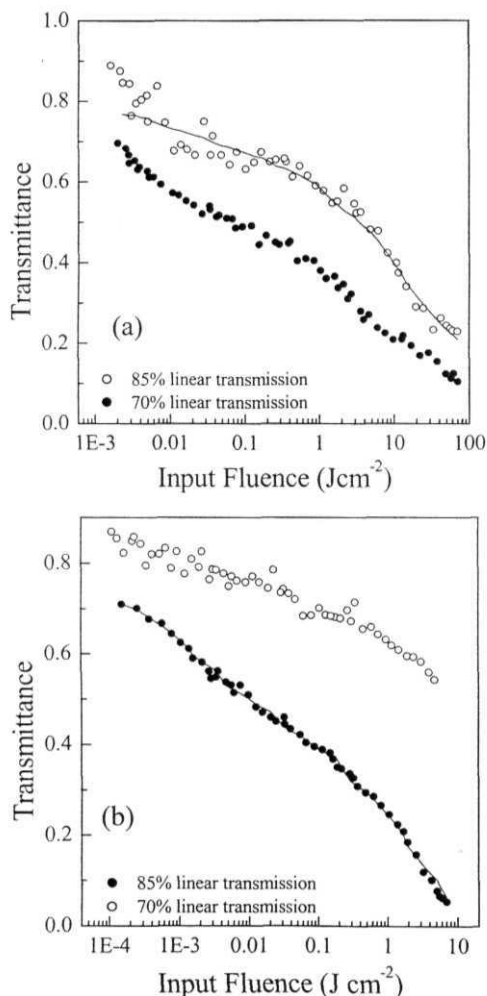
Fig 4.9: OL curves of (a) Sn(IV)TTP monomer and (b) Sn-Sn dimer at 85% and 70% linear transmission. Sold lines show theoretical fits.
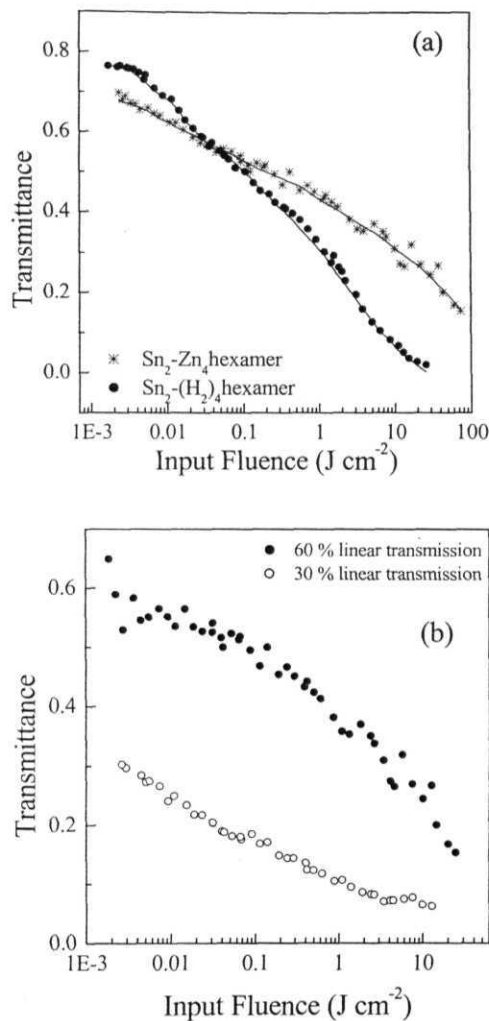
Fig 4.10: OL curves showing (a) the effect of heavier mctalloporphyrin with in hexamer arrays. Solid lines show theoretical fits. (b) OL curves showing the effect of concentration in Sn_2-$Zn_4(TTP)_6$ array.

However, with the introduction of heavier metalloporphyrin in the axial position in place of free-base porphyrin, in trimer and hexamer donor-acceptor homologues, lead to slightly reduced limiting response. OL curves for hexamers

with free-base and Zn porphyrins in axial position are shown in Fig. 4.10. Though the limiting threshold has not varied greatly the onset of limiting is certainly at lower input fluences for the oligomers with freebase porphyrin. Throughput fluences from these hybrids are as low as 35 - 52 mJcm^{-2} with input fluences in the range of ~ 26 - 74 Jcm^{-2} making them very good optical limiters at higher intensities. Decreasing linear transmission to ~ 60%, we are able to achieve much better limiting performance in all these molecules. With increase in the concentration the ESA increases, thereby leading to improved nonlinear absorption behaviour. At higher concentrations we have not observed any scattering due to thermal blooming of the solution as reported earlier in suspensions of carbon black and ink [30]. No aggregation in the porphyrin solutions is observed even at higher concentrations.

Limiting threshold values for the oligomers with 6ns pulses are shown in Table 4.4. Figure of merit (σ_{ex}/σ_0), which describes the capability of a material for optical limiting, and τ_{ISC} estimated from the theoretical fits is also given in table 4.4. The contribution from all the processes like PET and EET and both the radiative and nonradiative processes towards the lifetimes are taken as the effective singlet lifetime used in the rate equations. The values of σ_{ex}/σ_0 are estimated using a generalized five-level model and from the rate equations explained in section 2.11 of this thesis. The lifetime of the higher excited singlet state S_n (τ_{Sn}) and triplet (τ_{Tn}) are taken as ~ 100 fs and the lifetimes of the first excited singlet state is taken as given **in** table 4.1.

Porphyrin	$I_{1/2}$ 0 cm^{-2})	σ_{ex}/σ_0	τ_{isc} (psec)
SnTTP	12.30	3.24	1000
Sn-Sn (TTP)$_2$	0.16	21.53	1X0
Sn-(H$_2$)$_2$(TTP)$_3$	2.91	7.26	3X0
Sn-Ni$_2$(TTP)$_3$	3.46	6.21	550
Sn$_2$-(H$_2$)$_4$(TTP)$_6$	0.46	19.45	220
Sn$_2$-Zn$_4$(TTP)$_6$	1.16	6.73	600

Table 4.4: Limiting threshold with 6 ns at 75% linear transmission at 532 nm.

Singlet state lifetime and the ESA from $S_1 \rightarrow S_n$ in addition to $T_1 \rightarrow T_n$ are found to be responsible for the enhanced limiting performance of higher homologues. Simultaneous occurrence of strong EET and less prominent PET lead to a drastic change and stabilization of S_1 states in these molecules, making the S_1 state metastable in comparison with the excitation laser pulse width. The effective ESA cross-sections from both singlets and triplet states is taken as σ_{ex}.

Even though the contribution due to ESA from S_1 to S_n is present in these molecules as the lifetime of S_1 is longer and comparable to laser pulse width, due to the low fluorescence yields most of these molecules seem to transfer to T_1 with a time given by the longer decay. However high triplet yields in these molecules indicates that intersystem crossing plays an important role in these systems at the nanosecond timescales. Such a longer intersystem crossing has been reported in the unaggregated solutions of edge linked zinc porphyrin oligomers [31] and in monomer, dimer and polymer films [32]. The intersystem crossing time obtained from the theoretical fits is around 180 ps to 600 ps for these oligomers. Similar decay times arc reported in zinc porphyrin oligomers [32] obtained from pump-probe measurements using a 0.8 ps pulse. Highly efficient triplet-triplet energy transfer and enhanced intersystem crossing is reported in rigidly linked metal and free-base porphyrin hybrids [33] and also in porphyrins linked via Ruthenium complex [34]. As the excitation pulse is of 6 ns duration, the longer lifetimes of S_1 in these arrays will help in enhanced ESA from the S_1 states, in addition to the ESA from the triplet states, which lead to better optical limiting performance. With the introduction of ZnTTP in case of hexamer and NiTTP in case of trimer in the place of the free-base TTP, we have observed reduced limiting performance of the molecule, due to the variation in the singlet state properties. When compared with the H_2TTP, NiTTP and ZnTTP monomers these oligomers show a better limiting performance under the similar experimental conditions. Substitution of Zn as central metal atom in porphyrin ring is reported to vary the singlet state properties and triplet state formation quite significantly [35]. Population relaxation times studied using DFWM-ps technique has been reported to have faster relaxations for ZnTTP and NiTTP compared to that of SnTTP and H_2TTP [36]. Population relaxation times studied using DFWM-ps technique has

shown just the autocorrelation trace that is similar to that obtained for CS_2 shows that the relaxations are certainly fast < 25 ps.

4.4.2   With 25 ps pulses

With 25 ps pulse excitation the nonlinear absorption behaviour is completely different compared to that observed with 6 ns pulses.   SnTTP monomer shows a regular RSA behaviour at lower concentrations (corresponding to 75-80% linear transmission at 532 nm) and at lower intensities.   At higher intensities the ESA saturates and SA followed by RSA is observed as shown in Fig.4.11 (a).   At higher concentrations the nonlinear absorption shows a sudden transition to RSA at higher intensities within SA behaviour (Fig.4.11 (b))..
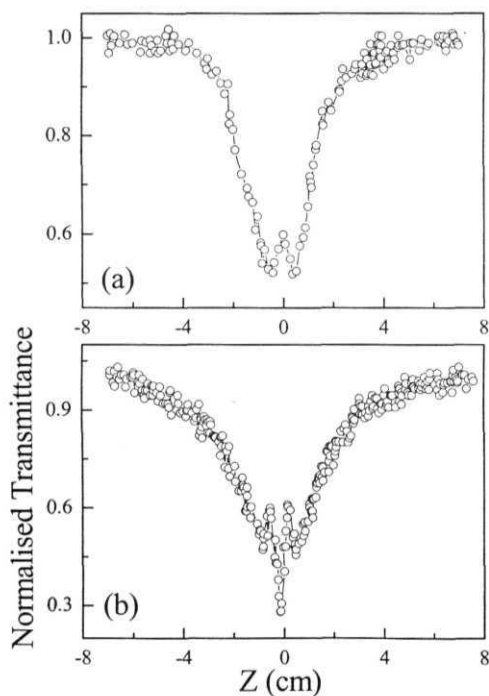
Fig **4.11:** Sn monomer at (a) low (~14 GW cm^{-2}) and (b) high input intensities (~38 GW cm^{-2}) at lower concentration. Solid line is guide to the eye.

In the case of dimer at lower intensities only RSA (Fig. 4.12 (a)) is observed and as the intensity increases, the switching of the nonlinear absorption from RSA to SA and then back to RSA (Fig. 4.12 (b)) with intensity is observed. As the intensity increases the SA behaviour after RSA goes down as the RSA behaviour becomes more dominant (Fig. 4.12 c).
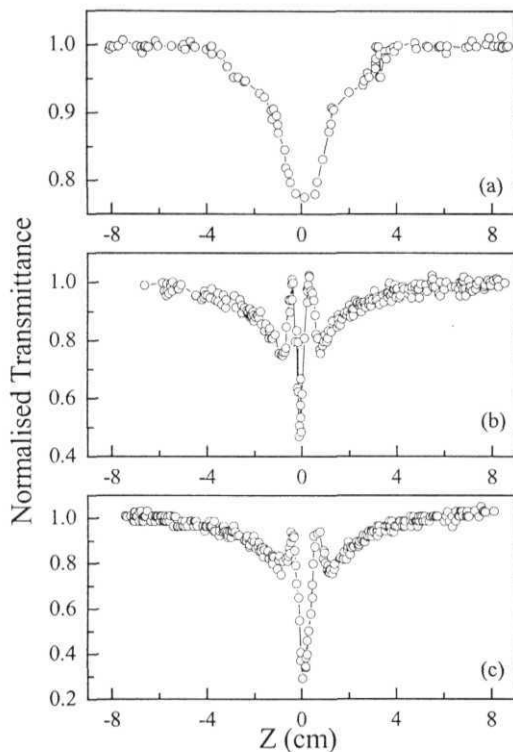
Fig **4.12:** Sn dimer at low concentration, at (a) 5.6 GWcm^{-2} (b) 19 GWcm^{-2} and (c) 46 GW cm^{-2}. Solid line is guide to the eye.

In the case of trimers, at lower concentrations and at lower intensities RSA is observed and with increasing intensity saturation of the ESA is observed. The saturation has increased with increasing input intensity. The open aperture Z-scan curves for Sn-$(H_2)_2$ $(TTP)_3$ are shown in Fig. 4.13. For Sn-Ni_2 $(TTP)_3$, the substitution of NiTTP in axial position in place of H_2TTP lead to a total reversal

in the nonlinear absorption behaviour. At lower concentrations and at lower intensities SA is observed (Fig 4.1 a). With gradual increase in the input intensity the RSA phenomenon started taking over as RSA followed by SA is observed (Fig 4.14b) and at higher intensities pure RSA was observed (Fig 4.14c). At higher concentrations (60% linear transmission at 532 nm) the behaviour remained pure RSA similar to as shown in Fig 4.14c. As the intensity is increased the behaviour of RSA (Fig 4.14 (b)) started to take over and at higher intensities completely RSA dominates (Fig 4.14 (c)) probably due to TPA assisted ESA.
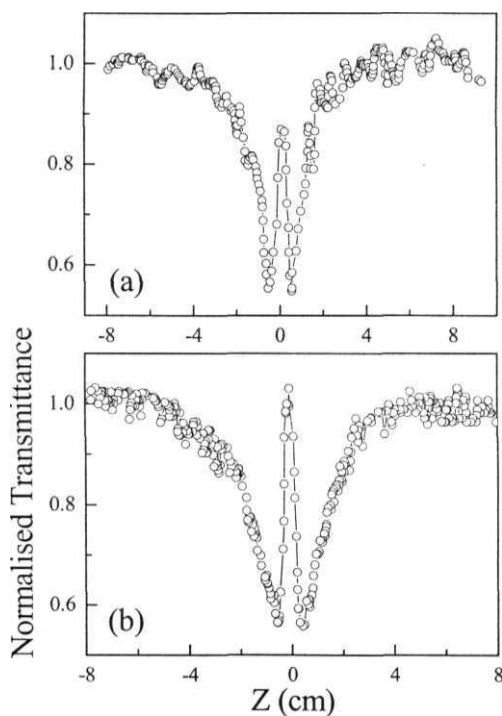
Fig 4.13: Sn-(H$_2$)$_2$ trimer at low concentration and at (a) 26.2 GW cm^{-2} and (b) 44.5 GW cm^{-2} . Solid line is guide to the eye.

For Sn-Ni$_2$(TTP)$_3$ with 532 nm excitation that falls in the edge of the absorption band, we have observed SA behaviour (Fig 4.14 (a)) at lower

intensities. With 532 nm excitation, the lowest of the S_1 energy levels get excited and therefore one expects more localization of the energy [37], which thereby leads to saturation at lower intensities. When the pump excitation is into the lower side of the absorption band, there is more localization of the energy before it decays to the ground state, leading to resonant TPA.
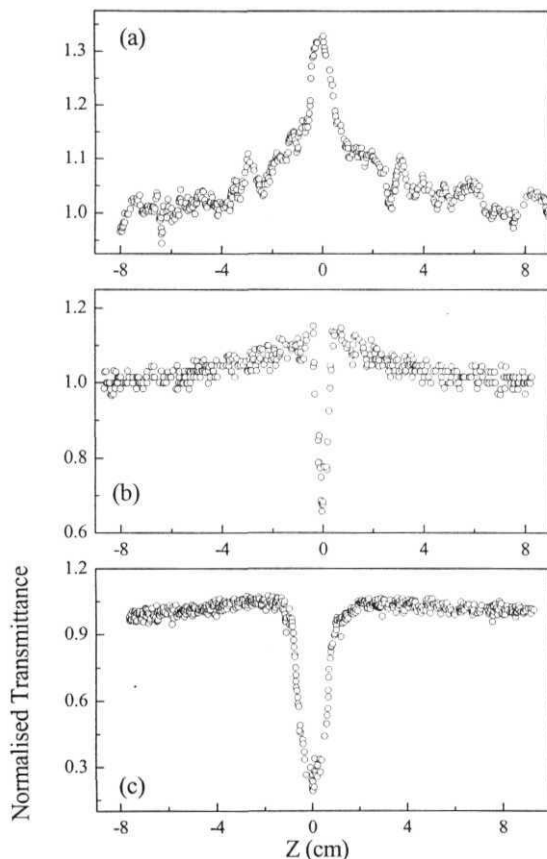
Fig 4.14: Sn-Ni$_2$ trimer at low concentration and at intensities (a) 4.5 GWcm^{-2} (b) 24.3 GW cm^{-2} and (c) 47.5 GW cm^{-2}

In the case of Sn-(H$_2$)$_2$ (TTP)$_3$ and Sn$_2$-(H$_2$)$_4$ (TTP)$_6$, both at lower and higher concentrations and at higher intensities saturation due to the excited states

is observed (Fig 4.13 and **4.15**). At higher intensities the saturation has increased quite considerably. However in Sn_2-$Zn_4(TTP)_6$ at lower concentrations and at lower intensities a transition from SA to RSA due to two-photon/multi-photon absorption is observed (Fig 4.16). At higher concentrations and at lower intensities saturation of absorption due to excited states is observed (Fig. **4.17** (a)). As the intensity increased to ~ 52.5 GWcm^{-2} RSA is observed after saturation of absorption due to the excited states (Fig **4.17** (b)).
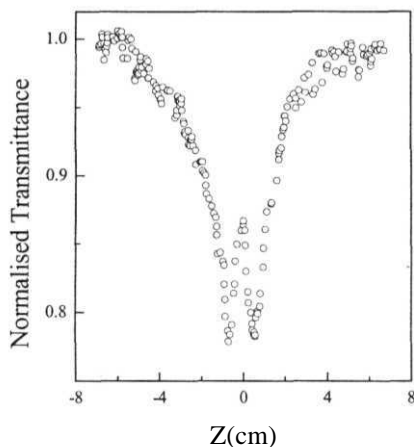
Fig 4.15: Sn_2-$(H_2)_4$ hexamer at 75% linear transmission and at I_{00} ~ 22.5 GWcm^{-2}
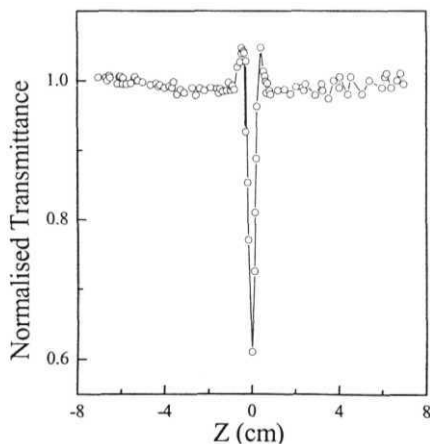
Fig 4.16: Sn_2-Zn_4 hexamer at 75% linear transmission and at I_{00} ~ 27.0 GWcm^{-2}. Solid line is guide to the eye.
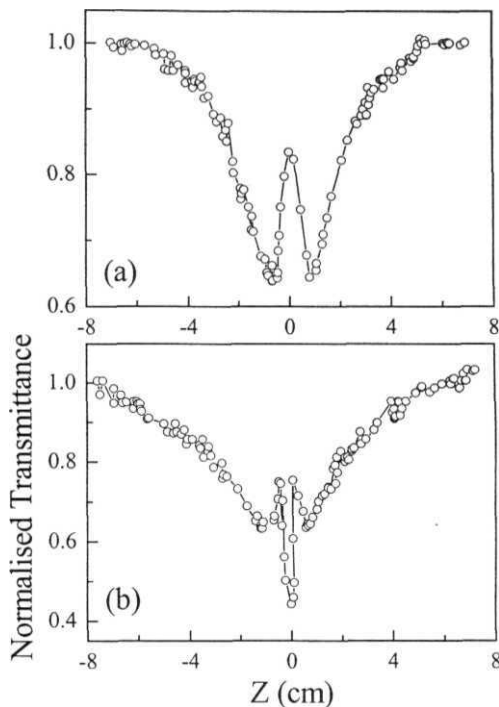
Fig **4.17**: Sn_2-Zn_4 hexamer at high concentration (60% linear transmission) at intensities of (a) 28.5 GW cm^{-2} and (b) 52.5 GW cm^{-2} respectively. Solid line is guide to the eye.

Depending on the input pulse duration, nonlinear absorption in these materials normally occurs through transitions from $S_o \rightarrow S_n$ states by instantaneous TPA or from $S_0 \rightarrow S_1 \rightarrow S_n$ states by a two-step resonant ESA (if $S_1 \rightarrow S_n$ occurs after vibrational transitions or diffusion within the singlet states) or $T_1 \rightarrow T_n$ states by means of ESA. From the equilibrium level S_1 the molecules may relax radiatively or nonradiatively to the ground state or transfer to the lower level of triplet manifold, T_1. Efficient RSA for picosecond pulses requires that the recovery rate from the S_1 state be slow compared to the optical pumping rate. Intra-band vibrational relaxation times also play an important role for RSA. The higher excited states of the singlet manifold relax to the lower vibrational states,

leading to absorption of the pump from the lower singlet level to the higher excited states through ESA. At the intensities and the pulse width used one need to consider the effect of multi-photon absorption (MPA) process also. Two-photon and Three-photon processes leading to optical limiting are well reported in various organic compounds [38]. Presence of MPA is generally resolved using upconverted fluorescence [39], transient absorption [40] using pump-probe and four-wave mixing experiments with femtosecond pulses [41]. For porphyrins the intersystem crossing time (τ_{ISC}), which is of the order of few nanoseconds in general and few hundreds of picoseconds in some specific cases, is of minor consequence because of the 25 ps pulse width of the laser. For the ps excitation we therefore can neglect intersystem crossing and hence the contribution of the T_1 state, which makes the singlet states responsible for the observed behaviour at these time scales.

At the wavelength of excitation, 532 nm, the lowest of the S_1 energy levels get excited, and therefore one expects more localization of the energy, which thereby leads to saturation at lower intensities. As the intensity increased, the behavior switched to RSA, as shown in Fig. 4.14 (b)&(c). The intensities used are 4.5 x 10^9 and 24.3 x 10^9 Wcm^{-2} for a concentration corresponding to 70% linear transmission at 532 nm. For increasing intensities (>34 x 10^9 Wcm^{-2}) the behavior shows a complete switchover from SA to RSA, which could probably be due to either TPA or step-wise ESA, TPA generated ESA or multi-photon absorption. At very large intensities the behavior was completely dominated by RSA.

Behavior of RSA followed by initial SA has been observed earlier for zinc meso-tetra (p-methoxyphenyl) tetrabenzoporphyrin (ZnmpTBP) [42], polymethine dye [43], and coordination compounds [44] and in Rhodamine B [45]. In ZnmpTBP [38] the behavior was attributed to the excitation of population into higher excited states (T_n) at higher intensities, giving rise to RSA; and the SA behavior was given as due to the saturation of the T_1 state. In polymethine dye [43] this behavior was attributed to irreversible damage induced by the input pulses. For ruthenium and osmium complexes of modified terpyridines [44], the saturation curve was explained as being due to the

compounds and the RSA portion as being due to TPA of the solvent. In RhB [45] the cross over from SA to RSA is observed with increasing concentrations and intensities in methanol when excitation is at near resonance with the absorption band and for RhB in water transition from RSA to SA is observed. The cross over is attributed to the formation of aggregates at higher concentrations that vary the singlet state lifetimes greatly. Zhan *et al*. [46] observed a transition from RSA to SA in a charge-transfer salt of with increasing intensity that was attributed to the fifth-order nonlinearity, as the excitation wavelength was 1064 nm and absorption peaked near 532 nm for their sample. Transition from RSA to SA with intensities and concentration depends on the higher excited state relaxation times. The most plausible explanation for the observed behavior in our case is that due to the PET and EET processes occurring simultaneously the excited singlet states become more and more localized thereby causing considerable changes in the absorption from the S_1 to the S_n states, which follows the square law for intensity dependence, leading to enhanced TPA. Though PET is reported to lead to saturation of excited states, the contribution from the lifetimes also plays a crucial role [47].

4.5   Ultrafast relaxation - DFWM-ps results

Population relaxation from the excited states becomes very important parameter in these molecules. Relaxation of the molecules out of the excited states occurs rapidly (<1ps) into an equilibrium level in the highest singlet S_1 state. The relaxation of S_n state would be unresolvable in our case due to the laser pulse width being larger than the expected lifetime. Population relaxation times studied using DFWM-ps technique has shown just the autocorrelation trace that is similar to that obtained for CS_2 shows that the relaxations are certainly faster < 25 ps. The recovery of the ground-state population can occur in times shorter than the measured fluorescence decay times under high laser fluence. This has been attributed to exciton-exciton annihilation. The rapid ground state recovery is common for porphyrin and phthalocyanine based systems in which

the excitons are strongly coupled [32]. This process could also lead to a rapid excited-state nonlinearity.

Ultrafast relaxations of the order of few hundred femtoseconds are well known in porphyrin-acceptor systems due to electron transfer [48]. Photoinduced charge separation, thermal charge recombination electron transfer due to porphyrin localized charge transfer character in a directly linked pyromellitimide-(porphyrinato) Zn(II) complex and similar donor-acceptor systems are reported to be in the timescales of 770 and 5200 fs [49]. Competition between internal conversion and energy transfer in the upper excited singlet state of the porphyrin-ruthenium complexes are also reported [50]. Lammi *et.al.* [51] reported energy and charge transfer between the adjacent states leading to excited state quenching at timescales < 11 ps and between different sites by super exchange assisted energy transfer at timescales of < 55 ps in diphenyl ethyne linked porphyrin dyads and triads and the relaxation rates can be tuned using the porphyrin-linker connection motif. Ultrafast excitation energy transfer processes are reported to be in the order of 12 ± 3 ps in Zn(II) porphyrin box [52]. Increasing number of porphyrin units has also reported to accelerate the relaxation dynamics of the lowest excited states from 4.5 ps for dimer to 0.3 ps for hexamer [53]. O'Keefe *et. al.* [54] reported a two-component decay, of approximately 700 fs and 170 ± 50 ps due to exciton-exciton annihilation and exciton diffusion to recombination centers on the polymer chain from femtosecond transient photoinduced transmission measurements on Zinc conjugated porphyrin polymer. Similar faster decay of 13 ± 5 ps is also reported for dimer [54] due to the rotational diffusion of the excited molecule in solution. Relaxations of ~ 6 ps are also reported in ethylene bridged side-to-side OEP porphyrin dimer [55]. Excited-state energy transfer is reported to be operative at timescales of 3.5 ps and 10 ps in *p*-phenylene linked porphyrin dimers [56], which varies with the bridge linker. Ultrafast fast kinetics of a hexameric benzo-porphyrin compound investigated by femtosecond transient absorption spectroscopy shows that in the hexamer a 20 ps decay component is present which is attributed to an intramolecular interchromophoric excited-state process [57]. In cofacial lanthanide porphyrin macrocycles two relaxation processes with time constants of ~ 1.5 and 10 ps are

reported [58]. Energy transfer to the nearest porphyrin in chelate assembly separated by approximately 15-18.5 A is reported to occur in ~ 10 ps, which varies with the separation [59]. The transition from SA due to the excited states to RSA observed in the Sn^{IV} oligomer arrays at higher intensities and the contribution from different nonlinear absorptive processes can be better understood with the help of relaxation/decay dynamics from the higher excited singlet states/energy transfer in these molecules.

4.6 Conclusions

> In the ns regime OL performance increases as one moves to higher homologues.

> Within trimers and hexamers, substitution of heavier metalloporphyrin reduced limiting performance slightly.

> Linearly linked Sn-Sn dimer shows a better OL performance than the axial-bonding type trimers and hexamers.

> In the ps regime these molecules show SA at higher intensities after initially showing RSA at lower intensities. At very high intensities RSA again takes over.

> Higher order nonlinearities in the ps regime indicate the presence of two-photon/ multi-photon absorption process.

> Ultrafast relaxations show a very fast relaxation < 25 ps in these molecules.

4.7 References

1. J.L. Bredas, C. Adant, P. Tackx, A. Persoons, and B.M. Pierce, *Chem. Rev.* 94, 243 (1994).

2. H.S. Nalwa, *Adv. Mater.* 5, 341 (1993); R.R. Tykwinski, U. Gubler, R.E. Martin, F. Diederich, C. Bosshard, and P. Gunter, *J. Phys. Chem. B* **102,** 4451 (1998).

3. P.N. Prasad and D.J. Williams, *"Introduction to nonlinear optical effects in molecules and polymers",* John Wiley and Sons Inc., (1991); H.S. Nalwa, *Adv. Mater.* 6, 341 (1994).

4. G. Horowitz, F. Garnier, A. Yassar, R. Hajaoui, and F. Kouki, *Adv. Mater.* 8, 52 (1996); W. Schrof, S. Rozouvan, T. Hartmann, H. Mohwald, V. Belov, and E. Van Keuren, *J. Opt. Soc. Am. B* 15, 889 (1998);

5. H.S. Nalwa, A. Katua, and A. Mukoh, *Chem. Phys. Lett.* **203,** 109 (1993); H.L. Anderson, S.J. Martin, and D.D.C. Bradley, *Angew. Chem. Int. Ed. Engl.* 33, 655 (1994); S. Guha, K. Kang, P. Porter, J.F. Roach, D.E. Remy, F.J. Aranda, and D.V.G.L.N. Rao, *Opt. Lett.* 17, 264 (1992); M.K. Casstevens, M. Samoc, J. Pfleger, and P.N. Prasad, J. *Chem. Phys.* 92, 2019 (1990); M.A. Diaz-Garcia, I. Ledoux, J.A. Duro, T. Torred, F. Agullo-Lopez, and J. Zyss, *J. Phys. Chem.* 98, 8761 (1994); H.S. Nalwa, A. Kakuta, and A. Mukoh,/ *Phys. Chem.* 97, 1097 (1993); G.L. Wood, M.J. Miller, and A.G. Mott, *Opt. Lett.* 20, 973 (1995).

6. P.N. Taylor, J. Huuskonen, G. Rumbles, R.T. Aplin, E. Williams, and H.L. Anderson, *Chem. Commun.* 909 (1998); A. Grand, A. Kaltbeitzel, A. Mathy, R. Schwarz, C. Bubeck, P. Vermehren, and M. Hanack, ./. *Phys. Chem.* 96, 7450 (1992); M.E. Orczyk, M. Samoc, J. Swiatkiewicz, N. Manickam, M. Tomoaia-Cotisel, and P.N. Prasad, *Appl. Phys. Lett.* 60, 2837 (1992); J.P. Hermann, and J. Ducing,./. *Appl. Phys.* 45, 5100 (1974); K.-H. Hass, A. Ticktin, A. Esser, H. Fisch, J. Paust, and W. Schrof, *J. Phys. Chem.* 97, 8675 (1993); L. Yang, R. Dorsinville, Q.Z. Wang, P.X. Ye, and R.R. Alfano, *Opt. Lett.* 17, 323 (1992); L. Yang, R. Dorsinville, R.R. Alfano, W.K. Zou, and N.L. Yang, *Opt. Lett.* 16, 758 (1991).

7. W.J. Feast, J. Tsibouklis, K.L. Pouwer, L. Groenendaal, and E.W. Meijer, *Polymer,* 37, 5017 (1996); *Conjugated Polymers,* eds. J.L. Bredas, and R. Silbey, Kluwer Academic, Dordrecht, 1991.

8. H.L. Anderson, *Chem. Commun.* 2323 (1999); Z. Bao, and L. Yu, ***Trends Polym. Sci.*** 3, 159(1995).

9. T. Kobayashi, *Nonlinear Opt.* 1, 91 (1991); S.V. Kershaw, in *Optoelectronic Properties of Inorganic compounds,* eds. D.M. Rondhill, and J.P. Fackler, Plenum, New York, 1999.

10. C.W. Spangler, *J.Mater. Chem.* 9, 2013 (1999).

11. H.S. Nalwa, *Adv. Mater.* 5, 341 (1993); T. Kaino, and S. Tomaru, *Adv. Mater.* 5, 172 (1993).

12. P.P. Kiran, N.K.M.N. Srinivas, D.R. Reddy, B.G. Maiya, A.S. Sandhu, A. Dharmadhikari, G.R. Kumar, and D.N. Rao, *Opt. Commun.* 202, 347 (2002); P.P. Kiran, D.R. Reddy, B.G. Maiya, A. Dharmadhikari, G.R. Kumar, and D.N. Rao, *Applied Optics, LPEO* 41, 7631 (2002); A. Krivokapic, H.L. Anderson, G. Bourhill, R. Ives, S. Clark, and K. J. McEwan, *Adv. Mater.* 13, 652 (2001).

13. F.Z. Henari, W.J. Blau, L.R. Milgrom, G. Yahioglu, D. Phillips, and J.A. Lacey, *Chem. Phys. Lett.* 267, 229 (1997); K.A. Sinha, B. Bihari, B.K. Mandal, and L. Chen, *Macromolecules* 28, 5681 (1995); M. Terazima, H. Shimizu, and A. Osuka, *J. Appl. Phys.* **81,** 2946 (1997); M.R. Wasielewski, *Chem. Rev.* 92, 435 (1992); Z.N. Bao, Y.M. Chen, and L.P. Lu, *Macromolecules* 27, 4629 (1994).

14. D.P. Arnold, G.A. Heath, and D.A. James, *New J. Chem.* 1377 (1998); D.P. Arnold, and D.A. James, *J. Org. Chem.* 3460 (1997); S.M. Lecours, S.G. DiMagno, and M.J. Therien, *J. Am. Chem. Soc.* **118,** 11854 (1996); V.S.-Y. Lin, S.G. DiMagno, and M.J. Therien, *Science* 264, 1105 (1994); P.J. Angiolillo, V.S.-Y. Lin, J.M. Vanderkooi, and M.J. Therien,*./. Am. Chem. Soc.* 117, 12514 (1995).

15. J.R. Reimers, T.X. Lu, M.J. Crossley, and N.S. Hush, *Chem. Phys. Lett.* 256, 353 (1996); L. Jaquinod, M.O. Senge, R.K. Pandey, T.P. Forsyth, and K.M. Smith, *Angew. Chem. Int. Ed. Engl.* 35, 1840 (1996); L. Jaquinod, O. Siri, R.G. Khoury, and K.M. Smith, *Chem. Commun.* 1261 (1998); C.K. Johnson, and D. Dolphin, *Tetrahedron Lett.* 39, 4753 (1998).

16. H.L. Anderson, *Chem. Commun.* 2323 (1999).

17. K.M. Kadish, Q.Y.Y. Xu, B.G. Maiya, J.-M. Barbe, and R. Guilard, *J. Chem. Soc.,Dalton Trans.* 1531 (1989).

18. A.A. Kumar, L. Giribabu, D.R. Reddy, and B.G. Maiya, *Inorg. Chem.*, 40, 6757 (2001).

19. L. Giribabu, T.A. Rao, and B.G. Maiya, *Inorg. Chem.,* 38, 4971 (1999).

20. S.V. Rao, N.K.M.N. Srinivas, D.N. Rao, L. Giribabu, B.G. Maiya, R. Philip, and G.R. Kumar, *Opt. Commun.* **182,** 255 (2000).

21. J. Hein, H. Bergner, M. Lenzner, and S. Rentsch, *Chem. Phys.* **179,** 543 (1994); J.P. Hermann, and J. Ducuing, *J. Appl. Phys.* 45, 5100 (1974); T. Johr, W. Werncke, M. Pfeiffer, A. Lau, and L. Dahne, *Chem. Phys. Lett.* 346, 521 (1995).

22. M. Terazima, H. Shimizu, and A. Osuka, *J. Appl. Phys.* **81,** 2946 (1997); D. Kim, and A. Osuka,*J. Phys. Chem.A,* **107,** 8791 (2003).

23. W. Werncke, M. Pfeiffer, A. Lau, W. Grahn, H.-H. Johannes, and L. Dahne, *J. Opt. Soc. Am. B,* **15, 863 (1998).**

24. J.R.G. Thorne, S.M. Kuebler, R.G. Denning, I.M. Blake, P.N. Taylor, and H.L. Anderson, *Chem. Phys.* **248,** 181 (1999).

25. S.M. Kuebler, R.G. Denning, and H.L. Anderson, *J. Am. Chem. Soc.* **122,** 339 (2000); T.E.O. Screen, K.B. Lawton, G.S. Wilson, N. Dolney, R. Ispasoiu, T. Goodson III, S.J. Martin, D.D.C. Bradley, and H.L. Anderson, *J. Mater. Chem.* **11,** 312(2001).

26. R. Kumble, S. Palese, V.S.-Y. Lin, M.J. Therien, and R.N. Hochstrasser, *J. Am. Chem. Soc.* **120,** 11489 (1998).

27. C. Zhan, D. Li, D. Wang, D. Zhang, Y. Li, W. Xu, Z. Lu, L. Zhao, Y. Nie, and D. **Zhu,** *Chem. Phys. Lett.* 347, 410 (2001).

28. Optical phase conjugation ed. R.A. Fischer, Academic Press, (1983).

29. E.J. Canto-Said, D.J. Hagan, J. Young and E.W. Van Stryland, *IEEE. J. Quant. Electron.* 27, 2274(1991).

30. K.M. Nashold, and D. P. Walter, *J. Opt. Soc. Am. B* 12, 1228 (1995); K. Mansour, M.J. Soileau, and E.W. Van Stryland, *J. Opt. Soc. Am. B* 9, 1100 (1992).

31. D. Beljonne, G.E. O'Keefe, P.J. Hamer, R.H. Friend, H.L. Anderson, and J.L. Bredas, *J. Chem. Phys.* **106,** 9439 (1997).

32. F.M. Qureshi, S.J. Martin, X. Long, D.D.C. Bradley, F.Z. Henari, W.J. Blau, E.C. Smith, C.H. Wang, A.K. Kar, and H.L. Anderson, *Chem. Phys.* **231,** 87 (1998).

33. M.A. Someda, and Y. Kaizu, *Inorg. Chem.* 38, 2303 (1999).

34. L. Flamigni, F. Barigelletti, N. Armaroli, B. Ventura, J.P. Collin, J.P. Sauvage and J.A.G. Williams, *Inorg, Chem.* 38, 661 (1999).

35. K. Kalyanasundaram, Ch. 13, in "*Photochemistry of polypyridine and porphyrin complexes",* Academic Press, (1992).

36. S. V. Rao, N.K.M.N. Srinivas, D.N. Rao, L. **Giribabu,** B.G. Maiya, R. Philip, and G.R. Kumar, *Opt. Commun.* 192, 123 (2000).

37. G. B. Talapatra, D. N. Rao, and P. N. Prasad, J. Phys. Chem. 88, 4636 (1984).

38. J.D. Bhawalkar, G.S. He, and P.N. Prasad, *Rep. Prog. Phys.* 59, 1041 (1996); G.S. He, G.C. Xu, P.N. Prasad, B.A. Reinhardt, J.C. Bhatt, and A.G. Dillard, *Opt. Lett.* 20, 435 (1995); G.S. He, J.D. Bhawalkar, C.F. Zhao, and P.N. Prasad, *Appl. Phys. Lett.* 67, 2433(1995).

39. J.D. Bhawalkar, G.S. He, and P.N. Prasad, *Opt. Commun.* **119,** 587 (1995); G.S. He, J.D. Bhawalkar, and P.N. Prasad, *Opt. Lett.* 20, 1524 (1995); G.S. He, J. Zieba, J.T. Bradshaw, M.R. Kazmierczak, and P.N. Prasad, *Opt. Commun.* **104,** 102 (1993).

40. Y. Pang, M. Samoc, and P.N. Prasad, *J. Chem. Phys.* 94, 5282 (1991).

41. M.T. Zhao, Y. Cui, M. Samoc, P.N. Prasad, M.R. Unroe, and B.A. Reinhardt, *J. Chetn. Phys.* 95, 3991 (1991).

42. N. K. M. N. Srinivas, S. V. Rao, D. V. G. L. N. Rao, B. K. Kimball, M. Nakashima, B. S. Decristofano, and D. N. Rao, J. *Porphyrin. Phthalocyanine.* 5, 549 (2001).

43. O. V. Przhonska, J. H. Lim, D. J. Hagan, E. W. Van Stryland, M. V. Bondar, and Y. L. Slominsky, *J. Opt. Soc. Am. B* **15,** 802 (1998).

44. M. Konstantaki, E. Koudoumas, S. Couris, P. Laine, E. Amouyal, and S. Leach, *J. Phys. Chem. B* **105,** 10797 (2001).

45. N.K.M.N. Srinivas, S.V. Rao, and D.N. Rao, J. *Opt. Soc.Am B* **20,** 2470 (2003).

46. C. Zhan, W. Xu, D. Zhang, D. Li, Z. Lu, Y. Nie, and D. Zhu, *J. Mater. Chem.* **12,** 2945 (2002).

47. P.P. Kiran, D.R. Reddy, B.G. Maiya, A.K. Dharmadhikari, G.R. Kumar, and D.N. Rao, *Appl. Opt.* **41,** 7631 (2002); S. Huges, G. Spruce, B.S. Wherrett, K.R. Welford, and A.D. Lloyd, *Opt. Commun.* **100,** 113 (1993); X. Deng, X. Zhang, Y. Wang, Y. Song, S. Liu, and C. Li, *Opt. Commun.* **168**, 207 (1999).

48. M. Andcrsson, "*Tuning electron transfer reactions by selective excitation in porphyrin-acceptor assemblies",* Ph.D. Thesis, Uppsala (2000).

49. N.P. Redmore, I.V. Rubstov, and M.J. Therien, *Inorg. Chem.* **41,** 566 (2002); *ibid, J. Am. Chem. Soc.* **125,** 8769 (2003).

50. A. Harritnan, M. Hissler, O. Jrompette, and R. Ziessel, *J. Am. Chem. Soc.* **121,** 2516 (1999).

51. R.K. Lammi, A. Ambroise, R.W. Wagner, J.R. Dicrs, D.F. Bocain, D. Holten, and J.S. Lindsey, *Chem. Phys. Lett.* **341,** 35 (2001).

52. I.W. Hwang, H.S. Cho, D.H. Jeong, D. Kim, A. Tsuda, T. Nakamura, and A. Osuka *J. Phys. Chem. B.* **107,** 9977 (2003).

53. H.S. Cho, D.H. Jeong, S. Cho, D. Kim, Y. Matsuazaki, K. Tanaka, A, Tsuda, and A. Osuka, *J. Am. Chem. Soc.* **124,** 14642 (2002).

54. G.E. O'Keefe, G.J. Denton, E.J. Harvey, R.T. Phillips, R.H. Friend, and H.L. Anderson,./. *Chem. Phys.* **104,** 805 (1996).

55. M. Chachisvilis, V.S. Chirvony, A.M. Shulga, B. Kallebring, S. Larsson, and V. Sundstrom, *J. Phys. Chem.* **100,** 13867 (1996).

56. S.I. Yang, R.K. Lammi, J. Seth, J.A. Riggs, T. Arai, D. Kim, D.F. Bocian, D. Holten, and J.L. Lindsey, J. *Phys. Chem B* **102,** 9426 (1998).

57. G. Schweitzer, G. De Belder, L. Latterini, Y. Karni, A.E. Rowan, R.J.M. Nolte, and F.C. De Schryver, *Chem. Phys. Lett.* 303, 261 (1999).

58. O. **Bilsel, J.** Rodriguez, and D. Holten, *J. Phys. Chem.* 94, 3508 (1990).

59. I.V. Rubstov, Y. Kobuke, H. Miyaji, and K. Yoshihara, *Chem. Phys. Lett.* **308,** 323 (199).

Chapter 5

$Bi_{12}SiO_{20}$ and $Bi_{12}SiO_{20}$:Fe crystals

Optical limiting characteristics of $Bi_{12}SiO_{20}$(BSO) and $Bi_{12}SiO_{20}$: Fe (BSO.Fe) crystals at different wavelengths in the visible region at 435, 532, 600 and 683 nm in the nanosecond regime are presented. Studies reveal the contributions of both two-photon absorption (TPA) and charge carrier absorption from the traps, leading to nonlinear absorption. Pump-probe studies with 25 ps pulses revealed ~ 60 ps relaxation of excited carriers. The effect of relaxation of excited charge carriers on the nonlinear absorption behavior is also discussed.

5.1 Photorefractive materials for NLO applications

Electro-optic photoconductive materials present many interesting phenomena, one among them is the photorefractive effect with a variety of potential applications in nonlinear optics and photonics which include phase conjugation, optical interconnections, optical spatial solitons, and optical signal processing [1]. The phenomenon of photorefraction arises on the nonuniform illumination of such materials and with the diffusion of the ensuing photogenerated carriers towards lesser-illuminated regions with the associated electric fields that, through the Pockels effect, cause localized changes in the refractive index. This photoionization occurs from relatively deep energy levels within the bandgap that are not normally thermally ionized. The light induced absorption due to the photoinduced charge transport has been studied widely **in** the field of photorefractive nonlinear optics because it plays an important role in the construction of passive optical limiters and optical threshold elements in optical processing systems [2].

In photorefractive materials, at higher input intensities, the mechanism of charge carrier generation and transport process involve impurity levels which leads to the greater possibility of the combined effect of trap assisted charge carrier absorption (TACCA) and TPA [3]. Here the former is an accumulative nonlinearity, which requires time for energy transfer from field to medium and hence depends on energy density deposited in the medium. This nonlinearity can

also be nonlocal due to the drift or diffusion of photogenerated charge carriers in the medium and hence can in principle only depend on the input fluence. The later is an instantaneous nonlinearity, which depends on the input light intensity, can be effective over broadband of the spectrum and for very short pulses. TPA can also act as a significant loss mechanism when a material is subjected to a strong beam of photons of energy ħω, with ħω $< E_g < 2\hbar\omega$, where E_g is the energy gap of the material. High sensitivity optical storage by the photorefractive process using multi-photon absorption was demonstrated in LiNbO$_3$ and in KTN [4]. Permanent and reversible changes of refractive index of pure and doped LiNbO$_3$ have been obtained by multi-photon absorption that results in increased sensitivity for optical storage and holography [5].

In this chapter, we compare the optical limiting behavior exhibited due to combined effect of TPA, free carrier absorption and trap assisted charge carrier absorption (TACCA) in photorefractive crystals of pure and iron doped BSO in the visible spectral range using nanosecond pulses at 435, 532, 600 and 683 nm. An excellent passive limiting behavior is demonstrated for the first time using these crystals in visible region. In our qualitative modeling of the effect, we account the absorptive changes due to combined effect of TACCA and TPA. Consequently, we present the precise role of the internal defects due to impurity centers present in the crystal lattice, to help in the understanding and obtaining optimum samples for enhanced optical limiting from these photorefractive materials.

5.2   Bi$_{12}$SiO$_{20}$ and Bi$_{12}$SiO$_{20}$: Fe

The sillenite family crystals, in particular, BSO is considered attractive candidate for applications due to its strong photorefractive properties like high sensitivity, fast response time, comparable electro-optic coefficient with other crystals of the family and interesting piezoelectric, optically-active and many other interesting properties like beam deflection, switching, holography, phase conjugation and optical memories [6]. It has been reported that out of three non-zero electro-optic coefficients r_{41}, r_{52}, and r_{63}, the element r_{41} is important for

device applications [7]. BSO has cubic symmetry, belonging to point group 23. In BSO the standard photorefractive effect is based on the absorption of photons by impurity levels. One can improve the performance by means of increasing the impurity levels by doping. In BSO, a large number of trap levels in the energy gap predicted from the spectral response of the photoconductivity [8] and the traps with high concentration were observed experimentally [9]. In addition to distinguishable shallow trap levels reported, there appears to be many overlapping levels that are not distinguishable at deep energy levels below the conduction band [10]. Attard [11] predicted the Fermi level shift in BSO via photon induced trap occupation. The shift of Fermi level is dependent on the density of trap sites in the bandgap, the radiation induced occupation density, and the energy levels of the traps. Investigations report that photorefractive materials doped with iron leads to favourable photorefractive properties such as small response time and high sensitivity [12]. It is also shown that optical properties and light induced absorption changes are affected due to iron doping [13]. Investigations on the possibilities for practical applications of sillenites have revealed that doping can conveniently be used to modify the absorption in a way suitable for the particular application. In BSO too, doping with various elements leads to significant changes in the electrical, photoelectrical and optical properties. Nagao and Mitnura [14] have investigated the influence of a large number of transition metals on the transmission and photoresponse of BSO. The general conclusion made about photoresponse is that the transition metal impurities in BSO crystals quench the photoconductivity. An intuitive explanation proposed for the quenching is the formation of recombination centers [15]. When the light intensities are strong enough, effects that are caused by TPA can become important [16] and can also be enhanced by the existence of intermediate energy levels inside the forbidden bandgap because of the impurities. It is found that addition of significant amount of Fe^{34} ions as impurities can easily change the valence state and may play a critical role in charge carrier mobility as well as intensity dependent absorption. Recent study of this effect [7] in pure BSO crystal examined the CW recording under applied electric field at low intensities of a CW laser. Optical limiting has been studied

in $BaTiO_3$ by using photorefractive nonlinearities [17] and by utilizing the photo induced lensing in BSO [18] at low intensities of a CW laser. Light controlled electro-optic power limiter has also been demonstrated in BSO crystal [7].
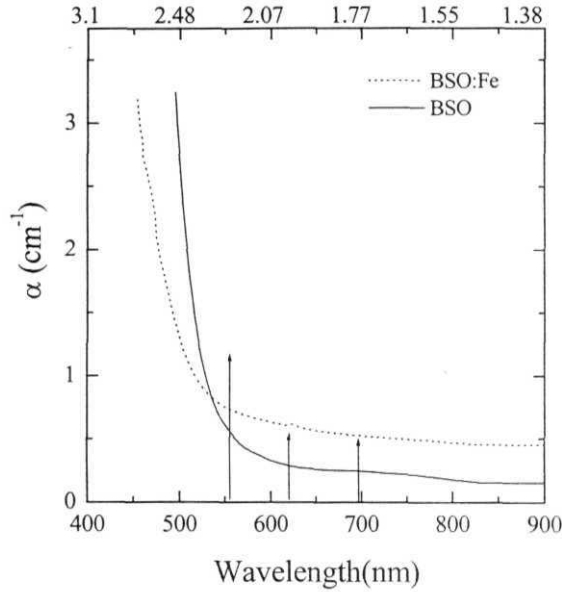
Figure 5.1: Absorption spectra of BSO and BSO: Fe.

Since the revelation of polymorphy of bismuth trioxide [19] various efforts were made for the growth and characterization of BSO single crystals [20]. An undoped BSO crystal bought from Fujian Castech Crystals Inc., China with dimensions of 10 mm x 10 mm x 5 mm, and a Fe-doped BSO crystal obtained from Alabama University, USA [21] with dimensions 5 mm x 4 mm x 4 mm, are cut to have thickness of 1 mm along c-axis are used for optical limiting and nonlinear absorption studies. The surfaces of the crystal were polished to minimize the scattering. Optical limiting studies are also done with 4 mm thick crystals. The amount of iron incorporation in the crystal is determined using Inductive Coupled Plasma - Atomic Emission Spectroscopy (ICP-AES). The

result has shown that 150-ppm Fe is incorporated in the crystal as impurity. In principle, during the growth Fe can replace Bi as well as Si in BSO. **But** from ICP - AES study it is also found that the doped crystal grown from melt having no Si deficit. Hence it can be assumed that Fe atoms incorporated only on the Bi sites in our sample.

The absorption spectrum of the crystals used in this study is shown in Fig 5.1. The absorption spectrum shows a very large absorption above 3eV and matches well with that reported in literature [10,22]. As one can see from the absorption spectrum a long tail in the absorption edge goes all the way to 900 nm (1.38eV). This implies that the crystal possess large number of donor sites. The absorption centers/traps responsible for the absorption in the above region are reported as due to either silicon vacancy complex or bismuth substituting for silicon or Fe^{3+} impurities. And these are raised to conduction band by optical excitation with photons in energy region 1.7eV to 3.5eV.[l 1]. The change in the absorption spectrum with various metals as dopants and different growth conditions has been reported earlier in various photorefractives like $BaTiO_3$, $LiNbO_3$ and in $PbBaNb_2O_6$ [23] with major variation in the visible region. Doping of impurities like iron [10], cobalt [15] and transition metals [14] has been reported to change the optical absorption spectrum in the visible region. The crystal structures of both pure and iron doped BSO are studied using single crystal X-ray diffraction technique revealed body centered cubic structure with lattice constants of (10.0935 ± 0.003) A and (10.0335 ± 0.006) A respectively. The result shows that the lattice constants are slightly varied due to doping process without change in crystal structure and are in good agreement with earlier reports in the literature [20].

5.3   Energy levels due **to iron impurity in BSO**

The energy levels of iron are spread in the energy gap below the conduction band of BSO. This is a very important result for the understanding of the excitation (both thermal and light induced) and recombination processes and their influences on photorefractive measurements. In any case, it cannot be

assumed, as in the case of a semiconductor like silicon, that the dopant introduces a single, well-defined energy level in the band gap. An impurity atom with a certain valence can capture an electron and change its valence accordingly if the newly created state is stable. For example the Fe^{4+} centre can capture an electron in the reaction $Fe^{4+} + e" \rightarrow Fe^{3+}$. On the other hand, an electron of Fe^{3+} can be photoexcited leading to a Fe^{4+} centre and an electron in the conduction band. The Fe^{4+} centre has both empty and occupied levels near mid gap. The centre Fe cannot capture an electron because the Fe^{2+} center appears to be unstable: its upper occupied energy level has energy higher than the energy of the lowest conduction band states. This centre becomes stable if the unit cell is slightly more distorted than assumed. It can also be stabilized by local charge compensation. The higher the ionicity of the impurity is, the lower are its energy levels. This is a general rule.
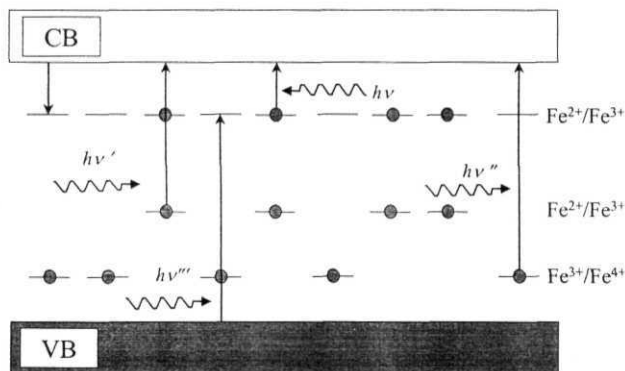
Figure 5.2: Qualitative representation of the intra band-gap energy levels introduced by Fe impurity. Each level represents a photoionisation energy. The ability to trap an electron and to obtain a centre with such a photoionisation energy is indicated by a line. The presence of a photoexcitable electron is indicated with a grey dot. The levels are labelled with the photoionisation transition they represent.

When the nominal ionicity of the impurity increases, the *d* states of the transition metal (in the above example iron) move down in energy with respect to the valence band (oxygen *2p* orbitals). Under illumination the impurities with lower ionicity (e.g. Fe^{24}) behave more as electron donors, and the impurities with

higher ionicity (e.g. Fe^{4+}) tend to be electron acceptors, or hole donors. Another general result valid for the Si ion as well as for the substituent Fe ion is that the environment of the metal atom (Si or Fe) has a strong influence on its energy levels: a low symmetry of the environment produces a splitting of degenerate energy levels and a general downward shift in energy. This effect can be produced by a phase transition to a phase with lower symmetry or by a modification of the local environment of the ion.

Fig. 5.2 is a schematic representation of the level structure of an impurity Fe atom in different valence states. Here Fe^{2+} is assumed to be stable and to have two occupied energy levels with different energies inside the band gap. For this band diagram, we adopted a simplified notation that is useful in the context of a thermodynamic discussion. The energy levels that correspond to a certain ionization process (e.g. $Fe^{2+} \rightarrow Fc^{3+} + e^{-}$) are identified by a series of horizontal bars (labeled Fe^{2+} / Fe^{3+}). The energy difference between a level and the lower edge of the conduction band represents the minimum energy that is necessary to photoexcite an electron from the impurity state to the conduction band. A solid dot is present if an electron exists with such ionisation energy. Absence of a solid dot means that the level is able to bind an electron and act as an electron trap. There arc two levels labelled Fe^{2+} / Fe^{3+} in Fig. 5.2 because there are two electron states with different ionisation energies. An elcctron can be photoexcited from both states to create a centre Fc^{3+}. A solid dot in the upper Fe^{2+} / Fc^{3+} level represents the centre Fe^{2+}, with the ionization energy of the upper electron given by the position of the level in the energy diagram. An empty line in the upper Fe^{2+} / Fe^{3+} level represents a Fe^{3+} centre which is able to trap an electron to become the centre Fe^{2+}. The centre Fe^{2+} has two occupied energy levels with different energies inside the band gap and has therefore two ionisation energies. The level corresponding to the electron with higher photoionisation energy is also drawn in Fig. 5.2. Photoexcitation of an electron from one of this two levels leads always, after thermalisation, to the formation of the centre Fe^{3+}. In Fig. 5.2, when empty levels are drawn, they can always capture an electron; their energy corresponds to the photoionisation energy of the captured electron. The levels that correspond to excited states of an impurity that

are present inside the conduction band are not drawn. The method used to draw energy levels concentrates more on the photoionisation and recombination process, that are of primary importance to the photorefractive effect rather than on the possible electronic states in the band gap.

Note that the centre Fe^{3+}, which represents an empty site in the Fe^{2+}/Fe^{3+} level, is shown as a full site in the Fe^{3+}/Fe^{4+} level. In the band diagram of Fig. 5.2, empty levels appear to have the same energy as the filled ones, but at the same time they can be interpreted as donors at a lower energy in the band diagram (with a higher photoionisation energy). The occupation of the ionisation levels (i.e. the valence state of the impurity atom) is connected with the difference between the Fermi energy and the energy of the particular ionisation level. When the Fermi level is below one particular level, that level will be essentially empty and when the Fermi level is higher, the level will be primarily filled. For a level to be partially full (that is, for an impurity atom to appear at the same time in two valence states that act as donor and acceptors), the energy of the Fermi level must be close to the energy of the impurity level. An important conclusion, which is valid, also if there are many different impurities, is that in thermal equilibrium there can be only one partially filled level for any particular value of the Fermi energy (the distance between different levels is generally greater than $k_B T$). This means that in thermal equilibrium a certain impurity centre is expected to appear in the host crystal in at most two valence states.

Above we have described only the photoexcitation of electrons to the conduction band. The symmetric case of photoexcitation of an electron in the valence band to an empty level like Fe^{3+} is also possible. This transition is often described as photoexcitation of holes and Fe^{3+} acts as a "hole donor". The changes in level occupation induced by this transition are analogous to what was described above in the case of transitions to the conduction band and we do not describe them any further. In Fig. 5.2 three possible electron photoexcitation transitions are drawn. Which transition will be favoured under illumination depends on the photoionisation cross section of the impurities and on the wavelength of the light. As an example, photoexcitation of Fe^{3+} in Fig. 5.2 (Fe^{3+} / Fe^{4+} level) requires light with a shorter wavelength than photoexcitation of Fe^{2+}.

Thus, the concentrations of active photorefractive acceptors or donors are determined by the extent to which each level is filled or empty and by the wavelength of the light. The number of filled centres that can be photoexcited using a certain wavelength gives the number of active donors. The empty levels give the number of active traps. In the example shown in the diagram of Fig. 5.2 the centre Fe $^+$ (**in** the upper Fe^{2+} / Fe^{3+} level) acts as a trap with small ionisation energy. This trap disappears if Fe^{3+} is photoionised to produce Fe^{4+}. The centre Fe^{4+} (in the lower Fe $^+$ / Fe^{4+} level) is an electron trap with much larger photoionisation energy. {One can also say that photoionisation of Fe^{3+} transforms a trap with small ionization energy into a trap with higher ionisation energy.} The total number of trap levels available for electron recombination increases with the ionicity of the impurity (in the example of Fig. 5.2 the centre Fe^{4+} can trap two electrons: $Fe^{4+} + 2\ e'' \rightarrow$ Fe $^+$). Since the ionicity of the impurity atoms is connected with the position of the Fermi level, the number of electron donors and traps also depends on the Fermi energy. We assume all donor impurities are identical and have exactly the same energy and lie in the middle of the bandgap. Absorbing photons ionizes these donor impurities and as a result ionization electrons are generated in the conduction band leaving empty trap states behind, which are capable of capturing electrons. The impurities due to the presence of Fe atoms may be in the form of Fe^{3+} or Fe^{21} states.

5.4   **Optical limiting** and **Nonlinear absorption**

Optical limiting and nonlinear absorption measurements are performed with <110> direction of the crystal coinciding with the Z-axis of the beam propagation. Open aperture Z-scan studies are done with 1 mm thick crystals and OL curves arc recorded with both 1 and 4 mm thick crystals. The sample satisfied the **"thin"** sample condition $L < n_0 z_0$, where L is the sample thickness, n_0 the linear refractive index and z_0 the diffraction length of the focused beam for Z-scan studies. No external electric field is applied across the crystal. Beam fanning is observed in the far field from BSO:Fe while performing Z-scan and OL measurements. Proper precautions are taken to collect all the transmitted

light by bringing the collecting lens closer to sample and by using large diameter lens for collecting the output. Beam fanning is well known phenomenon in Fe doped photorefractive crystals arising from scattering due to the impurities within the crystal [24]. At room temperature BSO behaves as a two-photon absorber at 532, 600 and 683 nm as the band gap obey $\hbar\omega < Eg < 2\hbar\omega$. We find, from the theoretical modeling, that the nonlinear absorption is due to TPA assisted by free carrier absorption and trap assisted charge carrier absorption from TL to CB_L. Absorption from trap levels has been discussed earlier for $BaTiO_3$ [25] and BSO [26]. The excitation of charges from shallow traps to the conduction band is also reported [27]. The domination of photogenerated carrier absorption with nanosecond pulsed lasers is reported earlier [28] in direct band gap semiconductors.
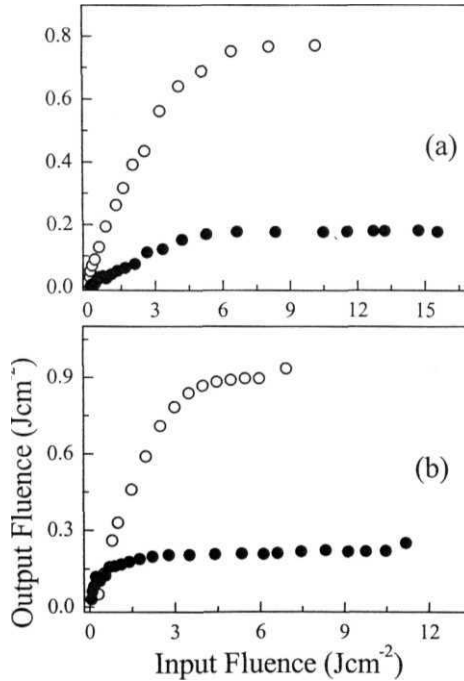
Figure 5.3: Optical limiting response of BSO (o) and BSO: Fe (•) at (a) 532 nm and (b) 600 nm with 4mm thick crystals.

The transfer of the conduction electrons to trap levels and the recombination with the VB holes increases with the number density of excited electrons in the CB. This leads to more absorption of the electrons from the trap levels to the conduction band. However, for very short pulses (ps), transitions from lower conduction band to trap levels can be neglected. Pure TPA is reported in another crystal of sillenite family $Bi_{12}GeO_{20}$ (BGO) at 532 nm using a 16 ps pulse width Nd: YAG laser [16]. Optical limiting behavior of BSO and BSO: Fe at 532 nm and 600 nm with 4 mm crystal is shown in Fig.5.3.

The damage threshold is identified as the intensity at which a strong scattering appeared at the output followed by the darkening and then damage formed on the crystal. The optical limiting performance and the damage threshold have increased considerably with the presence of iron impurity. The limiting and damage thresholds of the crystals are given in table 5.1. Fig 5.4 shows the open aperture Z-scan curves of BSO and BSO: Fe at 532 nm with different peak intensities. Open aperture Z-scan curves of BSO: Fe appear slightly broader compared to that of BSO and nonlinear absorption has increased quite considerably even at lower intensities. At all the excitation wavelengths similar increase in nonlinear absorption is observed. Open aperture Z-scan curves of both the crystals at 600 nm is shown in fig 5.5.
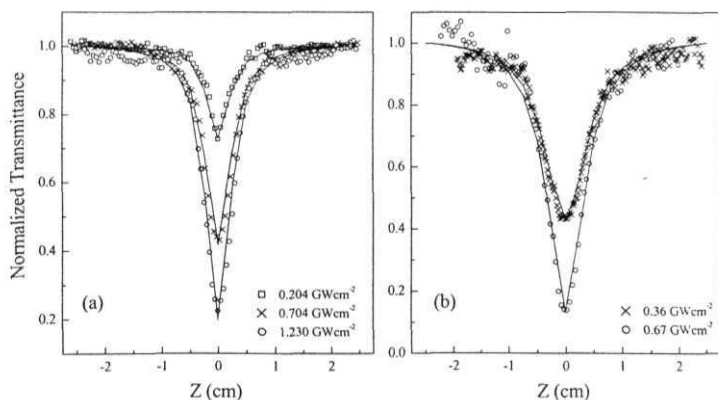
Figure 5.4: Open aperture Z-scan curve of (a) BSO and (b) BSO: Fe at 532 nm, 6ns pulses. Solid lines show **the** theoretical fits generated using **the** model explained in section 5.5.
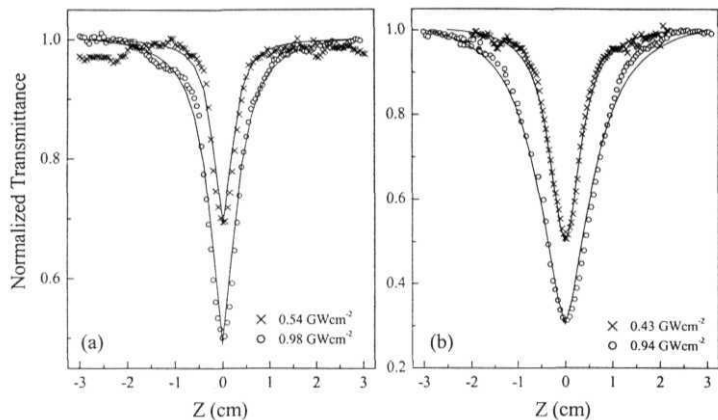
Figure 5.5: Open aperture Z-scan curve of (a) BSO and (b) BSO: Fe at 600 nm, 6ns. The solid lines are theoretical fits generated using the model explained in section 5.5.

λ_{ex}	Limiting Threshold (Jcm^{-2})		Damage Threshold (Jcm^{-2})	
	BSO	BSO: Fe	BSO	BSO: Fe
532 nm	3.38±0.4	1.29±0.2	9.6±0.3	15.6±0.2
600 nm	5.88±0.5	3.29±0.3	6.4±0.2	10.6±0.3
683 nm	---	---	4.7±0.2	7.7±0.3

Table 5.1: Limiting and damage thresholds of BSO and BSO: Fe with 6 ns pulses with 1 mm crystal.
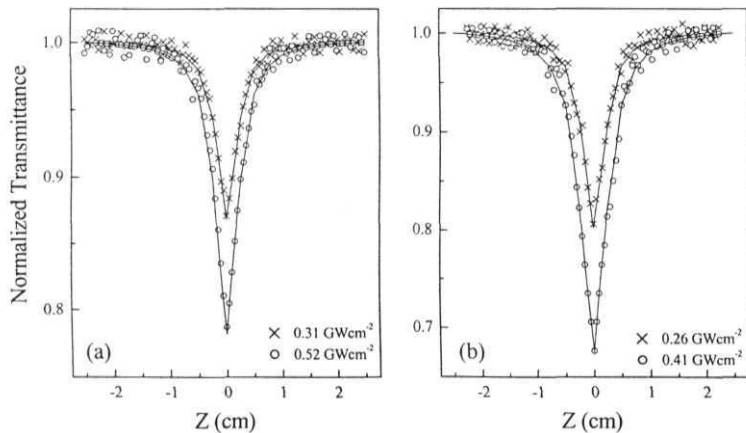
Figure 5.6: Open aperture Z-scan curves of BSO and BSO: Fe at 683 nm.

Open aperture Z-scan curves of these crystals at Raman shifted wavelength of 683 nm are shown in Fig 5.6. As we move towards the red side of the spectrum, the nonlinear absorption has reduced slightly. But the overall contribution of TPA has remained almost same at the excitation wavelengths. It is the contribution from the trap levels and the FCA playing a very significant role in the nonlinear absorption. As one moves towards the longer wavelength region more contribution from the TPA can be expected.

The limiting threshold ($Il/2$) is decreasing and the damage threshold increases with iron incorporation in these crystals. As one moves towards the longer wavelengths the $l_{1/2}$ increases gradually and the damage threshold decreases. This may be due to the fact that at the longer wavelengths the contribution from the trap levels and free carrier absorption may be decreasing, where as the contribution of TPA remaining almost constant.

5.4.1   Open aperture Z-scan and Pump-probe and measurements with 25 ps pulses

Open aperture Z-scan experiment is performed with 25 ps pulses at 532 nm and a good nonlinear absorption is observed (Fig 5.7). Pump-probe measurements are done to find out the relaxation of the excited carriers at these timescales. The ratio of the intensity of the pump to probe beam is 1000:1. Pump energy is 300 μJ and the probe is kept at 0.3μJ. At the probe energy used no nonlinear absorption is observed for BSO. Probe is delayed with respect to pump and its transmittance is monitored with delay. Probe transmittance has reduced considerably at the zero delay and as the probe moves away the transmittance starts to increase back to the linear transmittance (Fig. 5.8). In the pump-probe experiment, probe transmittance reduced in the presence of the pump pulse for a large range of delay times. The measurements showed that photoinduced absorption could occur even within a picosecond time scale. From the curve we can see that there is no original induced absorption before pump excitation (~ -300 ps). Also for a delay (~ 200 ps) there is saturation in the transmittance. We observed that the induced absorption reaches its maximum

within the first 70 ps and then decays slowly. And for longer delays the induced absorption is still present.
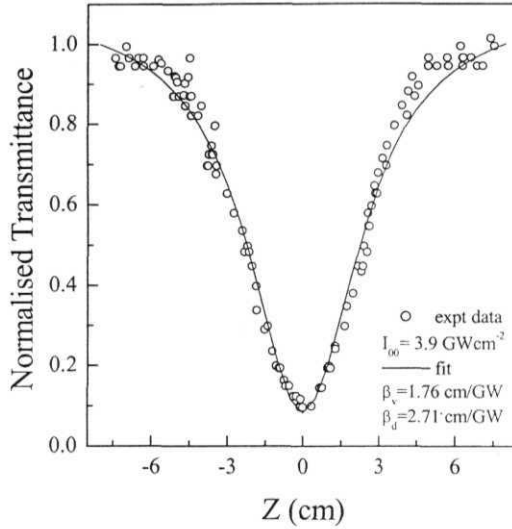
Figure 5.7: Open aperture Z-scan curve of BSO at 532 nm, 25 ps pulse width. Circles represent experimental data the theoretical fit is shown by solid line obtained using the model explained in section 5.5.

The inset in fig 5.8 shows the decay of probe absorption ~ 60 ps, which gives the relaxation of the excited charge carriers. Similar photoinduced absorption has been observed in BaTiO3 which gives the hole recombination time of ~ 60 ps with secondary centers [29]. Measurements done with 1 ps pulse excitation at 596 nm [30] revealed two distinct features, first one is a pronounced rapidly recovering induced absorption at zero delay with a width indistinguishable from the width of the pulse duration consistent with an absorption process that depends on the instantaneous irradiance in the crystal which is attributed to TPA and the second is a long-lived induced absorption at positive delays. There are two processes that can contribute to the long-lived induced absorption: free-carrier absorption and redistribution of charge among the impurity levels. Although the relative contributions of these two processes

cannot be determined uniquely, long decay time of the induced absorption suggests that charge redistribution plays a significant role.
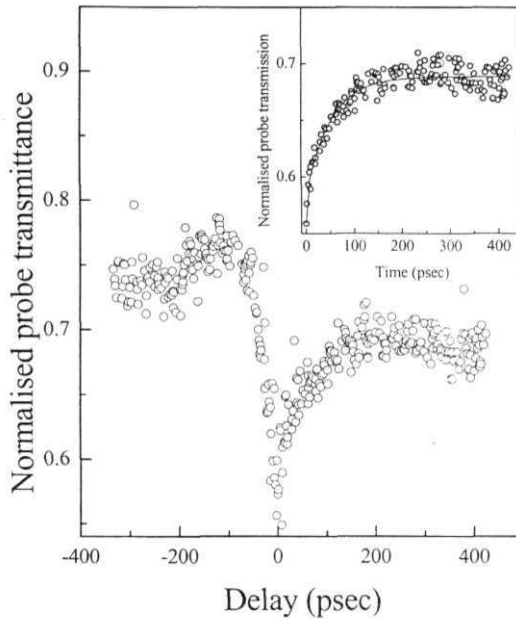
Figure 5.8: Temporal response of excited carriers from Pump-probe experiment for BSO at 532 nm, with 25 ps pulses. Inset shows the fit to get the relaxation of the excited carriers.

5.5   Model for optical limiting

The early model of photorefractive effect, i.e., the single level deep-trap model [31], assumes that only one donor level in which the charge carriers can be excited and trapped by both donor and acceptor levels in a crystal. The model predicts that the optical absorption, beam coupling gain coefficient, and the effective Debye screening length are intensity independent. According to this model, the response time increases linearly with intensity if the dark conductivity is small compared with the photoconductivity, and the magnitude of the two-beam coupling coefficient is the same whether a beam is depleted or amplified.

However, many anomalous behaviors have been observed in photorefractive crystals. For example, a sublinear relationship between the response time and the optical intensity has been found [32,33]. The intensity dependence of the photorefractive beam-coupling gain coefficient and the effective Debye screening length [34], and the intensity dependence of the absorption coefficient [25,35] are inconsistent with the single-trap model. An asymmetry in the two-beam coupling strength when the weak beam was amplified or depleted has also been observed [36]. Subsequently, several photorefractive models were proposed. Strohkendl *et al.* [37] and Valley [38] proposed a model involving electron-hole competition from a single level. This model explained the change of sign in the two-beam coupling gain coefficient observed in $BaTiO_3$ at 442 nm by Klein and Valley [39]. Motes and Kim [35] showed that part of the asymmetry between gain and depletion in the two-beam coupling is caused by the bulk light-induced absorption in the crystal. Brost *et al.* [25] showed that light-induced absorption requires more than one active level in the crystal. The sublinear dependence of the photoconductivity of $BaTiO_3$ was explained using a model that included an additional trap level [33]. Tayebati and Mahgerefteh [27] analytically solved the charge-transport equations for a photorefractive crystal with shallow and deep traps. They theoretically explained the light induced absorption, the sublinear dependence of photoconductivity on optical intensity, and the intensity dependence of the two-beam coupling strength and the effective Debye screening length in photorefractive crystals. Cudney *et al.* [in Ref. 34] theoretically solved for more general cases, in which multiple levels [40] are involved in charge distribution process in a photorefractive crystal. They obtained an analytical solution for absorption gratings from the band transport equations [31], taking the trap gratings into account [41] assuming that the polarizability of a filled trap differs from that of an empty one, i.e., the trapping sites themselves alter the susceptibility of the crystal. In all these models explaining different photorefractive properties two beams are applied, whereas in our case we used only a single beam to study the optical limiting properties.

The photoionization occurs from relatively deep energy levels within the band gap that are not thermally ionized. A variety of techniques such as

photoluminescence or thermally stimulated conductivity (TSC) are used to establish the presence of deep energy levels and their position inside the bandgap. Many TSC measurements have shown that deep trap levels are invariably present in sillenites such as BSO [42]. The deep energy/defect levels are attributed to arise from the specific crystalline defect or from a particular residual impurity that is introduced during the growth process. Various experimental studies have been performed on sillenite crystals to exactly find out the origin and position of the defect levels leading to photorefractive and photoionization process. Even with occasional variations in the growth parameters, such as deviating from the exact stoichiometric melt composition, provided remarkably similar TSC spectra and photoconductive properties [43]. The role of traps has been widely used for restoration of holographic images in BSO [44]. Considerable redistribution of impurity level populations, leading to varying lifetimes of mobile carriers, thus changing the dynamics of holographic recording with irradiation at different wavelengths in BSO has been reported [45]. Observations done on the decay dynamics of laser-induced phase gratings have been reported to be consistent with the assumption of multiple shallow and deep trap levels. From these studies three major types of trapping centers, one electron trapping center with a very short decay constant, a second electron trapping center with a longer decay time constant and a hole trapping center with a still longer time constant are found to be present [46]. Further photoconductive properties investigated revealed different mechanisms out of which hopping mechanisms appear to be important [8]. Evidence for the existence of multiple traps and the trapping mechanisms in BSO is described in detail in literature [46,47]. The electron mobility has been modulated 3-4 orders of magnitude due to trapping [48], where the filling of traps increased the mobility. Comparison of the photorefractive and photoconductive effects demonstrated that charge transport processes could not be explained by the effective-mass approximation to the "nearly free electron in the conduction band" model. The calculated drift length for the electron based on the photorefractive and conductivity measurements is inconsistent with the drift length required to explain the photoconductive measurements and charge transport via phonon-assisted tunneling (hopping model) is suggested as a major

contributor. **Krainak** and Davidson [49] investigated two-wave mixing in BSO with applied alternating electric fields and presented evidence that supports the hopping model for charge transport. All these earlier reported theoretical and experimental investigations provides a base for the band model used to explain the optical limiting behavior in BSO and BSO: Fe.
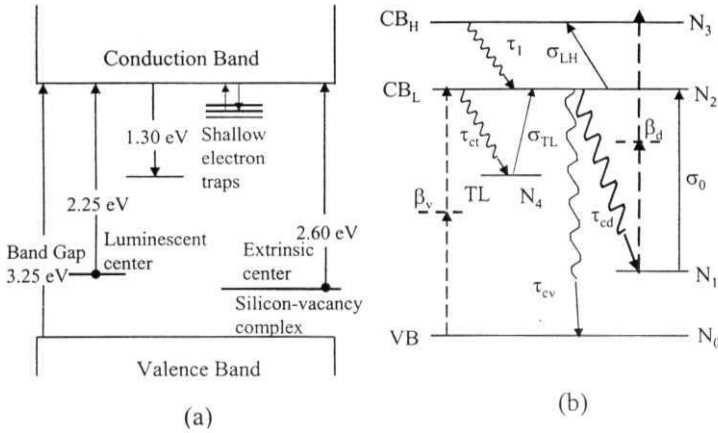
Figure 5.9: (a) Band model and (b) the equivalent five level diagram used for the modeling.

The energy band structure [8, 50] and the equivalent five level energy diagram used to explain the nonlinear absorption are shown in Fig. 5.9 (a) and (b) respectively. The following assumptions are made to explain the observed optical limiting and nonlinear absorption behavior explaining various properties of in these crystals:

- Extrinsic silicon-vacancy center is taken as donor level
- All the shallow and deep trap levels from which light induced absorption is possible are considered to be originating from a single trap level (TL).
- Recombination rate with valance-holes from the deep level of the crystal is exceptionally small [51].
- Thermal excitation/decay effects are neglected in the modeling as they are of the time scale of few ms to sec.

- Two paths of TPA are taken into consideration; one from VB to CB and the other from donor level to CB.

In fig 5.9(b) VB is the valence band, TL is the trap level, DL is the donor level, CB_L is the lower energy levels of the conduction band and CB_H is taken as the high energy levels of the conduction band. The extrinsic center (silicon-vacancy complex) is considered as N_l from where the photo absorption is possible. The shallow traps, deep traps and secondary photorefractive centers are taken as TL (N_4). CTI.H and τ_1 represent the contributions of free-carrier absorption coefficient and recombination times respectively inside the levels of conduction band.

The rate equations for the five level model assumed to explain the observed nonlinear absorption are given below:

$$\frac{dN_0}{dt} = -\frac{\beta_v I^2}{2\hbar\omega} + \frac{N_2}{\tau_{cv}} \tag{5.1}$$

$$\frac{dN_1}{dt} = -\frac{\beta_d I^2}{2\hbar\omega} - \frac{\sigma_0 I N_1}{\hbar\omega} + \frac{N_2}{\tau_{cd}} \tag{5.2}$$

$$\frac{dN_2}{dt} = \frac{\beta_v I^2}{2\hbar\omega} + \frac{\sigma_0 I N_1}{\hbar\omega} - N_2 \left(\frac{1}{\tau_{cv}} + \frac{1}{\tau_{cd}} + \frac{1}{\tau_{ct}} \right) + \frac{N_3}{\tau_1} - \frac{\sigma_{LH} I N_2}{\hbar\omega} + \frac{\sigma_{TL} I N_4}{\hbar\omega} \tag{5.3}$$

$$\frac{dN_3}{dt} = \frac{\beta_d I^2}{2\hbar\omega} + \frac{\sigma_{LH} I N_2}{\hbar\omega} - \frac{N_3}{\tau_1} \tag{5.4}$$

$$\frac{dN_4}{dt} = -\frac{\sigma_{TL} I N_4}{\hbar\omega} + \frac{N_2}{\tau_{ct}} \tag{\textbf{5.5}}$$

Intensity transmitted through the sample is given by

$$\frac{dI}{dz} = -\sigma_0 I N_1 - \sigma_{LH} I N_2 - \sigma_{TL} I N_4 - \beta I^2 \tag{5.6}$$

with

$$I = I_{00} \times \left(\frac{\omega_0^2}{\omega^2(z)} \right) \times \exp\left(-\frac{t^2}{\tau_p^2} \right) \times \exp\left(-\frac{2 \times r^2}{\omega^2(z)} \right) \tag{5.7}$$

and

$$\omega(z) = \omega_0 \left\{ 1 + \left(\frac{z}{z_0} \right)^2 \right\}^{\frac{1}{2}} \;\; ; \;\; z_0 = \frac{\pi \times \omega_0^2 \times n_0}{\lambda}; \;\; \beta = \beta_v + \beta_d$$

where σ_0 is the absorption cross-section from the donor levels, β_v is the two photon absorption coefficient from the valence band to the conduction band, β_d is the two photon absorption coefficient from the donor levels to the higher conduction band leading to an effective two photon absorption coefficient, $\beta = \beta_v + \beta_d$, σ_{TL} is the charge carrier absorption cross-section from the trap levels (TL) to the lower conduction band (CBL), σ_{LH} is the free carrier absorption cross-section within the conduction band to the intraband absorption. Both these absorptions are effectively considered as $\sigma_{l\,eff}$. N_i's are the corresponding carrier densities in different states, r,'s are the lifetimes of the states, and $1/\tau_{CT}$ is the crossing rate to TL from conduction band, $1/\tau_{CV}$ is the crossing rate from CB_L to VB, $\backslash TCD$ is the crossing rate from CB_L to DL. Relaxation of the excited charge carriers obtained from the pump-probe experiment with 25 ps pulses is taken as τ_{CT}. The refractive index n_0 of BSO at 532, 600 and 683 nm and is taken as 2.6, 2.55, and 2.52 respectively [52]. The differential equations arc solved numerically using Runge-Kutta fourth order method as explained in section 2.11. The carrier density [53] of the extrinsic absorption center N_l is taken as $\sim 10^{19}$ cm$^{"3}$. Ground state absorption cross-section σ_0 is calculated from the absorption spectrum shown in Fig.5.1, and is given in table 5.2.

At higher intensities, BSO has shown nanosecond timescale relaxation rates [54]. Nanosecond and picosecond recombination rates were also reported for $KNbO_3$ [55] and $BaTiO_3$ [29,30] at higher intensities. Since the intensities used in the present study are very high ($>10^8$ Wcm^{-2}), the following relaxation (recombination) times, $\tau_l =$ O.lpsec, $\tau_{cd} = 10$ nsec, and $\tau_{cv} = 10$ nsec [56,57] are used for the theoretical modeling. The excited charge carrier relaxation τ_{ct} is taken as ~ 60 psec from the pump-probe measurements. The solid lines in the figures 5.4, 5.5, 5.6 and 5.7 are the theoretical curves generated using the above

mentioned relaxations and the values of β_{eff} and σ_{leff} are then estimated through least square fit of the experimental data and are given in the Table 5.3. The effect of τ_{ct} = 4 nsec [58,59] and different β_{eff} on the nonlinear absorption is shown in Figs 5.10 to 5.12.

λ (nm)	σ_0 (× 10^{-20} cm^2)	
	BSO	BSO: Fe
532	9.15	8.53
600	3.30	6.34
683	2.49	5.34

Table 5.2: σ_0 calculated from the absorption spectrum for BSO and BSO: Fe

λ_{ex} (nm)	β_{eff} (cm/GW)	BSO		BSO:Fe	
		Intensity (GWcm^{-2})	σ_{leff} x 10^{-19} (cm^2)	Intensity (GWcm^{-2})	σ_{leff} × 10^{-19} (cm^2)
532	4.47	0.21	15	0.36	41
		0.70	21	0.67	91.8
		1.23	43		
600	5.02	0.54	16.8	0.43	
		0.98	39.4	0.94	54
683	4.36	0.31	8.0	0.26	10.5
		0.52	11.0	0.41	16.5

Table 5.3: σ_{leff} calculated at 532, 600 and 683 nm at different input intensities with 6 ns pulses for BSO and BSO:Fe.

From the pump-probe and open aperture Z-scan curves with 25 ps pulses the relaxation of the excited charge carriers and TPA coefficient are evaluated. These values are used to find out the contribution of TACCA in these crystals with ns pulse excitation. With ns pulse excitation various processes will come into picture and the data can be fitted using all the effects TPA, FCA, and TACCA or any one of them and with the relaxation times of the excited carriers. The effective TPA coefficient, which is a sum of the effects from valence bands and donor levels; is 4.47 cm/GW. From the theoretical considerations given by earlier reports [66] the TPA value is nearly around K ~ 1940 cm/GW (eV)$^{5/2}$, value given assuming the two level band model. Ratio of σ_{leff}/σ_0, which is considered as one of the figures of merit for optical limiters is found to increase

with increasing input intensity as can be seen from table 5.3. In iron doped crystal the contribution from the trap levels is found to be more, which increases with increasing intensity. Intensity dependent absorption is observed in PR crystals with low-intensity CW beams [25,35]. The effect is attributed to the photoinduced shift of the carriers from a primary trap with a lower absorption cross-section to a secondary trap with a higher absorption cross-section. Motes *et al.* [35] showed that this is not a photorefractive effect. It exists in unpoled crystals, can be induced at one wavelength and observed at a second wavelength, and has a rise time of the induced absorption that is an order of magnitude faster than the grating formation time. The contribution of the thermal effects is also ruled out as the absorption decreases with increasing temperature [60]. Similar induced absorption due to resonant TPA occurring in steps and free carrier absorption due to the trap levels is also reported in BSO [26]. Intensity dependent absorption and light induced absorption (LIA) have been studied in various doped and undoped photorefractive crystals like $BaTiO_3$ [61], $LiNbO_3$ [62], $KNbO_3$ [63] and in sillenites $Bi_{12}TiO_{20}$ [64]. In all these crystals, LIA and intensity dependent absorption are explained using the contributions from shallow and deep trap levels. In the doped crystals the contribution of the shallow levels is reported to be more.

Out of the two major phenomenon contributing to nonlinear absorption in these materials, TPA plays a decisive role in these materials with ultrashort pulses. There have been two basic approaches to the calculation of degenerate TPA coefficients in a crystalline solid. First, second order perturbation theory can be used to calculate the transition rate from valence band to conduction band (resulting from the absorption of two photons). Second, first-order perturbation theory can be used with electronic wavefunctions that have been dressed to include the acceleration of the electrons as a result of the ac light field developed by Keldysh and is often termed as tunneling theory [65]. Fermi's golden rule derived from the second-order time dependent perturbation theory provides the form of the two-photon transition rate:

$$W_2 = \frac{2\pi}{\hbar} \sum_{vc} \left| \sum_i \frac{\langle \psi_c | \hat{H}_{OPT} | \psi_i \rangle \langle \psi_i | \hat{H}_{OPT} | \psi_v \rangle}{E_{iv}(\bar{k}) - \hbar\omega} \right|^2 \delta\left(E_{cv}(\bar{k}) - 2\hbar\omega\right) \qquad (5.8)$$

$$\hat{H}_{OPT} = \left(\frac{e}{mc}\right) \bar{A} \cdot \bar{p} \qquad (5.9)$$

H_{opt} is the optical interaction Hamiltonian applicable to solids; ψ_c (ψ_v) is the bloch wave function for the conduction (valence band) and E_{cv} is the energy difference between the bands. The sum over all possible intermediate states i and over all possible transitions starting from a filled and ending at an empty state (usually valence band to conduction band for an intrinsic semiconductor), i.e., a sum over bands and the electronic wave vector.

We have compared our experimental results and the fits with simple two-parabolic band model describing both semiconductors and dielectric materials. The energy-gap dependence of the TPA coefficient was determined by measurements on a variety of materials with gaps ranging from 1.4 to 3.7 eV [28,66,67] predicting a scaling relation for the degenerate TPA coefficient given by

$$\beta(\omega) = K_{ph} \frac{\sqrt{E_p}}{n_0^2 E_g^3} F_2\left(\frac{\hbar\omega}{E_g}\right) \qquad (5.10)$$

Where

$$F_2 = (2x - 1)^{3/2} / (2x)^5 \qquad for\, 2x > 1 \qquad (5.11)$$

is the dispersion function for the TPA, and is only a function of the ratio of the photon energy to E_g i.e., optically coupled states. E_g being the bandgap of the material and E_p is the Kane momentum parameter

$$E_p = 2 \frac{|p_{vc}|^2}{m_0} \approx 21\, eV \qquad (5.12)$$

p_{vc} is the interband momentum matrix element given by

$$\vec{p}_{vc} = \frac{i}{\hbar} \int d^3r\, \psi_c^*(\bar{k}, r) \nabla \psi_v(\bar{k}, r) \qquad (5.13)$$

K_{pb} is a material independent constant:

$$K_{pb} = \frac{2^9 \pi}{5} \times \frac{e^4}{\sqrt{m_0}c^2}$$
(5.14)

which has a value of 1940 in units cm/GW $(eV)^{5/2}$ such that β is in cm/GW and E_g and E_p are in eV. A wealth of experimental and theoretical work regarding TPA in semiconductors and crystalline materials exists. The best fit to the data [28] using equations (10), (11) and (13) gave $K_{pb} = 3100$ cm/GW $(eV)^{5/2}$. While second-order perturbation calculation for a four-band model gave $K_{pb} = 5200$ cm/GW $(eV)^{5/2}$ for parabolic bands neglecting any coulomb interaction [68]. The value of β_{eff} obtained from the open aperture Z-scan curve with 25 ps pulses and at 532 nm is in close agreement with the value obtained using $E_p = 21$eV, and $K_{pb} = 1940$ cm $(eV)^{5/2}$/GW. These values are used to estimate the absorption from the trap levels and the free carriers.

The energy gaps are taken as 3.25 eV and 2.65 eV for the calculation of β_v and β_d respectively. The values of the estimated TPA values for β_v and β_d and the effective theoretical TPA coefficient β_{th} is given in table 5.4.

λ_{ex} (nm)	β_v	β_d	β_{eff}
532	1.801	2.766	4.567
600	1.701	3.328	5.029
683	0.956	3.510	4.466

Table 5.4: Estimated values of β_{eff} different wavelength excitations used with $E_p = 21$ eV and $K_{pb} = 1940$ cm $(eV)^{5/2}$/GW. β has units of cm/GW.

From table 5.3, it is clear that TPA plays a dominant role and the intraband processes inside the conduction band and the excitation of the carriers from the trap levels to the CB assist TPA for reverse saturable absorption. TPA coefficient is evaluated in various photorefractive crystals like BGO [16], BaTiO₃ [30] and LiNbO₃ [68], at different wavelengths and pulse widths. In all these reports a large deviation from the value calculated using equations (5.10) - (5.14) has been reported. Boggess *et al.* [30], with 1 ps excitation in BaTiO₃ found that the estimated value is an order of magnitude higher than the measured value and Adinolfi *et.al.* [68], found almost 50 % variation in LiNbO₃. With ps and shorter

pulses only TPA is playing a major role. Though pump-probe studies show approximately 50-60 ps decay of the excited carriers, the contribution from the traps is negligible compared to TPA. With ns pulses TPA as well as TACCA comes into picture.
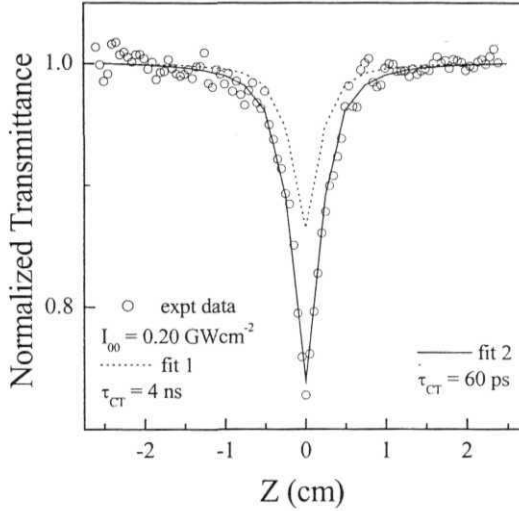
Figure 5.10: Effect of τ_{CT} on nonlinear absorption at constant $\beta_{eff} = 12.24$ cm/GW (corresponding to $K_{pb} = 5200$) and $\sigma_{Ieff} = 8 \times 10^{-19}$ cm^2

By considering (*1* (with $K_{pb} = 5200$ cm/GW (eV)$^{5/2}$) we are able to fit with high TPA only at higher intensities and at lower intensities more contribution coming from TACCA; which is not matching with the earlier reported theoretical and experimental observations in literature. Whereas with low TPA in the ns regime (with $K_{pb} = 1900$ cm eV$^{5/2}$/GW); with increasing intensity TACCA increases, which matches well with the earlier secondary center models. Theoretical fits with two different τ_{ct} (4 ns and 60 ps) and different values of β (with $K_{pb} = 1940$ and 5200 cm (eV)$^{5/2}$/GW) are shown in Fig 5.10 to fig 5.12 to give an idea of the effect of these factors on nonlinear absorption in these crystals.
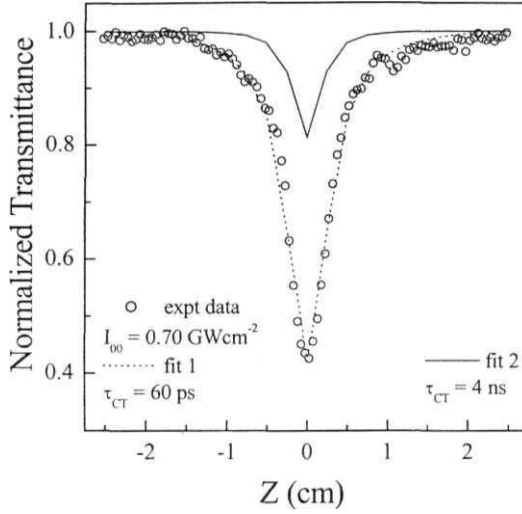
Figure 5.11: Effect of τ_{CT} on nonlinear absorption at constant β_{eff} = 4.43 cm/GW (corresponding to K_{pb} =1900 from the ps data) and σ_{leff} = 21 x 10^{-19} cm^2

Figure 5.12: Effect of TPA coefficient β nonlinear absorption at constant τ_{CT} (= 60 ps) and σ_{leff} (= 43× 10^{-19} cm^2)

5.6   Conclusions

➢   Broadband response in the visible wavelength region

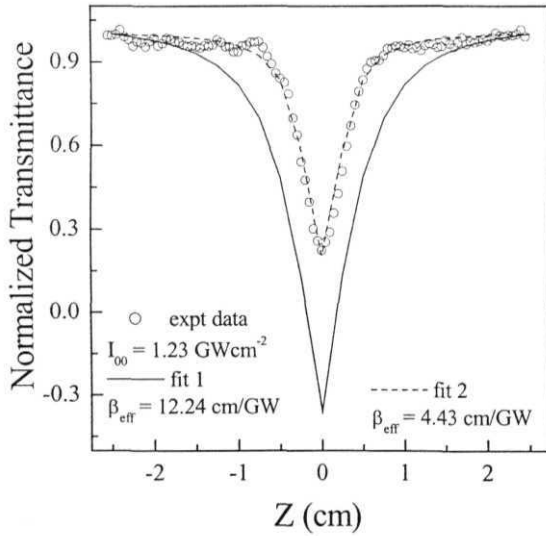➢   The crystals are found to have a very strong nonlinear absorption with major contribution from TPA assisted by intraband carrier absorption and charge carrier absorption from trap levels.

➢   In the ps regime TPA plays a dominant role and in the ns regime absorption from the trap levels and free carrier absorption also come into play.

➢   Low limiting thresholds and high damage threshold with iron doping makes the material suitable for limiting purposes even for short pulse duration and high energy sources over broadband region.

➢   Relaxations of the excited carriers in the timescales of ~ 60 ps and TPA make these crystals very good materials for ultrashort pulse applications.

5.7   References

1. P. Yeh, "Introduction to photorefractive nonlinear optics", John-Wiley, (1993); "*Photorefractive Optics*", ed: F.T.S. Yu. and S. Yin, Academic Press, (2000); J. Feinbcrg, *Physics Today,* 46, October, (1988); P. Gunter, *Phys. Rep.* 93, 199 (1982); M.C. Golomb, *Opt. Commun.* 89, 276 (1992); J.P. Huignard, *Proc. SPIE*, **1127,** 205 (1989); K.D. Shaw, and M.C. Golomb, *Opt. Commun.* 65, 301 (1988)

2. J.A. Hermann and J. Staromlynska, ***Int. J. Nonlin. Opt. Phys.*** 2, 271 (1993). 1. Golub and Y. Beadoin, *Nonlinear optics* 11, 71 (1995); H. Krose, R. Scharfschwerdt, O.F. Schirmer, and H. Hesse, *Appl. Phys. B* 61, 1 (1995); K. Buse, *Appl. Phys. B* 64, 273 (1997); A. Mazur, U.V. Stevendaal, K. Buse, M. Weber, O.F. Schirmer, H. Hesse, and E. Kratzig, *Appl. Phys. B* 65, 481 (1997).

3. D.N. Rao and P.P. Kiran, *Nonlinear Optics* 27, 347 (2001).

4. D.V.D. Linde, A.M. Glass, and K.F. Rodgers, *Appl. Phys. Lett.* 25, 155 (1974).; *ibid. Appl. Phys. Lett.* 26, 22 (1975).

5. C.T. Chen, D.M. Kim, and D. Von der Linde, *IEEE J. of Quantum. Electron.* **QE-16,** 126,(1980).

6. G. Pauliat, and G. Roosen, *J. Opt. Soc. Am. B* 7, 2259 (1990); R. Grousson, M. Henry, and S. Mallick, *J. Appl. Phys.* 56, 224 (1984); M.G. Jani and L.E.

Halliburton, *J. Appl. Phys.* 64, 2022 (1988); F. Holler, and H.J. Tiziani, *Opt. Commun.* 58, 20 (1986); H.C. Pederson, D.J. Webb, and P.M. Johansen, *J. Opt. Soc. Am. B* 15, 2439 (1998); S.I. Stepanov, V.V. Kulikov, and M.P. Petrov, *Opt. Commun.* 44, 19 (1982); G. Hussain, and R.W. Eason, *Opt. Commun.* 86, 106 (1991); A. Marrakchi, R.V. Johnson, and A.R. Tanguay, Jr., *J. Opt. Soc. Am. B* 3, 321 (1986); G. Pauliat, J.P. Herriau, A. Delboulbe, G. Roosen, and J.P. Huignard, *J. Opt. Soc. Am. B* 3, 306 (1986); K. Tada, Y. Kuhara, M. Tatsumi, and T. Yamaguchi, *Appl. Opt.* 21, 2953 (1982); J.P. Herriau, J.P. Huignard, and P. Aubourg, *Appl. Opt.* 17, 1851 (1978); J.P. Herriau, and J.P. Huignard, *Appl. Opt.* 17, 2671 (1978); P.M. Johansen, *J. Phys. D: Appl. Phys.* 22, 247 (1989); P. Jayanth, R.K. Mohan, and C.K. Subramanian, *Opt. Commun.* 147, 33 (1998); J.P. Huignard, and A. Marrakchi, *Opt. Commun.* 38, 249 (1981); S.L. Hou, and D.S. Oliver, *Appl. Phys. Lett.* 18, 325 (1971).

7. J. Guo, T.Y. Chang, I. McMichael, J. Ma, and J.H. Hong, *Opt. Lett.* 24, 981 (1999).

8. A.E. Attard, *Appl. Opt.* 28, 5169 (1989).

9. N. Benjelloun, M. Tapiero, J.P.Zielenger, J.C. Launay, and F. Marsaud, *J. Appl. Phys.* 64, 4013 (1988).

10. B.C. Grabmaier and R. Oberschmid, *Phys. Stat. Sol. (a)* 96, 199 (1986).

11. A.E. Attard, *J. Appl. Phys.* 71, 993 (1992).

12. A. Mazur, C. Veber, O.F. Schirmer, C. Kuper and H.Hesse, *J. Appl. Phys.* 85, 6751 (1999).

13. D. Nesheva, Z. Aneva and Z. Levi, *J. Phys. Chem. Solids.* 55, 889 (1994); M. Gospodinov, and D. Doshkova, *Mater. Res. Bull.* 29, 681 (1994).

14. Y. Nagao, and Y. Mimura, *Mat. Res. Bull.* 24, 239 (1989).

15. D. Nesheva, Z. Aneva and M. Gospodinov, *J.Phys. Chem. Solids.* 54, 857 (1993).

16. B. Taheri, S.A. Holmstorm, R.C. Powell, Jin Joo Song, F. Munoz, 1. Foldvari, A. Peter, *Optical Materials* 3, 251 (1994).

17. M.C. Golomb, and A. Yariv, *J. Appl. Phys.* 57, 4906 (1985).

18. S. Thai, J. Malowicki, and Q. Wang song, C. Zhang, X. Dang, Q. Sheng, and J. Tian, *Optical Memory and Neural Networks* 3, 399 (1994).

19. B. Aurivillius and L. G. Sillen, *Nature* 155, 305 (1945)

20. A.I. Safonov, S.A. Baryshev, T.I. Nikiforova, G.N. Antonov, and S.A. Fedulov, *Soviet Phys.-Crystallography.* 13, 797 (1969); M.D. Aggarwal, R. Metzl, W.S. Wang, and J. Choi, *Rev. Sci. Instru.* 66, 3939 (1995); S. C. Abrahams, P. B. Jamieson, and J. L. Bernstein, *J. Chem. Phys.* 47, 4034 (1967); G.A. Babonas, E.A.

Zhogova, Y.G. Zaretskii, G.A. Kurbatov, Y.I. Ukhanov **and** Y.V. Shmartsev, *Sov. Phys. Solid State* 24, 921 (1982); W.B. Leigh, J.J. Jarkin, M.T. Harris, and R.N. Brown, *J. Appl. Phys.* 76, 660 (1994).

21. M.D. Aggarwal, W.S. Wang, J. Choi, J.C. Cochrane, and Z.Y. Wang, *J. Cryst. Growth* **137,** 132(1994).

22. E.V. Mokrushina, M. A. Bryushinin, V. V. Kulikov, A. A. Petrov, and I. A. Sokolov, *J. Opt. Soc. Am. B* 16, 57 (1999).

23. A. Mazur, O.F. Schirmer, and S. Mendricks, *Appl. Phys. Lett.* **70,** 2395 (1997); L. Kovacs, R. Sommerfeldt, Y. Ming, and E. Kratzig, *Phys. Stat. Sol.(a)* **113,** K75 (1989); A. Liu, M. Lee, L. Hesselink, S.-H. Lee, and K.-S. Lirn, *Opt. Lett.* 23, 1618 (1998).

24. P.P. Banerjcc and R.M. Misra, *Opt. Commun.* **100,** 166 (1993); G. Pauliat, J.P. Herriau, A. Delboulbc, G. Roosen, and J.P. Huignard, *J. Opt. Soc. Am. B* 3, 306 (1986); Q. Sun, S. Liu, G. Y. Zhang, Q. Fang, G. Tian and J. Xu, *Optik,* **105,** 74 (1997); E.M. Avakyan, S.A. Alaverdyan, K.G. Bclabaev,.V.Kh. **Sarkisov,** and K.M. Tumanyan, *Sov. Phys. Solid. State,* 20, 1401 (1978); E.M. Avakyan, K.G. Bclabaev, and S.G. Odulov, *Sov. Phys. Solid. State,* 25, 1887 (1983); G. Zartov, T. Tenev, K. Parrajotov, E. Popov, R. Peyeva, H. Theinpent, and I. Veretcnnicoff, *J. Opt. Soc. Am. A* **18,** 174(2001).

25. G.A. Brost, R.A. Motes, and J.R. Rotge, *J. Opt. Soc. Am. B* 5, 1879 (1988).

26. B.Kh. Bairamov, B.P. Zakharchenya, and Z.M. Khashhkhozhcv, *Sov. Phys. Solid State* **14,** 2357 **(1973).**

27. P. Tayebati and D. Mahgerefteh, *J. Opt. Soc. Am. B* 8, 1053 (1991).

28. E. W. Van Stryland, H. Vanherzeele, M. A. Woodall, M. J. Soilcau, A. L. Smirl, S. Guha, and T. F. Boggess, *Opt. Engg.* 24, 613 (1985).

29. P. Ye, A. Blouin, C. Demers, M-M. D. Roberge, and X. Wu, *Opt. Lett.* 16, 980 (1991).

30. T.F. Boggess, J.O. White, and G.C. Valley, *J. Opt. Soc. Am.B* 7, 2255 (1990).

31. N. V. Kukhaterev, V. B. Markov, S. G. Odulov, M. S. Soskin, and V. L. Vinetskii, *Ferroelectrics*, 22, 949 (1979).

32. S. Ducharme, and J. Feinberg, *J. Appl. Phys.* 56, 839 (1984); G.A. Brost, and R.A. Motes, *Opt. Lett.* **15,** 1194 (1990).

33. L. Holtmann, *Phy. Stat. Solidi A* **K89,** 113 (1989); D. Mahgerefteh, and J. Feinberg, *Phys. Rev. Lett.* 64, 2195 (1990).

34. M.H. Garrett, J.Y. Chang, H.P. Jenssen, and C. Warde, *J. Opt. Soc. Am. B.* 9, 1407 (1992); M.H. Garrett, P. Tayebati, J.Y. Chang, H.P. Jenssen, and C. Warde, *J. Appl. Phys.* 72, 1965 (1992); J.Y. Chang, M.H. Garrett, H.P. Jenssen, and C. Warde, *J. Appl. Phys.,* 75, 43 (1994); R.S. Cudney, R.M. Pierce, G.D. Bacher, and J. Feinberg, *J. Opt. Soc. Am. B* 8, 1326(191).

35. A. Motes and J.J. Kim, *J. Opt. Soc. Am. B* 4, 1379 (1987).

36. A. Motes and J.J. Kim, *Opt. Lett.* 12, 199 (1987).

37. F.P. Strohkendl, J.M.C. Jonathan, and R.W. Hellwarth, *Opt. Lett.* 11, 312 (1986).

38. G.C. Valley, J. *Appl. Phys.* 59, 2363 (1986).

39. M.B. Klein and G.C. Valley, *J.Appl. Phys.* 57, 4901 (1985).

40. D.D. Nolte, D.H. Olson, and A.M. Glass, *Phys. Rev. Lett.* 63, 891 (1989).

41. R.M. Pierce, R.S. Cudney, G.D. Bacher, and J. Feinberg, *Opt. Lett.* 15, 414 (1990).

42. R.B. Lauer, *J. Appl. Phys.* 42, 2147 (1971); T. Takamori and D. Just J. *Appl. Phys.* 67,848(1990).

43. D.E. Davies and J.J. Larkin *Appl. Phys. Lett.* 67, 188 (1995); F.P. Strohkendl, P. Tayebati and R.W. Hellwarth, *J.Appl. Phys.* 66, 6024 (1989).

44. A.E. Attard, *J. Appl. Phys.* 66, 3211 (1989).

45. A.A. Kamshilin, and M.G. Miteva, *Opt. Commun.* 36, 429 (1981); M.G. Miteva, *Opt. Commun.* 50, 79 (1984); *IEEEJ. Quant. Electron.* QE-22, 1365 (1986).

46. A.E. Attard, and T.X. Brown, *Appl. Opt.* 25, 3253 (1986).

47. A.E. Attard, *Appl. Opt.* 27, 232 (1988); *J. Appl. Phys.* 66, 3211 (1989), *Appl. Opt.* 28, 5169 (1989).

48. B.K. Kostyuk, A.Y. Kudzin, and G.S. Sokolyanskii, *Sov. Phys. Solid. Stat.* 22, 1429 (1980).

49. M.A. Krainak, and F.M. Davidson,./. *Opt. Soc. Am. B* 6, 634 (1989).

50. M. Peltier and F. Micheron, *J. Appl. Phys.* 48, 3683 (1977); S.L. Hou, R.B. Lauer, and R.E. Aldrich, *J. Appl. Phys.* 44, 2652 (1973).

51. U. Van Stevendaal, K. Buse, H. Malz, and E. Kratzig, *Opt. Lett.* 24, 908 (1999).

52. R.E. Aldrich, S.L. Hou, and M.L. Harvill, *J. Appl. Phys.* 42, 493 (1971).

53. S.L. Hou, R.B. Lauer, and R.E. Aldrich, *J. Appl. Phys.* 44, 2652 (1973); G.C. Valley ans M.B. Klein, *Opt. Engg.* 22, 704 (1983).

54. M. Sylla, D. Rouede, R. Chevalier, X. Nguyen Phu and G. Rivoire, *Opt. Commun.* 90,391 (1992).

55. M. Zgonik, 1. Biaggio, U. Bertele, and P. Gunter, *Opt. Lett.* 16, 977 (1991); I. Biaggio, M. Zgonik, and P. Gunter, *J. Opt. Soc. Am. B* 9, 1480 (1992).

56. A. Miller, D.A.B. Miller, and S.D. Smith, *Adv. Phys.* 30, 697 (1981).

57. A.R. Beattie and P.T. Landsberg, *Proc. Roy. Soc. A* **249,** 16 (1959).

58. J.P. Hermann, J.P. Herriau, and J.P. Huignard, *Appl. Opt.* 20, 2173 (1981).

59. G. Lesaux, J.C. Launay, and A. Brun, *Opt. Commun.* 57, 166 (1986); G. Lesaux, G. Roosen, and A. Brun, *Opt. Commun.* 58, 238 (1986).

60. A. Motes, G. Brost, and J.J. Kim, *Opt. Lett.* 13, 509 (1988).

61. C. Yang, Y. Zhang, X. Yi, P. Yeh, Y. Zhu, M. Hui, and X. Wu, *J. Appl. Phys.* 78, 4323 (1995); K. Buse and T. Bierwirth, *J. Opt. Soc. Am. B* **12**, 629 (1995); J. Zhang, H. Gao, S.X. Dou, Y. Zhu, and P. Ye, *J. Appl. Phys.* 82, 5295 (1997); H. Song, S.X. Dou, M. Chi, H. Gao, Y. Zhu, and P. Ye, *J. Opt. Soc. Am. B* **15**, 1850 (1998); R.K. Banyal and B.R. Prasad, *J. Appl. Phys.,* 93, 9466 (2003).

62. S. Sunarno, Y. Tomita, and G. Zhang, *Appl. Phys. Lett.* 81, 4505 (2002); G. Zhang and Y. Tomita, *J. Appl. Phys.* 91, 4177 (2002); G. Panotopoulos, M. Luennemann, K. Buse, and D. Psaltis, *J. Appl. Phys.* 92, 793 (2002).

63. K. Buse and E. Kratzig, *Opt. Mat.* 1, 165 (1992); L. Holtmann, K. Buse, G. Kuper, A. Groll, H. Hesse, and E. Kratzig, *Appl. Phys. A* 53, 81 (1991); H. Mabuchi, E.S. Polzik, and H.J. Kimble, *J. Opt. Soc. Am. B,* 11, 2023 (1994); L. **Shiv,** J.L. Sorensen, E.S. Polzik, and G. Mizell, *Opt. Lett.* 20, 2270 (1995).

64. L. Mosquera, I. De Oliveira, J. Frejlich, A.C. Hernandes, S. Lanfredi, and J.F. Carvalho, *J. Appl. Phys.* 90, 2635 (2001).

65. L.V. Keldysh, *Sov. Phys. JETP* **20**, 1307 (1965).

66. E.W. Van Stryland, M.A. Woodall, H. Vanerzeele, and M.J. Soileau, ***Opt. Lett.*** 10, 490(1985).

67. M. Sheik-Bahae, D.C. Hutchings, D.J. Hagan and E.W. Van Stryland, ***IEEE J. Quantum Electron.*** 27, 1296 (1991); M. Sheik-Bahae, D.J. Hagan, and E.W. Van Stryland, ***Phys. Rev. Lett.*** 65, 96 (1990); R. DeSalvo, A.A. Said, D.J. Hagan, E.W. Van Stryland and M. Sheik-Bahae, *IEEE J. Quantum Electron.* 32, 1324 (1996); D.C. Hutchings and E.W. Van Stryland, *J. Opt. Soc. Am. B* 9, 2065 (1992).

68. M.H. Weiler, *Solid State Commun.* 39, 937 (1981).

69. A. Adinolfi, T. Cassano, R. Tommasi, and M. Ferrara, *Nonlinear Optics* 21, 327 (1999).

Chapter 6

Ag-Cu nanoclusters co-doped in SiO$_2$ Sol-Gel films

Role of surface plasmon resonance (SPR) on optical limiting properties of Ag-Cu nanoclusters co-doped in SiO$_2$ matrix, prepared by Sol-Gel technique with Cu/Ag molar ratio of 1,2 and 3 respectively is presented. Excitation near SPR of Cu resulted in enhanced optical limiting behaviour with increasing Cu concentration. No such concentration dependence is observed when excited near SPR of Ag. However, limiting threshold has reduced approximately 10-17 times. Excitation at wavelengths far below the SPR of Ag and Cu has not shown any optical limiting behaviour. The major contribution towards optical limiting is observed to be from interband absorption and from a possible energy transfer within the higher unoccupied states of Cu and Ag. Although nonlinear scattering is observed at higher intensities its contribution is found to be very less in comparison to that of nonlinear absorption assisted by energy transfer.

6.1   Metal nanoclusters/particles

A *nanocluster* or *nanocrystal* is a fragment of solid comprising somewhere between a few atoms and a few tens of thousands of atoms. Over the past few years huge advances have been made both in the synthesis of size-tunable, monodisperse nanoclusters of various chemical compositions and in the development of techniques for their assembly into well-ordered nanostructured solids. Alongside the advances in nanocluster synthesis, spectroscopies capable of studying individual clusters have been developed and these together with more conventional structural, electronic and optical probes have produced detailed information on and key insights into the properties of single clusters, cluster ensembles and cluster-based materials [1]. Metal nanoparticles have been the subject of growing interest both theoretically and experimentally over the years due to the fascinating electrical and optical properties that are different from bulk materials [2]. Most of the optical properties of metal nanoparticles are different from those of the bulk materials because of the dielectric and quantum confinement effects, which arise due to the reduction in particle size to few nanometers. The quantum confinement gives rise to discrete energy levels in an otherwise continuous band. However, such size effects are significant only for

particles of sub-nanometer (<lnm size).   On the other hand, dielectric confinement effects can be observed even in bigger particles. These effects are also found to enhance the nonlinear susceptibilities to a great extent [3].

A very important feature of small metal particles is the existences of a strong surface plasmon band in the UV-visible region of the spectrum. Surface plasmons are coherent fluctuations in electron density occurring at a "free-electron" metal/dielectric interface.   Mie theory and Maxwell-Garnet theory explained SPR in terms of higher moment oscillation and particle size [4]. On decreasing the particle size, the energy level spacing increases as a result of quantum size confinement of the electron wave function causing changes in the electronic absorption spectrum [5]. The surface plasmon resonance (SPR) band in metal nanoparticles arises from the oscillations of the free electrons in the conduction band occupying energy states near the Fermi level. Although in the dipole approximation SPR is independent of the particle size, it has been found that the width and peak position of the SPR depends on the particle size, shape and environment [6]. In case of metals, when particle size is reduced, the plasmon peak of the bulk (usually in the deep UV region) gets down shifted in energy to near UV or visible region.

Metal nanoparticles are used in variety of applications due to their small size, large surface area and surface plasmon resonances. The small size shortens the average diffusion time for charge carriers to migrate onto the surface and increases the efficiency and yield of charge transfer and surface reactions. The large surface area is highly desirable in applications such as heterogeneous catalysis.   Nanometer sized metal and semiconductor particles are used as fundamental building blocks of advanced electronic and optoelectronic devices [7] and in biotechnology [8]. SPR in nanoparticles is being used in diverse areas aimed at making real-time biomolecular interaction analysis possible like bio and imaging sensors [9]. Metal clusters and nanoparticles are promising materials for different nonlinear optical processes like optical limiting [10], optical switching, and computing because of their ultrafast nonlinear optical response [11]. Interaction of light with noble metal nanoparticles has been a significant stimulus for scientific research. Out of various metal nanoparticles Cu [12] and Ag [13]

are extensively studied in semi-continuous thin films, colloids, and in different glass matrices for their nonlinear optical properties. Different metal alloy nanoclusters and composites are also studied in this aspect [14,15]. Preparation and characterization of the nanoparticles for nonlinear optical studies is a challenging task where lot of progress has been made **[16].** Sol-gel method of making glasses with different matrices is one of the emerging techniques [17]. Different nanoparticles [18], organic nanocrystals [19], fullerenes [20] doped in sol-gel glasses are well studied for nonlinear optical and optical limiting applications. In this chapter, optical limiting and nonlinear optical properties of Cu-Ag nanoclusters with Cu/Ag molar ratio of 1,2 and 3 respectively, deposited on silica glass by the sol-gel process are presented.

6.2   Ag-Cu codoped metal nanoclusters

The composite materials formed by Ag and Cu nanoclusters embedded in silica glass matrix are prepared by sol-gel technique. A constant $(Ag+Cu)/SiO_2$ molar ratio of 0.175 is maintained while preparing the films. The synthesis and properties of the films used in this study are reported elsewhere [21]. The films were reheated at 600°C for 1 hour in $8\%H_2$ - 92% N_2 atmosphere to remove any oxidation of silver and copper metals embedded in the film. No noticeable change in the absorption spectra is observed before and after heat treatment. The AFM images revealed that the films exhibit same surface characteristics and films have not deteriorated with time. The samples having the Cu/Ag molar composition of 1,2,3 are called as 1 Ag1Cu, 1 Ag2Cu and 1 Ag3Cu respectively.

All these films show reasonably homogenous distribution of clusters throughout 150+10 nm thickness and the Ag/Cu atomic ratios are well maintained. The size and distribution of the clusters is clearly dependent on the composition of the film. A distribution of small clusters of 5 nm and 40-50 nm in diameter is observed in 1Ag1Cu films, where as in case of 1Ag3Cu sample the diameter of clusters is 5-20 nm with more homogenous distribution. With increasing concentration of Cu, the clusters became more spherical in shape. In

lAg2Cu film relatively larger clusters are spheroid and in case of lAg3Cu the clusters are spherical [21]. The properties of these films used for this study are given in Table 6.1.
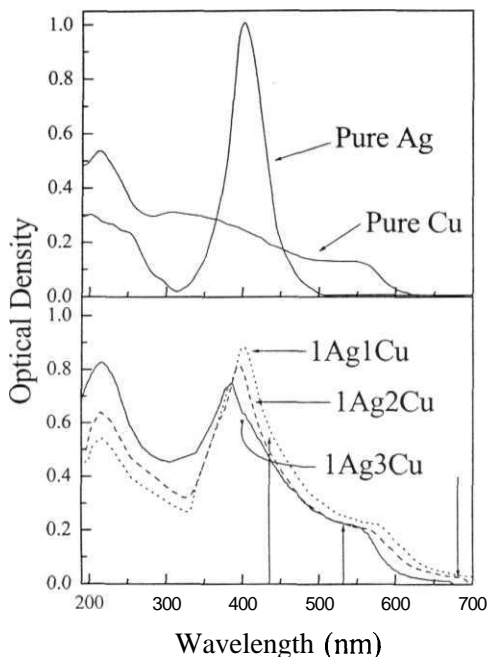
Figure 6.1: Absorption spectrum of Ag-Cu nanoclusters co-doped in SiO₂ sol-gel matrix. Arrows indicate the excitation wavelengths used.

Surface plasmon resonance bands corresponding to both Ag and Cu are clearly seen in Ag-Cu codoped films, indicating that these nanoclusters are not forming alloys and retaining their individuality. In case of alloy formation, a single surface plasmon resonance should come between the position of surface plasmon band of Ag and Cu as reported earlier in case of Au-Cu system and also in Au-Ag system [Kreibig and Vollmer in 4, 22]. In TEM/ED studies we observed both spots corresponding to Ag and Cu fcc phases indicating the presence of Ag and Cu mixed nanocrystals. The surface plasmon band, which arises from the oscillations of the free electrons in the conduction band occupying

energy states near the Fermi level is shifted in these samples compared to that of pure Ag and Cu nanoclusters embedded in SiO_2.
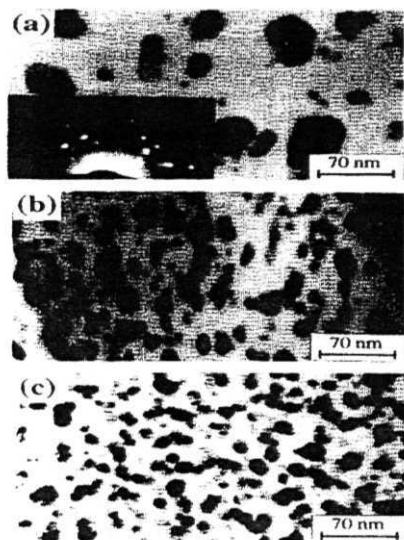
Figure 6.2: TEM micrographs of (a) 1Ag1Cu, (b) 1 Ag2Cu and (C) 1 Ag3Cu films

     The pure Ag and Cu samples show surface plasmon bands at 403 ± 1 nm (3.08 eV) and about 562 nm (2.21 eV) respectively. The shift increases with Cu concentration. SPR reaches 384 ± 1 nm (3.23 eV) for 1Ag3Cu sample with Cu/Ag ratio of 3. Since the Ag clusters are too large to show SPR peak at a wavelength less than 400 nm, the blue shift may not be due to the size effect. On the other hand, Ag colloids are good electron acceptors, therefore the large blue shift of Ag SPR can be attributed to electron transfer to the Ag clusters filling up its 5s band [23]. The increase of the s-electron density gives rise to the increasing of fermi energy of the plasmon frequency. The increasing blue shift with increasing Cu/Ag ratio could be due to an interaction between Ag and Cu clusters, which should depend on the cluster concentration and the cluster separation [24]. The distance between the clusters decrease with increasing Cu concentration and is much smaller than the wavelength of analysing light.

Molar ratio Ag:Cu	Size (nm)	Shape	Linear transmission (%)	
			532 nm	435 nm
1:1	40-50	Spheroid	77.5	58.5
1:2	25-35	Spheroid & spherical	75	49.5
1:3	15-20	Spherical	72	47.2

Table 6.1: Size and shape of the nanoclusters in Ag-Cu:SiO₂ films. Linear transmission at λ_{ex} ~ 532 and 435 nm are also given.

Three different excitation wavelengths are used to study the contribution of SPR for optical limiting. Frequency doubled Nd:YAG laser (532 nm) with 6 ns, 10 Hz repetition rate, the first Stokes line for 532 nm at 683 nm ($14642 \ cm^{-1}$) and the first anti-Stokes at 435.7 nm ($22952 \ cm^{-1}$) generated from a Raman cell filled with H_2 gas (vibration mode $4155 \ cm^{-1}$) are used as excitation wavelengths. The pump, Stokes and anti-Stokes lines are separated by means of a Pellin-Broca prism mounted on a rotating stage. Optical limiting studies are performed using f/30 geometry for excitation at 532 nm and f/15 geometry for excitations at 435 and 683 nm. Intensity dependent scattering measurements were done simultaneously at different angles (9) from the axis of propagation. Input fluence is varied from 30 μJcm^{-2} to 60 Jcm^{-2} for 532 nm excitation and from 10 μJcm^{-2} to 23 Jcm^{-2} for λ_{ex} ~ 435 nm. Open and closed aperture Z-scan studies are done by focusing 532nm laser pulses on to the sample using a lens of 80 mm focal length with beam waist of 40 μm at focus leading to peak intensities in the range of 0.38 – 1.2 $GWcm^{-2}$.

6.3   Nonlinear Optical Properties

The peak-valley trace in closed aperture Z-scan shows that these films have self-defocusing (negative, $n_2 < 0$) nonlinearity. Though earlier reports (Hamanaka *et al,* Haglund *et al,* Ballesteros *et al)* with femtosecond and picosecond pulses have observed positive nonlinearity (valley-peak trace) using closed aperture Z-scan technique, for Cu nanoclusters, nonlinear absorption measurements using open-aperture Z-scan did not give detectable changes of the

transmitted intensity with femtosecond pulses at high fluences. Whereas, we
have observed good nonlinear absorption with nanosecond pulses. Though
permanent sample colour changes due to laser pulse induced deformation [25]
and change in the sign of the nonlinear refractive index n_2 with increasing
incident intensities are reported earlier in Ag nanoparticles in soda lime glass [26]
we have not observed any such change. Closed and open aperture Z-scan curves
for the lAg2Cu sample are shown in Fig.6.3. The nonlinear refractive index is
calculated from the difference between the normalized peak-valley transmittance
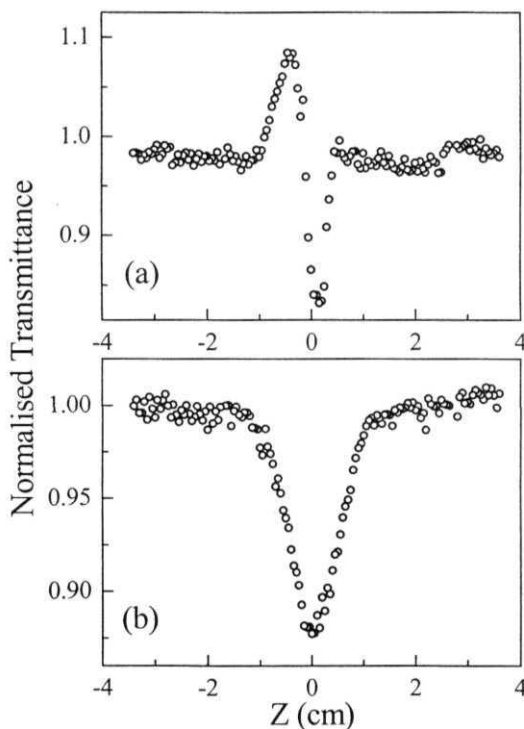ΔT_{p-v} in closed aperture Z-scan.

Figure 6.3 Closed and open aperture Z-scan curves of lAg2Cu:SiO₂ films at peak
intensities of $I_m \sim 0.52$ GWcm^2

The nonlinear refractive index n_2 is defined in terms of the ordinary linear index n_0 and the complex third-order nonlinear dielectric susceptibility $\chi^{(3)}$ in Gaussian units [27] by $n - n_0 + n_2 I$

$$n_2 (cm^2 \, W^{-1}) = \frac{0.0395}{n_0^2} \chi^{(3)} (esu) \qquad (6.1)$$

where I is the laser intensity. Estimated values of n_2 and $\chi^{(3)}$ for different films with ns are given in Table 6.2. For a fixed value of S, with increasing input intensity, the value of ΔT_{p-v} has increased with dominating valley in the closed aperture Z-scan curve, indicating the presence of nonlinear absorption in these films. The values of n_2 measured for $\Delta T_{p-v} \sim 15\%$ are of the order of 10^{-9} cm²/W for all the three films. The closed aperture Z-scan curves with the undoped silica film shows a transmission variation $\Delta T_{p-v} < 15 - 2\%$, whereas for the doped glass samples the variation is $> (15-20) \pm 2$ % which increases with increasing laser intensity. With increasing copper concentration we observed that the nonlinear refractive index reduced, but the nonlinear absorption increases. Table 6.2 also gives the normalized transmittance at focus $(T_{z=0})$ for open aperture Z-scan curves at the peak intensities I_{00} at focus. Nonlinear refractive index n_2 values measured with 6 ns and 25 ps pulses [23] at 10 Hz repetition rate are nearly the same. Further both ns and ps measurements show a decrease in the value of n_2 while going from a film with low absorbance of 0.225 (1Ag1Cu) to a film of high absorbance of 0.28 (1 Ag3Cu). This result clearly shows that n_2 is predominantly electronic in origin rather than due to thermal nonlinearity. If the thermal contributions were to be dominating, then we would have seen an increase in n_2 with increase of absorption.

The n_2 values measured with 25 ps pulses show higher values than with ns pulses. These values also match with the earlier measurements with 6 ps, 15.2 MHz repetition rate pulses [21]. Thermal loading effects were reported only at high repetition rate of 76 MHz leading to an increase in the nonlinearity by an order of magnitude [21,28]. The figure of merit for the third order nonlinearity $\chi^{(3)}/\alpha$ measured using two-beam degenerate four-wave mixing configuration by Uchida et al. [11] shows an increase with the particle size of Cu as well as Ag,

with a ratio of 1.7 for 40 nm to 15 nm Cu particles. Our values measured from closed aperture Z-scan match well with theirs for ns data, but give a ratio of 1.1 for ps data [29]. We therefore attribute the steady increase in the n_2 values to the increase of $\chi^{(3)}$ as a function of particle size from 1Ag3Cu to 1Ag1Cu.

Sample	n_2 ($\times 10^{-9}$ cm²/W)	$\chi^{(3)}$ ($\times 10^{-7}$ esu)	$T_{Z=0}$, I_{00} (GWcm⁻²)
1Ag1Cu	3.08 ± 0.4	1.65 ± 0.21	0.86, 1.14
1Ag2Cu	2.14 ± 0.2	1.15 ± 0.12	0.83, 0.93
1Ag3Cu	1.66 ± 0.3	0.89 ± 0.16	0.88, 0.72

Table 6.2: Measured values of nonlinear refraction from closed aperture and normalized transmittance from open aperture.

6.4   Optical limiting properties

The limiting curves for the Ag-Cu nanoclusters at 532 nm laser excitation are shown in Fig. 6.4. It clearly shows that the increasing Cu/Ag ratio enhances limiting property. Optical limiting curves of these nanoclusters excited at 435 nm are shown in Fig 6.5. Excitation at 435 nm has shown good optical limiting properties for all the three films however no specific enhancement in the limiting property with increasing Cu/Ag ratio is observed. At 532 nm excitation the limiting threshold has decreased with increasing Cu/Ag ratio, from 47.22 Jcm⁻² to 27.88 Jcm⁻². Whereas, at 435 nm excitation the limiting threshold was reduced to ~2.74 Jcm⁻², but no concentration dependence is observed. Excitation at 683 nm has not shown any optical limiting behaviour in these films. The limiting threshold ($I_{1/2}$) values are given in Table 6.3. The reason for a drastic change in the limiting properties at 435 nm, could be due to the contribution of SPR of both Ag and Cu nanoclusters towards nonlinear absorption, as the excitation energy is above the SPR of Cu and closer to SPR of Ag. It becomes difficult to exactly find out the individual contribution from Cu and Ag at 435 nm. No observed variation in the limiting threshold with increasing Cu concentration at this excitation energy gives an indication to this fact.
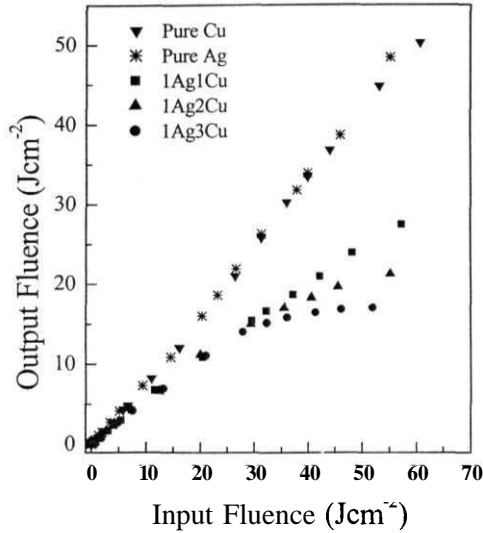
Figure 6.4: Optical limiting curves of Ag-Cu films excited at 532 nm. OL curves of pure Cu and Ag nanocrystals are also shown for comparison.
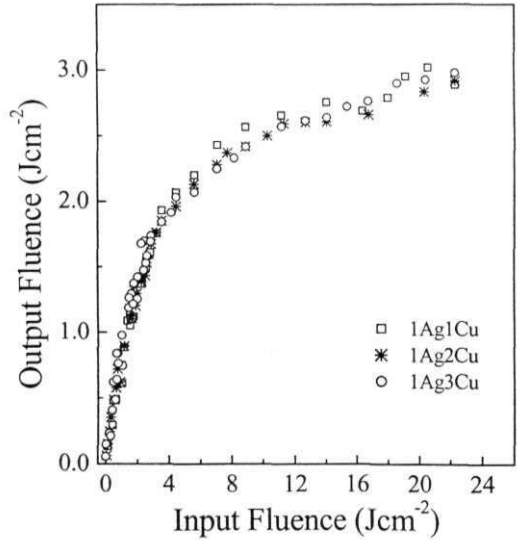
Figure 6.5: **Optical limiting** curves of the **films at** 435nm

Different processes like transient absorption, nonlinear absorption due to interband / intraband transition [30], photoejection of electrons [31] and nonlinear scattering [32] are reported to be operative in nanoclusters leading to optical limiting. The possible processes are depicted in fig 6.6. In our case as the excitation energy is closer to the interband transition threshold of one of the constituents Cu, interband transitions play a major role in optical limiting. A laser pulse can cause an interband or intraband absorption in the metal nanoparticle system, depending on the excitation wavelength and incident intensity. While considering the interband/intraband absorption one needs to consider the electron dynamics in metal nanoparticles [33] occurring in several steps, whose behavior is different from the one observed in the corresponding bulk metal. Initially the energy is transferred to the electrons by absorption of photons via interband and intraband transitions. During this quasi-instantaneous process, the phase memory is conserved between the electromagnetic field and the electronic states, and the density of excited states depends on the spectral shape of the laser pulse leading to non-thermal distribution. The next step involves electron-phonon coupling, which leads to an equilibrium of the electron and lattice temperatures, which takes place with in a few picoseconds time scale. The two mechanisms are not entirely independent. The nonthermal regime is accompanied by an acceleration of the energy transfer to the lattice. In addition to these processes, the heat transfer to the surrounding medium should also be considered in metallic nanoparticles. The relaxation dynamics of metal nanoclusters depends on the energy absorbed by the nanoparticles, size of the nanoparticles and the surrounding matrix and the excitation wavelength [34]. The relaxation time decreases with the particle diameter, by which further excitation of the free carriers is possible. The relaxation time is reported to show an increase at the surface plasmon resonance. In case of Cu nanoparticles electron-electron and electron-phonon relaxations are around few picoseconds; 1-4 ps and 0.7 ps respectively and in Ag nanoparticles they are around ~ 500 fs to 1.4ps [35-38]. The faster relaxations make further excitation of the relaxed electrons and further transfer of energy via electron-electron and electron-phonon

interaction possible as the excitation 6 ns laser pulse is present over much wider time scales compared to the relaxation times.
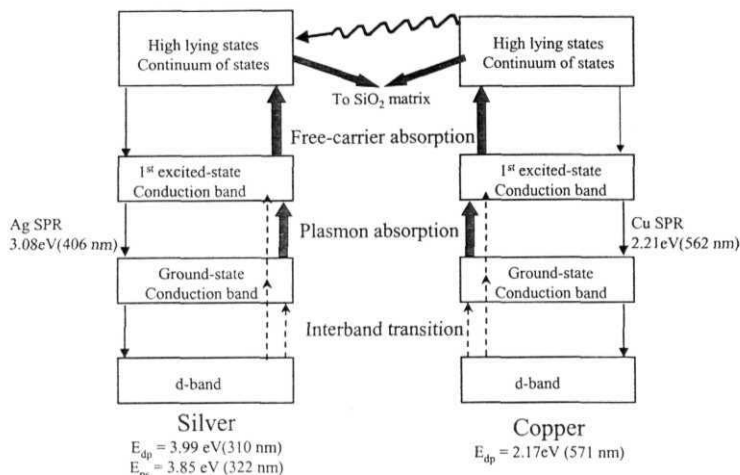
Figure 6.6: Scheme of electron dynamics in Ag-Cu nanoclusters for laser excitation. The down arrows, and filled block arrows represent the electronic relaxations, and plasmon/free-carrier absorption respectively. The broken arrows represent weaker interband and two-photon transitions.

In the case of Cu, SPR is situated near the interband transitions $d \rightarrow p$ (E_{dp} = 2.17eV or 571 nm) from the filled d band to the unoccupied states in the p conduction band and for Ag, SPR is situated well below the interband transition thresholds $d \rightarrow p$ (E_{dp} = 3.99 eV or 310 nm) and $p \rightarrow$ (E_{ps} = 3.85 eV or 322 nm) from the occupied p states to the unoccupied s states. With 532 nm (2.33 eV) and 435 nm (2.86 eV) excitation in Ag nanoclusters only plasmon absorption from SPR is possible, whereas in Cu both interband transitions and plasmon absorption are possible. When excited at 532 nm and 435 nm the electrons in the filled d band of Cu will get excited to the unoccupied states in the p conduction band. These excited electrons are free carriers possessing both kinetic and potential, immediately after the absorption. The potential energies are those of the formerly

unoccupied states within the conduction band. This excitation leads to the bleaching of the ground-state plasmon band.

This process is accompanied by the nascent excited state showing a transient absorption due to the free carrier absorption. Now the hot electrons (excited electrons) will exchange energy with each other to form an internally thermalised distribution. These electrons lose their energy further by electron-electron coupling which takes place in few hundreds of femtoseconds and also by externally thermalising with the lattice through electron-phonon interactions. This electron thermalization with the lattice is synchronous with a substantial recovery of the ground-state plasmon absorption band, so that the fast phase of the transient absorption phenomenon is over within a few picoseconds from the point of laser excitation. Because of the phonon-phonon relaxation process that follow, thermal energy will be dumped into the surrounding dielectric, thereby influencing plasmon frequency of the nanoclusters. The result is that the full recovery of the ground-state plasmon band is delayed further, which is reported to be ~ 90 ps for 40-60 nm diameter Ag colloids [31].

At 532 nm excitation, with increasing Cu concentration more free carriers are generated and these excited carriers can relax to the conduction band or SPR of Ag via electron-electron interaction, electron-phonon coupling and energy transfer leading to further bleaching of the Cu surface plasmon band, as the excitation energy is closer to the SPR and interband threshold of Cu. This possible mechanism explaining the processes leading to optical limiting is shown in Figure 6.6 and forms the basis for obtaining the theoretical curves for the optical limiting data. The solid block upward arrows show the strong SPR absorption and free carrier absorption and dotted lines show a weak interband and two-photon absorption. Block arrows at an angle show the dissipation of energy to the surroundings. Similar energy transfer coupling of two-photon absorption from one molecular system to reverse saturable absorption in another molecular system, leading to enhanced optical limiting is reported in organic systems [39]. At 435nm excitation, in addition to the processes occurring at 532 nm excitation, the contribution from the SPR of Ag nanoparticles also need to be considered. No drastic variation in the limiting threshold with increasing Cu concentration

may also be considered to explain the contribution of Ag nanoparticles to OL, as the excitation energy is closer to the SPR of Ag. The contribution of SPRs of both Ag and Cu nanoclusters towards nonlinear absorption with major contribution from Ag bands could be the reason for a drastic reduction in the limiting threshold at 435 nm.

6.5   Nonlinear Scattering

In addition to the processes mentioned above, we have also observed nonlinear scattering at high energies from these films, which is clearly observed in the far field. Nonlinear scattering is a well-known process leading to optical limiting in colloidal suspensions of silica particles [40], carbon particle suspensions [41], fullerenes [42] and nanoparticles [32]. The nonlinear transmittance and scattering collected at an angle of 3.3° from the beam axis for 1Ag2Cu are shown in Fig. 6.7.

Different mechanisms are reported to lead to nonlinear scattering. In **a** medium consisting of two components at low energy, the medium is rendered homogenous by a good refractive index matching between the two components, whereas at high energy, the intense laser light propagating through the medium makes it a heterogeneous scattering medium because of the photoinduced refractive index mismatch between the two components. In case of nanoparticles, nonlinear scattering phenomenon is proposed to be due to the induced pseudo-absorbance to the vaporization or the fragmentation of the metal nanoparticles inducing a large light-scattering center around the initial particles. Such vaporization or fragmentation induced by a thermal effect has been reported earlier [43]. The energy concentrated in each particle and available to form the scattering centers is more in the nanoclusters of larger size, and the size of the induced scattering centers increases with time to reach a maximum, leading to more nonlinear scattering. In case of nanoclusters suspended in solutions at high fluences the scattering centers produces more numerous fragments confined in the same scattering center. This increases the probability of recombination with the solvent and a more efficient cooling of the scattering centers. Such effects

can be efficient in case of nanoclusters in solution state, where as in thin films such a process can lead to an irreversible damage, which was observed at higher energies. We have observed surface damage at the fluence around 75 Jcm^{-2} where the transmission has reduced drastically and the films undergo irreversible damage. Observed scattering is therefore due to the metal nanoparticles not due to the damage to the film. Sol-gel films are well known to remain stable upto the very high fluence, as high as 300 Jcm^{-2} in the nanosecond regime [44].
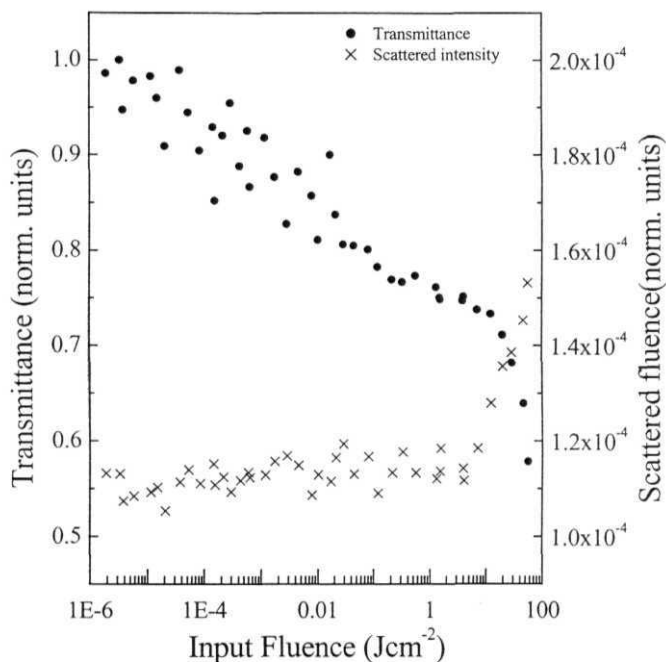
Figure 6.7: Nonlinear transmittance and Scattering of 1 Ag2Cu:SiO$_2$ **film.**

Size effects on optical limiting are observed in case of gold nanoparticle systems [32] where optical limiting effects are observed at lower intensities for larger particles (~15 nm), where as smaller particles ~ 2 nm does not show any limiting effects. Nonlinear scattering recorded at different angles from the axis of propagation (θ) reduced with increasing angle. Fig 6.8(a) shows the scattering

curves for 1 Ag1Cu film at 6 ~3.3° and 10°. At higher angles the scattering starts reducing drastically and for 0 > 27° scattering is not observed. Fig 6.8(b) compares the scattering from two films 1Ag2Cu and 1Ag3Cu. Though the nonlinear scattering has decreased with decreasing particle size from 1Ag1Cu (40-50 nm) to 1Ag3Cu (15-20 nm), the optical limiting performance has increased with increasing Cu concentration and reduced particle size. This implies that the nonlinear absorptive processes contribute more to the optical limiting performance. This is due to the fact that the excitation wavelength is closer to the SPR of Cu nanoclusters (565 nm) as surface palsmon band is sensitive to laser excitation.
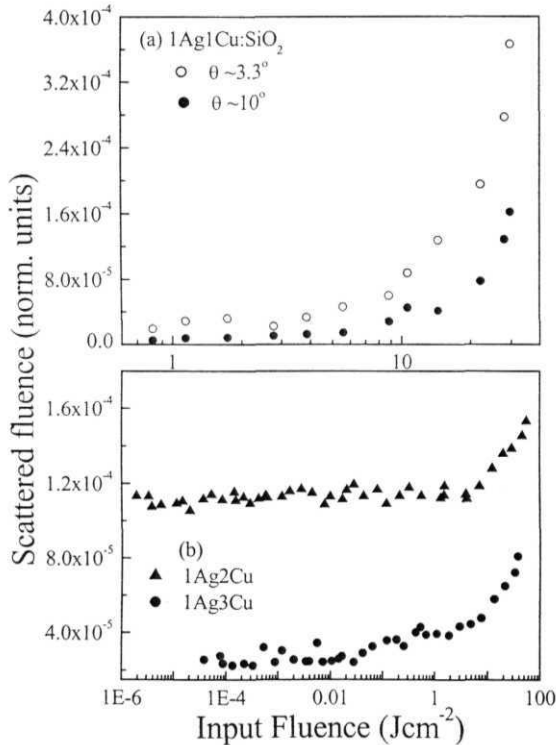
Figure 6.8: Scattering curves (a) at $\theta \sim 3.3°$ and 10° for 1 Ag1Cu film, (b) at 3.3° for 1Ag2Cu and 1Ag3Cu films for $\lambda_{ex} \sim 532$ nm

6.6   Surface Plasmon Band and Model for Optical Limiting

In a crystalline solid, electrons occupy effectively continuous energy bands with the occupation, width and separation of these bands determining the fundamental electrical, optical and magnetic properties of the solid. At the other end of the length scale, for individual atoms and molecules the electronic state density is discrete, resulting in, for example, intrinsically sharp spectral linewidths. In some respects the electronic structure of a nanocluster or nanocrystal might be said to fall somewhere between these two extremes. A striking property of a colloidal solution of noble-metal nanoclusters is its intense colour. It was the dependence of solution colour on Au colloid size that prompted Mie [4] to apply Maxwell's equations, with the appropriate boundary conditions for spherical particles, to the calculation of the absorption spectra of small Au clusters. A key feature of the absorption spectra of noble-metal nanocrystals is the presence of a strong band **in** the visible region, arising from the collective oscillation of conduction electrons (i.e. surface plasmons) in response to the external electromagnetic field [4] (Bohren and Huffman 1983). As discussed by, for example, Link and El-Sayed [6], although the total extinction cross-section for the particles, κ due to both absorption and scattering, arises from a summation over all electromagnetic multipole oscillations for nanocrystals which are small compared to the wavelength of the exciting radiation ($\leq 0.1\lambda$) the dipole approximation may be used. Mie theory leads to the following expression for κ [45] of the composite can be expressed in terms of the complex dielectric function of the metal nanoparticles $\varepsilon(\omega) = \varepsilon_r(\omega) + i\varepsilon_i(\omega)$ as

$$\kappa = \frac{9V\varepsilon_m^{3/2}}{c} \frac{\omega\varepsilon_i(\omega)}{\left[\varepsilon_r(\omega) + 2\varepsilon_m\right]^2 + \varepsilon_i^2(\omega)} \qquad (6.2)$$

where ε_m is the dielectric constant of the dielectric matrix and will be assumed frequency independent and real, V is the (spherical) particle volume, ω the angular frequency of the exciting radiation, ε_m the dielectric constant of the

medium surrounding the particle and ε_r and ε_i the real and imaginary parts of the dielectric function of the particle material respectively. The absorption is resonantly enhanced close to the frequency, minimizing the denominator, which is the condition for the surface plasmon resonance. This resonance is associated with enhancement of the electric field of the optical wave inside the particle as compared to the applied field.

From the above equation, Mie theory predicts that the bandwidth and peak height of the plasmon resonance (which occurs when $\varepsilon_r(\omega) = -2\varepsilon_m$ if ε_i is small or weakly dependent on *co*) are determined solely by ε_i. Thus, on the basis of eqn. 6.2, there should be no dependence of resonance position or width on particle size, only a volume-dependent variation in resonance intensity. However, a large number of experimental studies [46] have clearly demonstrated that as nanoclusters size decreases there is a dramatic increase in the plasmon resonance bandwidth, which maybe accompanied by shifts in the resonance position [47]. To account for these findings, the basic Mie theory has been extended [4] to include the fundamental assumption that the dielectric function of metal nanoparticles is size dependent, thus explaining the dependence of resonance bandwidth on particle radius.

Following the model given by Qu *et al.* $\varepsilon_i(\omega) > 0$, $\varepsilon_r(\omega) < 0$, and $|\varepsilon_i(\omega)|$ « $|\varepsilon_r(\omega)|$, we can omit $\varepsilon_i^2(\omega)$ in the denominator of the extinction coefficient.

Again,
$$\varepsilon(\omega) = n^2(\omega) = [n'(co) + in''(\omega)]^2$$
$$= n^2(\omega) - n''^2(\omega) + i2n'(co)n''(\omega),$$
$$\varepsilon_r(\omega) = n^2(\omega) - n''^2(\omega), \qquad \varepsilon_i(\omega) = 2n'(\omega)n''(\omega) \qquad (6.3)$$

The refractive index $n'(\omega)$ and attenuation index $n''(\omega)$, are related to the input intensity /. Now assuming that the refractive index, $n'(\omega)$, is unchanged with the increasing intensity, while the attenuation index, $n''(\omega)$, changes with / the real and imaginary parts of the dielectric can be written as

$$\varepsilon_r(\omega,I) = \varepsilon_r(\omega) + \Delta\varepsilon_r(I)$$
$$= n^2(\omega) - [n''(co) + An''(I)]^2$$

$$= n'^2 - n''^2 - 2\,n''\Delta n'' - (\Delta n'')^2, \tag{6.4}$$

$$\varepsilon_i(\omega,I) = \varepsilon_i(\omega) + \Delta\varepsilon_i(I) = 2\,n'(n'' + \Delta n'') \tag{6.5}$$

let $\Delta n'' = \beta_2 I + \beta_3 I^2 + \dots$, where β_2 and p_3 are the first and second order nonlinear attenuation coefficients. For the input intensities used we can neglect $(\Delta n'')$, $\beta_3 I^2$ and the parts containing the higher-order powers of I.

By substituting (6.4) and (6.5) into (6.2) the modified extinction coefficient containing the nonlinear attenuation at higher intensity is given by

$$\kappa \approx a\,\frac{1 + \dfrac{\beta_2}{n''}I}{1 - \dfrac{2\beta_2}{b}I}, \tag{6.6}$$

where $\beta_2 I$ describing the nonlinear attenuation performance is comparable with the nonlinear attenuation index, n'', for the strong nonlinear absorption. Substituting the above equation into the light transmission equation $dI/dz = -\alpha I$ and integrating, we obtain

$$I_{out} = T \times I_{in} = T_0 \left(\frac{1 + \dfrac{\beta_2}{n''}I_{out}}{1 + \dfrac{\beta_2}{n''}I_{in}} \right)^{1+(2n''/b)} \tag{6.7}$$

Where $T_0 = e^{\kappa_0 L}$ is the linear transmittance of the films

$$a = \frac{9\pi N V \varepsilon_m^{3/2} n''}{\lambda n'^2}, \quad b = \frac{n'^2 - n''^2 + 2\varepsilon_m}{2n'} \quad \text{and}$$

$$\kappa_0 = \frac{a}{b^2}\,n' = \frac{36\pi N V n' n'' \varepsilon_m^{3/2}}{\lambda(n'^2 - n''^2 + 2\varepsilon_m)^2},$$

Using the above equation optical limiting curves for Ag-Cu nanoparticles are fitted. This is valid to describe the optical properties of small metal particles for the SPR and also for interband and weaker intraband transitions. The

theoretical fits for the Ag-Cu clusters at 532 nm and 435 nm are shown in Fig 6.9(a) and (b) respectively. The fitting parameters are tabulated in Table 6.3. At 532 nm the increase of β_2/n " from 1Ag1Cu to 1Ag3Cu film and no variation at 435 nm clearly explains the observed results.
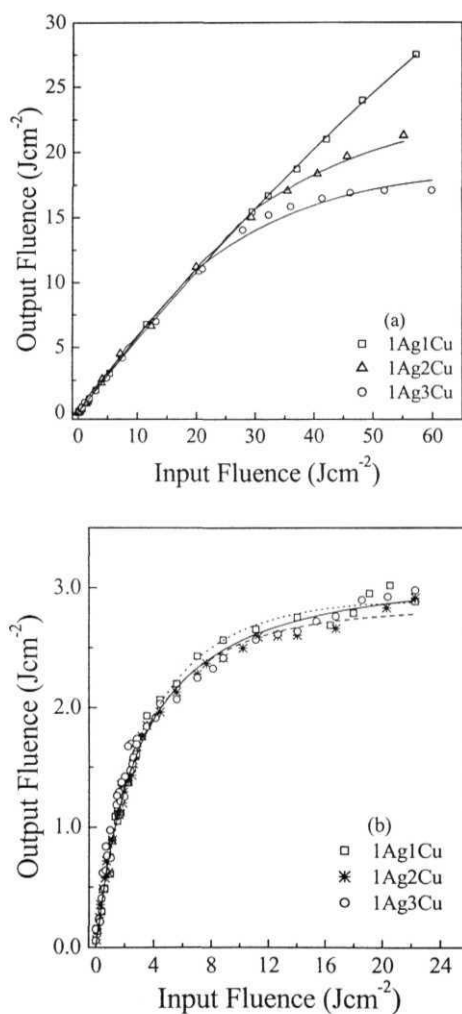
Figure 6.9: OL curves with theoretical fits (solid and dashed lines) for Ag-Cu metal nanoclusters in Sol-gel matrix at (a) 532 nm and (b) 435 nm from Raman shifter.

Molar ratio	Limiting threshold, $I_{1/2}$ (Jcm^{-2})		β_2/n'' (cm^2/J)	
Ag:Cu	532 nm	435 nm	532 nm	435 nm
1:1	48.2	1.37	0.00275	0.518
1:2	35.5	1.35	0.01114	0.520
1:3	27.88	1.37	0.01388	**0.521**

Table 6.3: Limiting thresholds and the interband transition coefficients for Ag-Cu:SiO₂ films.
β_2/n'' gives the measure of the interband transition coefficient.
$1+(2n''/b)$ is taken from the best fit to the data where the χ^2 is minimum and $1+(2n''/b) \sim$ 1.575 and 1.113 for $\lambda_{ex} \sim$ 532 nm and 435 nm.

6.6   Conclusions

➢ Optical limiting properties of Ag-Cu codoped nanoclusters are investigated at three different wavelengths that are in resonance with the SPR and below the SPR.

➢ Excitation closer to the SPR (532 nm) of Cu nanoclusters resulted in reduction of limiting threshold with increasing Cu concentration.

➢ Excitation well above the SPR of Cu and nearer to that of Ag (435 nm) resulted in reduction of limiting threshold approximately by 10-17 times.

➢ Excitation at 683 nm has not shown any nonlinear absorption.

➢ Though the nonlinear scattering has decreased from 1Ag1Cu to 1Ag3Cu, **the** optical limiting performance has increased with increasing **Cu** concentration and decreasing particle size.

➢ The nonlinear absorptive processes associated with energy transfer among the high lying states of Cu and Ag found to contribute more to the optical limiting performance.

6.7   References

1. P. Moriaty, Rep. Prog. Phys. 64, 297 (2001); Handbook of nanostructured materials and nanotechnology, ed: H.S. Nalwa, Vol.1-5, Academic Press, 2000.

2.   A.E. Hughes and S.C. Jain, *Adv. In Phys.* **28,** 717 (1979); J.A.A.J. Perenboom, P. Wyder, P. Meier, *Phys. Rep.* 78, 173 (1981).

3.   G.L. Fischer, R.W. Boyd, R.J. Gehr, S.A. Jenekhe, J.A. Osaheni, J.E. Sipe, and L.A. Weller-Brophy, *Phys. Rev. Lett.* 74, 1871 (1995); R.W. Boyd, R.J. Cher, G.L. Gischer, and J.E. Sipe, *Pure Appl. Opt.* 5, 505 (1996); C. Flytzanis, F. Hache, M.C. Klein, D. Ricard, P. Roussignol, vol. XXIX, 321 in: E. Wolf Ed., Progress in Optics, North Holland, Amsterdam, (1991); F. Hache, D. Ricard, and C. Flytzanis, *J. Opt. Soc. Am.* **53,** 1647(1986).

4.   G. Mie, ***Ann.*** *Phys. (Leipzig)* 25, 377 (1908); C.F. Bohren and D.R. Huffman, *Absorption and scattering of light by small particles,* Wiley, New York, 1983; U. Kreibig and M. Vollmer, *Optical properties of metal clusters,* springer, Berlin, 1995; T.S. Ahmadi, S.L. Logunov and M.A. El-Sayed, J. Chem. Phys. 100 8053 (1996); R.H. Ritche, Phys. Rev. **106,** 874 (1957)

5.   U. Kreibig, *J.Phys.* **F4,** 999 (1974); J.R. Heath, *Phys. Rev.* **B40,** 9982 (1989).

6.   S. Link, C. Burda, Z.L. Wang, M.A. El-Sayed, *J. Chem. Phys.,* **111,** 1255 (1999); S. Link and M.A. El-Sayed,/ ***Phys. Chem. B***, **103,** 8410 (1999).

7.   C. Larpent and E. Bernard, J. Cehm. Soc. Chem. Commun. 7, 535 (1992); Y. Chen and U. Nickel, J. Chem. Soc, Faraday Trans. 89, 2479 (1993); A. Bezryadin and C.Dekker, Appl. Phys. Lett., 71, 1273 (1997); M.S. Fuher, J. Nygard, L. Snih, M. Forero, Y-G. Yoon, M.S.C. Mazzoni, H.J. Choi, J. Ihm, S.G. Louie, A. **Zettl,** P.L. McEuen, *Science,* **288,** 494 (2000); H. Ditlbacher, J.R. Krenn, **B.** Lamprecht, A. Leitner, and F.R. Aussenegg, *Opt. Lett.25,* 563 (2000).

8.   C.M. Niemeyer, Angew. Chem. Int. Ed. **40,** 4128 (2001).

9.   M.J. Natan and L.A. Lyon, *Surface plasmon resonance biosensing with colloidal Au amplification;* D.L. Feldheim and C.A. Foss, Jr., Eds.; Metal nanoparticles; Marcel-Dekker: New York.

10. Y-P. Sun, J.E. Riggs, K.B. Henbest, and R.B. Martin, *./. Nonlinear Opt. Phys & Materials. 9,* 481 (2000); Y-P. Sun and J.E. Riggs, ***Int.*** *Rev. Phys. Chem.* **18,** 43 **(1999);** Y-P. Sun, J.E. Riggs, H.W. Rollins, and R. Guduru, *J. Phys. Chem.* 103, *11* (1999); 7071-7076 (2000); B. Yu, Y. Gu, Y. Mao, C. Zhu, and F. Gan, *J. Nonlinear Opt. Phys & Mater.* 9, 117 (2000); B. Yu, G. Yin, C. Zhu, and F. Gan, *Opt. Materials.* **11,** 17 (1998); N. Sun, Z.X. Guo, L. Dai, D. Zhu, Y. Wang, Y. Song, *Chem. Phys. Lett.* **356,** 175 (2002); S.X. Wang, L.D. Zhang, H. Su, Z.P. Zhang, G.H. Li, G.W. Meng, J. Zhang, Y.W. Wang, J.C. Fan, and T. Gao, ***Phys. Lett. A*** **281,** 59 **(2001);** N. Sun, Y. Wang, Y. Somg, Z. Guo, L. Dai, and D. Zhu, ***Chem.*** *Phys. Lett.*

344, 277 (2001); B. Yu, C. Zhu, F. Gan, and Y. Huang, *Opticla Materials* 7, 103 (1997); S. Qu, Y. Song, C. Du, Y. Wang, Y. Gao, S. Liu, Y. Li, and D.Zhu, *Opt. Commun.* 196, 317 (2001).

11. D. Ricard, Ph. Roussignol, and C. Flytzanis, *Opt. Lett.* 10, 511 (1985); K. Uchida, S. Kaneko, S. Omi, C. Hata, H. Tanji, Y. Asahara, A.J. Ikushima, T. Tokizaki, and A. Nakamura, *J. Opt. Soc. Am. B* 11, 1236 (1994); N. Del Fatti and F. Vallee, *Appl. Phys. B* 73, 383(2001).

12. J.M. Ballesteros, J. Bollis, R. Serna and C.N. Afonso, *Appl. Phys. Lett.,* 74, 2791 (1999); T. Tokizaki, A. Nakamura, S. Kaneko, K. Uchida, S. Omi, H. Tanji, and Y. Asahara, *Appl. Phys. Lett.,* 65, 941 (1994); L. Chae, M. Lee, H.K. Kim, D.W. Moon, *Bull. Korean Chem. Soc,* 18, 886 (1997); R.F. Haglund, Jr., L. Yang, R.H. Magruder III, J.E. Wittig, K. Becker, R.A. Zuhr, *Opt. Lett.* 18, 373 (1993); Li. Yang, K. Becker, F.M. Smith, R.H. Magruder III, R.F. Haglund, Jr., L. Yang, R. Dorsinville, R.R. Alfano, R.A. Zuhr, *J. Opt. Soc. Am. B,* 11, 457 (1994); J. Olivares, J. Requejo-isidro, R. del Coso, R. de Nalda, J. solis, C.N. Afonso, A.L. Stephanov, D. Hole, P.D. Townsend, and A. Naudon,./. *Appl. Phys.* 90, 1064 (2001).

13. Y. Hamanaka, A. Nakamura, S. Omi, N. Del Fatti, F. Vallee and C. Flytzanis, *Appl. Phys. Lett.,* 75, 1712 (1999); M. Kyoung, and M. Lee, *Opt. Commun.,* 171, 145 (1999); K.P. Unnikrishnan, V.P.N. Nampoori, V. Ramkrishnan, M. Umadevi, and C.P.G. Vallabhan, *J. Phys. D: Appl. Phys.* 36, 1242 (2003); Q.F. Zhang, W.M. Liu, Z.Q. Xuc, J.L. Wu, S.F. Wang, D.L. Wang, and Q.H. Gong, *Appl. Phys. Lett.* 82, 958 (2003); Y. Watanabe, M. Inoue and T. Tsuchiya, *J. Appl. Phys.,* 84, 6457 (1998).

14. R. Philip, G. Ravindra Kumar, N. Sandhyarani and T. Pradeep, *Phys. Rev.* #62, 13160(2000).

15. M. Falconieri, G. Salvetti, E. Cattaruzza, F. Gonella, G. Mattei, P. Mazzoldi, M. Piovesan, G. Battaglin, and R. Polloni, *Appl. Phys. Lett.* 73, 288 (1998); H. Zhang, D.E. Zelmon, L.Deng, H.-K. Liu and B.K. Teo, *J. Am. Chem. Soc.* 123, 11300 (2001); R.G. Aspasoiu, L. Balogh, O.P. Varnavski, D. Tomalia, and T. Goodson III, *J. Am. Chem. Soc.* 122, 11005-11006 (2000);

16. R.F. Haglund Jr., *Material Science and Engineering A* 253, 275 (1998); G.V. Prakash, M. Cazzanelli, Z. Gaburro, L. Pavesi, F. Iacona, G. Franzo, and F. Priolo, *J. Appl. Phys.* 91, 4607 (2002); C.L. Haynes, and R.P. Van Duyne, *J. Phys. Chem. B* 105, 5599(2001).

17. J. Zarzycki, Chapter 7, Glass Science and Technology, Vol.2, Eds: D.R. Uhlmann and N.J. Kreidl, Acadameic Press 1984; L.L. Hench, and J.K. West, *Chem. Rev.*

90,33 (1990); G. De, *J. Sol-Gel Sci. and Tech,* **11,** 289 (1998); M. Catalano, E. Carlino, G. De, L. Tapfcr, F. Gonella, P. Mazzoldi and G. Battaglin, *Philosophical Magazine* **B76,** 621-628 (1997); G. De, M. Gusso, L. Tapfer. M. Catalano, F. Gonella, G. Mattei, P. Mazzoldi, and G. Battaglin, *J. Appl. Phys.* 80, 6734-6739 (1996).

18. K.V. Yumashev, N.N. Posnov, I.A. Denisov, P.V. Prokoshin, V.P. Mikhailov, V.S. Gurin, V.B. Prokopenko and   A.A. Alexeeno, *J. Opt. Soc. Am B***17**, 572 (2000); A.M. Malyarcvich, K.V. Yumashev, N.N. Posnov, V.P. Mikhailov, V.S. Gurin, V.B. Prokopenko, A.A. Alexeenko, and I.M. Melnichenko, J. Appl. Phys. 87, 212 (2000); P. Innocenzi, G. Brusatin, M. Gugliemi, R. Signorini, R. Bozio, M. Maggini, *J. Non-crystalline Solids* **265,** 68 (2000); Y.Z. Gu, Z.J. Liang, F.X. Gan, *Optical Materials* **17,** 471 (2001); K. Dou, J.Y. Du, Edward T. Knobbc, *J. of Luminescence,* **83-84,** 241 (1999); H.I. Elim, W. Ji, A.H. Yuwono, J.M. Xuc, and J. Wang, *Appl. Phys. Lett.***82,** 2691 (2003).

19. N. Sanz, P.L. Baldeck, and A. Ibanez, *Synthetic Metals.* **115**, 229 (2000); N. Sanz, A. Ibanez, Y. Morel and P.L. Baldeck, *Appl. Phys. Lett.* **76**, 2569 (2001); Y. Morel, P. Najechalski, N. Sanz, A. Ibanez, C. Nguefack, C. Andraud, P.L. Baldeck, *Synthetic Metals* **109,215** (2000).

20. R. Signorini, M. Meneghetti, R. Bozio, M. Maggini, G. Scorrano, M. Prato, G. Brusatin, P. Innocenzi, M. Gugliemi, *Carbon* 38, 1653 (2000); J. Schell, D. Brinkmann, D. Ohlmann, B. Honerlage, R. Levy, M. Joucla, J.L. Rehspringer, J. Serughetti and C. Bovier, *J. Chem. Phys.* **108,** 8599 (1998); J. Schell, D. Ohlmann, B. Honerlage, R. Levy, M. Joucla, J.L. Rehspringer, J. Serughetti and C. Bovier, *Carbon*, 36, 671-674, (1998); M. Meneghetti, R. Signorini, S. Sartori, R. Bozio, M. Maggini, G. Scorrano, M. Prato, G. Brusatin, M. Guglielmi, *Synthetic Metals* **103,** 2474 (1999); M. Meneghctti, R. Signorini, M. Zcrbetto, R. Bozio, M. Maggini, G. Scorrano, M. Prato, G. Brusatin, E. Menegazzo, and M. Guglielmi, *Synthetic Metals* 86,2353(1997).

21. G. De, L. Tapfer, M. Catalano, G. Battaglin, F. Caccavale, F. Gonella, P. Mazzoldi, and R.F. Haglund, Jr., *Appl. Phys. Lett.68,* 3820 (1996).

22. G. De, G. Mattei, P. Mazzoldi, C. Sada, G. Battaglin, and A. Quaranta, *Chem. Mater.* **12,** 2157(2000).

23. G. De, A. Licciulli, C. Massaro, L. Tapfer, M. Catalano, G. Battaglin, C. Meneghini, and P. Mazzoldi, *J. Non Cryst. Solids* **194,** 225(1996).

24. H. Tamaru, H. Kuwata, H. T. Miyazaki and K. Miyano, *Appl. Phys. Lett.* 80, 1826 (2002); W. Rechberger, A. Hohenau, A. Leitner, J.R. Krenn, B. Lamprecht, F.R. Aussenegg, *Opt. Commun.* **220,** 137 (2003).

25. M. Kaempfe, T. Rainer, K.-J. Berg, G. Seifert and H. Graener, *Appl. Phys. Lett.*, 74, 1200 (1999); M. Kaempfe, H. Hofmeister, S.Hopfe, G. Seifert, and H. Graener, *J. Phys. Chem.B* **104,** 11847 (2000).

26. D.H. Osborne, Jr., R.F. Haglund, Jr., F. Gonella and F. Garrido, *Appl. Phys. J,* 66, 517(1998).

27. R.W. Boyd, Ch. 4, "*Nonlinearoptics*", Academic Press, Sandiego, Calif, 1992.

28. P. Mazzoldi, G.W. Arnold, G. Battaglin, F. Gonella, and R.F. Haglung. Jr., *J. Nonlinear Optical Physics & Materials.* 5, 285 (1996).

29. P.P. Kiran, G. Dc, and D.N. Rao, *IEE Proc.-Circuits and Devices,* **150,** 559 (2003).

30. S. Qu, Y. Song, H. Liu, Y. Wang, Y. Gao, S. Liu, X. Zhang, Y. Li, and D. Zhu, *Opt. Commun.* **203,** 283 (2002).

31. P.V. Kamat, M. Flumiani and G.V. Hartland, J. *Phys. Chem.B* **102,** 3123 (1998)

32. L. Francois, M. Mostafavi, J. Belloni, J-F. Delouis, J. Delaire, and P. Feneyrou, *J.Phys.Chem.B* **104,** 6133 (2000).

33. W.S. Fann, R. Storz, H.W.K. Tom, and J. Bokor, ***Phys. Rev. Lett.68,*** 2834 (1992); R.H.M. Groeneveld, R. Spirk, and A. Lagendijk, *Phys. Rev. B* **51,** 11433 (1995); C.K. Sun, F. Vallee, L.H. Acioli, E.P. Ippen, and J.G. Fujimoto, ***Phys. Rev.B*** 48, 12365 (1993); 50, 15337 (1994); C. Suarez, W.E. Bom, and T. Juhasz, ***Phys. Rev. Lett.*** 75, 4536 (1995); H.E. Elsayed-Ali, T.B. Norris, M.A. Pessot, and G.A. Mourou, ***Phys. Rev. Lett.58,*** 1212 (1987); J.-Y. Bigot, V. Halte, J.-C. Merle, and A. Daunois, *Chem. Phys.* **251,** 181 (2000); N. Del Fatti, F. Vallee, C. Flytzanis, Y. Hamanaka, and A. Nakamura, ***Chem. Phys.*** **251,** 215 (2000).

34. V. Halte, J.-Y. Bigot, B. Palpant, M. Broyer, B. Prevel, and A. Perez, *Appl. Phys. Lett.,* 75, 3799(1999).

35. N. Del Fatti, F. Vallee, "Ultrafast optical nonlinear properties of metal nanoparticles", *Appl. Phys. B* 73, 383 (2001)

36. T.V. Shahbazyan, I.E. Perakis, "Surface collective excitations in ultrafast pump-probe spectroscopy of metal nanoparticles", *Chem. Phys.* **251,** 37 (2000); S. Stagira, M. Nisoli, S. De silvestri, A. Stella, P. Tognini, P. Cheyssac, R. Kofman, *Chem. Phys.* **251,** 259 (2000); J. Hohlfeld, S.-S. Wellershoff, J. Gudde, U. Conrad, V. Jahnke, E. Matthias, *Chem. Phys.* **251,** 237 (2000).

37. J.-Y. Bigot, J.-C. Merle, O. Cregut, and A. Daunois, *Phys. Rev. Lett.* 75, 4702 (1995); A. Stella, M. Nisoli, S. De Silvestri, O. Svelto, G. Lanzani, P. Cheyssac, and R. Kofman, *Phys. Rev.* B 53 15497(1996); Roberti T W, Smith B A and Zhang J ZJ. *Chem. Phys.* **102** 3860((1995).

38. M. Perner, S. Gresillon, J. Marz, G. von Plessen, J. Feldmann, J. Porstendorfer, K.-J. Berg and G. Berg, *Phys. Rev. Lett.* **85,** 792 (2000); T.V. Shahbazyan, I.E. Perakis, *Phys. Rev.B* **60,** 9090 (1999); H. E. Elsayed-Ali, T.B. Norris, M.A. Pessot and G.A. Mourou, *Phys. Rev. Lett.* **58,** 1212(1987); C. Viosin, D. Christofilos, N. Del Fatti, F. Vallee, B. Prevel, E. Cottancin, J. Lerme, M. Pellarin and M. Broyer, *Phys. Rev. Lett.,* **85,** 2200 (2000); T.V. Shahbazyan, I.E. Perakis and J.-Y. Bigot, *Phys. Rev. Lett.,* 81,3120(1998).

39. M.P. Joshi, J. Swiatkiewicz, F. Xu, P.N. Prasad, B.A. Reinhardt, and R. Kannan, Opt. Lett. 23,1742(1998).

40. V. Jourdier, P. Bourdon, F. Hache, and C. Flytazanis, *Appl. Phys.* **567,** 627 (1998); *Appl. Phys. B***70**, 105(2000).

41. K.M. Nashold and D.P. Walter, *J. Opt. Soc. Am.* **B12,** 1228-1237 (1995); R. Goedert, R. Becker, A. Clements, and T. Whittaker III, *J. Opt. Soc. Am.* **B15,** 1442-1462(1998).

42. G.S. Maciel, N. Rakov, and Cid B. de Araujo, *Opt. Lett.* 27, 740-742 (2000); S.R. Mishra, H.S. Rawat, M.P. Joshi, S.C. Mehendale, *Appl. Phys. A***63**, 223-226 (1996); S.R. Mishra, H.S. Rawat, M.P. Joshi, and S.C. Mehendale, *J. Phys. B: At. Mol. Opt. Phys.*27, L157-L163 (1994);

43. S. Link, M.A. El-Sayed, *J. Phys. Chem.* **5103,** 8410 (1999); A. Takami, H. Kurita, S. Koda, *J. Phys. Chem.* **5103,** 1226, (1999); H. Fujiwara, S. Yanagida, P.V. Kamat, *J. Phys. Chem.* **5103,** 2589 (1999).

44. L. Smilowitz, D. McBranch, V. Klimov, M. Grigorova, B.J. Weyer, A. Koskelo, B.R. Mattes, H. Wang, and F. Wudl, *Synthetic Metals* 84, 931 (1997).

45. G.C. Papavassiliou. *Prog. Solid State Chem.* **12** 185 (1980).

46. J. Hellier, J. Turkevich, and P.C. Stevenson, *Trans. Faraday Soc. Discuss.* **11** 55 (1951); J.P. Wilcoxon, J.E. Martin, F. Parsapour, B. Wiedenman, and D.F. Kelley, *J. Chem. Phys.* **108** 9137 (1998); J.P.Wilcoxon, R.L. Williamson, and R. Baughman, *J. Chem. Phys.* 98 9933 (1993).

47. U. Kreibig, and U. Genzel, *Surf. Sci.* **156,** 678 (1985).

Chapter 7
Summary and future perspective

To summarize, we have studied three different classes of materials: tetratolylporphyrins, pure and doped photorefractive crystals and co-doped metal nanoclusters to identify new materials for all-optical limiting mechanisms based on Reverse Saturable Absorption (RSA) that lead to optical limiting in the visible wavelength region.

In porphyrins, two classes of modified tetratolylporphyrins are studied. First class of porphyrins has central phosphorus (V) atom with different axial **ligands,** like (OH), Cl, and azoarene units and is studied for heavy atom effect and the presence of charge-transfer states. Second class of porphyrins are axial-bonding type hybrid porphyrin arrays, dimer, trimers and hexamers based on tin(lV) TTP scaffold and with free base and Ni and Zn in the periphery.

In P (V) TTP's with heavier axial chlorine substitution in place of (OH) group, has lead to a faster intersytstem crossing and high excited state coefficients from the triplet states in the ns regime and limiting threshold has decreased drastically by ~ 30 times. In the ps regime where only the singlet levels play a role in the nonlinear absorption, at lower intensities ESA is observed and the limiting threshold has decreased ~ 3 times. However, at higher intensities ESA duc to the excited singlet states get saturated leading to saturation of absorption (SA) behaviour after initial RSA. With axial azoarene substitution photoinduced electron transfer and the charge transfer states come into play. The limiting threshold has lowered by approximately a factor of 2 in the ns regime. However in the ps regime at higher intensities SA due to the excited singlet is observed. But compared to the heavy atom substitution, the saturation of ESA in the excited singlet states has decreased as the population can decay rapidly from the higher singlet states to ground state via CT states. **Both the** axial chlorine and azoarene substitutions lead to variation in the vibrational relaxations of the singlet

states. With the axial chlorine substitution the throughput fluences are as low as 100 mJcm^{-2} are achieved.

In 'axial-bonding' type hybrid arrays based on Sn (IV) TTP scaffold, the limiting threshold has decreased as one moves to higher homologues. But within the trimer and hexamer hybrid arrays, replacing the free-base porphyrin with metallo porphyrin has lead to reduction in the limiting threshold and the figure of merit. Linearly linked Sn-Sn dimer shows a better limiting performance than the axial bonding type arrays. Though the limiting thresholds are almost same as that of P (V) TTP's the onset of limiting is at lower fluences and the throughput is as low as 35 mJcm^{-2} at fluences of ~ 70 Jcm^{-2}. In all these hybrid arrays excitation energy transfer also plays an important role in addition to the PET. All these hybrid arrays show higher order nonlinearities and ultrafast relaxations in the ps regime.

Pure and iron doped $Bi_{12}SiO_{20}$ crystals are studied and both the crystals show good optical limiting and nonlinear absorption properties at three different wavelengths in the visible region. The crystal is found to have a very strong nonlinear absorption with major contribution from TPA assisted by intraband carrier absorption and charge carrier absorption from trap levels. The damage threshold has increased at all the wavelengths with Fe doping. Ultrafast relaxations of the excited carriers with ps pulses excitation are found to make these crystals good optical limiting materials over a wide range of wavelengths and time scales.

The effect of surface plasmon resonance on the optical limiting response in Ag-Cu nanoclusters codoped in SiO_2 sol-gel matrix is studied. Optical limiting properties are investigated at three different wavelengths that are nearly in resonance with the SPR and below the SPR. Nonlinear absorption and nonlinear scattering are observed to be present in these films. Though the nonlinear scattering has decreased with decreasing particle size from 1Ag1Cu to 1Ag3Cu, the optical limiting performance has increased. Excitation closer to the SPR (532 nm) of Cu nanoclusters resulted in reduction of limiting threshold with increasing Cu concentration and excitation well above the SPR of Cu and nearer to that of

Ag (435 nm) resulted in reduction of limiting threshold approximately by 10-17 times.   Whereas, excitation below the SPR at 683 nm has not shown any nonlinear absorption. The nonlinear absorptive processes associated with energy transfer among the high lying states of Cu and Ag found to contribute more to the optical limiting performance.

Since the mechanism of optical limiting in all the three classes of the materials depends on the absorption of excited molecules/electrons/carriers and the nonlinearity, it is important to characterize the excited state dynamics in order to exactly evaluate parameters like TPA coefficients, lifetimes/relaxation times of the high lying states, bands etc. to optimize them in making a realistic device.

Higher order nonlinearities, presence of two-photon/multi-photon absorption and ultrafast relaxations in the porphyrin arrays can be resolved using fs pump-probe, transient absorption and FWM experiments.   In metal nanoclusters the energy transfer mechanism in the codoped clusters can be better understood from the fs transient absorption and pump-probe studies. All these studies will give better insight into the processes leading to nonlinear absorption and optical limiting phenomenon.

Publications from the work presented in thesis

In refereed journals:

1. P.S. Aithal, <u>P. Prem Kiran</u> and D. Narayana Rao, "Optical limiting studies in photorefractive Pure and iron-doped $Bi_{12}SiO_{20}$ crystals", *Journal of Nonlinear Optical Physics & Materials* 9, 217-225 (2000).

2. D. Narayana Rao and <u>P. Prem Kiran</u>, "Optical limiting studies of BSO crystal using a nanosecond laser source", *Nonlinear Optics* 27, 347-355 (2001).

3. <u>P. Prem Kiran</u>, N.K.M. Naga Srinivas, D. Raghunath Reddy, B.G. Maiya, Aravinder S. Sandhu, Aditya Dharmadhikari, G. Ravindra Kumar and D. Narayana Rao, "Heavy atom effect on nonlinear absorption and optical limiting characteristics of 5,10,15,20-(tetratolyl) porphyrinato phosphorus (V) dichloride", *Opt. Commun.* 202, 347-352 (2002).

4. <u>P. Prem Kiran</u>, D. Raghunath Reddy, B.G. Maiya and D.Narayana Rao, "Third order nonlinearity and optical limiting studies in phosphorus (v) porphyrins with charge transfer states", *Optical Materials* 21, 565-568 (2002).

5. <u>P. Prem Kiran</u>, D. Raghunath Reddy, B.G. Maiya, Aditya Dharmadhikari, G. Ravindra Kumar and D. Narayana Rao, "Enhanced optical limiting and nonlinear absorption properties of azoarene appended phosphorus (V) tetratolylporphyrins", *Appl. Opt.* LPEO 41, 7631-7636 (2002).

6. <u>P. Prem Kiran</u>, Goutam De and D. Narayana Rao, "Nonlinear optical properties of copper and silver nanoclusters in SiO_2 Sol-Gel films", to appear in *IEE Proceedings - Circuits, Devices and Systems* 150, 559-562 (2003).

7. <u>P. Prem Kiran</u>, Shiv Kiran N. Bhakta B, Goutam De, and D. Narayana Rao, "Effect of surface plasmon band on optical limiting and nonlinear optical properties of Ag-Cu nanoclusters codoped in SiO_2 sol-gel films" (Manuscript submitted to *J. Appl. Phys.*).

8. P. <u>Prem Kiran</u>, D. Raghunath Reddy, B.G. Maiya, Aditya Dharmadhikari, G. Ravindra Kumar and D. Narayana Rao, "Effect of axial ligation on excited-state dynamics in Phosphorus (V) tetratolylporphyrins" (Manuscript to submitted to *J. Porphyrin Phthalocyanines*).

9. <u>P. Prem Kiran</u>, D. Raghunath Reddy, B.G. Maiya, Aditya Dharmadhikari, G.Ravindra Kumar and D. Narayana Rao, "Nonlinear optical and optical limiting characteristics of tin (IV) tetratolylporphyrin oligomer arrays" (Manuscript to be communicated to *Client. Phys. Lett.*).

10. <u>P. Prem Kir</u>an and D. Narayana Rao, "Optical limiting characteristics of $Bi_{12}SiO_{20}$ and $Bi_{12}SiO_{20}$:Fe crystals in the visible region" (Manuscript to be communicated to *Opt. Commun.*).

Book Chapters:

1. D. Narayana Rao, <u>P. Prem Kiran</u>, D. Raghunath Reddy and B.G. Maiya, "Study of the excited state dynamics to improve the optical limiting performance of tetra tolylporphyrins", Page 65-70, in Current Developments in Atomic, Molecular, and Chemical Physics with Applications, Kluwer Academic/Plenum publishers Jan 2003. (Proceedings of an International Conference held March 20-22, 2002, in Delhi, India).

Poster/Oral presentations at **National/International** Conference proceedings:

1. P. Prem Kiran. P.S. Aithal, and D. Narayana Rao, *"Nonlinear absorption and optical limiting in $Bi_{12}SiO_{20}$ crystal"*, Proc. of National Laser Symposium, Pg.155, University of Hyderabad, December 15-17, (1999).
2. D. Narayana Rao and P. Prem Kiran. "Optical limiting studies of BSO crystal using a nanosecond laser source", Presented at Second International Symposium on Optical Power Limiting, Venice, Italy, July 2-5, (2000).
3. P. Prem Kiran. D. Raghunath Reddy, B.G. Maiya and D. Narayana Rao, "Studies of third-order optical nonlinearity and optical limiting in a new class of phosporus azoarene porphyrins", Proc. of National Laser Symposium, Pg.184, Laser Science and Technology Center, December **13-15,** (2000).
4. P. Prem Kiran. D.Raghunath Reddy, B.G. Maiya and D. Narayana Rao, "Third order nonlinearity and optical limiting studies in phosphorus (V) porphyrins with charge transfer states", Invited student presentation at International Conference on Photoresponsive Organics and Polymers (ICPOP'2001), Cheju, Korea.
5. P. Prem Kiran. N.K.M. Naga Srinivas, D. Raghunath Reddy, Bhaskar G. Maiya, Aditya Dharmadhikari, Arvinder S. Sandhu, G. Ravindra Kumar and D. Narayana Rao, "Optical limiting characteristics of 5,10,15,20-(tetratolyl) porphyrinato phosphorus (V) dichloride - enhancement due to heavy atom effect", Poster presentaion at the National Laser Symposium-2001, Center for Advanced Technology, Indore. (Post deadline paper)
6. P. Prem Kiran. Goutam De and D. Narayana Rao, "Nonlinear optical and optical limiting properties of copper and silver nanoclusters in SiO_2 Sol-gel films", Poster presentation at PHOTONICS-2002 Sixth international conference on optoelectronics, Fiber optics and Photonics, Tata Institute of Fundamental Research, Mumbai, December 16-18, 2002.
7. P. Prem Kiran, D. Raghunath Reddy, Bhaskar G. Maiya, and D. Narayana Rao, "Optical limiting characteristics of tin (IV) tetratolyl porphyrin hexamers", Poster presentation at Recent Developments and Challenges in Physics, School of Physics, University of Hyderabad, December 19-22, 2002.
8. P. Prem Kiran, D. Narayana Rao, D. Raghunath Reddy, Bhaskar G. Maiya, "Tin(IV) tetratolylporphyrin arrays for nanosecond optical limiting", Poster presentation at The third International Symposium on Optical Power Limiting *ISOPL-3*, Sedona, 28 Sept – 3 Oct, 2003.
9. D. Narayana Rao, P. Prem Kiran. and Goutam De, "Role of surface plasmon resonance towards optical limiting in Ag-Cu nanoclusters codoped in SiO_2 sol-gel films", Poster presentation at The third International Symposium on Optical Power Limiting *ISOPL-3*, Sedona, 28 Sept - 3 Oct, 2003.
10. P. Prem Kiran, D. Raghunath Reddy, Bhaskar G. Maiya, and D. Narayana Rao, "Sn(IV)TTP axial-bonding type arrays for optical limiting: Role of excited singlet states", Proc. of DAE-BRNS, National Laser Symposium, Pg. 405, Indian Institute of Technology, Kharagpur, December 22-24, 2003.

Publications from outside the thesis work

<u>**In** refereed journals:</u>

1. P.S. Aithal, <u>P. Prem Kiran</u> and D. Narayana Rao, *"Self-focussing, self-trapping, and optical limiting of light beams in photorefractive $Bi_{12}SiO_{20}$: Fe crystal"*, *Proc. SPIE,* 3899,406-416(1999).
2. B.R. Kimball, M. Nakashima, B.S. DeCristofano, N.K.M. Naga Srinivas, <u>P. Prem Kiran</u>, D. Narayana Rao, A. Panchangam and D.V.G.L.N. Rao, "Solvent effect on optical limiting in zinc tetrabenzoporphyrins", *Proc. SPIE,* **4106,** 264-271 (2000).

<u>Poster/Oral presentations at National/International Conference proceedings:</u>

1. <u>P. Prem Kiran</u>, P.S. Aithal, and D. Narayana Rao, *"Observation of 1-D self trapping of optical beams in photorefractive $Bi_{12}SiO_{20}$: Fe Crystal",* Proc. of National Laser Symposium, Pg. 157, University of Hyderabad, December 15-17, (1999).
2. P.S. Aithal, <u>P. Prem Kiran</u> and D. Narayana Rao, *"Self-trapping of Optical beams in an unbiased photorefractive $Bi_{12}SiO_{20}$: Fe crystal*", presented at International Conference on Lasers and Applications, St. Joseph's College, Trichy, March 1-4, 2000. Published as special issue of Asian J. Physics vol. 9, 376-381 (2000).